THERMODYNAMIC OPTIMIZATION OF SUSTAINABLE ENERGY SYSTEM: APPLICATION TO THE OPTIMAL DESIGN OF HEAT EXCHANGERS FOR GEOTHERMAL POWER SYSTEMS

by

PENI Junior YEKOLADIO

Submitted in partial fulfillment of the requirements for the degree

MASTER OF ENGINEERING (Mechanical Engineering)

in the

Faculty of Engineering, the Built Environment and Information Technology

UNIVERSITY OF PRETORIA

Pretoria

Supervisors: Prof. TUNDE BELLO-OCHENDE and Prof. JP MEYER

May 2013

Abstract

Title : Thermodynamic Optimization of Sustainable Energy System: Application to the optimal design of heat exchangers for geothermal power systems
Author : PJ Yekoladio
Supervisor : Prof. Tunde Bello-Ochende and Prof. JP Meyer
Department : Mechanical and Aeronautical Engineering
Degree : Master of Engineering

The present work addresses the thermodynamic optimization of small binary-cycle geothermal power plants operating with moderately low-temperature and liquid-dominated geothermal resources in the range of 110^{o}C to 160^{o}C, and cooling air at ambient conditions of 25^{o}C and 101.3 kPa, reference temperature and atmospheric pressure, respectively. The thesis consists of an analytical and numerical thermodynamic optimization of several organic Rankine cycles (ORC) to maximize the cycle power output. The thermodynamic optimization process and entropy generation minimization (EGM) analysis were performed to minimize the overall exergy loss of the power plant, and the irreversibilities associated with heat transfer and fluid friction caused by the system components. The effect of the geothermal resource temperature to impact on the cycle power output of the ORC was studied, and it was found that the maximum cycle power output increases exponentially with the geothermal resource temperature. In addition, an optimal turbine inlet temperature was determined, and observed to increase almost linearly with the increase in the geothermal heat source. Furthermore, a coaxial geothermal heat exchanger was modeled and sized for minimum pumping power and maximum extracted heat energy from the Earth's deep underground. The geofluid circulation flow rate was also optimized, subject to a nearly linear increase in geothermal gradient with depth. In both limits of the fully turbulent and laminar fully-developed flow, a nearly identical diameter ratio of the coaxial pipes was determined irrespective of the flow regime, whereas the optimal geofluid mass flow rate increased exponentially with the flow Reynolds number. Several organic Rankine Cycles were also considered as part of the study. The basic types of the ORCs were observed to yield maximum cycle power output. The addition of an IHE and/or an OFOH improved significantly the effectiveness of the conversion of the available geothermal energy into useful work, and increased the thermal efficiency of the geothermal power plant. Therefore, the regenerative

ORCs were preferred for high-grade geothermal heat. In addition, a performance analysis of several organic working fluids, namely refrigerants R123, R152a, isobutane and n-pentane, was also conducted under saturation temperature and subcritical pressure operating conditions of the turbine. Organic fluids with higher boiling point temperature, such as n-pentane, were recommended for the basic type of ORCs, whereas those with lower vapour specific heat capacity, such as butane, were more suitable for the regenerative ORCs.

Keywords: Geothermal energy, Organic Rankine Cycles, Optimization, Exergy analysis, Entropy Generation Minimization analysis, binary cycle, Enhanced Geothermal System.

Acknowledgements

The author acknowledges with gratitude the support from the University of Pretoria and his supervisors. The funding obtained from Hitachi Power Africa and the National Research Foundation (NRF-DST) is duly appreciated.

To my Lord and God who made it all possible!

Table of Contents

List of tables

List of figures

Nomenclature

Alphabetic Symbols

A	Heat transfer area, m^2
A_{min}	Minimum cross-sectional flow area, m^2
A_{fin}	Fin heat transfer area, m^2
A_{fr}	Flow entrance frontal area, m^2
A_T	Total heat transfer area, m^2
B	Baffle spacing, m
Bo	Boiling number
C	Mass flow parameter
Cp	Isobaric specific heat capacity, J/kg.K
CL	Tube layout constant
CTP	Tube count constant
D	Diameter, m
D_h	Hydraulic diameter, m
E, F, H	Dimensionless factors
$\dot{E}x$	Exergy rate, W
f	Fanning friction factor
F	Flow-arrangement correction factor
Fr	Froude number
g	Gravitational acceleration, m/s^2
G	Mass flux, kg/m^2s
h	Convective heat transfer coefficient, $W/m^2.K$, or specific enthalpy, J/kg
H	Height
h_{fg}	Latent heat of vaporization, J/kg
ΔH_{is}	Isentropic enthalpy difference in the turbine, J
$\dot{I}$	Exergy destruction (irreversibility), W
j	Temperature bin number
$I\dot{P}$	Exergetic improvement potential
k	Thermal conductivity, W/m.K
K	Local loss coefficient

L	Length, m, or latent heat, J/kg
$\dot{m}$	Mass flow rate, kg/s
M	Merit function
m_{es}	Extended surface geometric parameter
n_f	Number of fins
n_L	Number of tubes in the longitudinal direction
n_T	Number of tubes in the transversal direction
N_E	Exergy destruction number
N_s	Non-dimensional entropy generation number
$N_{s,aug}$	Augmented entropy generation number
Nu	Nusselt number
P	Pressure, Pa
ΔP	Pressure drop, Pa
P_f	Fin spacing, m
p_r	Reduced pressure
Pe	Perimeter, m
Pr	Prandtl number
q	Heat flux, W/m^2
$\dot{Q}$	Heat transfer rate, W
r	Diameter ratio
R	Radius, m, or thermal resistance, W/m^2.K
R_e	Equivalent radius, m
Re	Reynolds number
s	Specific entropy, J/kg.K
S_D	Tube pitch in the diagonal direction, m
S_L	Tube pitch in the longitudinal direction, m
S_T	Tube pitch in the transversal direction, m
$\dot{S}_{gen}$	Entropy generation rate, W/K
$\dot{S}'_{gen}$	Entropy generation rate per unit length, W/K.m
SP	Size parameter
St	Stanton number

Sv Svelteness

T Temperature, ^{o}C

$\Delta T_{lm,cf}$ Counter-flow logarithmic mean temperature difference, ^{o}C

u Flow velocity, m/s

U Overall heat transfer coefficient, W/m^2.K

V Volume, m^3

$\dot{V}$ Volumetric flow rate, m^3/s

$\dot{W}$ Power, W

We Weber number

x Vapour quality, or axial distance along the tube/pipe, m

Y_s Heat exchange reversibility norm (HERN)

z Tube clearance, m

Abbreviations

ATL Atmospheric Lifetime

Btu British Thermal Unit

CA Cooling Air

CS Cooling System

HC Hydrocarbons

HE Heat exchanger

HFC Hydrofluorocarbons

$HCFC$ Hydrochlorofluorocarbons

HDR Hot-Dry-Rock

GWP Global Warming Potential

K Kelvin

kg Kilogram

kJ KiloJoule

kPa KiloPascal

kWh Kilowatt-hours

MW Megawatt

$O\&M$ Operating and Maintenance

ODP Ozone Depletion Potential

$OECD$ Organization for Economic Cooperation and Development

ORC Organic Rankine Cycle

$SExI$ Specific Exergy Index

TW Terawatt

TWh Terawatt-hours

Greek symbols

α, β Constant parameter

δ_f Fin thickness, m

ε Void fraction or effectiveness, %

η_I First Law efficiency, %

η_{II} Second Law efficiency, %

η_f Fin efficiency, %

η_o Overall surface efficiency, %

θ angle with respect to the horizontal, ^{o}

μ Dynamic viscosity, kg/m.s

ν Specific volume, m^3/kg, or vapour

Φ Two-phase multiplier

ρ Density, kg/m^3

σ Surface tension, N/m

τ Dimensionless temperature difference

χ Diameter ratio function

ψ Specific exergy, J/kg

Other subscripts

0 Reference state

1-15 Thermodynamic states

a Annular space or air-side

ac Actual

aug Augmentation

b Bulk

B Baffle

C	Condenser or cold stream
cr	Critical value
D	Diameter
$dest$	Destruction
e	Equivalent
E	Evaporator
el	Electrical
ext	Extraction
f	Fin or fouling
fr	Frontal
$frict$	Friction
G	Gas- (or vapour) phase
geo	Geothermal fluid
gen	Generation
H	Homogeneous or hot stream
i	Inner
in	Inlet
is	Isentropic
j	Bin number
L	Liquid-phase
lam	Laminar flow
m	Mean
max	Maximum
min	Minimum
mom	Momentum
net	Net
o	Outlet or overall
opt	Optimal
p	Pump or pass
pp	Pinch point
PH	Preheater
R	Rational

rej	Rejection
res	Reservoir
rev	Reversible
s	Shell or surface
sat	Saturation
sp	Specific
$stat$	Static
St	Stanton number
t	Turbine or tube
th	Thermal
tp	Two-phase
$turb$	Turbulent flow
vap	Vaporization
w	Wall
wh	Wellhead
$W-S$	Witte-Shamsundar

Superscripts

$*$	Non-dimensional
CH	Chemical
KN	Kinetic
PH	Physical
PT	Potential

CHAPTER 1

INTRODUCTION

1.1. Background

The unexpected global demographic growth and rapid industrial and economic development of developing countries such as China and India, has resulted to a significant increase in the worldwide energy consumption, namely 1.4 percent per year for the past decades. As illustrated by Fig. 1.1, the world energy consumption is expected to rise from 522 quadrillion Btu in 2010 to 770 quadrillion Btu, as projected in 2035, according to the annual energy outlook 2012 published by the U.S. Energy Information Administration [1].

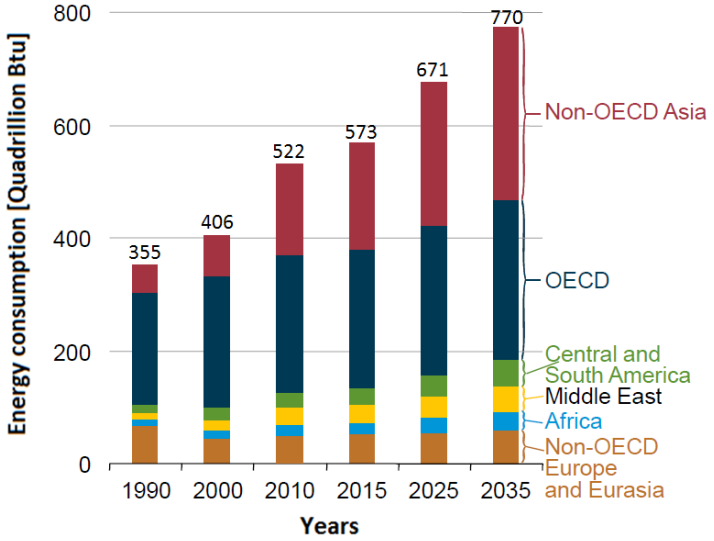

Figure 1. 1: World energy consumption by region, projection through 2035 [1]

Although electricity has been generated from various fuels (e.g. coal, liquid fuels and other petroleum), natural gas-fired (e.g. diesel and kerosene), and sustainable sources such as the renewable and nuclear power plants, fossil fuel constitutes the widest source of energy in use worldwide for power generation purposes (Fig. 1.2). Coal, representing a highly carbon-intensive energy source, raises concern about the environmental impacts, global warming and the greenhouses effects.

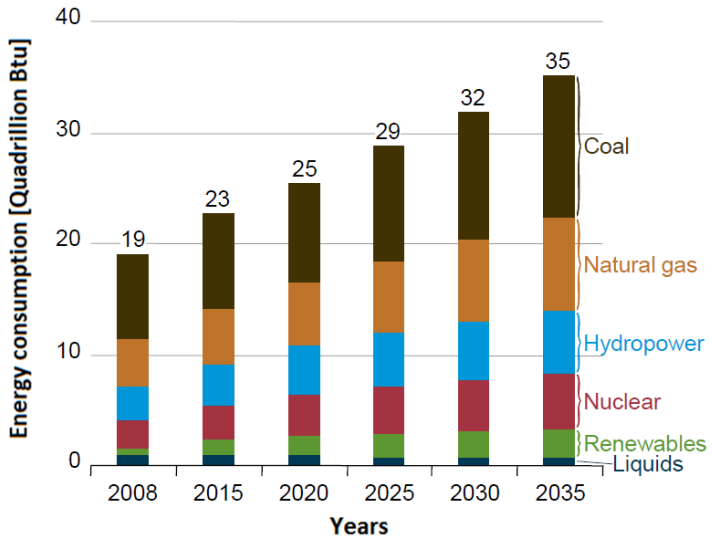

Figure 1. 2: World net electricity generation by fuel, projection through 2035 [1]

Scientific theories have strongly proven the causes and effects of global warming, such as the increase in the atmospheric heat-reflecting potential, changes in rainfall patterns, heat waves and unusual periods of warm weather, ocean warming and rise in sea levels, glaciers melting, flooding, shift in seasons, etc., which affect directly or indirectly both living matters (humans, plants, animals and microbes) and non-living materials such as paints, metals and fabrics. Surely so many solutions and guidelines policies against global warming have been proposed and implemented thus far. These include the global warming awareness conferences and debates, the reduction of CO_2 emission in accordance to the Kyoto Protocol, development of alternative forms of energies besides oil and coal, recycling processes, protection of natural resources, conservation of the forest worldwide as well as the implementation of more energy-efficient and environmental friendly technologies [2]. Among diverse studies conducted to reduce the environment defects of global warming, greenhouse effect, air pollution and waste of natural resources, one may recognize the solar and nuclear energies, wind, tidal and wave powers, hydroelectricity, biomass, biofuel and geothermal energies.

The earth's geothermal energy was originally conceived from the formation of planets, and is replenished at approximately 80% by radioactive decay of minerals (i.e. uranium, thorium and potassium) at a rate of 30 TW [3], and 20% by the residual heat from the earth's interior such as volcanic activities and solar energy absorbed by the earth surface [4,5]. Thus, the geothermal energy is the earth's internal heat, naturally presents in the earth's core, mantle and crust (Fig. 1.3), and flowing to the surface by conduction at a rate of 44.2 TW [3,6].

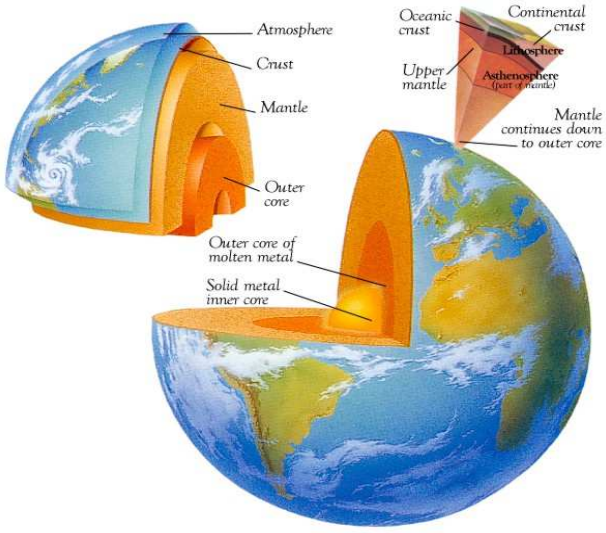

Figure 1. 3: Earth's composition [6]

Traditionally, the constructions of geothermal power plants were restricted to areas near the edges of tectonic plates, volcanic sites, sedimentary hot sources as well as hot wet fractured granite where the presence of subterranean hot water or steam reservoirs facilitated geothermal energy production. However, with the development of the power cycle systems and the improvements in deep drilling and extraction technology, the exploitation of the heat energy in all geological and geographical locations was enabled, irrespective of the presence of subterranean reservoirs of heated water or steam [3].

An estimated worldwide geothermal installed capacity of 10,898 MW_{el} has been approximated by the international energy agency (IEA), as of 2010, producing 67,246 MWh_{el} per annum mostly from liquid-dominated geothermal reservoirs, out of $3x10^{15}$ TWh of the total Earth's heat content [1,7]. Therefore, electricity produced by means of geothermal energy represents only 0.3% of the global electricity demand up to present, and is expected to increase significantly in the near future with the development of advanced geothermal energy extraction technologies [8].

An additional 18,000 MW_{el} of direct geothermal heating capacity is installed worldwide, generating about 63 TWh_{th} per year [9]. Recent figures have shown an annual growth in geothermal energy output of about 3.8% and 10% for electricity generation and direct use, respectively, over the past five years [10].

1.2. Problem statement

A thermodynamic optimization process and entropy generation minimization (EGM) analysis were conducted for small binary-cycle geothermal power plants operating with moderately low-temperature and liquid-dominated geothermal resources in the range of 110^{o}C to 160^{o}C, and cooling air at ambient conditions of 25^{o}C and 101.3 kPa, reference temperature and atmospheric pressure, respectively. The analysis was implemented to minimize the overall exergy loss of the power plant, and the irreversibilities due to heat transfer and fluid friction caused by the system components. Optimal operating conditions, which maximize the cycle power output of the energy conversion systems and reduce the cost of production of the geothermal electricity, were determined.

1.3. Purpose of the investigation

For decades, diverse studies have been conducted to develop renewable and sustainable energies while reducing the environment defects of global warming, greenhouse effect, air pollution and waste of natural resources. Among a diversity of energy-efficient and environmental friendly technologies identified for power generation, the geothermal energy has been proven itself to be an alternative energy source for electric power generation due to its economic competitiveness, operational reliability of its power plants, and its environmentally friendly nature [11].

Current research activities undertaken worldwide have aimed at reducing the cost of geothermal electricity production either in resource exploration and extraction, reservoir stimulation, drilling techniques, or energy conversion systems [12,13]:

a. **Resource exploration and extraction**: This research area focuses on developing more accurate, cost-effective and reliable instrumentation for locating, mapping and extracting economically viable geothermal resources, to minimize the high capital cost and associated risks of exploring deep reservoirs.

   Innovation: Development of High-temperature electrical submersible downhole pumps, improved computer models and better instrumentation operating in high-temperature environment, such as geographical information system (GIS) mapping geothermal indicator for field test temperature, stress, fluid, depth, and airborne identification.

b. **Reservoir stimulation**: This research area aims at maximizing both the production rate and service life of the geothermal reservoirs in order to avoid local depletion of the aquifers and cooling down of the underground.
   Innovation: Development of high-temperature packers, novel well interval isolation techniques, etc.

c. **Drilling techniques**: This research area strives to reduce the cost of drilling through hard rocks present in high-temperature and corrosive environments. This accounts for up to half the geothermal field development cost.
   Innovation: Improved drilling control and tools such as continuous drilling, monobore casting, casting while drilling, high-temperature tools, etc.

d. **Energy conversion systems**: This research area aims at improving the performance and efficiency of the geothermal power plant, maximizing the cycle power output, and minimizing the O&M costs.
   Innovation: Implementation of the supercritical Rankine cycle, novel binary fluids, new designs of both the water-cooled and air-cooled condensers, development of low-cost heat exchanger linings system shielding from corrosion and scaling, improved maintenance techniques, etc.

Likewise, the thesis has aimed at maximizing the cycle power output and reducing the cost of production of the geothermal electricity by investigating and optimizing the energy conversion systems employed in the geothermal power plants. Although various studies have been conducted in this regard, more focus has been directed to the energetic and exergetic analysis and the performance evaluation of the geothermal energy based on the Second-law analysis. Limited attention was spent, however, to the Second-law based performance criteria using the entropy generation as the critical evaluation criteria for the design, analysis, performance evaluation and optimization of sustainable energy systems in general, and the geothermal energy in particular. Among others, we may acknowledge Bejan [14] who developed alternatives to thermodynamic performance and optimization of system subject to physical constraints such as entropy generation minimization (EGM); and Yilmaz et al. [15] who conducted a Second-law based performance evaluation criteria using both entropy and exergy as evaluation parameters to assess the performance of the heat exchangers.

An exergetic analysis briefly conducted by Koroneos et al. [16] on solar thermal, geothermal and wind energy power systems, was extended by Hepbasli [17] to include the performance evaluation of a wide range of renewable energy resources (RERs), namely solar, wind, geothermal, biomass and their hybrid systems. Kanoglu [18], on the other hand, focused on an existing 12.4 MW dual-level binary geothermal power plant, and revealed significant fraction of exergy loss occurring in the condenser, the reinjection process of the brine, the turbine-pump assembly and the preheater-vaporizer, which accounted for 22.6, 14.8, 13.9 and 13.0% of the total exergy input to the plant, respectively. Yari [19] confirmed that more than 51% of the exergy input from high-temperature geothermal resources was lost.

The First- and Second-law efficiencies were also quantified by many other researchers based on either the energy or exergy input into the power generating cycle. The study on flash-steam cycles by Bodvardson and Eggers [20], yielded an exergetic efficiency of 38.7% and 49%, for the single-flash and double-flash cycle, respectively, based on 250^{o}C resource water temperature and 40^{o}C sink temperature. Binary Rankine cycles were rated, by Kanoglu and Bolatturk [21] at 5-15% and 20-54% First- and Second-law efficiency, respectively. Franco [22] approximated the First- and Second-law efficiencies of the geothermal binary power plants in the range of 5-10% and 25-45% respectively, resulting to large heat transfer surfaces for both the heat recovery and condensation systems. DiPippo [23] concluded that binary plants operating with low-temperature, thus low exergy, geothermal resources could achieve 40% or higher exergetic efficiencies with geofluids having specific exergies of 200 kJ/kg or lower, as a result of primarily the optimum design of the heat exchangers to minimize the loss of exergy during the heat transfer processes, and secondarily, the availability of low-temperature cooling water to allow a once-through system for waste heat rejection [19].

The choice of the working fluids was found to be crucial to the design and performance of the geothermal power plants, to the extent of affecting significantly both the power plant capital cost and the cost of operation and maintenance (O&M) [24].

Various other studies were conducted by diverse authors proposing innovative methods to improve the efficiency of the geothermal power plants operating with moderately low-temperature geothermal resources. Kanoglu [18] discussed dual-level binary geothermal power plant. Gu and Sato [25] studied supercritical cycles. DiPippo [26] proposed a recovery heat exchanger (RHE) with a cascade of evaporators with both high- and low-pressure turbines

operating in a Kalina cycle. Desai and Bandyopadhyay [27] recommended an incorporation of both regeneration and turbine bleeding to the basic organic Rankine cycles, whereas Gnutek and Bryszewska-Mazurek [28] suggested multicycle with different thermodynamic properties.

With regard to achieving optimal design of the binary cycle power plants for maximum cycle power output, the sole objective of this thesis, we may acknowledge the study conducted by Borsukiewicz-Gozdur and Novak [29] who maximized the working fluid flow to increase the power output of the geothermal power plant by repeatedly returning a fraction of the geofluid downstream of the evaporator to completely vaporize the working fluid prior expanding in the turbine; Madhawa Hettiarachchi et al [30] who presented a cost-effective optimum design criterion based on the ratio of total heat transfer area to the net cycle power output as the objective function, for the simple ORC employing low temperature geothermal resources.

In most of the literatures mentioned above, the minimization of the geothermal fluid flow rate (or specific brine consumption) for a given cycle power output was addressed as the objective function for optimum design of the ORCs using low-temperature geothermal heat sources. The present study, however, focuses on maximizing the cycle power output for a given geothermal fluid flow rate while minimizing the geothermal plant exergy destruction (or irreversibility) with careful design of the heat exchangers utilized in the geothermal power systems.

1.4. Method, scope and limitations

The thesis consisted of a thermodynamic optimization process and entropy generation minimization (EGM) analysis of small binary-cycle geothermal power plants operating with moderately low-temperature and liquid-dominated geothermal resources in the range of 110^{o}C to 160^{o}C to maximize the cycle power output of several ORCs and reduce the cost of production of the geothermal electricity. A dry cooling system was considered with the cooling air at ambient conditions of 25^{o}C and 101.3 kPa, reference temperature and atmospheric pressure, respectively.

The analysis was organized in three steps, namely:

- To determine the optimal operating conditions, which maximize the cycle power output of the selected Organic Rankine Cycles (ORC), and minimize the overall exergy loss of the power plant, and the irreversibilities due to heat transfer and fluid friction caused by the system components;

- To size a downhole coaxial heat exchanger for an application to an enhanced geothermal system (EGS) by optimizing the geofluid circulation flow rate, which ensured minimum pumping power and maximum extracted heat energy from the Earth's deep underground;
- And to design, model and size the system components for the optimal operating conditions.

For the simplicity of the analysis, a nearly linear increase in the geothermal gradient with depth was assumed. The transient effect or time-dependent cooling of the Earth underground, and the optimum amount and size of perforations at the inner pipe entrance region to regulate the flow of the geothermal fluid were disregarded. The pressure drops in the evaporator, condenser and piping systems were ignored when estimating the thermodynamic performance of the ORCs, and taken into account when sizing the system components.

CHAPTER 2

LITERATURE REVIEW

2.1. Technology Analysis

2.1.1. Overview and applications

The Earth's geothermal gradient, notably 2.4 to 4.5^{o}C per 100 meter on average, is the natural increase of the temperature with depth, and varies from different location depending on the porosity and the degree of liquid saturation of the rock and sediments, their thermal conductivity, heat storage capacity and the vicinity of magma chambers or heated underground reservoirs of liquid [3,31]. The geothermal heat can be extracted at near surface (200 to 400 meters) for direct usage or from the deep underground (2km and deeper below the surface) for an indirect use [32]. The geothermal energy finds its application in various domains of power generation: Direct or indirect, large or small scale production operating with one or multiple working fluids cycle system and subject to the geothermal gradient.

The direct or passive use of the geothermal energy includes space heating and cooling (geothermal heat pump), hot water system and swimming pool heating, underfloor (district) heating, spa (Fish farm), agriculture applications, desalination, industrial processes (food processing and refrigeration plants), etc., in proportion shown in Fig. 2.1 [31]. The indirect use is to generate mainly electricity from dry- or flash-steam, binary or combined (hybrid) cycles depending on the temperature of the geothermal resources [3,33].

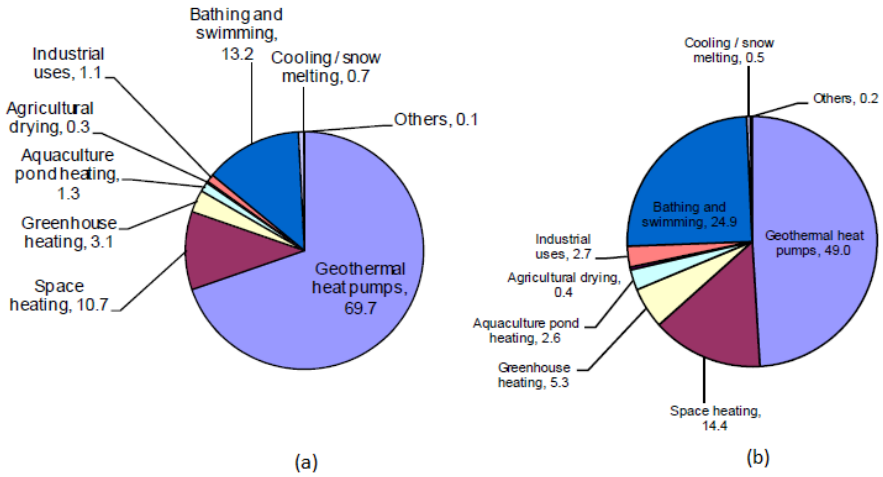

Figure 2. 1: Direct or passive use of geothermal energy (a) Installed capacity, (b) Utilisation [31]

2.1.2. Technology description

The overwhelming majority of existing geothermal power plants draw energy from hydrothermal reservoirs containing either vapour- or liquid-dominated resources [34], which are extracted at their hottest state from the aquifer on the edges of tectonic plates, volcanic or magmatic sites, sedimentary hot sources, as well as from hot wet fractured granite [3]. The most abundant and widely distributed geothermal sources are, however, petrothermal or deep-crust heat reservoirs, wherein the heat transfer medium (e.g. water) is firstly injected at its coldest state in the hot dry fracture granite and then pumped back to the surface as hot geothermal fluid [3,34]. The geothermal power can also be generated from the underground geopressured deposits of heated brine, which contain dissolved methane and are found in conjunction with oil and natural gas reserves [34].

Geothermal power plants can be categorized into four technology options [35]:

- **Dry-steam power plant:** This is a one-cycle system using naturally occurring dry, saturated or slightly superheated steam, from large steam reservoirs at temperature greater than 170^{o}C, to directly drive the turbine. A rock-catcher is installed just before the turbine to prevent small rocks carried along with the steam from the reservoir to damage the turbine blades. The condensed water flows through the injection well back into the geothermal reservoir (Fig. 2.2) [3,33].

  Operating plants: PG&E, unit 18, 120 MW (The Geysers, California) and Valle Secolo, unit 2, 57 MW (Larderello, Tuscany, Italy) [11].

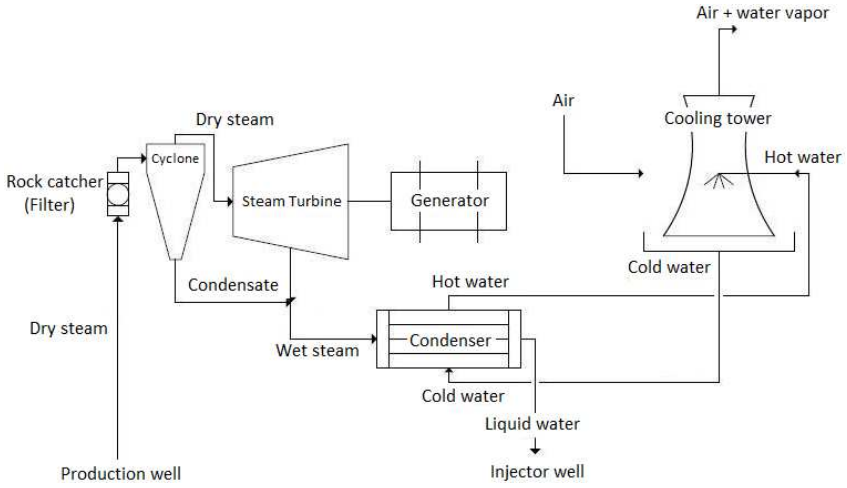

Figure 2. 2: Dry-steam power plant [33]

- **Flash-steam plant:** This is also a one-cycle system, extracting deep, high-pressure super-heated water at temperatures greater than 170^{o}C, into low-pressure tanks, where it vaporizes and drives the turbines. Waste or condensed water is either re-injected back into the geothermal reservoir to be reheated (Single-Flash plants, Fig. 2.3) [3,33], or flashed to a much lower-pressure tank by means of a control valve or an orifice plate, to generate additional steam, which drives the low-pressure turbine or a dual-pressure, dual-admission turbine (Double-Flash plants) [11].

  Operating plants: Single-Flash plants: Miravalles, unit 1, 55MW (Guanacaste, Costa Rica), and Blundell, 24 MW (Milford, Utah). Double-Flash plants: Hatchobaru unit 2, 55MW (Kyushu, Japan), and Beowawe, 16.7 MW (Beowawe, Nevada) [11].

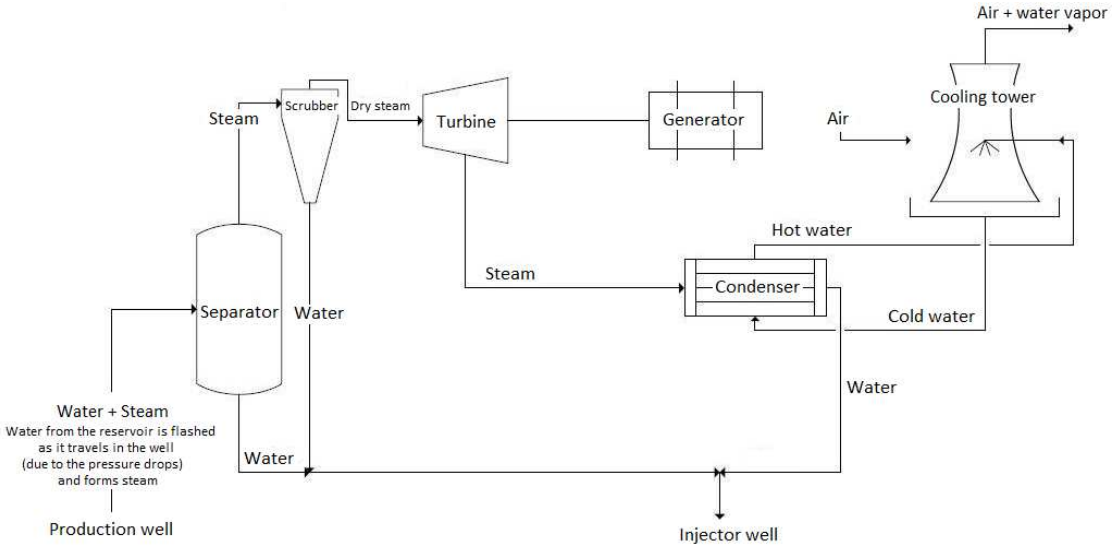

Figure 2. 3: Single-Flash-steam power plant [33]

- **Binary-cycle plant:** This is a two-cycle system exchanging moderately hot geothermal water energy, at temperature lower than 170^{o}C, through a closed pipe system heat exchanger, to a secondary or binary fluid with a lower boiling point and higher vapour pressure. The vapour from the binary fluid then drives the turbine whereas the cooled geothermal water is re-injected into the reservoir (Fig. 2.4) [3,33,36]. The binary fluid could either be an organic compound (e.g. propane, isobutene, isopentane hydrocarbons) or water-ammonia mixture.

  Operating plants: Heber binary demonstration, 65 MW (Heber, California), Second Imperial Geothermal Co., 12x 40 MW (Heber, California), Mammoth-Pacific, unit 1, 2x 10 MW (Mammoth, California), and Amedee, 2x 2 MW (Wendel, California) [11].

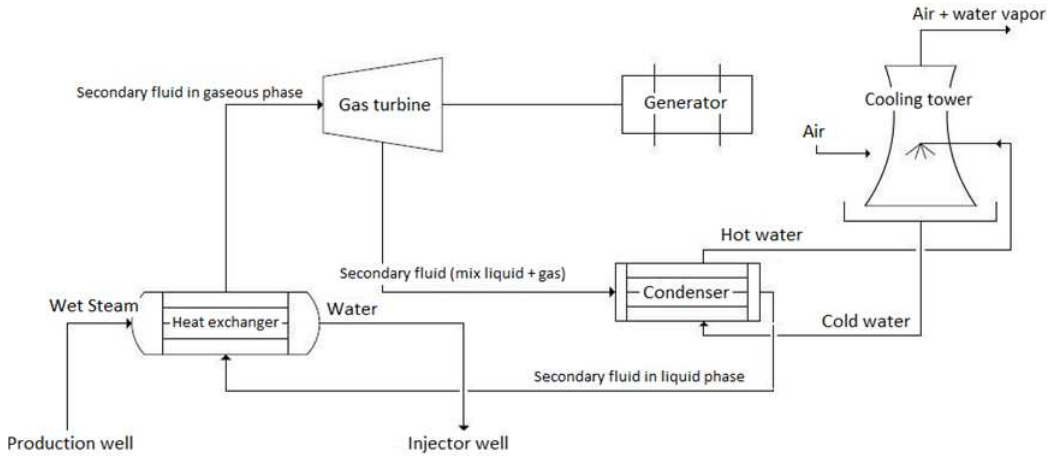

Figure 2. 4: Binary-cycle power plant [33]

- **Combined or Hybrid plant:** This is a combined-cycle system, utilizing steam and hot water as working fluids for the power generation process [3,33]. The hybrid plant can be subdivided into:

  - **Direct-Steam Binary plant**: A combination of a dry-steam unit, containing high concentrations of noncondensable gases, with a binary-cycle unit. In this type of plant, the back-pressure turbine exhaust steam of the dry-steam cycle exchanges heat to a secondary fluid through a heat exchanger, acting as a condenser (Fig. 2.5) [11].
    Shutdown plant: Cove Fort -Sulphurdale (CFS), 10.8 MW total (Millard and Beaver, Utah) [11].

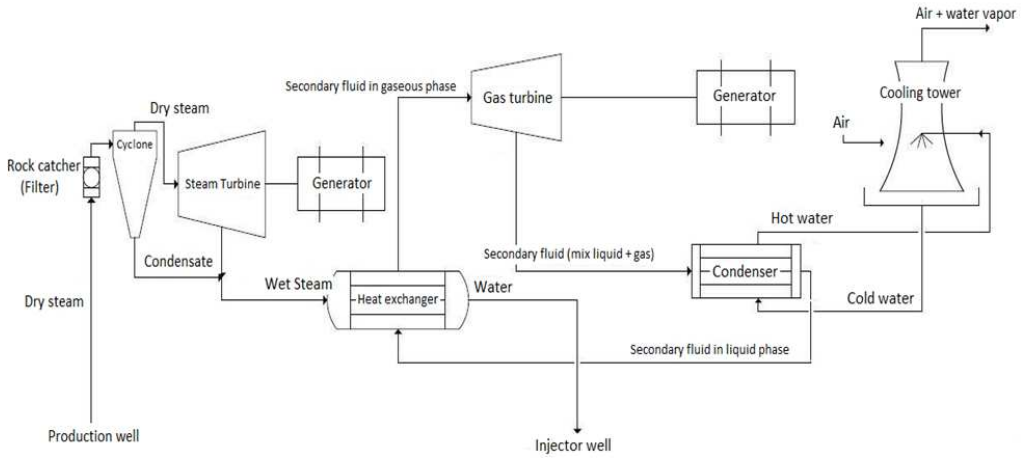

Figure 2. 5: Direct-Steam Binary Hybrid power plant [33]

- **Single-Flash Binary plant**: A combination of a single-flash unit with a binary-cycle unit. In this type of plant, the waste hot geothermal water extracted from the separator is used as a heat transfer medium to a secondary fluid through a closed pipe system heat exchanger either in a condensing steam turbine or back-pressure steam turbine arrangements (Fig. 2.6) [11].

  Operating plants: Puna Geothermal Venture, 25 MW (Puna, Hawaii) [11].

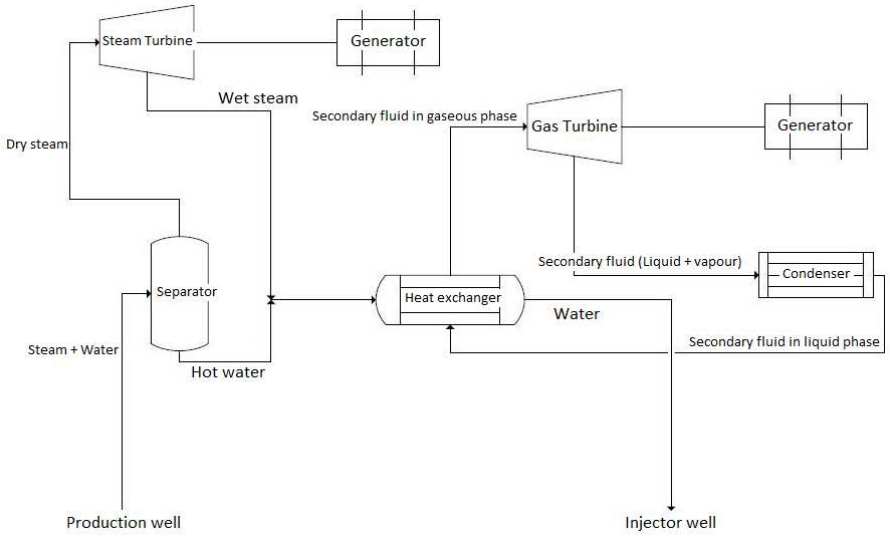

Figure 2. 6: Single-Flash (back-pressure steam turbine arrangements) Binary Hybrid power plant [33]

- **Integrated Single- and Double-Flash plant**: An integration of one or multiple single-flash units with a double-flash unit. In this type of plant, the waste hot geothermal water extracted from the separators of the single-flash units are flashed to a much lower-pressure tank by means of a control valve or an orifice plate, to generate additional steam, which drives a low-pressure turbine or a dual-pressure, dual-admission turbine of the Double-Flash plant [11].

  Operating plants: Cerro Prieto I, 4x 37.5 MW single-flash units and one 30 MW double-flash unit (Mexico); and Ahuachapán, 2x 30 MW single-flash units and one 35 MW double-flash unit (El Salvador) [11].

- **Flash Crystallizer and Reactor Clarifier plant**: A combination of a series of separators and flash crystallizers with a reactor clarifier vessel. In this type of plant, the high-temperature clean steam is separated from a high-salinity and corrosive fluid extracted

from the production well. The settled particulates are disposed, dried and used for other commercial applications [11].

Operating plant: Salton Sea, 185 MW (Imperial Valley, California) [37].

- **Hybrid Fossil-Geothermal system**: A combination of a fossil-fuel with a geothermal plant. In this type of plant, a fossil-fuel exhaust (e.g. natural gas) supplements superheat to the geothermal fluid harnessed from a dry- or flash-steam cycle, as a "geothermal steam plant with a fossil-fuel assist" [38]. Alternatively, the geothermal fluid, at low- to moderate-temperature, is utilised as the heat transfer medium for the lower-temperature feedwater heaters of the conventional fossil-fuel plant as a "fossil-fuel plants with a geothermal assist" [39].

  Operating plant: Hybrid wood-waste/geothermal plant, 30 MW (Honey Lake, California)

2.1.3. Current status of the technology development

The production of electricity by geothermal technology, has found its first industrial exploitation in 1914 in Larderello (Italy) where the world's first commercial geothermal power plant was built, and rated at 250 kW_{el}, to extract boric acid from a volcanic mud [41]. Traditionally, the construction of geothermal power plants was restricted to areas near the edges of tectonic plates, volcanic sites, sedimentary hot sources as well as hot wet fractured granite. The presence of subterranean hot water or steam reservoirs facilitated the hydrothermal energy to flow either vertically by convection or horizontally through convection, advection and diffusion due to the difference in pressure of the extracted and re-injected geothermal fluid [3]. These active, high heat-flow areas comprise the region around the "Pacific Ring of Fire" (i.e. Central America, Indonesia, Japan, New Zealand, Philippines and the west cost of the United States), and the "Great Rift Valley" zones of Iceland, east of Africa and eastern Mediterranean (Fig. 2.7) [9,42].

The development of the binary-cycle power plants and the improvements in deep drilling and extraction technology enabled exploitation of the heat energy by means of petrothermal systems (also known as hot-dry-rock geothermal energy in Europe and enhanced geothermal system in North America) in all geological and geographical locations, irrespective of the presence of the subterranean reservoirs of heated water or steam. The hot-dry-rock (HDR) geothermal energy consists of one or multiple injection and production wells, where the injected water is initially pressurized to cause hydraulic fracturing of hot, dry basement rocks. The technology has

however, been proven to induce seismic activities and yet not economically viable, as the injected geothermal fluid is not harnessed in sufficient quantity for the production wells [3,43].

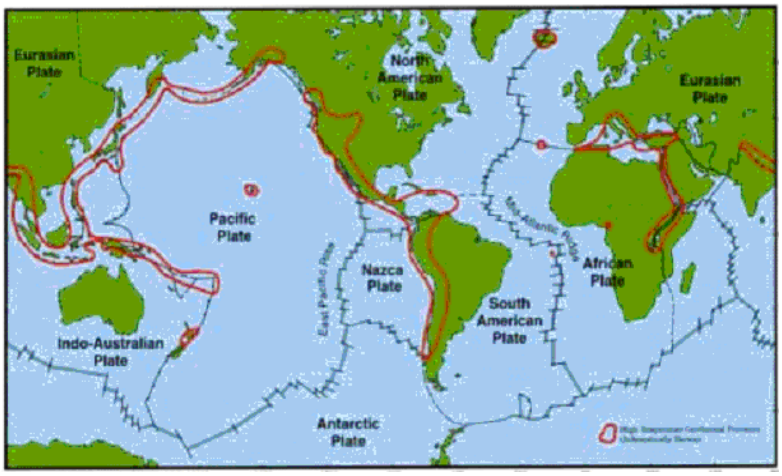

Figure 2. 7: World geothermal resources potential [9]

In Table 2.1, the major developments achieved in deep drilling, resource exploration and extraction, and energy conversion systems of the geothermal technology are listed [13].

Technique	State of art	Barriers	Innovation	Application
Drilling	Rotary table rigs; Trone roller and PDC bits; Telescoping casing; Wireline downhole.	Costs & Temperature limits: designed for oil & gas fields	Continuous drilling; Monobore casting; Casing while drilling; High-temperature tools.	Hydrothermal fields, EGS
Reservoir stimulation	Demo projects: 25 kg/s flow rate, and 1 km^3 reservoir volume	Immature technique, 40 to 80 kg/s flow rates needed	High-temperature packers, novel well interval isolation techniques, 'first to-commercial'	Marginal hydrothermal fields, EGS
Downhole pumps	Line-Shaft Pumps to 600m, Electric Submersible to 175^oC	Temperature and depth limits	High-temperature electrical Submersible pumps	EGS, hydrothermal fields 175 - 200^oC
Energy conversion systems power plants	Binary cycle (isobutene): 100 -200^oC, Cooling towers, Air-cooled condensers	Efficiency limits, low power output at high room temperature	Supercritical Rankine cycle, novel binary fluids, advanced cooling	Medium-low temperature hydrothermal fields, EGS

Exploration and resource tests	Surface evidence; Ground heat-flow tests; Well exploration; Stress field analysis (EGS)	Costly well exploration & drilling; time (years) to prove a field	GIS mapping geothermal indication to assess resources novel techniques for field test temperature, stress, fluid, depth, airbone identification	hydrothermal fields, EGS

Table 2. 1: Development of the geothermal technology

An advanced geothermal energy extraction technology, implemented in Switzerland, Germany and Austria consists of a single gravel-filled well, closed-loop system where the heat transfer fluid is continuously circulated through the earth in a closed pipe system without ever directly contacting the soil or water in which the loop is buried or immersed. The well is filled with gravel for the purpose of stabilization and better water flow regulation, and a set of thermal-insulated and perforated production pipes fitted with pumps to regulate the flow of water (Fig. 2.8). The pipe dimensions, water circulation speed and the amount and size of perforations need to be, however, optimized to ensure maximum extracted energy [3].

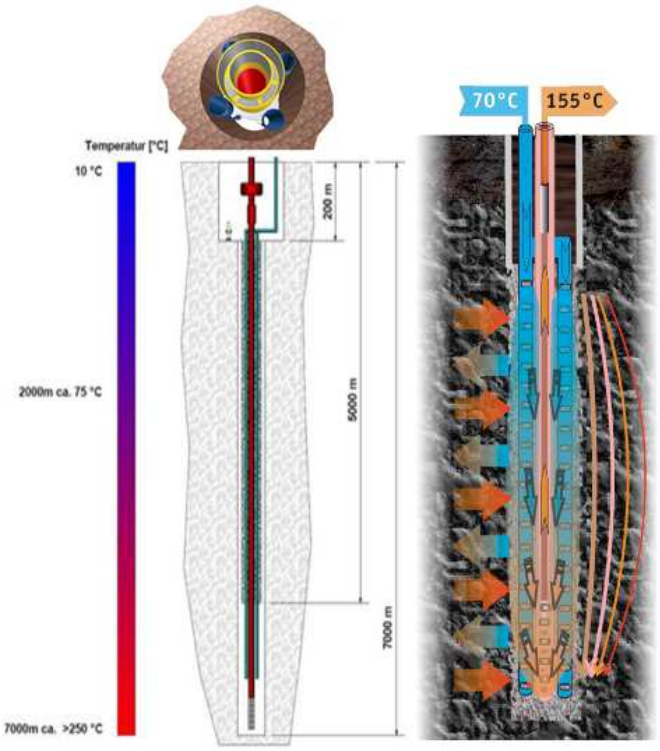

Figure 2. 8:Advanced geothermal energy extraction technology [3]

The advantages of the advanced geothermal energy extraction technology over the conventional geothermal power plants are [3]:

1. The technology can be applied anywhere in the world, irrespective of the local geological ground structure;
2. Much higher geothermal energy can be extracted;
3. Environmental impact such as seismic activities and local depletion of the aquifers related to water injection rate and capacity respectively, is minimized;
4. The risks related to exploration, such as location of hot water reservoirs and fracturing of deep-seated rock can be minimized;
5. The cost as a result of drilling dual or multiple injection or production wells is reduced since a single well is required;
6. The extended life of power plants without noticeable depletion of the geothermal heat output.

2.2. Economics of the geothermal power

The economics of the geothermal power can be defined as the costs associated with building, operating and maintaining a geothermal power plant. They vary widely with [11]:

- The resource chemistry as harnessed from the deep underground geothermal reservoir, namely steam or hot water;
- The resource temperature and pressure;
- The reservoir depth, permeability and productivity performance;
- The power plant size, rating and type;
- The state of the geothermal field development: greenfield versus brownfield;
- The environmental regulations;
- And the cost of capital and labour.

While the first three factors mentioned above, influences the number of wells to be drilled at a typical cost of $100 to $400 per kilowatt for a single production well, the next two factors determine the capital cost of the energy conversion system. The last factor, on other hand, accounts for the cost of operation and maintenance (O&M) [11].

The development of the binary-cycle power plants and the improvements in deep drilling and extraction technology has significantly reduced the capital and electricity production costs of the geothermal power to an estimated value of \$3,400/kW_{el} and \$90/MWh, respectively, at present. It is expected to come down modestly to \$3,150/kW_{el} and \$70/MWh in 2030 [44]. In Table 2.2, the costs of capital, electricity generation and O&M for small Binary Geothermal Plants, based on the geothermal resource temperature and power plant rating, are illustrated [45]. A more detailed analysis of the costs of small-scale geothermal plants in the western United States, with a net cycle power output below 1MW was investigated by Gawlik and Kutscherm [46].

Resource temperature, ^{o}C							
Net power, kW	**100**		**120**		**140**		**Total O&M cost, \$/year**
	Capital cost, \$/kW	**Electricity cost, \$/MWh**	**Capital cost, \$/kW**	**Electricity cost, \$/MWh**	**Capital cost, \$/kW**	**Electricity cost, \$/MWh**	
100	2535	34.7	2210	22.7	2015	18.8	19,100
200	2340	20.9	2040	13.7	1860	11.3	24,650
500	2145	12.2	1870	8.0	1705	6.6	30,405
1000	1950	9.0	1700	5.9	1550	4.9	44,000

Table 2. 2: Cost of capital, electricity generation and O&M for small Binary Geothermal Plants, as of 1993

2.3. Market Investigation

2.3.1. International market

According to the geothermal energy association (GEA) and the international geothermal association (IGA), the total worldwide geothermal power capacity and the number of countries producing geothermal power have dramatically increased and especially in Europe and Africa, over the last years (Fig. 2.9) [47]. Some of these countries are endowed with abundant geothermal resources. Of particular interest are Indonesia, the Philippines, Mexico, Japan, Italy, Kenya, and countries in Central America, namely Costa Rica, El Salvador, Guatemala, and Nicaragua [11].

In Fig. 2.10, the cumulative installed power capacity of geothermal plants from year 2000 and including prospect figures beyond year 2010 to 2020 are represented. Despite these growth trends, the potential of geothermal resources to provide clean energy appears to be under-realized since the number of countries with undeveloped geothermal resources is still high [47].

In Fig. 2.11, the worldwide installed capacity of geothermal electricity and the number of units by exploitation technology were quantified [48-50].

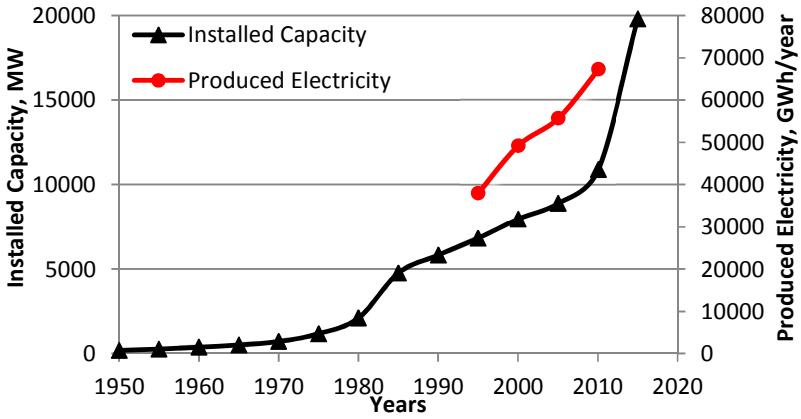

Figure 2. 9: World cumulative installed geothermal power capacity and produced electricity, 1950-2010, and forecast for 2015

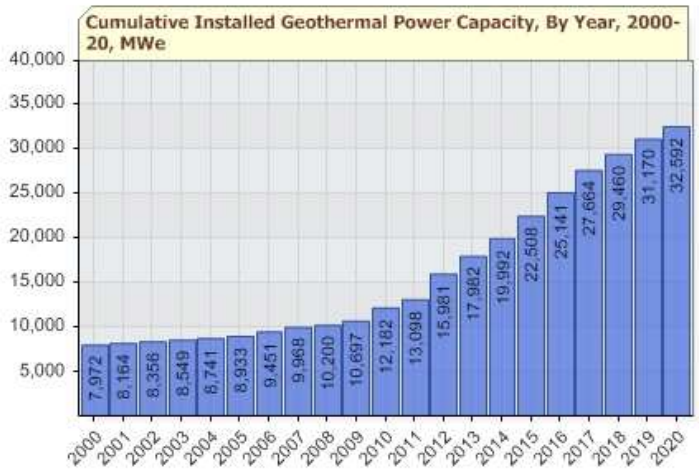

Figure 2. 10: Cumulative Installed Geothermal Power Capacity [47]

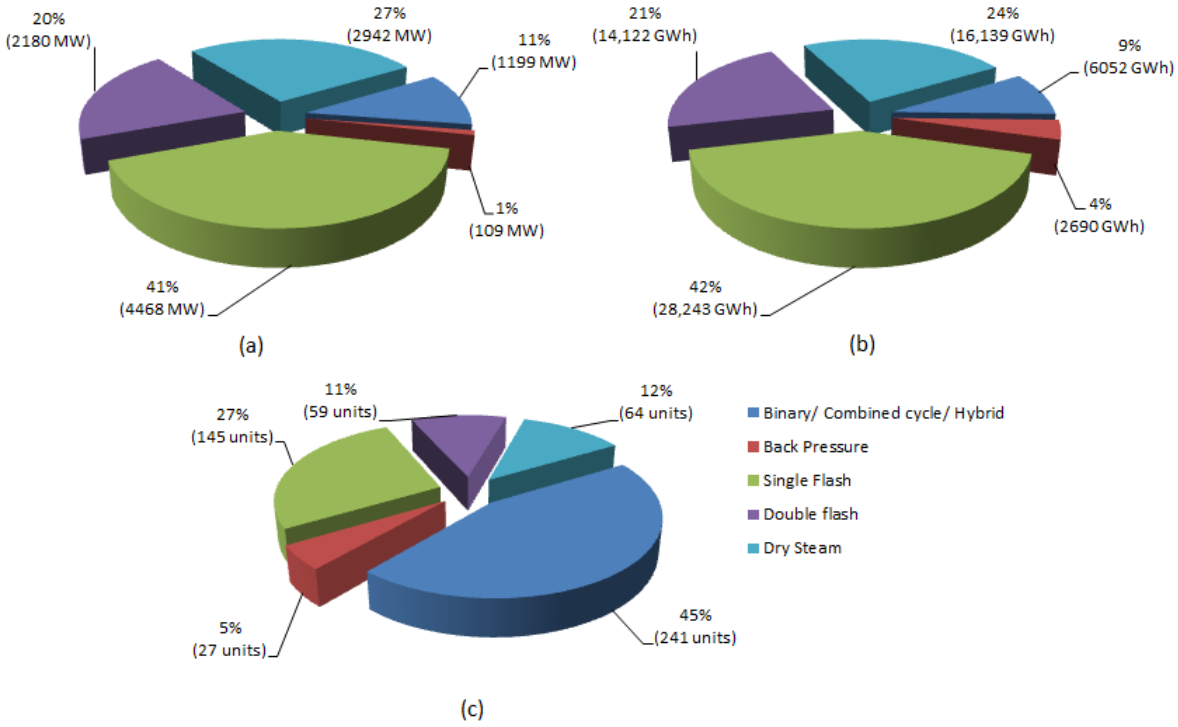

Figure 2. 11: (a) Installed capacity, (b) Electricity produced, and (c) Number of units by exploitation technology

2.3.2. African market

With massive resources, the geothermal energy is a key resource for the African countries along the volcanic region of the east African rift valley, with an estimated 9 GW of geothermal electricity-generating potential, out of which Kenya alone is known to engorge an exceeding 7 GW of geothermal power potential [42,47,51].

In 1999, the geothermal energy association (GEA) published a report on the international geothermal power potential, where 39 countries were identified to possess the potential to meet 100% of their electricity needs through domestic geothermal resources. These countries included 12 from the African continent, namely Burundi, Comoros Islands, Djibouti, Ethiopia, Kenya, Malawi, Mozambique, Rwanda, Somalia, Sudan, Tanzania and Uganda (Fig. 2.12). Up to now, only Ethiopia and Kenya have significantly developed their geothermal power production [47]. The remaining countries have not yet completed the exploration phase due to limited technical and financial resources, high capital investment costs and exploration risks [42].

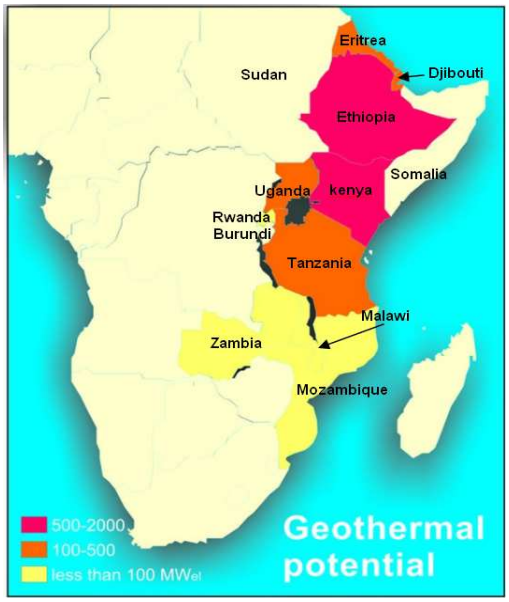

Figure 2. 12: African geothermal potential [47]

2.3.3. Geothermal projects under development in Africa

The growth in geothermal projects under consideration or under development in Africa is attributable to the national-level feed-in tariff mechanisms, international and multi-lateral support (i.e. The World Bank, European Bank for reconstruction and development and European Union), and global financial market in Australia, China, Germany, Iceland, Italy, Japan and the US for facilitating geothermal development projects around the world [42,52].

2.3.4. Feasibility of the geothermal energy exploration in South Africa

Although the Republic of South Africa has been producing 115 TJ per year geothermal energy output, as of 2008, for direct use only from 6 MW_{th} installed capacity [10], the country has, however, limited its prospects for geothermal electricity generation owing to the low price and ready availability of fossil-coal, geological challenges and the lack of knowledge of the new technology from the South African expertise [52,53].

The geological challenges include [11,52]:

- Significant depth to reach hot underground granite, at about 4,000 to 6,000 m below the Earth's surface, depending on the location;
- Relatively high exploration, reservoir characterization and drilling costs (about R1.45 billion for only 50MW geothermal power);

- And more sophisticated methods of monitoring and predicting the reservoir behaviour, prior and during exploitation.

Nevertheless, the organic Rankine cycle (ORC) technology could still be used for the South African geothermal energy production by generating high-pressure "steam" from lower quality heat (about 8°C to 40°C geothermal gradient) [47,52]. Alternatively, the country could integrate geothermal units circulating geothermal fluid, at low- to moderate-temperature, as heat transfer medium for the lower-temperature feedwater heaters of the conventional existing Fossil-fuel plants.

2.4. Peculiarities of the geothermal power

2.4.1. Advantages

- Sustainable energy: Earth's geothermal content is far more abundant than the projected heat extraction;
- Renewable energy: Re-injected water is reheated by the Earth and ready to be reused;
- Continuous availability: Constant underground Earth's temperature, independent of the season, weather nor daytime;
- Low to non-existent pollutant emitted: Carbon dioxide CO_2, sulphur dioxide SO_x, and typically no nitrogen oxides NO_x;
- No fuel required (except for pumps and fans);
- Reduced freshwater requirement;
- Safe and reliable energy;
- Low operating and maintenance costs;
- Minimal facility land used;
- Minimal wastes produced;
- Highly scalable to local geothermal resource, energy demand and available financing.

2.4.2. Disadvantages

- High capital cost and associated risks: Drilling and exploration for deep resources are very expensive;
- Exploration and exploitation difficulties: Locating subterranean reservoirs of heated water/steam or hot tectonic/volcanic and sedimentary sources;

- Low thermal efficiency: 10-23 %

2.4.3. Risk analysis: Environmental effects

Although the geothermal energy is a relatively benign source of energy and offers non-polluting impact to the environment, the minor risks associated with the development of geothermal fields include air and water quality, waste disposal, geological hazards, noise, biological resources and land use [10]. The widely used open-loop technology, such as dry-steam and flash-steam plants, could adversely affect the stability of the land resulting to seismic activity (e.g. Basel, Switzerland), local depletion of the aquifers (e.g. Wairakei, New Zealand and Staufen in Breisgau, Germany), and cooling down of the underground [3,54]. Moreover, the Earth's geothermal fluid, drawn from the deep underground, engorges in addition to noncondensable gases (e.g. carbon dioxide CO_2, hydrogen sulphide H_2S, methane CH_4, ammonia NH_3, etc.), trace amounts of toxic chemicals such as mercury, arsenic, boron, and antimony, susceptible to provoke corrosion, scaling and surface pollution [55]. Nevertheless, the modern practice of re-injecting cooled geothermal fluid back into the earth to stimulate production has significantly reduced the environmental risk of these toxic chemicals. It is therefore highly recommended that the geothermal fluid be treated before re-injection to remove dissolved chemicals and minerals, and thus avoiding any possible impact on the environment.

2.5. Second-law of thermodynamics and its application

2.5.1. Overview and applications

The Second-law of thermodynamics presents the essential tools required in the design, analysis, performance evaluation and optimization of energy systems. Of most importance are the reduction in heat transfer and fluid flow irreversibilities, minimization of the entropy generation, conservation of exergy, and increase in the Second-law efficiency of each components of the thermodynamic power cycle to maximize the system power output. Consequently, the Second-law (or exergy) analysis has extensively been used to investigate and quantitatively assess the causes of the thermodynamic imperfection of processes [17]. In the particular case of the geothermal energy, the application of the Second-law of thermodynamics is closely linked to the geothermal resource temperature, pressure and chemistry, as well as the permeability and productivity performance of the deep underground geothermal reservoir.

2.5.2. Irreversibility

The irreversibility is defined as a lost work, i.e. the difference between the reversible work and the actual work done. It is given by [56]

$$\dot{I} = \dot{W}_{rev} - \dot{W}_{ac} = T_o \dot{S}_{gen} \tag{2.1}$$

From Eq. (2.1), one can conclude that maximum work output is only achievable in reversible systems where irreversibility is minimized.

2.5.3. Entropy generation

As defined by Eq. (2.1), which is known as the Gouy-Stodola relation [15], the entropy generation term is observed to be directly proportional to the amount of available work lost in the process. Consequently, maximum work output is also equivalent to minimum entropy generation for a fixed and known reference temperature T_o.

At steady state, the rate of entropy generation is related to the rates of entropy transfer by [56]

$$\dot{S}_{in} - \dot{S}_{out} + \dot{S}_{gen} = 0 \tag{2.2}$$

*w*here

$$\dot{S}_{gen} = \sum \dot{m}_{out} s_{out} - \sum \dot{m}_{in} s_{in} - \sum \frac{\dot{Q}_j}{T_j} \tag{2.3}$$

2.5.4. Exergy

Exergy, also known as availability, accounts for the maximum theoretical possible amount of energy which can be extracted as useful work from a system interacting with an environment at fixed and known reference pressure P_o and temperature T_o [56]. For a general steady state, steady flow process, and negligible contribution from electrical, magnetic, surface tension and nuclear reaction effects, the total exergy of a system is associated to the random thermal motion, kinetic energy, potential energy and the concentration of species, relative to a reference state, also known as dead state.

The total exergy of a system can be expressed by [56-58]

$$\dot{E}x = \dot{E}x^{PH} + \dot{E}x^{KN} + \dot{E}x^{PT} + \dot{E}x^{CH} \tag{2.4}$$

The general exergy balance at steady state and negligible kinetic and potential changes was given by [56]

$$\sum \dot{E}x_{in} - \sum \dot{E}x_{out} = \sum \dot{E}x_{dest} \tag{2.5}$$

Where

$$\dot{E}x_{dest} = \dot{I} = \dot{E}x_{heat} - \dot{E}x_{work} + \dot{E}x_{mass,in} - \dot{E}x_{mass,out} \tag{2.6}$$

$$\dot{E}x_{heat} = \sum\left(1 - \frac{T_o}{T_j}\right)\dot{Q}_j \tag{2.7}$$

$$\dot{E}x_{work} = \dot{W} \tag{2.8}$$

$$\dot{E}x_{mass,in} = \sum \dot{m}_{in}\psi_{in} \tag{2.9}$$

$$\dot{E}x_{mass,out} = \sum \dot{m}_{out}\psi_{out} \tag{2.10}$$

The flow specific exergy was defined as

$$\psi = (h - h_o) - T_o(s - s_o) \tag{2.11}$$

2.5.5. Second-law analysis

A key concern for the assessment of renewable energy resources for a sustainable future is the depletion of natural resources such as oil, natural gas or coal, in the form of availability reserves. Thus, a sustainable development could eventually be attained while conserving and effectively utilizing these available reserves [56]. The losses associated with heat transfer and fluid flow irreversibilities, can be minimized by means of the Second-law analysis based on either entropy generation minimization (EGM), or exergy analysis, or an integrated approach of one of the above mentioned analysis, to the economic analysis, the so-called thermoeconomics [15]:

a. Entropy Generation Minimization (EGM): "The measure of entropy", as defined by the Second-law analysis based on EGM, is used by different authors in various forms as entropy generation rate, entropy generation number, augmentation entropy generation number, heat exchange reversibility norm (HERN), Witte-Shamsundar efficiency or the local entropy generation number [15]:

- The **entropy generation rate** accounts for the heat transfer irreversibility across a finite temperature difference and the fluid friction irreversibility at the boundary of the system as [15],

  $$\dot{S}_{gen} = \dot{S}_{gen,\Delta T} + \dot{S}_{gen,\Delta P} \tag{2.12}$$

- The non-dimensional **entropy generation number** (N_S) was obtained by dividing the entropy generation rate by either [59-62]

(i) The capacity flow rate $\dot{m}Cp$;

(ii) The heat transfer rate to temperature ratio $\dot{Q}/T$;

(iii) $\left(\dot{Q}^2 U\right)/\left(k\upsilon T^2\right)$ in external flow heat transfer devices;

(iv) Or a fixed and known reference entropy generation rate.

- The **augmentation entropy generation number** $(N_{S,aug})$ is commonly used to evaluate heat transfer augmentation, enhancement, or intensification, and was obtained by dividing the augmented entropy generation rate by a fixed and known reference entropy generation rate [63], i.e.

$$N_{S,aug} = \frac{\dot{S}_{gen,aug}}{\dot{S}_{gen,o}} \tag{2.13}$$

- The **heat exchange reversibility norm (HERN)** Y_S is a measure of the quality of energy conversion of a heat exchanger, and was defined by [15]:

$$Y_S = 1 - \frac{N_S}{N_{S,\max}} \tag{2.14}$$

- The **Witte-Shamsundar efficiency** (η_{W-S}) introduced by Professors Witte and Shamsundar was defined by [61]:

$$-\infty < \eta_{W-S} = 1 - \frac{T_o \dot{S}_{gen}}{\dot{Q}} \leq 1 \tag{2.15}$$

- The **local entropy generation number** represents the local production of entropy by either heat transfer or fluid flow irreversibilities.

b. Exergy analysis: Exergy can be defined as a measure of the ability of a resource to produce work [64,65]. The Second-law analysis based on exergy aims at minimizing the destroyed exergy and improving the system efficiency while conserving the resource [15]. In a similar manner, **"**the measure of exergy" as defined by the Second-law analysis is used by different authors in various forms, namely specific irreversibility, non-dimensional exergy destruction, rational (Second-law) effectiveness, merit function, exergy destruction number, exergetic efficiency (Second-law or rational efficiency), and specific exergy index [15]:

- The **specific irreversibility** is the ratio of a system irreversibility to the thermal exergy rate of the fluid at the inlet of a heat exchanger [66]. It was defined by

$$I_{sp} = \frac{I}{\dot{E}x_{heat}} \tag{2.16}$$

- The **non-dimensional exergy destruction** is the ratio of a system irreversibility (or exergy destruction) to the product of the capacity flow rate to a fixed and known reference temperature [67]. It was given by

$$I^* = \frac{\dot{I}}{\dot{m}T_o Cp} \tag{2.17}$$

- The **rational (Second-law) effectiveness** is the ratio of the gained to the dissipated exergy (availability). It was expressed by [68,69]:

$$0 < \varepsilon_R = \frac{\dot{m}_C \left(\psi_{out} - \psi_{in}\right)_C}{\dot{m}_H \left(\psi_{in} - \psi_{out}\right)_H} < 1 \tag{2.18}$$

- The **merit function** is the ratio of exergy transferred to the sum of exergy transferred and destroyed in the process [70]. It was defined by

$$M = \frac{\dot{Q}_o}{\dot{Q}_o + \dot{I}} \tag{2.19}$$

- The **exergy destruction number** is the ratio of the non-dimensional exergy destruction numbers of an augmented surface to the one of the smooth surface [67]. It was evaluated by

$$N_E = \frac{\dot{I}^*_{aug}}{\dot{I}^*_s} \tag{2.20}$$

- The **exergetic efficiency (Second-law or rational or utilization efficiency)** is explicitly defined by two different approaches, namely the "brute-force" and "functional" [23].

  The "brute-force" approach defines exergy as the ratio of the sums of all output to the input exergy terms,

$$\eta_{II} = \frac{\sum \dot{E}x_{out}}{\sum \dot{E}x_{in}} = 1 - \frac{\dot{E}x_{dest}}{\dot{E}x_{in}} \tag{2.21}$$

  The "functional" approach, however, defines exergy as the ratio of the exergies associated with the desired energy output to the energy expended to achieve the desired output [56]. In the instance of a geothermal power plant, DiPippo [71] defined the overall exergetic efficiency as a ratio of the net power output to the total exergy inputs into the plant at the wellhead or reservoir conditions,

$$\eta_{II,geo} = \frac{\dot{W}_{net,plant}}{\dot{E}x_{wh} or \dot{E}x_{res}} \tag{2.22}$$

- The **exergetic improvement potential (IP)** was proposed by Van Gool [72] as an evaluation parameter to measure the maximum improvement in the exergy efficiency for minimum exergy loss or irreversibility. It was computed as [17]

$$I\dot{P} = (1-\varepsilon)\left(\dot{E}x_{in} - \dot{E}x_{out}\right) \tag{2.23}$$

- The **specific exergy index (SExI)** was proposed by Lee [65] as an evaluation parameter to classify geothermal resources by exergy. It is expressed by

$$SExI = \frac{h_{brine} - 273.16 s_{brine}}{1192} \tag{2.24}$$

Where,

$$h_{brine} = \frac{\sum_{i}^{n} \dot{m}_{in} h_{in}}{\sum_{i}^{n} \dot{m}_{in}} \tag{2.25}$$

$$s_{brine} = \frac{\sum_{i}^{n} \dot{m}_{in} s_{in}}{\sum_{i}^{n} \dot{m}_{in}} \tag{2.26}$$

Therefore, the geothermal resources can be classified as [56]:

- Low-quality geothermal resources for $SExI < 0.05$;
- Medium-quality geothermal resources for $0.05 \leq SExI < 0.5$;
- High-quality geothermal resources for $SExI \geq 0.5$.

c. Thermoeconomic analysis: This is an integrated approach of one of the above mentioned analysis to the economic analysis, in order to achieve both a thermodynamic and economic optimum. The Second-law based thermoeconomic analysis, also known as exergoergonomics, can be defined as the minimization of the overall cost of entropy generation (or exergy destruction) with the annualized capital cost applied to system components, individually or as a whole [68].

2.5.6. Energy and exergy analysis

Mass, energy, and exergy balances for any control volume at steady state with negligible potential and kinetic energy changes can be expressed, respectively, by [19,21,73]

$$\sum \dot{m}_{in} = \sum \dot{m}_{out} \tag{2.27}$$

$$\dot{Q} - \dot{W} = \sum \dot{m}_{out} h_{out} - \sum \dot{m}_{in} h_{in} \tag{2.28}$$

$$\dot{E}x_{heat} - \dot{W} + \sum \dot{m}_{in} \psi_{in} - \sum \dot{m}_{out} \psi_{out} = \dot{I} \tag{2.29}$$

The cycle power output is determined by, [73]

$$\dot{W}_{net} = \dot{W}_t + \dot{W}_p \tag{2.30}$$

And the total exergy lost in the cycle and plant were defined respectively as [21,73]

$$\dot{I}_{cycle} = \sum_{all\ components} \dot{I}_i = \dot{I}_p + \dot{I}_{HEs} + \dot{I}_t + \dot{I}_c \tag{2.31}$$

$$\dot{I}_{plant} = \dot{I}_{cycle} + \dot{I}_{rej} + \dot{I}_{CS} = \dot{E}x_{in} - \dot{W}_{net} \tag{2.32}$$

Where the total exergy inputs to the ORC was determined by [21,23,74,75]

$$\dot{E}x_{in} = \dot{m}_{geo}\left[\left(h_{geo} - h_o\right) - T_o\left(s_{geo} - s_o\right)\right] \tag{2.33}$$

2.5.7. Performance analysis

The First- and Second-law efficiencies, based on the geothermal fluid state at the inlet of the primary heat exchanger and with respect to the reference temperature T_o, were defined respectively as [21,23,74,75]

$$\eta_I = \frac{net\ work\ output}{total\ energy\ inputs} = \frac{\dot{W}_{net}}{\dot{m}_{geo}\left(h_{geo} - h_o\right)} \tag{2.34}$$

$$\eta_{II} = \frac{net\ work\ output}{total\ exergy\ inputs} = \frac{\dot{W}_{net}}{\dot{m}_{geo}\left[\left(h_{geo} - h_o\right) - T_o\left(s_{geo} - s_o\right)\right]} \tag{2.35}$$

Based on the heat transfer or energy input to the cycle, the First- and Second-law efficiency were given by [21,23,74]

$$\eta_{I,2} = = \frac{\dot{W}_{net}}{\dot{m}_{geo}\left(h_{geo} - h_{rej}\right)} = \frac{\dot{W}_{net}}{\dot{m}_{wf}\left(h_{wf,out} - h_{wf,in}\right)} \tag{2.36}$$

$$\eta_{II,2} = \frac{\dot{W}_{net}}{\dot{m}_{geo}\left[\left(h_{geo} - h_{rej}\right) - T_o\left(s_{geo} - s_{rej}\right)\right]} \tag{2.37}$$

The performance of a binary-cycle geothermal power plant can also be evaluated using the cycle effectiveness, which represents the effectiveness of heat transfer to the cycle from the geothermal fluid, as [21,23,74,75]

$$\varepsilon = \frac{\dot{W}_{net}}{\dot{m}_{wf}\left[\left(h_{wf,out} - h_{wf,in}\right) - T_o\left(s_{wf,out} - s_{wf,in}\right)\right]} \tag{2.38}$$

As discussed by Subbiah and Natarajan [75], the First-law efficiency is a quantitative measure of the effectiveness of the conversion of the available geothermal energy into useful work. The cycle effectiveness measures both quantitatively and qualitatively the amount of available energy to be transferred, and the Second-law efficiency accounts for the overall exergy inputs to the cycle between the geothermal fluid temperature at the outlet of the resource well and the reference temperature T_o.

The performance analysis of individual component of the cycle can be evaluated using the following dimensionless parameters [17,19]

- Fuel depletion ratio:

$$\delta_i = \frac{\dot{I}_i}{\dot{E}x_{in}} \tag{2.39}$$

- Relative irreversibility:

$$\chi_i = \frac{\dot{I}_i}{\dot{I}_{plant}} \tag{2.40}$$

- Productivity lack:

$$\xi_i = \frac{\dot{I}_i}{\dot{W}_{net}} \tag{2.41}$$

- Exergetic factor:

$$f_i = \frac{\dot{E}x_i}{\dot{E}x_{in}} \tag{2.42}$$

CHAPTER 3

METHODOLOGY

3.1. Overview

Small binary cycle geothermal power plants operating with moderate low-grade and liquid-dominated geothermal resources in the range of 110^{o}C to 160^{o}C, and cooling air at ambient conditions of 25^{o}C and 101.3 kPa, reference temperature and atmospheric pressure, respectively, were considered. A similar study, conducted by Franco and Villani [76], has demonstrated, under the given operating conditions, a strong dependency of the power cycle performance on the geothermal fluid temperature at the inlet and outlet of resource well, the energy conversion system being used, as well as the selection of the organic working fluid [24] employed in the conversion of low-grade geothermal heat. Furthermore, DiPippo [23] concluded as follows: "The main design feature leading to a high-exergy efficiency lies in the design of the heat exchangers to minimize the loss of exergy during heat transfer processes. Another important feature that can result in high exergy efficiency is the availability of low-temperature cooling water that allows a once-through system for waste heat rejection.''

The thesis consisted of a thermodynamic optimization process and entropy generation minimization (EGM) analysis of four types of ORCs to minimize the exergy loss of the power plant, maximize the cycle power output and reduce the cost of production of the geothermal electricity. In addition, a diversity of organic working fluids was used as binary working fluids in the conversion of the low-grade geothermal heat, to demonstrate the extent at which they do affect the design and performance of the ORCs under saturation temperature and subcritical pressure operating conditions of the turbine.

The analysis was organized in three steps, namely:

- To determine the optimal operating conditions, which maximize the cycle power output of the ORCs and minimize the overall exergy loss of the power plant, and the irreversibilities due to heat transfer and fluid friction caused by the system components;
- To size a downhole coaxial heat exchanger for an application to an enhanced geothermal system (EGS) by optimizing the geofluid circulation flow rate, which ensured minimum pumping power and maximum extracted heat energy from the Earth's deep underground;

- And to design, model and size the system components for the optimal operating conditions.

3.2. Assumptions

The following assumptions were made:

1. The underground temperature increases almost linearly with depth from the Earth's surface. Hence, a constant wall heat flux was assumed on the outer diameter of the downhole coaxial heat exchanger;
2. The outer pipe of the downhole coaxial heat exchanger has a thin wall and is highly conductive. Consequently, its thermal resistance was neglected;
3. An effective layer of insulation onto the wall of the inner pipe ensures negligible heat transfer from the upflowing hot stream through the inner pipe to the downflowing cold stream in the annular space of the downhole coaxial heat exchanger;
4. The geothermal fluid collected from the downhole heat exchanger, was at a saturation liquid state.
5. The heat exchangers were well insulated so that heat loss to the surroundings was negligible;
6. The effectiveness of the heat exchangers remained constant;
7. The condensation process occurs with negligible temperature and pressure losses;
8. Heat loss through pipes were neglected;
9. All fluids flowing through tubes and piping systems were fully developed unless stated otherwise, and their thermodynamics properties were kept constant;
10. Changes in kinetic and potential energies of the fluid streams were negligible unless stated otherwise;
11. The heat transfer coefficients and the fouling factors were constant and uniform unless stated otherwise;
12. The effects of natural convection and radiation heat transfer were ignored.
13. All control volumes operated under steady-state condition;

3.3. Constraints, design variables and operating parameters

Although various design variables need to be considered while optimizing for the thermodynamic performance of a binary power cycle, this study has investigated a few in the

thermodynamic optimization process and entropy generation minimization (EGM) analysis, namely the geofluid circulation rate, the turbine inlet temperature and the condenser operating conditions with respect to the dead or reference state. For the simplicity of the analysis, a nearly linear increase in the geothermal gradient with depth was assumed. The transient effect or time-dependent cooling of the Earth underground, and the optimum amount and size of perforations at the inner pipe entrance region to regulate the flow of the geothermal fluid were disregarded. The pressure drops in the evaporator, condenser and piping systems were ignored when estimating the thermodynamic performance of the ORCs, and taken into account when sizing the system components.

Table 3.1 gives the basic design variables and operating parameters of the study,

Parameters	**values**
P_o [kPa]	101.3
T_o [^{o}C]	25
T_C [^{o}C]	40
T_{rej} [^{o}C]	50-110
T_{geo} [^{o}C]	110-160
(dT/dx)[^oC/ 100m]	2.4-4.8
η_p [%]	90
η_t [%]	80
η_{fan} [%]	90
ε_{IHE} [%]	80
V_t / V_w	0.11
D_o / D_i	1.2
δ_f [mm]	0.3

Table 3. 1: Operating parameters used in the simulation

3.4. Binary working fluids

The selection of the optimal organic fluid is subject to [77-80]:

- High thermodynamic performance (energetic and exergetic efficiencies) and good utilization of the available heat source;

- Thermodynamic properties: High boiling point, latent heat of vaporization, thermal conductivity, and density in gaseous phase; moderate critical temperature and pressure; and low viscosity, liquid specific heat, and density in liquid phase;
- Chemical stability at high temperature and compatibility with materials i.e. non-corrosive;
- Environmental impacts: low Ozone Depletion Potential (ODP), Global Warming Potential (GWP) and Atmospheric Lifetime (ATL).
- Safety concerns: non-flammable and non-toxic;
- Economical operation: Availability and cost.

In the literature, more than 50 pure and mixtures of organic compounds for ORC have been considered, and classified as “wet”, “dry” or “isentropic” organic fluids according to the slope of its saturated-vapour line [75]. This study considers refrigerants R123, R152a, isobutane and n-pentane as binary working fluids for the conversion of the low-to-moderate grade geothermal heat. Refrigerant R123 is an isentropic organic fluid with a near-vertical saturated vapour-phase line, thus a nearly infinitely large slope of the saturated-vapour line. Refrigerant R152a belongs to the wet type, thus having a negative slope of the saturated-vapour line. Isobutane and n-pentane represent dry organic compounds characterized by a positive slope of the saturated-vapour line. For subcritical pressure processes, dry organic compounds are usually preferred since the expansion process in the turbine ends in the superheated region. Isentropic fluids however, having a near-vertical saturated-vapour line, lead to saturated vapour at the later stages of the turbine, whereas wet fluids form a mixture of liquid and vapour, and thus require superheating to avoid the risk of the turbine blades erosion [78].

The thermodynamic phases of the selected working fluids are illustrated on a temperature versus entropy diagram in Fig. 3.1. In Table 3.2, the main thermo-physical properties of the selected binary working fluids are listed, as obtained from EES (Engineering Equation Solver) software [81].

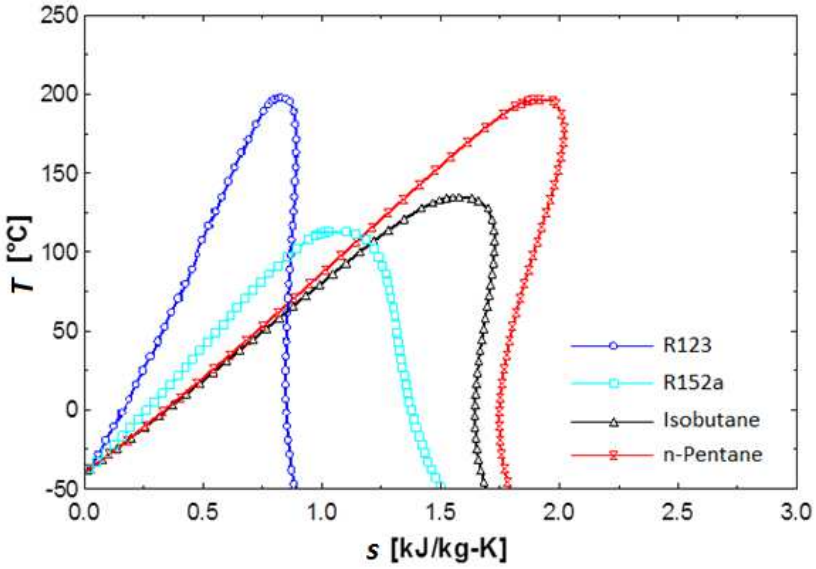

Figure 3. 1: *T-s* diagram of selected binary fluids for ORC

Working fluid	**R123**	**R152a**	**R600a**	**R601**
Name	2,2-Dichloro-1,1,1-trifluoroethane	1,1-Difluoroethane	Isobutane	n-Pentane
Chemical formula	$CHCl_2C-F_3$	CH_3CH-F_2	C_4H_{10}	C_5H_{12}
Type	*HCFC*	*HFC*	*HC*	*HC*
Organic type	Isentropic	Wet	Dry	Dry
Thermo-physical properties				
Molecular weight	152.93	66.05	58.12	72.15
T_{bp} @ 1atm [^oC]	27.82	-24.02	-11.67	36.0
T_{cr} [^oC]	183.68	113.26	134.67	196.55
P_{cr} [MPa]	3.662	4.517	3.62	3.37
Cp_v [J/kg.K]	738.51	1456.02	181.42	1824.12
L [kJ/kg]	161.82	249.67	303.44	349.00
Environmental characteristics				
ALT [$year$]	1.3	1.4	0.02	$\ll 1$
ODP [−]	0.02	0.000	0.000	0.000
GWP [100 $years$]	77	120	~20	11

Table 3. 2: Thermodynamic properties of selected binary fluids for ORC [30,78]

The thermodynamic properties of the selected working fluids listed in Table 3.2, have shown high latent heat of vaporization for dry fluids (i.e. n-pentane and isobutene), moderate value for

the wet organic fluid R152a, and low latent heat of vaporization for the isentropic fluid R123. As a consequence of the variation of the critical temperature of the selected organic fluids, positive normal boiling point temperatures were observed for R123 and n-pentane, whereas R152a and isobutene have negative normal boiling point temperatures. Based on the environmental impacts of the selected working fluids, dry organic fluids have shown low ODP, GWP and ATL. In conclusion, the preference of dry organic compounds as optimal organic fluids for the conversion of low-grade energy resources is verified as a result of their excellent thermodynamic properties and nearly clean environmental impact characteristics.

3.5. Organic Rankine Cycles

Considering the characteristics of the secondary or binary fluid, low-grade geothermal heat can suitably be recovered by an organic Rankine cycle (ORC) or Kalina cycle. The latter employs water-ammonia mixture as working fluid, whereas the former can either use hydrocarbons (HC), hydrofluorocarbons (HFC), hydrochlorofluorocarbons (HCFC), chlorofluorocarbons (CFC), perfluorocarbons (PFC), siloxanes, alcohols, aldehydes, ethers, hydrofluoroethers (HFE), amines, fluid mixtures (zeotropic and azeotropic) or inorganic fluids [82]. In addition to the ORC and the Kalina cycle, various other thermodynamic cycles are employed for the conversion of the low-grade energy sources, such as the supercritical Rankine cycle, Goswami cycle and the trilateral flash cycle [80]. For the purpose of the study, the ORC was preferred considering its widely use in the geothermal power generation, the simplicity of its power cycle, and the ease of maintenance required [75].

Four ORCs were analysed analytically and numerically, and their performance optimized to maximize the cycle power output. The selected ORCs are illustrated in Fig. 3.2. In Fig. 3.2a, a simple ORC type is shown. The primary heat transfer medium is pumped at high pressure and continuously circulated through the Earth in a closed pipe system [83]. The fluid is heated by the linearly increasing underground temperature with depth, as it flows down the well. A secondary or binary fluid with a lower boiling point and higher vapour pressure is completely vaporized and usually superheated by the primary fluid through a closed pipe system heat exchanger, to expand in the turbine and then condense either in an air-cooled or water-cooled condenser prior returning to the vaporizer and thus completing the Rankine cycle [21]. If the expansion process in the turbine terminates in the superheated region, a heat recuperator (or internal heat

exchanger, IHE) can be advantageous to preheat the binary working fluid prior evaporating in the heat exchanger, hence reducing the evaporator load and improving the thermal efficiency of the cycle (Fig. 3.2b) [19,73,84].

Further improvement of the heat exchange performance and the Rankine cycle overall efficiency can be achieved with the addition of a two-phase regenerative cycle [19,27], utilizing an open feed-heater to preheat the binary working fluid prior evaporating in the heat exchanger, with the extracted fluid from the turbine expanded vapour (Fig. 3.2c). A combination of regenerator and recuperator can also be employed to improve the performance of heat exchanger process (Fig. 3.2d) [19].

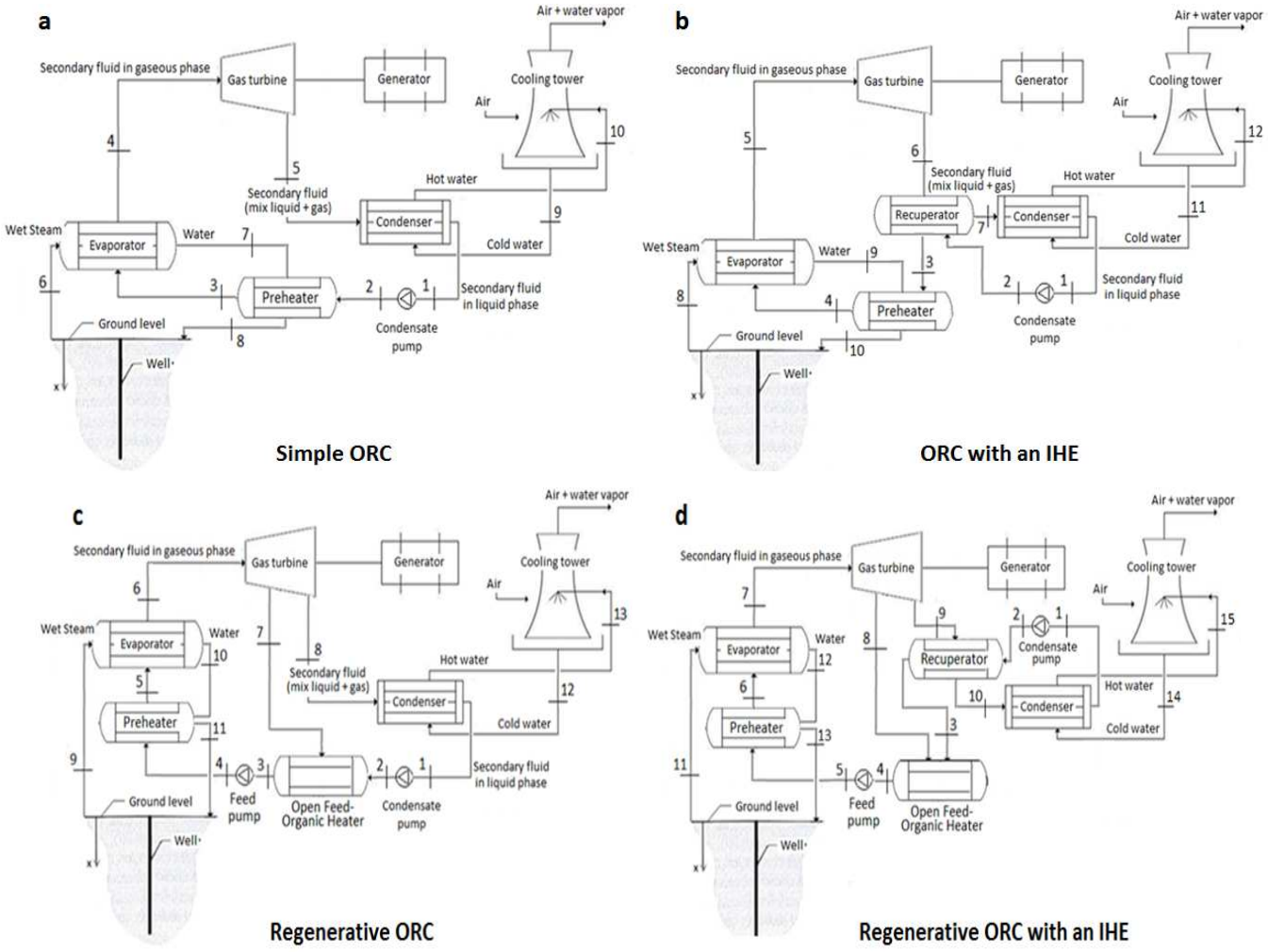

Figure 3. 2: Schematic diagrams of the binary-cycle geothermal power plants

The cycles' temperature versus entropy diagrams are illustrated in Fig. 3.3. For the simple ORC (Fig. 3.3a), processes 1-2 and 4-5 refers to reversible adiabatic pumping and expansion processes, respectively; whereas process 2-4 and 5-1 represent constant-pressure heat addition and rejection, respectively. The addition of an IHE to the simple ORC is represented by states 3 and 7 on the cycle T-s diagram shown in Fig. 3.3b.

In contrast to the basic ORC's, the regenerative cycles consist of three constant-pressure heat transfer processes (Fig. 3.3c). Ideally, the mixture of the turbine bleeding and the condensate at the exit of the open feed-organic heater is assumed at saturated liquid condition and at the evaporator pressure [85]. The addition of an IHE to the regenerative ORC is illustrated by states 3 and 10 on the cycle T-s diagram shown in Fig. 3.3d.

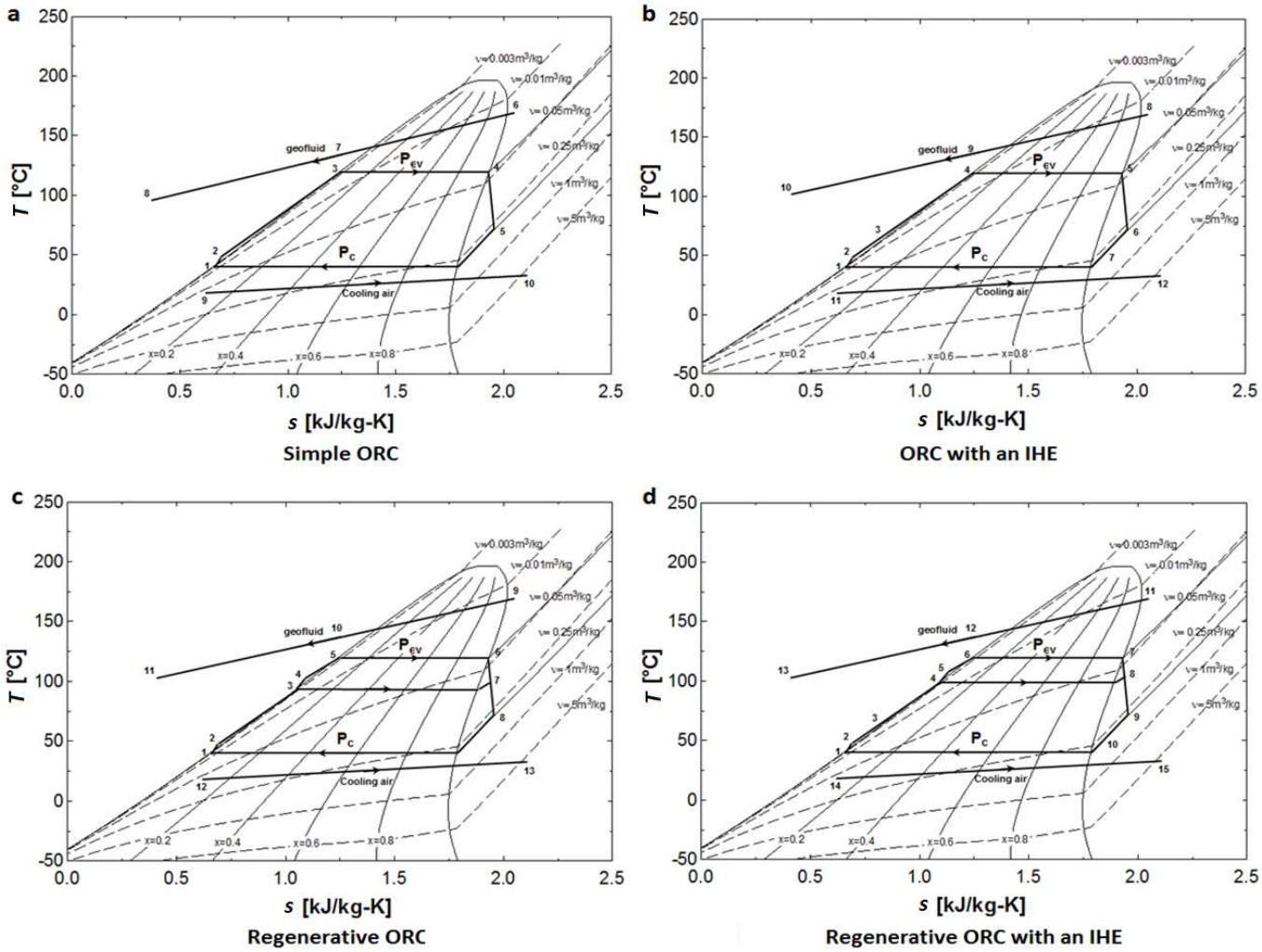

Figure 3. 3: T-s diagrams of the binary-cycle geothermal power plants

Many other power cycle designs have been proposed and studied in the literature for the conversion of low-to-moderate grade heat resources, and aiming at improving the performance of the binary-cycle power plant. For instance, a heat recovery exchanger with a cascade of evaporators employed in a Kalina cycle [23], a heat recovery cycle with a high and low-pressure turbine [74] or multiple pressure levels [28], a trilateral flash cycle [82], the Goswami cycle [82], a supercritical Rankine cycle [86], etc.

3.6. System component models

3.6.1. Downhole coaxial heat exchanger

In Fig. 3.4, a downhole coaxial heat exchanger for an enhanced geothermal system (EGS) is illustrated. It consists of a single gravel-filled well, closed-loop system where the heat transfer fluid is continuously circulated through the Earth in a closed pipe system without ever directly contacting the soil or water in which the loop is buried or immersed. The cold water is pumped downward through the annular space, and heated across the annular wall by the increasingly warmer rock material, as it flows. The heated stream returns, eventually to the surface through the inner pipe, which is effectively insulated to minimize any potential loss of heat to the surrounding.

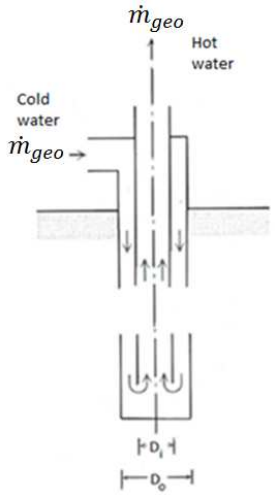

Figure 3. 4: Downhole coaxial heat exchanger

3.6.1.1. Pressure loss analysis

The optimization process began with an investigation of a potential local pressure loss [87], at the lower extremity of the well, caused by the sudden change in flow direction of the heated stream from the annular space of the downhole coaxial heat exchanger into the inner pipe to

return to the surface. This effect led to recirculation of the geofluid immediately downstream to the inner pipe entrance.

The local pressure drop was given by [57]

$$\Delta P_{local} = \frac{1}{2} K \rho U_i^2 \tag{3.1}$$

where the local loss coefficient was approximated as a sudden contraction,

$$K = 0.45\left[1 - \left(\frac{D_i}{D_o}\right)^2\right] \tag{3.2}$$

Defining the distributed losses as due to fully developed flow in the inner pipe, as

$$\Delta P_{distributed} = f_i \frac{4L_i}{D_i}\left(\frac{1}{2}\rho U_i^2\right) \tag{3.3}$$

The ratio of pressure drops was expressed by

$$\frac{\Delta P_{local}}{\Delta P_{distributed}} = \frac{0.45\left[1 - \left(\frac{D_i}{D_o}\right)^2\right]}{f_i \frac{4L_i}{D_i}} \tag{3.4}$$

The svelteness of the flow geometry was defined by Bejan [87] as follow

$$Sv = \frac{external\ flow\ length\ scale}{internal\ flow\ length\ scale} \cong \left(\frac{4}{\pi}\right)^{\frac{1}{3}}\left(\frac{L_i}{D_i}\right)^{\frac{2}{3}} \tag{3.5}$$

Thus, in term of svelteness, Eq. (3.4) was rewritten as

$$\frac{\Delta P_{local}}{\Delta P_{distributed}} = \frac{0.45\left[1 - \left(\frac{D_i}{D_o}\right)^2\right]}{4 f_i \left(\frac{4}{\pi}\right)^{\frac{1}{2}} Sv^{\frac{3}{2}}} \tag{3.6}$$

If the flow in the inner pipe is in the laminar fully-developed flow regime, then the fanning friction factor was a function of the Reynolds number and given by [88]

$$f_i = \frac{16}{\mathrm{Re}_i} \tag{3.7}$$

Substituting Eq. (3.7) into Eq. (3.6) and assuming that the ratio of the inner to the outer diameter of the coaxial pipes is much less than 1, the following equation was obtained

$$\left(\frac{\Delta P_{local}}{\Delta P_{distributed}}\right)_{lam} \cong \frac{\left(\frac{\mathrm{Re}_i}{126}\right)}{Sv^{\frac{3}{2}}} \tag{3.8}$$

From Eq. (3.8), the ratio of pressure drops was seen to be directly proportional to the inner pipe flow Reynolds number and inversely proportional to the svelteness. Hence, for $Sv >> 0.04\,\mathrm{Re}_i^{\frac{2}{3}}$, the local pressure loss at the lower extremity of the well could be neglected in the laminar fully-developed flow regime.

Similarly, if the flow is in the fully turbulent and fully rough regime, the friction factor was thus a constant and independent of the Reynolds number. Using the explicit approximation for smooth ducts [57]

$$f \cong 0.046\,\mathrm{Re}^{-\frac{1}{5}} \qquad (10^4 < \mathrm{Re} < 10^6) \tag{3.9}$$

Assuming that the fanning friction factor is of order 0.01 [26], the ratio of pressure drops in the fully turbulent and fully rough regime is expressed as,

$$\left(\frac{\Delta P_{local}}{\Delta P_{distributed}}\right)_{turb} \cong \frac{12.7}{Sv^{\frac{3}{2}}} \tag{3.10}$$

Consequently, for $Sv >> 5.44$, the local pressure loss at the lower extremity of the well could be neglected in the fully turbulent and fully rough regime.

The variation of the ratio of the pressure drops to the svelteness, for both laminar and turbulent fully-developed flow regimes was plotted in Fig. 3.5. As the svelteness increases, the ratio of the pressure drops decreases drastically. At the upper limit of the turbulent fully-developed flow regime and for Svelteness much greater than eight, the ratio of the pressure drops was minimum. Hence, from Eq. (3.5), it can be proved that the local pressure loss at the lower extremity of the well can be neglected, irrespective of the flow regime, for a coaxial pipe length greater than twenty times its diameter.

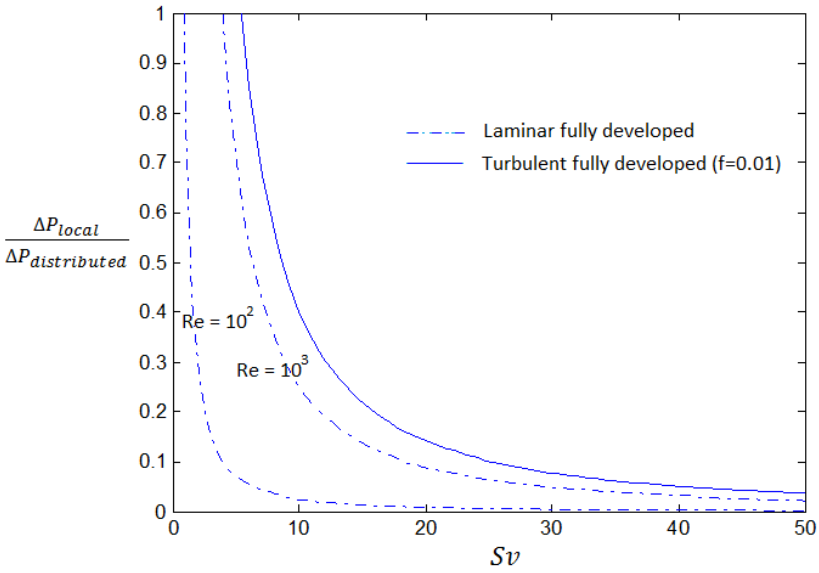

Figure 3. 5: variation of pressure drops ratio, local over distributed, to the svelteness

3.6.1.2. Optimal diameter ratio

For an inner diameter of the coaxial pipes much smaller than its outer diameter, it could be observed that the stream will be "strangled" as it flows upward through the inner pipe. On the contrary, that is the inner diameter being nearly as large as the pipe outer diameter, the flow will be hindered by the narrowness of the annular space [45,83]. In both cases, the total pressure drop to be overcome by the pump is extremely excessive. Hence, the need of determining an optimal diameter ratio of the coaxial pipes is essential to ensure minimum total pressure drop, thus minimum pumping power requirement.

The pressure drop per unit length in the inner pipe flow section of the downhole coaxial heat exchanger was given by [57]

$$\left(\frac{\Delta P}{L}\right)_i = \frac{2\rho}{D_o^5}\left(\frac{4}{\pi}\right)^2\left(\frac{\dot{m}}{\rho}\right)^2 \frac{f_i}{r^5} \tag{3.11}$$

where the diameter ratio r was defined as

$$r = \frac{D_i}{D_o} \tag{3.12}$$

Similarly, the pressure drop per unit length in the annular space region of the downhole coaxial heat exchanger can be expressed by

$$\left(\frac{\Delta P}{L}\right)_a = \frac{2\rho}{D_o^5}\left(\frac{4}{\pi}\right)^2\left(\frac{\dot{m}}{\rho}\right)^2 \frac{f_a}{(1-r)^3(1+r)^2} \tag{3.13}$$

Thus, the total pressure drop per unit length contributed by each portion of the coaxial pipe was evaluated by

$$\left(\frac{\Delta P}{L}\right)_{total} = \left(\frac{\Delta P}{L}\right)_a + \left(\frac{\Delta P}{L}\right)_i = \frac{1}{\rho}\left(\frac{\dot{m}}{\pi}\right)^2\left(\frac{2}{D_o}\right)^5 \chi_{turb} \tag{3.14}$$

where,

$$\chi_{turb} = \frac{f_a}{(1-r)^3(1+r)^2} + \frac{f_i}{r^5} \tag{3.15}$$

Eq. (3.15) can be minimized with respect to the diameter ratio r, to obtain the minimum total pressure drop and pumping power requirement.

In the large Reynolds number limit of the fully turbulent and fully rough regime, where the friction factors of both the inner pipe and annular space are constant and independent of the Reynolds number, an optimal diameter ratio of the coaxial pipes was obtained numerically as

$$r_{opt,turb} = 0.653 \tag{3.16}$$

In the laminar fully-developed flow regime, however, the friction factors being strongly dependent on the Reynolds number, was defined by [88]

$$f_i = \frac{16}{\mathrm{Re}_i} = \frac{16\mu\left(\frac{\pi}{4}\right)rD_o}{\dot{m}} \tag{3.17}$$

$$f_a = \frac{16\mu\left(\frac{\pi}{4}\right)(1-r)D_o}{\dot{m}} \frac{(1-r)^2\left(1-r^2\right)}{1-r^4-\frac{\left(1-r^2\right)^2}{\ln\left(\frac{1}{r}\right)}} \tag{3.18}$$

Substituting Eqs. (3.17) and (3.18) into Eq. (3.12) , the following equation of the total pressure drop per unit length contributed by each portion of the coaxial pipes in the laminar fully-developed flow regime was obtained

$$\left(\frac{\Delta P}{L}\right)_{total,lam} = \frac{\mu}{\rho}\left(\frac{\dot{m}}{\pi}\right)\left(\frac{2^7}{D_o^4}\right)\chi_{lam} \tag{3.19}$$

where,

$$\chi_{lam} = \frac{\frac{1-r}{1+r}}{1-r^4-\frac{\left(1-r^2\right)^2}{\ln\left(\frac{1}{r}\right)}} + \frac{1}{r^4} \tag{3.20}$$

Minimizing Eq. (3.20) with respect to the diameter ratio, one could obtain numerically

$$r_{opt,lam} = 0.683 \tag{3.21}$$

The same result can eventually be obtained numerically be assuming that the annular space is identical to a parallel-plate geometry positioned $\frac{\left(D_o - D_i\right)}{2}$ apart. Hence, the annular fanning friction factor was given by [83]

$$f_a = \frac{16}{\mathrm{Re}_a} = \frac{16\mu\left(\frac{\pi}{4}\right)D_o\left(1-r\right)}{\dot{m}} \tag{3.22}$$

And the total pressure drop as

$$\left(\frac{\Delta P}{L}\right)_{total,lam} = \frac{\mu}{\rho}\left(\frac{\dot{m}}{\pi}\right)\left(\frac{2^5}{D_o^4}\right)\chi_{lam} \tag{3.23}$$

where,

$$\chi_{lam} = \frac{24}{\left(1-r\right)^2\left(1+r\right)^2} + \frac{16}{r^4} \tag{3.24}$$

Eq. (3.24) can be minimized with respect to the diameter ratio to give the same result as in Eq. (3.21).

In brief, from Eqs. (3.16) and (3.21), the optimal diameter ratio of the coaxial pipes to yield minimum total pressure drop and minimum pumping power requirement, was observed to be nearly the same in both limits of the fully turbulent and laminar fully-developed flow regimes.

3.6.1.3. Entropy Generation Minimization (EGM) analysis

The entropy generation, as defined by Bejan [87], represents the measure of imperfection. Hence, minimizing the entropy generation term will yield maximum extracted heat energy for a given underground temperature gradient, according to Gouy-Stodola relation [56].

The mass balance (or continuity) equation was given by [59]

$$\sum \dot{m}_{in} = \sum \dot{m}_{out} = \dot{m} \tag{3.25}$$

Thus, the rate of entropy generation was related to the rate of entropy transfer as

$$\dot{S}_{gen} = \dot{m}(s_{out} - s_{in}) - \frac{\dot{Q}}{T_w} \tag{3.26}$$

Using thermodynamic relations [59,89] outlined below, and the incompressibility property of the geofluid (i.e. water)

$$dh = CpdT \tag{3.27}$$

$$Tds = dh - \frac{dP}{\rho} \tag{3.28}$$

$$d\dot{Q} = \dot{m}dh \tag{3.29}$$

The entropy generation rate per unit length of the downhole coaxial heat exchanger was given by

$$\dot{S}'_{gen} = \dot{m}Cp\frac{\Delta T}{T_m^2(1+\tau)}\left(\frac{dT}{dx}\right) + \frac{\dot{m}}{\rho T_m}\left(-\frac{dP}{dx}\right) \tag{3.30}$$

Eq. (3.30) can be rewritten as [15]

$$\dot{S}'_{gen} = \dot{S}'_{gen,\Delta T} + \dot{S}'_{gen,\Delta P} \tag{3.31}$$

The first term represents the entropy generation rate per unit length due to heat transfer irreversibility across a finite temperature difference along the outer wall of the annular space, while the inner pipe is effectively insulated to minimize any potential loss of heat to the surrounding. The second term accounts for the total fluid friction irreversibility as a result of the downward flow of the geofluid through the annular space then upward through the inner pipe, to return to the surface.

In Eq. (3.30), ΔT represents the temperature difference between the outer wall of the annular space and the mean temperature of the stream, i.e. $\Delta T = T_w - T_m$. Under the assumptions of uniform wall heat flux, constant fluid properties and fully developed flow regimes, both the outer wall and mean fluid temperatures increase linearly in the flow direction. Consequently, the local temperature difference between the wall and the stream does not change along the flow direction.

Considering an energy balance of a control volume of length dx of the coaxial pipes, the total rate of convective heat transfer was given by [83]

$$\dot{Q} = \dot{m}.Cp.dT = h.\pi D_o dx.\Delta T_{lm} \tag{3.32}$$

Hence the temperature difference ΔT, between the outer wall of the annular space and the mean temperature of the stream, increased linearly with the mean temperature gradient, and inversely with the convective heat transfer coefficient h, according to

$$\Delta T = \Delta T_{lm} = \frac{\dot{m}Cp}{h\pi D_o}\left(\frac{dT}{dx}\right) \tag{3.33}$$

Assuming that $\tau = \frac{\Delta T}{T_m} << 1$, the substitution of Eq. (3.33) into Eq. (3.30) yielded

$$\dot{S}'_{gen} = \frac{\dot{m}^2 Cp^2}{h\pi D_o T_m^2}\left(\frac{dT}{dx}\right)^2 + \frac{\dot{m}}{\rho T_m}\left(-\frac{dP}{dx}\right) \tag{3.34}$$

Since heat transfer occurs only across the outer wall of the annular space, the following equations from heat transfer principles applied [83]

$$h_a = St.\rho.Cp.u_a \tag{3.35}$$

$$Nu_a = \frac{hD_h}{k} = St.\,\mathrm{Re}_a\,.\,\mathrm{Pr} \tag{3.36}$$

$$u_a = \frac{4\dot{m}}{\rho\pi D_h^2} \tag{3.37}$$

Where

$$D_h = D_o - D_i = D_o(1-r) \tag{3.38}$$

Substituting Eqs. (3.35)-(3.38) into Eq. (3.30) and integrating along the length of the heat exchanger for a constant increment of the underground temperature with depth, the entropy generation rate per unit length can be expressed by

$$\dot{S}'_{gen} = \frac{\dot{m}Cp\,\mathrm{Re}_a\,\mathrm{Pr}\,D_o(1-r)^2}{4Nu_a T_m^2}\left(\frac{dT}{dx}\right)^2 + \frac{\dot{m}}{\rho T_m}\left(-\frac{\Delta P}{L}\right)_{total} \tag{3.39}$$

In the large Reynolds number limit of the fully turbulent and fully rough regime, the Nusselt number of the flowing geothermal fluid in the annular space of the coaxial pipes was approximated by Petukhov and Roizen correlation [90] for heat transfer at the outer wall of a concentric annular duct with its inner wall well-insulated, as

$$\frac{Nu_a}{Nu_i} = 1 - 0.14\left(\frac{D_i}{D_o}\right)^{0.6} \tag{3.40}$$

Where the Nusselt number of the upflowing stream in the inner pipe was given by [83]

$$Nu_i \cong 0.023\,\mathrm{Re}_i^{0.8}\,\mathrm{Pr}^{0.4} \qquad (0.7 < \mathrm{Pr} < 160,\ \mathrm{Re}_i > 10^4) \tag{3.41}$$

Substituting Eqs. (3.9), (3.14)-(3.15) and (3.40)-(3.41) into Eq. (3.39), the following equation was obtained

$$\dot{S}'_{gen,turb} = \frac{10.87\dot{m}Cp\,\mathrm{Re}_a\,\mathrm{Pr}^{0.6}\,D_o(1-r)^2}{\left(1-0.14r^{0.6}\right)T_m^2\,\mathrm{Re}_i^{0.8}}\left(\frac{dT}{dx}\right)^2 + \frac{1.472\dot{m}^3}{\pi^2\rho^2 T_m D_o^5}\left(\frac{\mathrm{Re}_a^{-\frac{1}{5}}}{(1-r)^3(1+r)} + \frac{\mathrm{Re}_i^{-\frac{1}{5}}}{r^5}\right) \tag{3.42}$$

The dimensionless Reynolds numbers for flow through straight pipes in terms of the pipe outer diameter were given by

$$\mathrm{Re}_a = \frac{4\dot{m}}{\pi\mu D_o(1-r)} \tag{3.43}$$

$$\mathrm{Re}_i = \frac{4\dot{m}}{\pi\mu r D_o} \tag{3.44}$$

Expressing Eq. (3.42) in terms of the Reynolds number of the flow in the annular space by substituting Eqs. (3.43)- (3.44) and eliminating D_o, the following equation was obtained

$$\dot{S}'_{gen,turb} = \frac{13.84\dot{m}^2 Cp\,\mathrm{Pr}^{0.6}(1-r)^{0.2}}{\mu\left(\frac{1}{r^{0.8}} - \frac{0.14}{r^{0.2}}\right)T_m^2\,\mathrm{Re}_a^{0.8}}\left(\frac{dT}{dx}\right)^2 + \frac{0.0446\,\mathrm{Re}_a^{4.8}\,\mu^5(1-r)^{4.8}}{\rho^2 T_m \dot{m}^2}\left(\frac{1}{(1-r)^{2.8}(1+r)^2} + \frac{1}{r^{4.8}}\right) \tag{3.45}$$

Eq. (3.45) was differentiated with respect to the geofluid mass flow rate and equalled to zero. The optimal mass flow rate of the geothermal fluid under turbulent flow conditions was determined for minimum entropy generation, thus maximum extracted heat energy for a given underground temperature gradient. The following relations were obtained

$$\dot{m}_{opt,turb} = 0.238\,\mathrm{Re}_a^{1.4}\,C_{turb}^{0.25} \tag{3.46}$$

where,

$$C_{turb} = \frac{\mu^6 T_m}{\rho^2 Cp\,\mathrm{Pr}^{0.6}\left(\frac{dT}{dx}\right)^2}(1-r)^{4.6}\left(\frac{1}{r^{0.8}} - \frac{0.14}{r^{0.2}}\right)\left(\frac{1}{(1-r)^{2.8}(1+r)^2} + \frac{1}{r^{4.8}}\right) \tag{3.47}$$

In the laminar fully-developed flow regime, the Nusselt number of the flowing geothermal fluid in the annular space of the coaxial pipes was approximated by Martin's correlation [90] for heat transfer at the outer wall of a concentric annular duct with inner wall well-insulated, as

$$Nu_a = 3.66 + 1.2\left(\frac{D_i}{D_o}\right)^{0.5} \qquad \left(0.1 < \mathrm{Pr} < 10^3, \mathrm{Re}_D < 2300, 0 < \frac{D_i}{D_o} < 1\right) \tag{3.48}$$

Substituting Eqs. (3.17)-(3.20) and (3.48) into Eq. (3.39), the following equation was obtained

$$\dot{S}'_{gen,lam} = \frac{\dot{m}Cp\,\mathrm{Re}_a\,\mathrm{Pr}\,D_o(1-r)^2}{4\left(3.66+1.2r^{0.5}\right)T_m^2}\left(\frac{dT}{dx}\right)^2 + \frac{128\dot{m}^2\mu}{\pi\rho^2 T_m {D_o}^4}\left(\frac{\frac{1-r}{1+r}}{1-r^4-\frac{\left(1-r^2\right)^2}{\ln\left(\frac{1}{r}\right)}}+\frac{1}{r^4}\right) \tag{3.49}$$

Expressing Eq. (3.49) in terms of the Reynolds number of the flow in the annular space and eliminating D_o, the following equation was obtained

$$\dot{S}'_{gen,lam} = \frac{0.318\dot{m}^2 Cp\,\mathrm{Pr}(1-r)}{\mu\left(3.66+1.2r^{0.5}\right)T_m^2}\left(\frac{dT}{dx}\right)^2 + \frac{15.50\,\mathrm{Re}_a^4\,\mu^5(1-r)^4}{\rho^2 T_m \dot{m}^2}\left(\frac{\frac{1-r}{1+r}}{1-r^4-\frac{\left(1+r^2\right)^2}{\ln\left(\frac{1}{r}\right)}}+\frac{1}{r^4}\right) \tag{3.50}$$

Similarly, Eq. (3.50) was differentiated with respect to the geofluid mass flow rate and equalled to zero. The optimal mass flow rate of the geothermal fluid was determined under laminar flow conditions, as

$$\dot{m}_{opt,lam} = 2.642\,\mathrm{Re}_a\,{C_{lam}}^{0.25} \tag{3.51}$$

where,

$$C_{lam} = \frac{\mu^6 T_m}{\rho^2 Cp\,\mathrm{Pr}\left(\frac{dT}{dx}\right)^2}(1-r)^3\left(3.66+1.2r^{0.5}\right)\left(\frac{\frac{1-r}{1+r}}{1-r^4-\frac{\left(1+r^2\right)^2}{\ln\left(\frac{1}{r}\right)}}+\frac{1}{r^4}\right) \tag{3.52}$$

Varying the Reynolds number of the flow in the annular space from the laminar to the turbulent limits, an optimal mass flow rate of the geothermal fluid was obtained from Eqs. (3.46) and (3.51). The outer diameter of the downhole coaxial heat exchanger was thereafter determined from Eq. (3.43) as

$$D_o = \frac{4\dot{m}_{opt}}{\pi\mu(1-r)\mathrm{Re}_a} \tag{3.53}$$

3.6.2. Preheater, Evaporator, Recuperator and Regenerator

3.6.2.1. Energy and exergy analysis

Assuming that the preheater, evaporator, recuperator and regenerator were all well-insulated so that heat transfer occurs only from one medium to the other, an energy balance around the component control volume (Fig. 3.6), can be expressed, under steady state and adiabatic operation with negligible potential and kinetic energy changes, by [26]

$$\dot{m}_H\left(h_{H,in}-h_{H,out}\right)=\dot{m}_C\left(h_{C,out}-h_{C,in}\right) \tag{3.54}$$

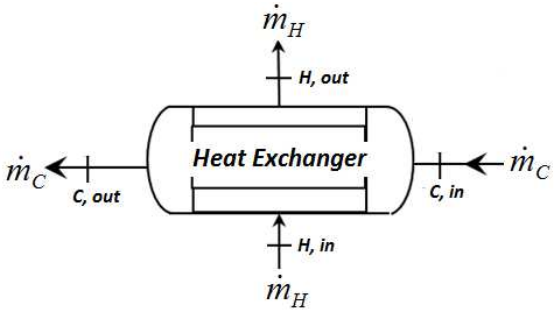

Figure 3. 6: Control volume around a heat exchanger

The energetic (or First-law) efficiency of a preheater, evaporator or recuperator, can be evaluated as [26]

$$\eta_{I,HE}=\frac{\left(T_{out}-T_{in}\right)_C}{T_{H,in}-T_{C,in}}=\frac{\left(T_{in}-T_{out}\right)_H}{T_{H,in}-T_{C,in}} \tag{3.55}$$

The exergetic (or Second-law) efficiency of a preheater, evaporator or recuperator, was defined as the ratio of increase in exergy of the cold stream to the decrease in exergy of the hot stream on a rate basis. It was given by [92]

$$\eta_{II,HE}=\frac{\left(\dot{E}x_{out}-\dot{E}x_{in}\right)_C}{\left(\dot{E}x_{in}-\dot{E}x_{out}\right)_H} \tag{3.56}$$

The regenerator exergetic efficiency was defined as the ratio of exergy outlet to exergy inlet to the system. It was determined by [93],

$$\eta_{II,OFOH}=\frac{\dot{E}x_{out}}{\dot{E}x_{in}}=\frac{\dot{E}x_{out}}{\dot{E}x_{out}+\dot{I}} \tag{3.57}$$

3.6.2.2. Irreversibility analysis

In Fig. 3.7a, the loss of exergy (irreversibility) generated during the heat transfer process occurring in the evaporator-preheater unit was represented by the marked area of the temperature

versus heat transfer diagram, assuming linearity of the geofluid cooling curve. This significant loss of exergy is a consequence of the large difference in enthalpy or temperature between the geothermal and the binary fluids [91]. The addition of an IHE to the simple ORC is demonstrated to reduce the irreversibility of the heat transfer process as the working fluid was preheated prior entering the preheater (Fig. 3.7b). A decrease in irreversibility can also be achieved while utilizing a regenerative Rankine cycle to improve the heat exchange performance (Fig. 3.7c). Further reduction in irreversibility is possible with a combination of a regenerator and recuperator (Fig. 3.7d).

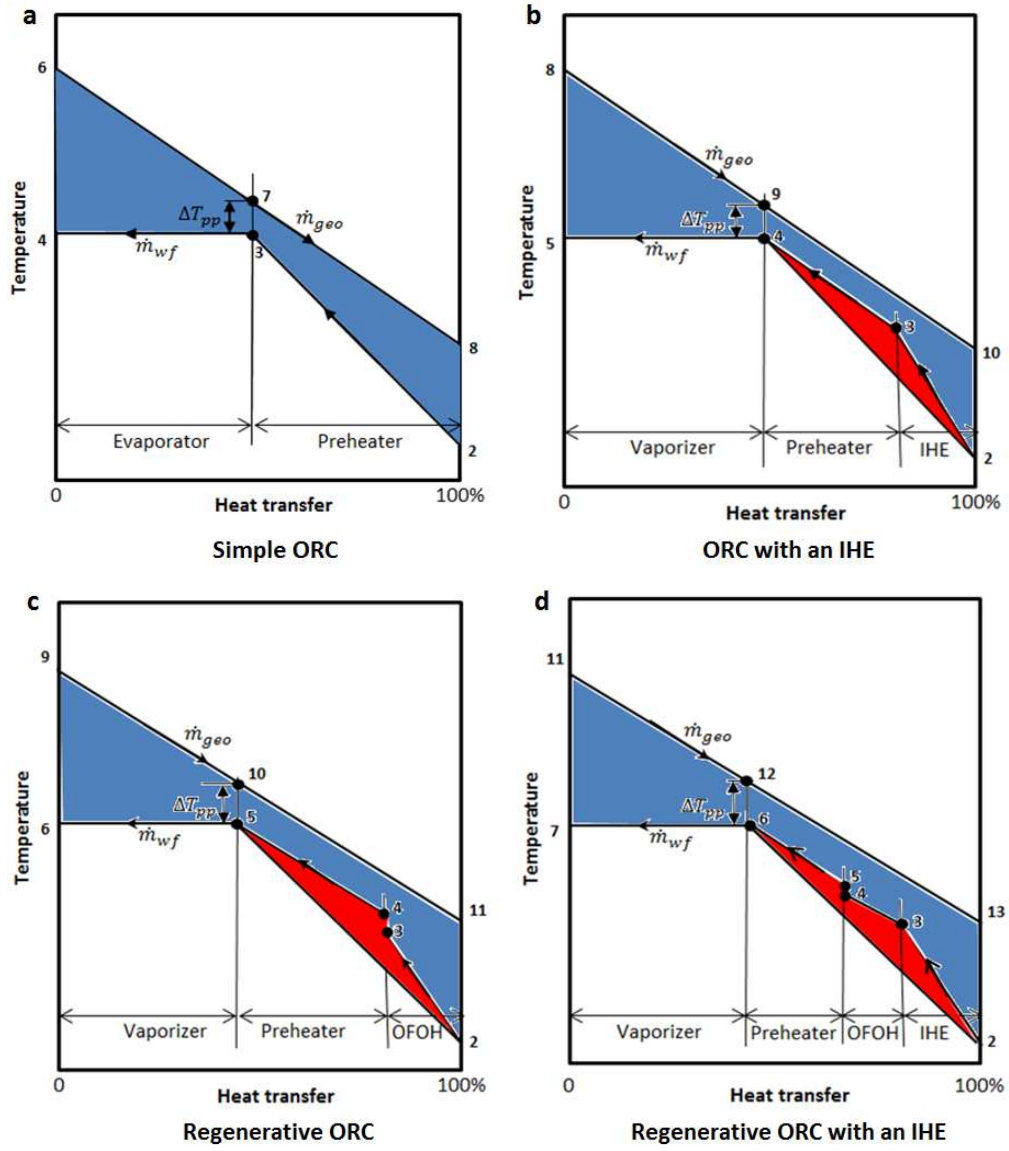

Figure 3. 7: *T-Q* diagrams of the heat exchange process in the Evaporator-Preheater unit

3.6.2.3. Constructional design

The preheater, evaporator and recuperator were assumed to be horizontal cylinder, liquid-liquid and shell-and-tube counterflow type (Fig. 3.8). This type of configuration is usually regarded as the most suitable type of design for the heat exchange process in the geothermal power plants [26,94,95]. A single tube-pass and shell-pass heat exchanger with square pitch tube layout was considered. The preheater and recuperator were single-phase heat exchangers type whereas the evaporator consisted of a two-phase flow. The working fluid was allowed to flow through the tube and the geothermal fluid on the shell side for the preheater-vaporizer unit, whereas, for the recuperator, the hot fluid flowed through the tubes and the cold fluid on the shell side.

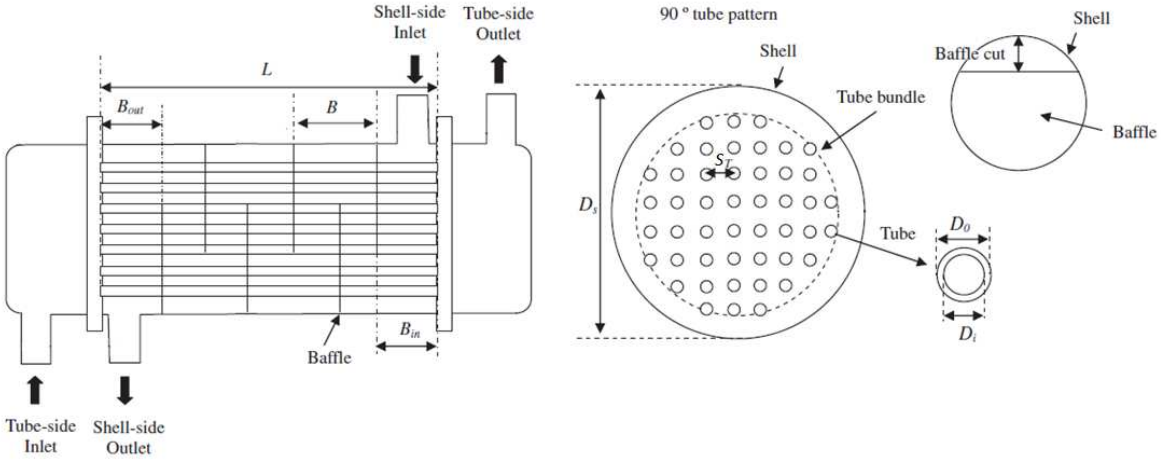

Figure 3. 8: Schematic of the shell and tube heat exchanger [96]

For the squared pitch tube layout, the constructional parameters were defined as followed [97,98]

$$D_e = \frac{4\left(S_T^2 - \frac{\pi D_o^2}{4}\right)}{\pi D_o} \tag{3.58}$$

$$A_s = \frac{D_s Bz}{S_T} \tag{3.59}$$

$$V_o = \frac{\pi}{4} L\left(D_s + 2\delta_w\right)^2 \tag{3.60}$$

$$V_w = \frac{\pi}{4} L\left[n_t\left(D_o^2 - D_i^2\right) + \left(\left(D_s + 2\delta_w\right)^2 - D_s^2\right)\right] \tag{3.61}$$

Where the tube pitch and clearance were defined by [98]

$$S_T = D_o + z \tag{3.62}$$

$$\frac{S_T}{D_o} = 1.5 \tag{3.63}$$

The number of tubes of the shell-and-tube heat exchangers was estimated by [98]

$$n_t = 0.785 \frac{CTP}{CL} \frac{D_s^2}{\left(\frac{S_T}{D_o}\right)^2 D_o^2} \tag{3.64}$$

With

$CL = 1.00$, for a square-pitch tube layout (3.65)

$CTP = 0.93$, for a one-tube pass tube count (3.66)

A recommended baffle spacing and baffle cut corresponding to about 40-60% and 25%-35% of the shell diameter were assumed, respectively.

3.6.3. Condenser

3.6.3.1. Energy and exergy analysis

Considering a control volume around the condenser (Fig. 3.9) and assuming steady state thermodynamic process and isobaric operation with negligible potential and kinetic energy changes, the required amount of heat rejection from the working fluid to the cooling air, was evaluated by [26]

$$\dot{Q}_C = \dot{m}_{wf}\left(h_{wf,in} - h_{wf,out}\right) = \dot{m}_{ca}\left(h_{ca,out} - h_{ca,in}\right) \tag{3.67}$$

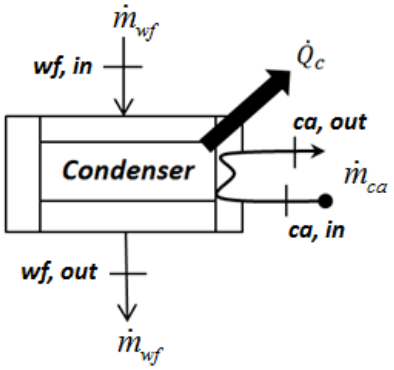

Figure 3. 9: Control volume around the Condenser

The energetic (or First-law) and exergetic (or Second-law) efficiencies were determined respectively, by [26,92]

$$\eta_{I,C} = \frac{(T_{out} - T_{in})_{ca}}{T_{wf,in} - T_{ca,in}} = \frac{(T_{in} - T_{out})_{wf}}{T_{wf,in} - T_{ca,in}} \tag{3.68}$$

$$\eta_{II,C} = \frac{\dot{m}_{ca} Cp_{ca} (T_{out} - T_{in})_{ca}}{\dot{m}_{wf} (\psi_{in} - \psi_{out})_{wf}} \tag{3.69}$$

3.6.3.2. Constructional design

The condenser was assumed to be a compact plate-fin-and-tube cross flow heat exchanger with multiple rows of staggered tubes (Fig. 3.10). The working fluid, flowing through the tube, was condensed by air, which was used as a cooling medium in a dry cooling system. The heat transfer process in the condenser had two main steps, namely desuperheating and condensing.

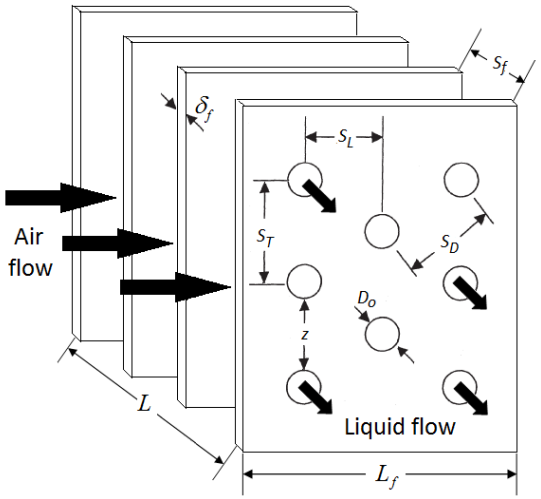

Figure 3. 10: Schematic of the plate-fin-and-tube heat exchanger

Assuming that the plates consisted of evenly divided hexagonal shaped fins that can be treated as circular fins, as suggested by Schmidt [99], the constructional parameters were defined as followed [100-102]

$$\frac{R_e}{r_o} = 1.27\alpha(\beta - 0.3)^{\frac{1}{2}} \tag{3.70}$$

$$A_{fr} = n_T D_e L \tag{3.71}$$

$$A_f = n_f L\left(\frac{\pi}{2}(D_e^2 - D_o^2) + \pi D_e \delta_f\right) \tag{3.72}$$

$$A_{uf} = n_t \pi D_o L - n_f \pi D_o \delta_f \tag{3.73}$$

$$A_o = A_f + A_{uf} \tag{3.74}$$

Where

$$\alpha = \frac{S_T}{D_o} \tag{3.75}$$

$$\beta = \frac{1}{S_T}\left(S_L^2 + \frac{S_T^2}{4}\right)^{\frac{1}{2}} \tag{3.76}$$

The air-side minimum flow area was given by [101,102]

$$A_{\min} = n_T L\left(S_T - D_o - \left(\frac{2z\delta_f}{z+\delta_f}\right)\right) \tag{3.77}$$

For $S_T > 2S_D - D_o - \left(\frac{2z\delta_f}{z+\delta_f}\right)$ (3.78)

Otherwise,

$$A_{\min} = 2n_T L\left(S_D - D_o - \left(\frac{2z\delta_f}{z+\delta_f}\right)\right) \tag{3.79}$$

The tube pitch and clearance were defined as [102]

$$S_T = D_o + z \tag{3.80}$$

$$\frac{S_T}{D_o} = 2.5 \tag{3.81}$$

$$\frac{S_L}{D_o} = 2 \tag{3.82}$$

$$S_D = \left(\left(\frac{S_T}{2}\right)^2 + S_L^2\right)^{\frac{1}{2}} \tag{3.83}$$

The fins parameters were given by [102]

$$S_f = \frac{1}{n_f} - \delta_f \tag{3.84}$$

$$L_f = \frac{D_e - D_o}{2} + \frac{\delta_f}{2} \tag{3.85}$$

The surface and fin efficiencies are given by [100-102]

$$\eta_o = 1 - \frac{A_f}{A_o}\left(1 - \eta_f\right) \tag{3.86}$$

$$\eta_f = \frac{\tanh(m_{es} R_e \phi)}{m_{es} R_e \phi} \tag{3.87}$$

Where

$$m_{es} = \left(\frac{h_{ca} Pe}{k_f A_f}\right)^{\frac{1}{2}} = \left(\frac{2h_{ca}}{k_f \delta_f}\right)^{\frac{1}{2}} \tag{3.88}$$

$$\phi = \left(\frac{R_e}{R_o} - 1\right)\left(1 + 0.35 \ln\left(\frac{R_e}{R_o}\right)\right) \tag{3.89}$$

3.6.4. Turbine

3.6.4.1. Energy and exergy analysis

Considering a control volume around the turbine (Fig. 3.11) and assuming steady state thermodynamic process and adiabatic operation with negligible potential and kinetic energy changes, the turbine output power was evaluated by [26]

$$\dot{W}_t = \dot{m}_{wf}\left(h_{wf,in} - h_{wf,out}\right) = \dot{m}_{wf}\eta_t\left(h_{wf,in} - h_{wf,out,is}\right) \tag{3.90}$$

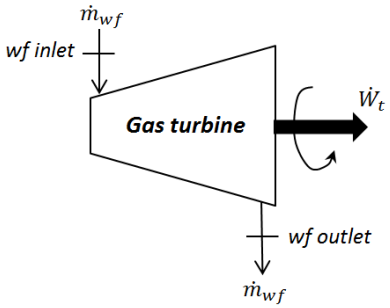

Figure 3. 11: Control volume around the Turbine

The exergetic efficiency of the turbine was determined as

$$\eta_{II,t} = \frac{\dot{W}_t}{\dot{W}_t + \dot{I}_t} \tag{3.91}$$

Subject to the binary-cycle utilized, the turbine inlet state is either a saturated vapour or superheated vapour at the evaporator pressure. The turbine outlet state was however strongly reliant on the type of working fluid employed. Superheated, saturated vapour or mixture of liquid and vapour, at the condenser pressure, was obtained for dry, isentropic and wet organic fluids, respectively.

3.6.4.2. Constructional design

The turbine was assumed to be an axial single-stage expander with a marginal capital cost and maintenance [103]. The actual turbine dimension was estimated by a turbine size parameter, which takes into account the turbine exit volume flow rate and the enthalpy drop during the expansion process [104].

The turbine size parameter was determined as

$$SP = \frac{\sqrt{\dot{V}_{out}}}{\Delta H_{is}^{\frac{1}{4}}} \tag{3.92}$$

3.6.5. Feedpump

Considering a control volume around the feedpump (Fig. 3.12) and assuming steady state thermodynamic process and adiabatic operation with negligible potential and kinetic energy changes, the feedpump input power was evaluated by [26]

$$\dot{W}_p = \dot{m}_{wf}\left(h_{wf,out} - h_{wf,in}\right) = \frac{\dot{m}_{wf}\left(h_{wf,out,is} - h_{wf,in}\right)}{\eta_p} \tag{3.93}$$

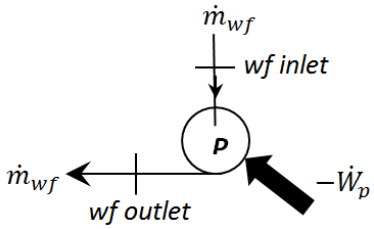

Figure 3. 12: Control volume around the Feedpump

The exergetic efficiency of the pump was computed by

$$\eta_{II,p} = \frac{\dot{W}_p - \dot{I}_p}{\dot{W}_p} \tag{3.94}$$

It is worth mentioning that the feedpump outlet state was a compressed liquid at the evaporator pressure.

3.7. Heat transfer and pressure drop models

3.7.1. Single-phase heat transfer coefficient and pressure drop correlations

The single-phase heat transfer coefficient was evaluated by

- For the tube-side: Gnielinski correlation [102,105]

$$Nu = \frac{h_i D_i}{k} = 0.012\left(\mathrm{Re}^{0.87} - 280\right)\mathrm{Pr}^{0.40} \tag{3.95}$$

With $0.50 < \mathrm{Pr} < 500$ and $3x10 < \mathrm{Re} = \frac{4\dot{m}}{\pi\mu D_i} < 10^6$

- The shell-side heat transfer coefficient was expressed as [97,98]

$$Nu = \frac{h_o D_e}{k} = 0.36\,\mathrm{Re}^{0.55}\,\mathrm{Pr}^{1/3}\left(\frac{\mu_b}{\mu_w}\right)^{0.14} \tag{3.96}$$

With $0.50 < \mathrm{Pr} < 500$ and $2x10^3 < \mathrm{Re}_s = \frac{G_s D_e}{\mu} < 10^6$

Where

$$G_s = \frac{\dot{m}}{A_s} \tag{3.97}$$

- The air-side heat transfer coefficient is given by Ganguli et al. correlation [106]

$$Nu = \frac{h_o D_o}{k_{air}} = 0.38\,\mathrm{Re}_d^{\,0.6}\,\mathrm{Pr}^{\frac{1}{3}}\left(\frac{A_{uf}}{A_o}\right)^{0.15} \tag{3.98}$$

With $1800 < \mathrm{Re}_d = \frac{G_s D_o}{\mu} < 10^5$

The total pressure drop across the heat exchanger was estimated as [97,107]

- For the tube-side:

$$\Delta P_t = \frac{G_t^2}{2\rho}\left(4f\frac{n_p L}{d_i} + 4\left(n_p - 1\right)\right) \tag{3.99}$$

With $f = \left(1.58\ln\mathrm{Re} - 3.28\right)^{-2}$ and $3000 < \mathrm{Re} < 5x10^6$

- For the shell-side:

$$\Delta P_s = \frac{fG_s^2\left(n_B + 1\right)D_s}{2\rho D_e\left(\frac{\mu_b}{\mu_w}\right)^{0.14}} \tag{3.100}$$

Where

$$n_B = \frac{L}{B} - 1 \tag{3.101}$$

$$f = \exp(0.576 - 0.19 \ln \mathrm{Re}_s) \tag{3.102}$$

- The air-side pressure drop of the compact plate-fin-and-tube cross flow heat exchanger was approximated by a combination of the effects due to both fins and tubes [100,108,109],

$$\Delta P_s = \Delta P_f + \Delta P_t \tag{3.103}$$

Where,

$$\Delta P_f = f_f \frac{G_s^2}{2\rho} \frac{A_f}{A_{\min}} \tag{3.104}$$

With

$$f_f = 1.7\, \mathrm{Re}_L^{-0.5} \tag{3.105}$$

$$\mathrm{Re}_L = \frac{G_s S_L}{\mu} \tag{3.106}$$

And

$$\Delta P_t = 18.03 \frac{G_s^2}{\rho} n_L\, \mathrm{Re}_d^{-0.316} \left(\frac{S_T}{d_o}\right)^{-0.927} \left(\frac{S_T}{S_D}\right)^{0.515} \tag{3.107}$$

With $200 < \mathrm{Re}_d = \dfrac{G_s D_o}{\mu} < 50000$

3.7.2. Evaporative heat transfer coefficient and pressure drop correlations

The evaporative two-phase flow heat transfer coefficient on the tube-side was evaluated by Gungor and Winterton [101,110]

$$Nu = \frac{h_i D_i}{k} = 0.023 \left(G_t (1-x) \frac{D_i}{\mu_l}\right)^{0.8} \mathrm{Pr}_l^{0.4} \left(1 + 3000 Bo^{0.86} + 1.12 \left(\frac{x}{1-x}\right)^{0.75} \left(\frac{\rho_l}{\rho_v}\right)^{0.41}\right) \tag{3.108}$$

Where,

$$Bo = \frac{q}{G_t h_{fg}} \tag{3.109}$$

The total pressure drop on the tube-side of the evaporator was estimated by [97,107]

$$\Delta P_o = \Delta P_{stat} + \Delta P_{mom} + \Delta P_{frict} \tag{3.110}$$

Where,

$$\Delta P_{stat} = \rho_{tp} g H \sin\theta \tag{3.111}$$

$$\Delta P_{mom} = G_t^2 \left(\left[\frac{(1-x)^2}{\rho_L (1-\varepsilon)} + \frac{x^2}{\rho_G \varepsilon} \right]_{out} - \left[\frac{(1-x)^2}{\rho_L (1-\varepsilon)} + \frac{x^2}{\rho_G \varepsilon} \right]_{in} \right) \tag{3.112}$$

$$\Delta P_{frict} = \Delta P_t \Phi_{fr}^2 \tag{3.113}$$

For horizontal flows, the static pressure drop can be neglected since there is no change in static head. The void fraction was approximated with Steiner correlation [111]

$$\varepsilon = \frac{x}{\rho_G} \left[(1 + 0.12(1-x)) \left(\frac{x}{\rho_G} + \frac{1-x}{\rho_L} \right) + \frac{1.18(1-x)\left[g\sigma(\rho_L - \rho_G) \right]^{0.25}}{G_t^2 \rho_L^{0.5}} \right]^{-1} \tag{3.114}$$

The two-phase multiplier from Friedel correlation was given by [112]

$$\Phi_{fr}^2 = E + \frac{3.24FH}{Fr_H^{0.045} We_L^{0.035}} \tag{3.115}$$

Where the dimensionless factors Fr_H, E, F and H were determined as follow

$$Fr_H = \frac{G_t^2}{g d_i \rho_H^2} \tag{3.116}$$

$$E = (1-x)^2 + x^2 \frac{\rho_L f_G}{\rho_G f_L} \tag{3.117}$$

$$F = x^{0.78} (1-x)^{0.224} \tag{3.118}$$

$$H = \left(\frac{\rho_L}{\rho_G} \right)^{0.91} \left(\frac{\mu_G}{\mu_L} \right)^{0.19} \left(1 - \frac{\mu_G}{\mu_L} \right)^{0.7} \tag{3.119}$$

$$f = \frac{0.079}{\mathrm{Re}^{0.25}} \tag{3.120}$$

The liquid Weber number and the homogeneous density were defined, respectively, as

$$We_L = \frac{G_t^2 d_i}{\sigma \rho_H} \tag{3.121}$$

$$\rho_H = \left(\frac{x}{\rho_G} + \frac{1-x}{\rho_L} \right)^{-1} \tag{3.122}$$

3.7.3. Condensation heat transfer coefficient and pressure drop correlations

For the condensing two-phase flow, the tube-side heat transfer coefficient was evaluated by Shah's correlation as [113]

$$Nu = \frac{h_i D_i}{k} = 0.023\left(G_t \frac{D_i}{\mu_l}\right)^{0.8} \mathrm{Pr}_l^{0.4}\left((1-x)^{0.8} + \frac{3.8x^{0.76}(1-x)^{0.04}}{p_r^{0.38}}\right) \tag{3.123}$$

The total pressure drop on the tube-side of the heat exchanger during the condensation process was estimated using the same correlations as for the evaporation [101].

3.7.4. Overall heat transfer coefficient

The overall heat transfer coefficient was given by [114]

$$\frac{1}{UA_s} = \frac{1}{U_i A_i} = \frac{1}{U_o A_o} = \frac{1}{h_i A_i} + R_{f,i} + \frac{\ln\left(\frac{D_o}{D_i}\right)}{2\pi k_w L} + R_{f,o} + \frac{1}{h_o A_o} \tag{3.124}$$

Neglecting the fouling effect at the inner and outer surfaces of the tubes, the overall heat transfer coefficient was simplified to

$$\frac{1}{U} \approx \frac{A_o}{h_i A_i} + \frac{A_o \ln\left(\frac{D_o}{D_i}\right)}{2\pi k_w L} + \frac{1}{h_o} \tag{3.125}$$

The overall heat transfer coefficient based on the unfinned inner surface of the tube was given by [115]

$$\frac{1}{U} \approx \frac{1}{h_i} + \frac{A_i \ln\left(\frac{D_o}{D_i}\right)}{2\pi k_w L} + \frac{A_i}{h_a \eta_o A_o} \tag{3.126}$$

3.8. Logarithmic Mean Temperature Difference (LMTD) approach

In order to size the preheater, evaporator, recuperator and condenser, each heat exchanger was divided into n small sections subject to identical enthalpy change and constant rate of heat transfer. The number of sections was chosen as large as possible to avoid any variation of the heat exchange area with subsequent subdivisions. For each small sections of the heat exchanger, an inlet and outlet fluid temperatures were computed, and the logarithmic mean temperature difference approach was implemented as [114]

$$\Delta T_{lm,cf} = \frac{\Delta T_{in} - \Delta T_{out}}{\ln\left(\frac{\Delta T_{in}}{\Delta T_{out}}\right)} \tag{3.127}$$

The effective length of the heat exchangers was therefore determined from the sum of the elemental areas obtained from the total rate of heat transfer expressed by [114]

$$\dot{Q} = UA_o F \Delta T_{lm,cf} \tag{3.128}$$

Where

$$A_o = n_t \pi D_e L \tag{3.129}$$

The stepwise calculation procedure explained above, for evaluating the heat transfer coefficients and pressure drops of the heat exchangers, was preferred to a single-point calculation, which was observed to yield unrealistic results.

The tube material was assumed to be made from stainless steel AISI316 with fixed wall thickness, whereas the correction factor was taken as unity for simplicity.

The following geometric variables were considered as dependent on the constructional variables:

- Shell diameter
- Tube pitch
- Clearance between adjacent tubes
- Baffle and fin spacing

3.9. Hydraulic performance of auxiliary components

The hydraulic performance of auxiliary components such as a downwell pump and fan were determined, respectively by [100,101]

$$W_{p,geo} = \frac{\dot{m}_{geo} \Delta P_{PH-E}}{\eta_p \rho} \tag{3.130}$$

$$\dot{W}_{fan} = \frac{G_s A_{\min} \Delta P_s}{\eta_{fan} \rho_{air}} \tag{3.131}$$

3.10. Model validation

The numerical results obtained, were validated with the work of Franco and Villani [76] who did perform an energy and exergy analyses to determine the upper limit to the First- and Second-law efficiency, based on the geothermal fluid state at the inlet of the primary heat exchanger. The results shown in Fig. 3.13 illustrate a very good agreement. It is worth mentioning that the work

by Franco and Villani [76] assumed zero lost work, thus zero entropy generation rate; whereas the present work used the minimum entropy generation rate produced by the system, which is, however, approaching zero.

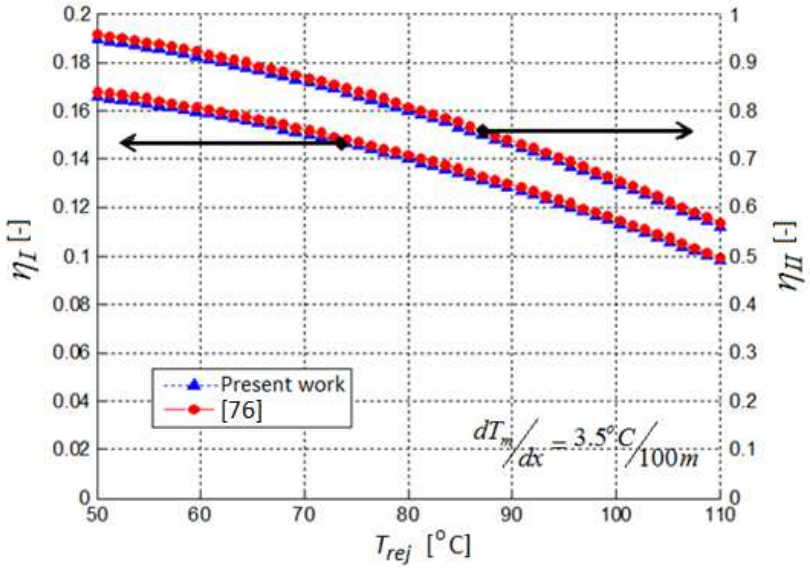

Figure 3. 13: Maximum First- and Second-law efficiency as a function of the geothermal rejection temperature

In addition, a thermodynamic performance of the selected ORCs was analysed using EES software [81]. The numerical data from the simulation were validated with the work of Yari [19] for refrigerant R123, at the operating conditions listed in Table 3.3.

Parameters	**Value**
P_o [kPa]	100
P_{ext} [kPa]	581 (for regenerative ORC with an IHE) 494 (for regenerative ORC)
T_o [°C]	25
T_c [°C]	40
T_E [°C]	120
T_{geo}[°C]	180
η_p[%]	90
η_t[%]	80
ΔT_{pp}[°C]	10

Table 3. 3: Operating parameters used in the validation of results

The comparison shown in Table 3.4 illustrates a very good agreement between the present work and the results of Yari [19].

Performance parameters	Simple ORC		ORC with IHE		Regenerative ORC		Regenerative ORC with IHE	
	Present work	[19]	Present work	[19]	Present work	[19]	Present work	[19]
$\dot{W}_{net}$ [kJ/kg]	50.29	50.38	50.29	50.38	44.13	43.61	43.88	44.02
$\dot{E}x_{dest}$ [kJ/kg]	79.67	80.25	79.67	80.25	85.84	85.98	86.09	86.59
η_I [%]	7.37	7.65	7.37	7.65	6.466	6.623	6.43	6.686
$\eta_{I,2}$ [%]	13.06	13.28	13.97	14.2	14.49	14.52	15.08	15.35
η_{II} [%]	37.84	38.76	37.84	38.76	33.2	33.56	33.01	33.87
$\eta_{II,2}$ [%]	48.56	49.06	50.92	51.4	50.64	50.39	52.20	52.73
ε [%]	63.28	64.33	64.75	65.82	62.5	62.67	64.25	65.41

Table 3. 4: Validation of the numerical model with published data [19]

3.11. Optimization model

The optimization process and entropy generation minimization (EGM) analysis were performed to minimize the exergy loss of the power plant. The steepest descent method [24] using EES software [81] was implemented to optimize the ORCs. For a given combination of the thermodynamic cycle and working fluid, the optimal operating conditions, i.e. evaporative and condensing temperatures, were determined for maximum cycle power output per unit mass flow rate of the geothermal fluid, as illustrated by the simulation flow chart in Fig. 3.14. The geothermal mass flow rate and the cooling air velocity in the condenser were varied to model, size, and optimize the power plant components using a stepwise calculation procedure.

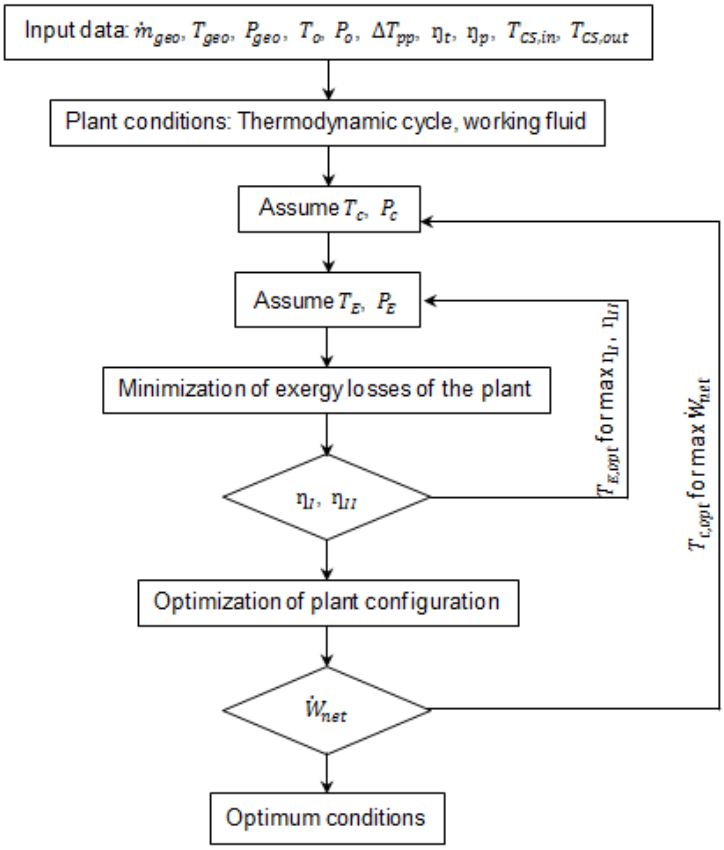

Figure 3. 14: Flow chart of the simulation procedure

CHAPTER 4

RESULTS AND DISCUSSIONS

4.1. Thermodynamic performance of the organic binary fluids

A thermodynamic performance of the selected organic binary fluids was studied for the simple and regenerative ORCs. A dry cooling system was considered with the cooling air at ambient conditions of 25^{o}C and 101.3 kPa, reference temperature and atmospheric pressure, respectively. The pinch-point and condensing temperatures were fixed at 5^{o}C and 40^{o}C respectively, while the turbine inlet temperature was varied from the limiting temperature of condensation to the geofluid input temperature.

In Fig. 4.1, the variation of the cycle power output per unit mass flow rate of the geofluid was plotted for both ORCs at subcritical pressure operating conditions. For a simple ORC (Fig. 4.1a), the binary organic fluids demonstrated an identical behaviour, whereas an optimal turbine inlet temperature and maximum cycle power output per unit mass flow of the geothermal fluid differed significantly for a regenerative ORC (Fig. 4.1b), depending on the thermodynamic properties of the organic fluids to behave with a fixed optimal turbine extraction pressure determined by Yari [19]. A brief comparison of Figs. 4.1a and 4.1b showed nearly identical thermodynamic performance for isobutane, whereas the addition of an OFOH to the binary cycle utilizing R152a, R123 or n-pentane as binary fluid resulted to a substantial reduction in the cycle power output by as much as 15%, 26% and 42%, respectively.

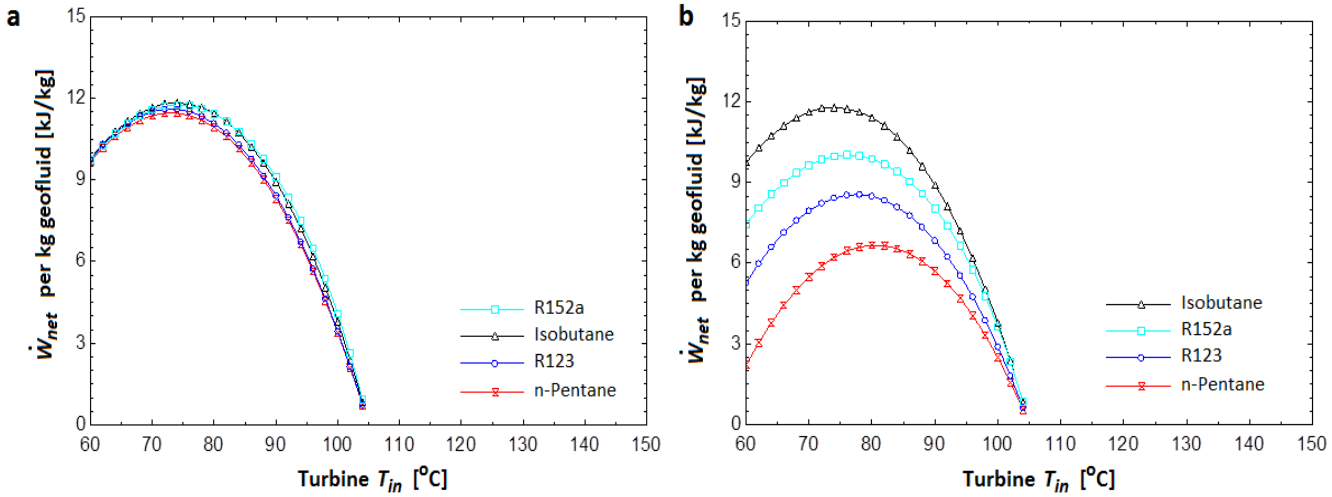

Figure 4. 1: Cycle power output per kg geofluid for geothermal resource temperature of 110^{o}C (a) Simple ORC and (b) Regenerative ORC

For the moderate-grade geothermal resource, the cycle power output per unit mass flow rate of the geofluid was plotted in Fig 4.2 for both ORCs against the turbine inlet temperature. Under subcritical pressure operating conditions, higher cycle power outputs were obtained at relatively higher optimal inlet operating conditions of the turbine for both ORCs as compared to the low-grade geothermal resource in Fig. 4.1.

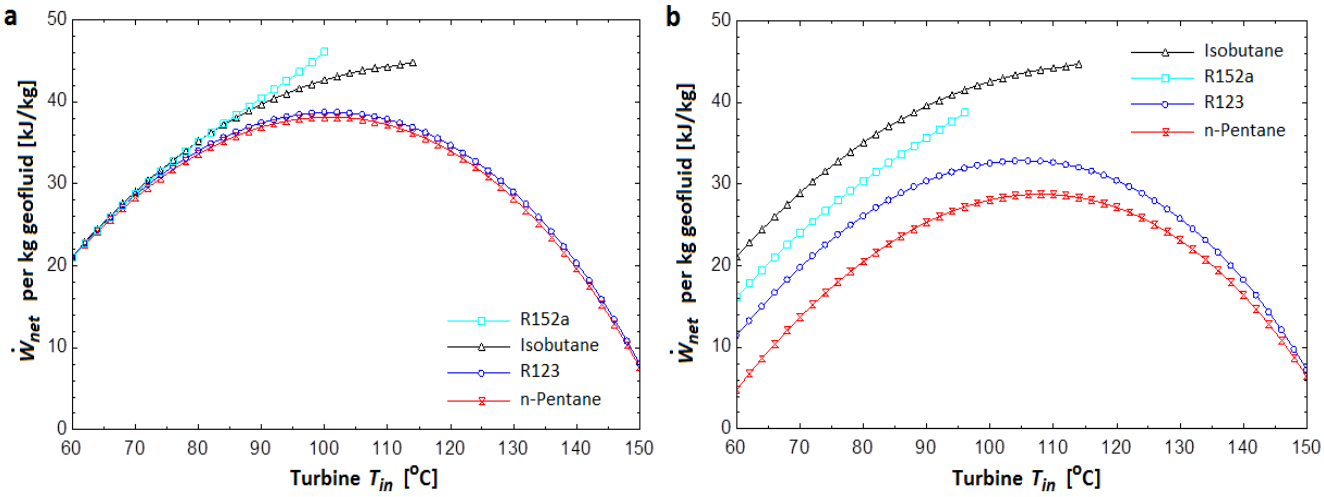

Figure 4. 2: Cycle power output per kg geofluid for geothermal resource temperature of 160°C (a) Simple ORC and (b) Regenerative ORC

In the studied range of heat source temperature, the lower the boiling point temperature of the organic fluid, the higher the evaporating temperature for its simple ORC (Fig. 4.3a). On the other hand, the supremacy of organic fluids with low vapour specific heat capacity, such as isobutane, to convert low-to-moderate geothermal resource temperature at relatively low evaporating temperature is remarkably demonstrated for the regenerative ORC (Fig. 4.3b). Hence, for the conversion of low-to-moderate grade geothermal heat, organic fluids with higher boiling point temperature, such as n-pentane, would be recommended for the simple ORC as discussed by Mago et al. [85], whereas organic fluids with lower vapour specific heat capacity, such as butane, would be more suitable for the regenerative ORC.

In Fig. 4.4, the variation of cycle thermal efficiency with the turbine inlet temperature was illustrated. Unlike the cycle power output, the thermal efficiency showed no extremum. The organic fluids with high boiling point temperature, such as R123 and n-pentane, had the best performance among the selected organic fluids for both configurations. Furthermore, a regenerative ORC was observed to yield high cycle thermal efficiency at higher turbine inlet temperatures as compared to a simple ORC.

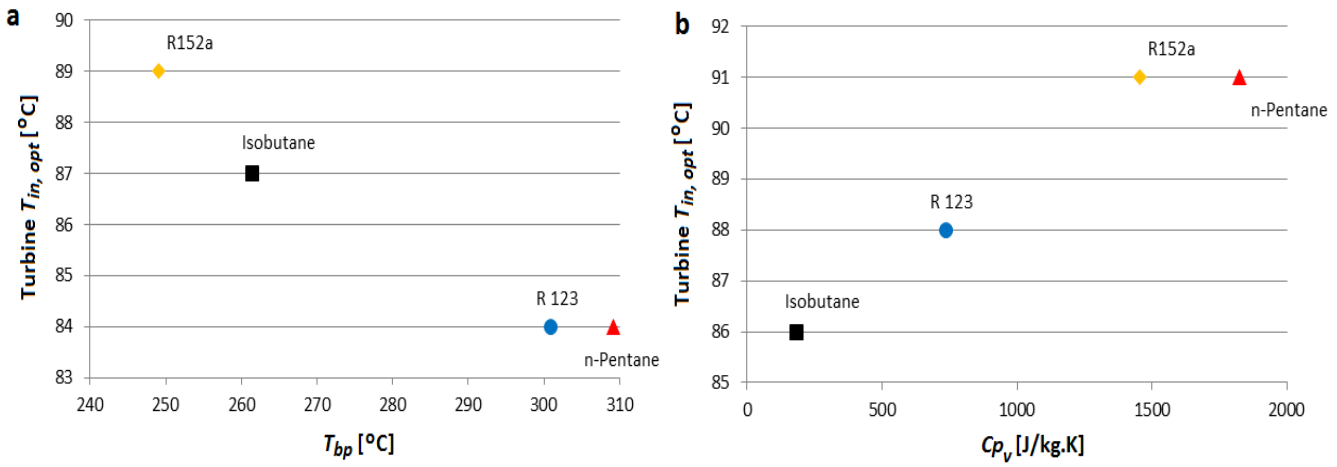

Figure 4. 3: Effect of fluid's (a) boiling point temperature, and (b) vapour specific heat capacity, on the optimal turbine inlet temperature for geothermal resource temperature of 130°C

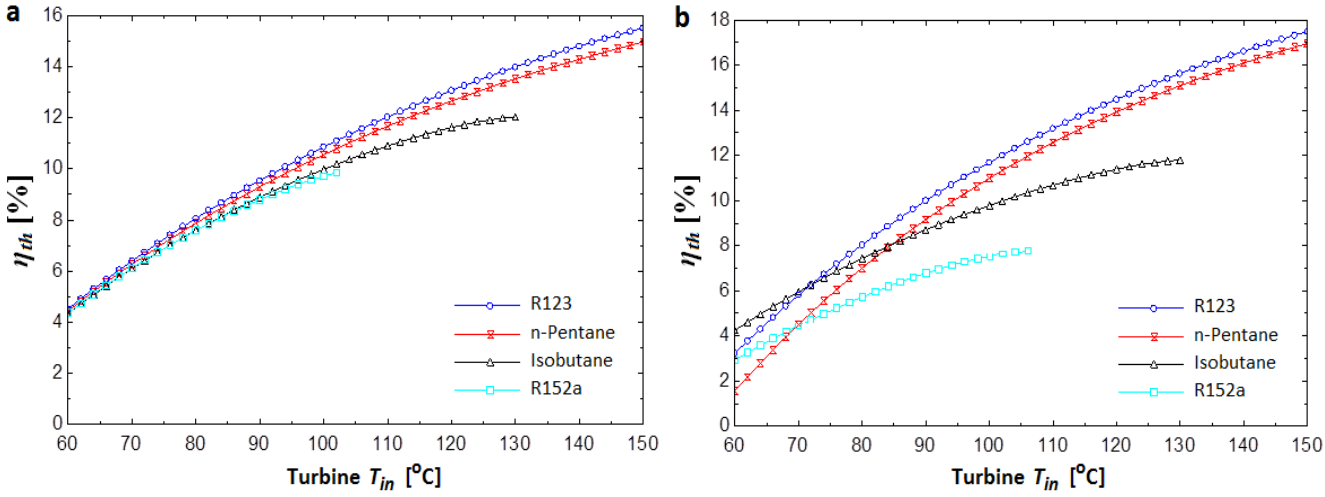

Figure 4. 4: Cycle thermal efficiency for (a) the simple ORC and (b) regenerative ORC

Likewise, the cycle effectiveness, which measures both quantitatively and qualitatively the amount of available energy to be transferred from the geothermal resource to the organic binary fluid was plotted in Fig. 4.5, as a function of the turbine inlet temperature. For a simple ORC, only a marginal difference in the cycle effectiveness was observed (Fig. 4.5a). For the regenerative ORC, however, isobutane showed better performance at low operating temperature of the turbine, whereas R123 and n-pentane demonstrated better conversion of the thermal energy at high turbine inlet temperatures.

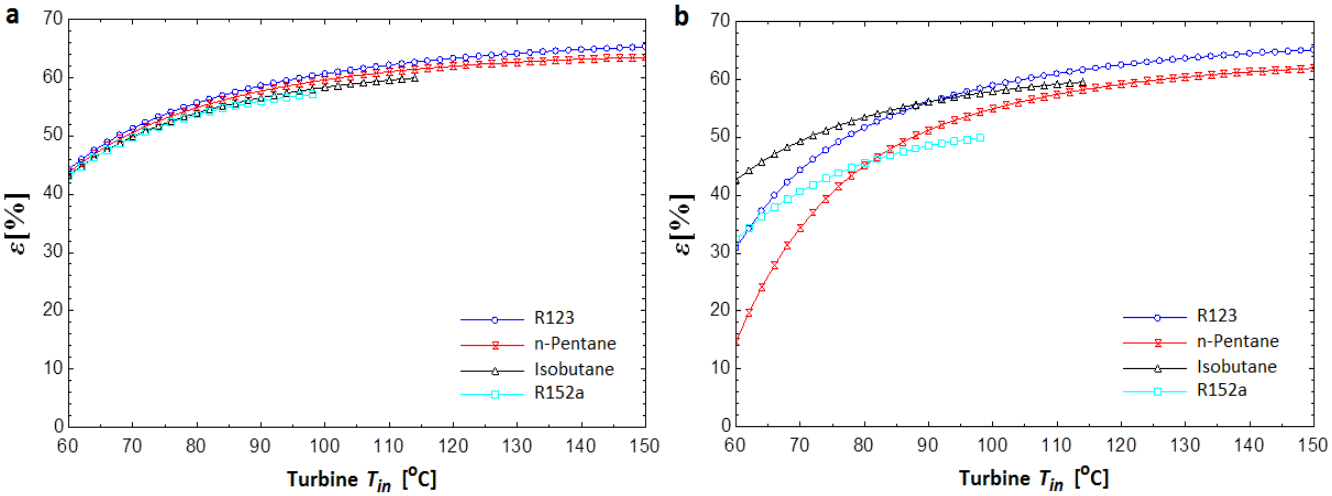

Figure 4. 5: Cycle effectiveness for (a) the simple ORC and (b) regenerative ORC

Although the present study limited itself to the thermodynamic performance of the selected organic fluids based on their thermodynamic properties, the selection of the optimal organic fluid is also subject to the chemical stability and compatibility with materials, the environmental impacts, the safety concerns, and the economical operation of the binary fluids [77-80].

4.2. Performance analysis of the Organic Rankine Cycles

An energy, exergy, irreversibility and performance analyses were conducted using mass, energy and exergy balances for any control volume at steady state with negligible potential and kinetic energy changes. N-pentane was chosen as the organic binary fluid for the conversion of the low-to-moderate grade geothermal heat.

4.2.1. Energy and exergy analysis

The First- and Second-law efficiencies with respect to the reference temperature T_o, were illustrated by Figs. 4.6 and 4.7, respectively. An optimal turbine inlet temperature was determined to maximize the First- and Second-law efficiencies. Based on the effectiveness of the conversion of the available geothermal energy and exergy into useful work, the regenerative cycles have been less efficient and less performing compared to the basic ORCs.

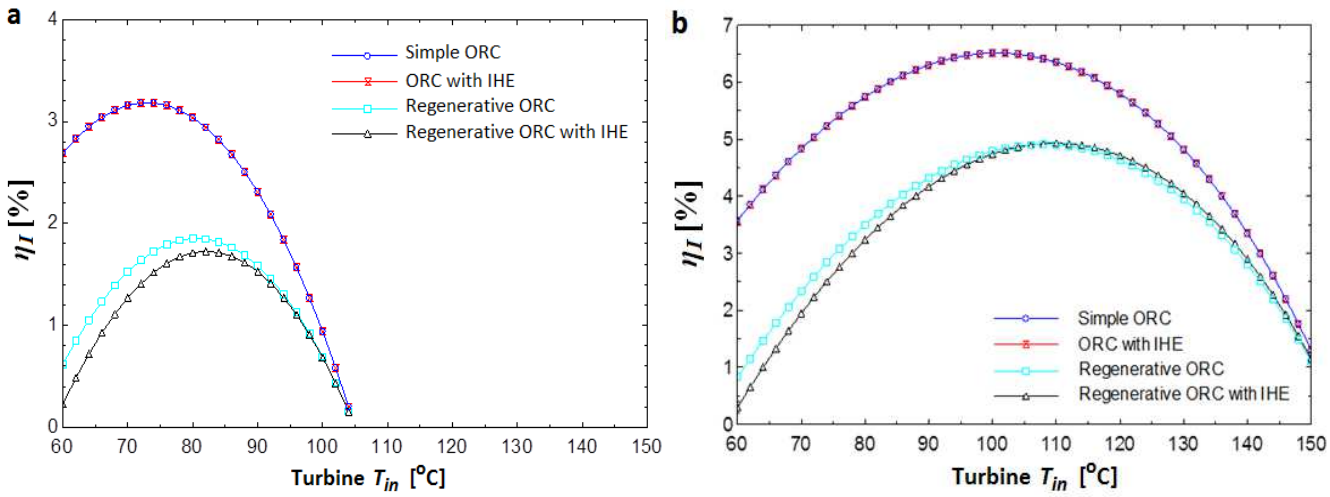

Figure 4. 6: First-law efficiency with respect to T_o for geothermal resource temperature of (a) 110°C and (b) 160°C

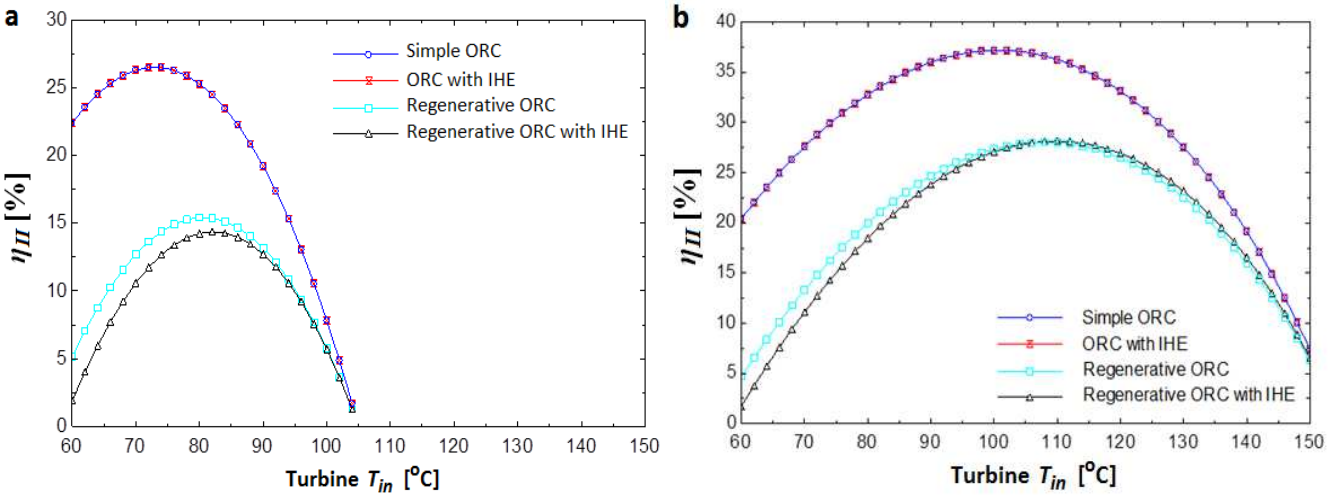

Figure 4. 7: Second-law efficiency with respect to T_o for geothermal resource temperature of (a) 110°C and (b) 160°C

Based on the energy input to the cycle, the First- and Second-law efficiencies were represented in Fig. 4.8. At low turbine inlet temperatures, the basic ORCs have been more efficient than the regenerative ORCs. As the turbine inlet temperature increased, the regenerative ORC with an IHE became the most efficient whereas the simple ORC showed a poor performance. This could be attributed to the ability of the regenerative cycles to minimize the exergy loss (irreversibility) during the heat transfer process. The noticeable lower First-law efficiency (Fig. 4.8a) can be attributed to the large difference in temperature between the geothermal resource and the organic binary fluid entering the primary heat exchanger [21].

The cycle effectiveness was plotted in Fig. 4.9, as a function of the turbine inlet temperature.

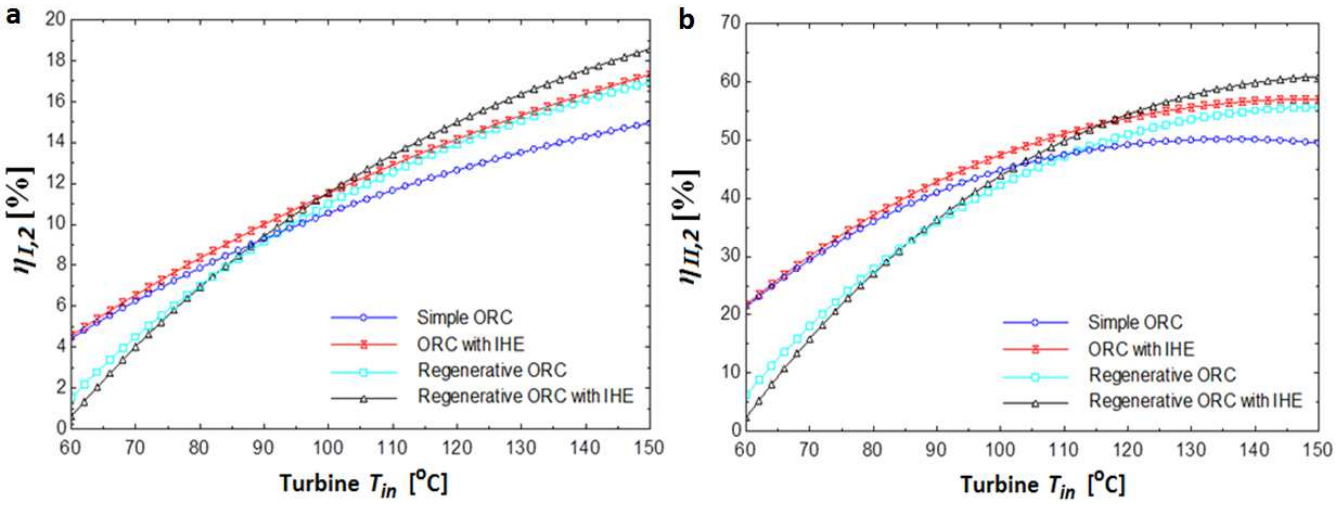

Figure 4. 8: (a) First- and (b) Second-law efficiency based on energy input to the ORC

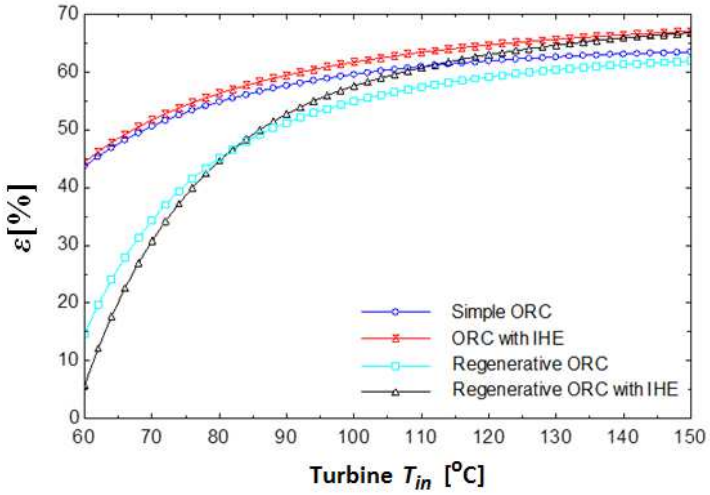

Figure 4. 9: Cycle effectiveness

The Second-law efficiency and the cycle effectiveness as illustrated by Fig. 4.8b and Fig. 4.9, respectively, were observed to yield an optimal turbine inlet temperature beyond which no substantial increase in both the Second-law efficiency and cycle effectiveness was noticeable.

4.2.2. Irreversibility analysis

An irreversibility analysis was conducted using the overall plant irreversibility as the objective function. It was defined as the sum of the exergy loss in each components of the cycle. In Fig. 4.10, the overall plant irreversibility was plotted against the turbine inlet temperature. An

optimal turbine inlet temperature was obtained to yield minimum overall plant irreversibility, which also produced maximum First- and Second-law efficiencies.

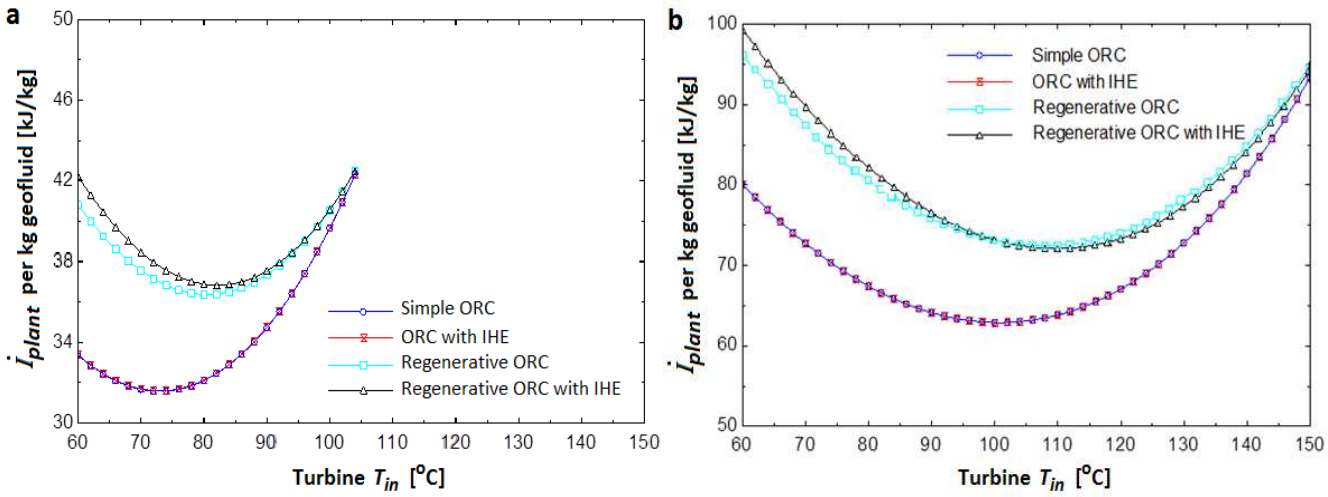

Figure 4. 10: Overall plant irreversibility for geothermal resource temperature o (a) 110°C and (b) 160°C

To analyse the exergy loss in each components of the cycle, a fuel depletion ratio was defined as the ratio of the exergy loss of the individual component to the total exergy input to the ORC. In Fig. 4.11, the fuel depletion ratio of the different components and the ORC itself were plotted as a function of the turbine inlet temperature. The major sites of exergy loss were the evaporator, the condenser and the turbine. The addition of an IHE yielded a significant decrease in the irreversibility of the preheater-evaporator unit, whereas adding an OFOH, reduced the exergy loss due to the condenser and turbine.

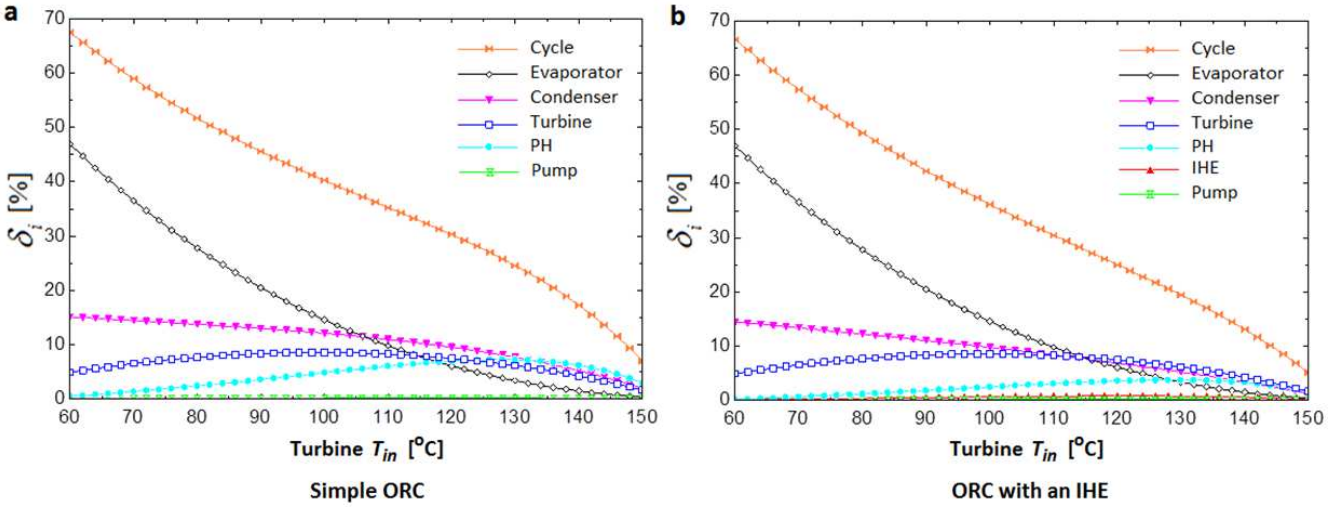

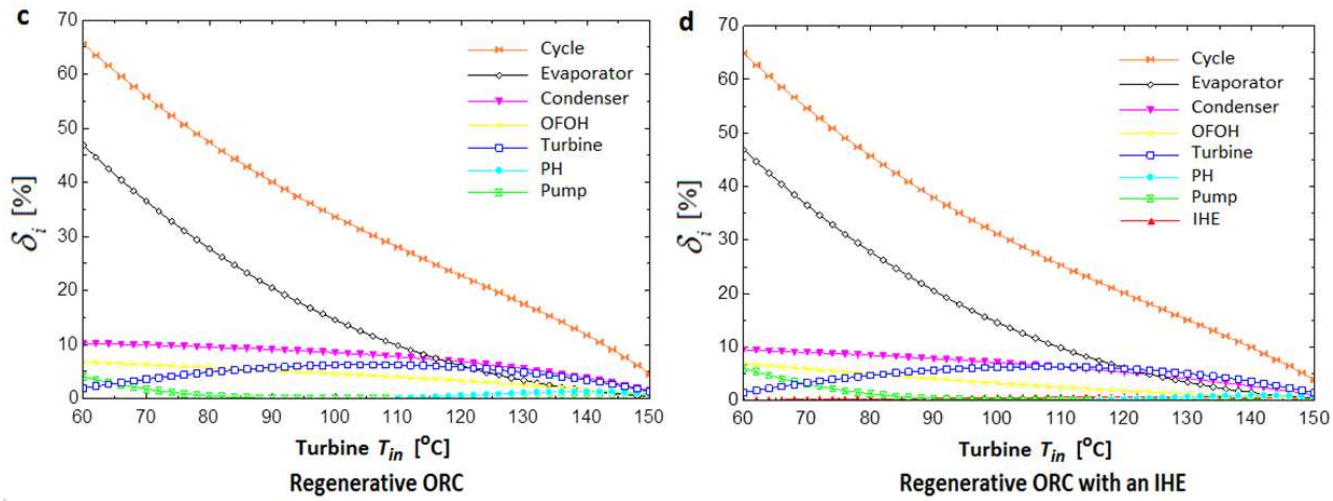

Figure 4. 11: Fuel depletion ratio for geothermal resource temperature of 160°C

4.2.3. Performance analysis

The cycle power output per unit mass flow rate of the geothermal fluid was plotted against the turbine inlet temperature (Fig. 4.12). As discussed by Lakew and Bolland [94], the increase in the turbine inlet temperature resulted in an increase of the enthalpy of the inlet fluid to the turbine and a decrease in the flow rate of the binary fluid. Consequently, an optimal turbine inlet temperature, which yielded maximum cycle power output per unit mass flow rate of the geofluid, was obtained for each type of ORC. Moreover, for the given operating conditions of the ORCs, one can conclude that the addition of an IHE did not really impact on the thermodynamic performance of the cycle, whereas the regenerative system reduced significantly the cycle performance.

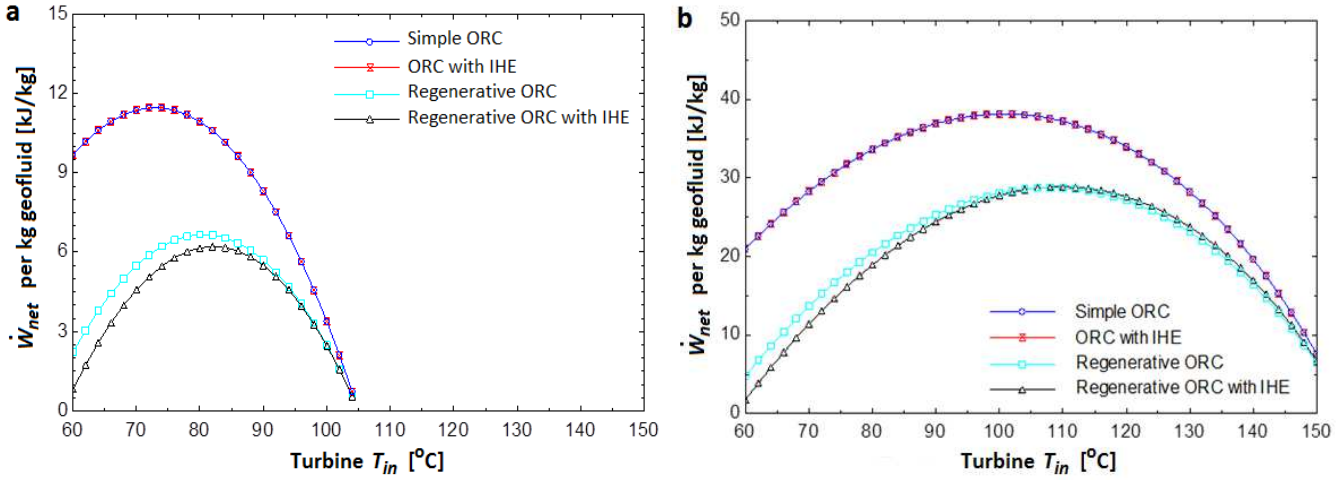

Figure 4. 12: Cycle power output per kg geofluid for geothermal resource temperature of (a) 110°C and (b) 160°C

4.3. Sensitivity analysis

Using cooling air at ambient conditions of 25^{o}C and 101.3 kPa, reference temperature and atmospheric pressure, respectively, in a dry cooling system; a sensitivity analysis was discussed in Fig. 4.13 for a change in operating evaporation temperature, decrease in condensing temperature and variation in the temperature of the geofluid resource:

- For a given geothermal fluid and condensing temperatures, an increment of 10^{o}C in the evaporating temperature resulted to a substantial increase in the rejection exergy loss, back to the exploitation reservoir, at approximately 16-27%, whereas the exergy loss of both the evaporative and condensation processes decreased by 20-40% and 20-25% respectively. In addition, the ability to convert the total exergy input to useful work output also dropped by approximately 15%;
- For a given geothermal fluid and evaporating temperatures, a decrease in condensing temperature of 10^{o}C yielded a decrease of roughly 71% in exergy loss of the condenser itself for cycles without an IHE and nearly 92% for those with an IHE. Moreover, the cycle power output was increased by 10-15%. Hence, the advantage of using an IHE was demonstrated to reduce also the condensing load;
- Finally, the effect of reduction in the temperature of the geofluid resource throughout the lifetime of the operation of the power plant was analysed. As the temperature of the geofluid resource was reduced by 10^{o}C, the cycle power output was reduced by approximately 18%. In short, a substantial decrease in work output can result from a small decrease in the geothermal resource temperature.

As illustrated by Fig. 4.13, the addition of an IHE to the binary cycle resulted in a reduction of the exergy loss in the evaporator-preheater unit, condenser and cooling air, by about 40-70%, 20-30% and 5-15% respectively. Adding an OFOH to the binary cycle, on the other hand, resulted in a remarkable reduction of the exergy loss in all individual components of the binary cycle, typically 80-90% for the evaporator-preheater unit, 25-35% for both the condenser and cooling air, 20-30% for the turbine, and 10-20% for the pumping system. The cycle power output was, however, reduced by 15-25%.

A major drawback with the addition of an IHE and/or OFOH resided in the increase in the rejection exergy loss: 0-20% with the addition of an IHE alone, 20-35% while adding only an

OFOH and up to 40% for incorporating both IHE and OFOH to the binary cycle. To avoid a susceptible thermal pollution of the environment caused by the geofluid being discarded as waste heat at relatively high temperature, a combined power generation and direct use in process or district heating applications as a cogeneration system can be an additional option to improve the geothermal energy utilization [21,116].

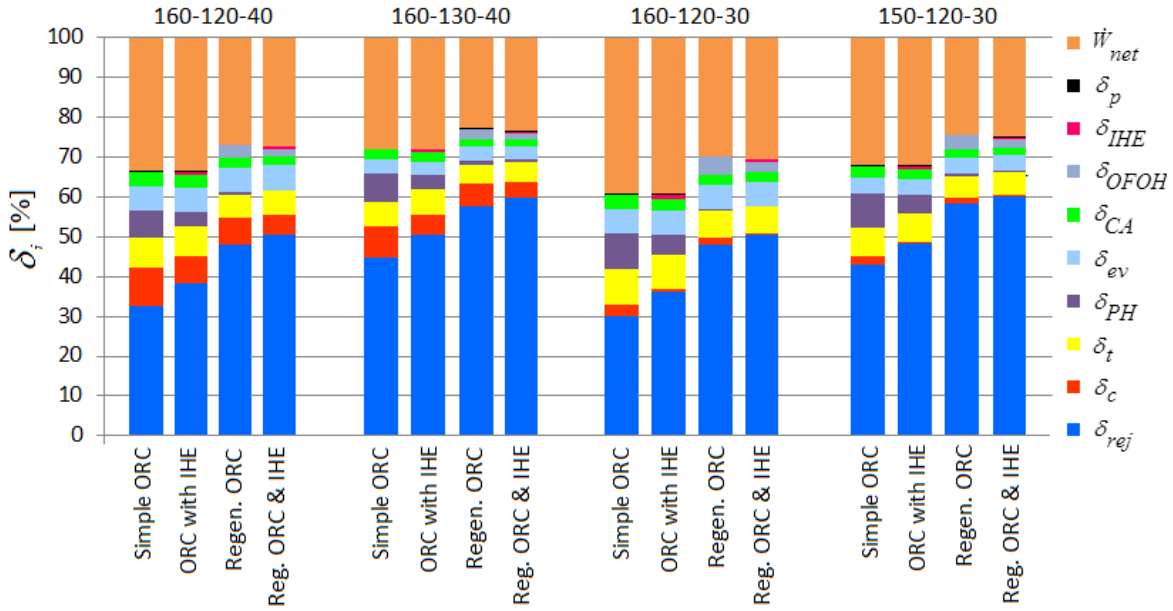

Figure 4. 13: Variation of Fuel depletion ratio with T_{geo}, T_E and T_c respectively (given in ^oC)

In addition, a sensitivity analysis was considered, using an ORC with an IHE and n-pentane as the organic binary fluid, to investigate the variation of the cycle power output with the changes in the geothermal resource temperature, condensing and pinch point temperatures for a unit mass flow rate of the geothermal fluid.

In Fig. 4.14, the effect of the variation of the cycle power output with the geothermal resource temperature was illustrated. The pinch point and condensing temperatures for the operation of the binary cycle were fixed at 5^{o}C and 40^{o}C respectively. The cycle power output per unit mass flow rate of geofluid was observed to increase with the increase in the geothermal resource temperature. An optimal turbine inlet temperature was determined for maximum cycle power output and observed to increase with the geothermal resource temperature.

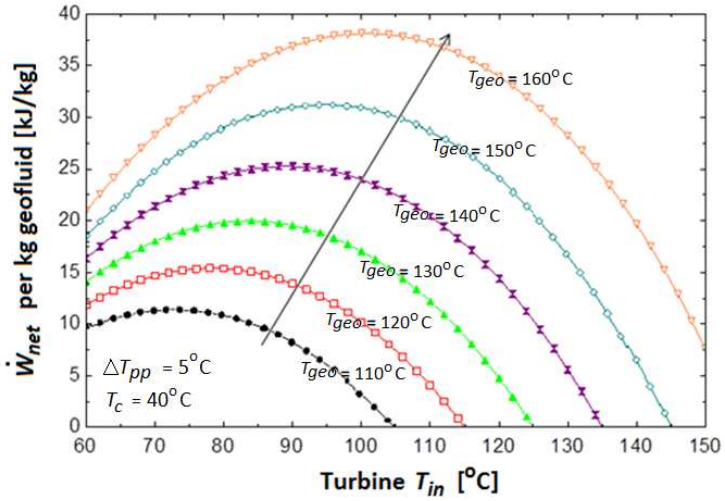

Figure 4. 14: Variation of the cycle power output with the geothermal resource temperature

For a given temperature of the geothermal resource and pinch point of the vaporizer unit, the reduction in condensing temperature to match the design environmental temperature T_o, yielded higher cycle power output and lower optimal turbine inlet temperature (Fig. 4.15). Although a remarkable increase in the cycle power output was obtained due to the increasing enthalpy difference in the expansion process, a substantial increment in the cooling air pumping power requirements was, however, observed. This limitation dictated the choice of the cycle condensing temperature, which is also subject to the site's ambient conditions, capital cost and chemical stability of the organic binary fluid [75].

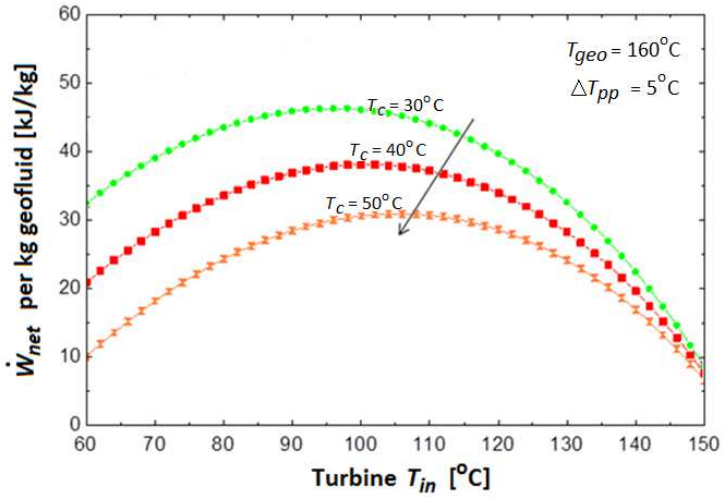

Figure 4. 15: Variation of the cycle power output with the condensing temperature

In terms of the variation of the cycle power output with the pinch point temperature, an optimal turbine inlet temperature was also obtained. The cycle power output was observed to decrease

with the increase in the pinch point temperature of the vaporizer unit due to the higher temperature difference between the geothermal resource and the organic binary fluid (Fig. 4.16). However, the very low pinch point temperatures were not justified since they resulted in high optimal turbine inlet temperature and just a marginal increase in the cycle power output.

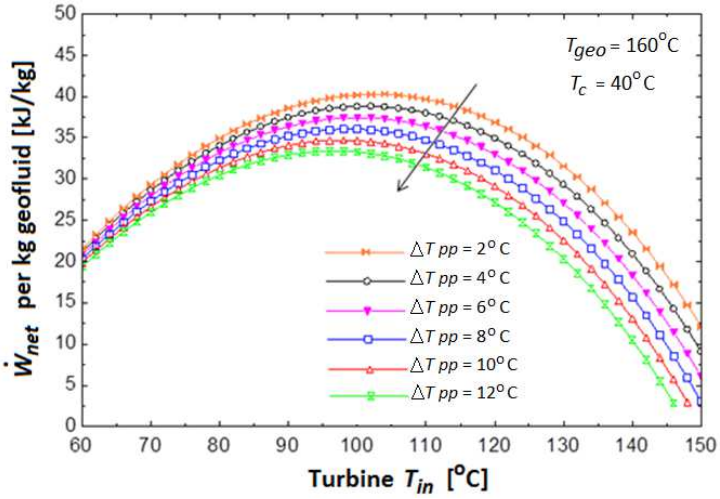

Figure 4. 16: Variation of the cycle power output with the pinch point temperature

4.4. Optimized solution

The optimization process and entropy generation minimization (EGM) analysis were performed to minimize the exergy loss of small binary cycle power plants operating with moderately low-temperature and liquid-dominated geothermal resources in the range of 110°C and 160°C, and cooling air at ambient conditions of 25°C and 101.3 kPa, reference temperature and atmospheric pressure, respectively. Parametric and thermodynamic optimizations were conducted with n-pentane as the organic binary fluid. Optimal operating conditions were determined for maximum cycle power output. An optimal First- and Second-law efficiency was also determined in the given range of the geothermal resource temperature.

As illustrated by Fig. 4.17, the optimal turbine inlet temperature was observed to increase almost linearly with the increase in the geothermal resource temperature. The addition of an IHE to the binary cycle has merely impacted on the optimal operating conditions of the ORCs, whereas adding an OFOH has required high optimal turbine inlet temperatures, approximately 10°C as compare to the basic Rankine ORCs.

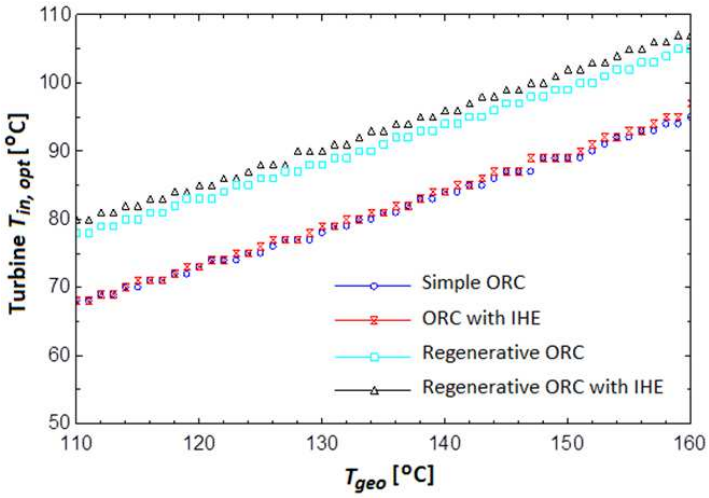

Figure 4. 17: Optimal turbine inlet temperature

In Fig. 4.18, an optimal First- and Second-law efficiency with respect to the reference temperature T_o were represented. Based on the geothermal fluid state at the inlet of the primary heat exchanger, the First- and Second-law efficiencies were in the range of 4-8% and 37-47% respectively for the basic ORCs; 2-6% and 19-33% respectively for the regenerative ORCs.

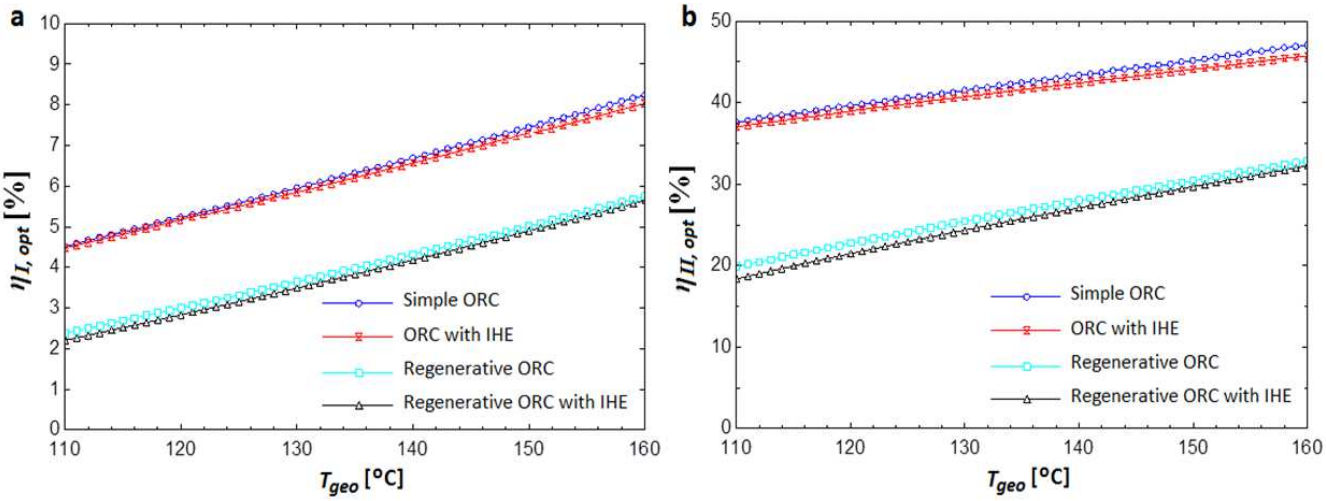

Figure 4. 18: Optimal (a) First- and (b) Second-law efficiency with respect to T_o

The minimum overall plant irreversibility and maximum cycle power output were plotted in Figs. 4.19a and 4.19b respectively, per unit mass flow rate of the geothermal fluid. The basic ORCs were rated at about 16-49 kW maximum cycle power output per unit mass flow rate of the geothermal fluid in the temperature range of 110-160°C, as compare to 8-34kW for the regenerative ORCs. With respect to the geothermal resource temperature, the minimum overall plant irreversibility was observed to increase almost linearly, whereas the maximum cycle power

output increased exponentially. Hence, with a slight increment in the geothermal resource temperature, a substantial increase in the cycle power output can be achieved in the expense of the plant irreversibility. Subbiah and Natarajan [75] proposed hybrid cycles operating with solar concentrators, bio-gas heating or fossil-fuel heating as an attempt to increase the cycle power output by increasing the resource fluid temperature.

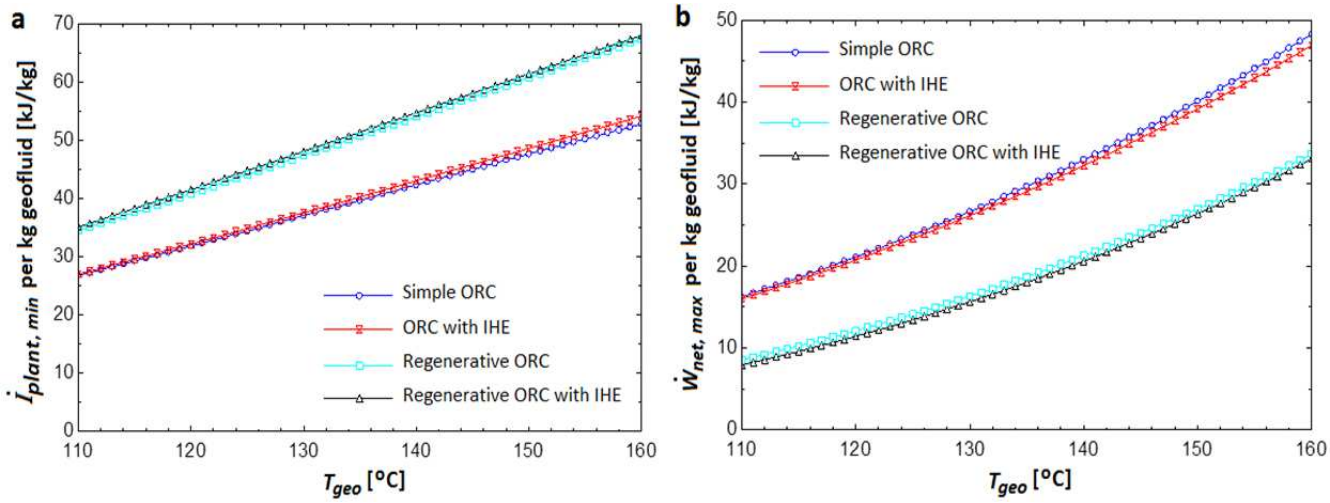

Figure 4. 19: (a) Minimum overall plant irreversibility and (b) maximum cycle power output per kg geofluid

Based on the energy input to the ORC, the First- and Second-law efficiencies were represented by Fig. 4.20. Within the range of the geothermal fluid temperature investigated in this thesis, the First-law efficiency was determined in the range of 8-15% for all ORCs (Fig. 4.20a), whereas a maximum of 56% in Second-law efficiency was achieved by the ORCs with an IHE (Fig. 4.20b). The advantage of adding an IHE and/or an OFOH to the binary cycle to improve the effectiveness of the conversion of the available geothermal energy into useful work was therefore noticeable. From Fig. 4.20a, the regenerative ORC with an IHE was observed to yield maximum thermal efficiency, while in Fig. 4.20b the use of the regenerative ORCs to convert high-grade geothermal heat was justified.

As illustrated by the cycle effectiveness (Fig. 4.21), a better heat transfer capability of the available energy to the organic binary fluid was demonstrated by the basic ORCs at 70-74%, as compared to 56-69% for the regenerative ORCs. Here, the high sensitivity of the regenerative ORCs to the variations in the geothermal resource temperatures was noticeable, as discussed by Franco and Villani [76].

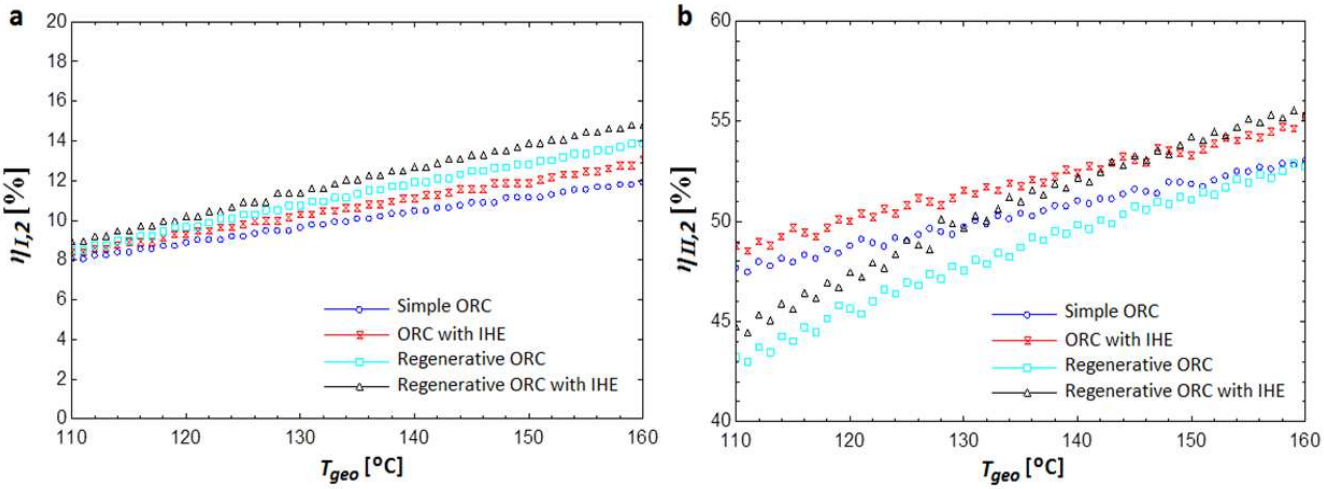

Figure 4. 20: (a) First- and (b) Second-law efficiency based on heat transfer input to the ORC at the optimal operating conditions

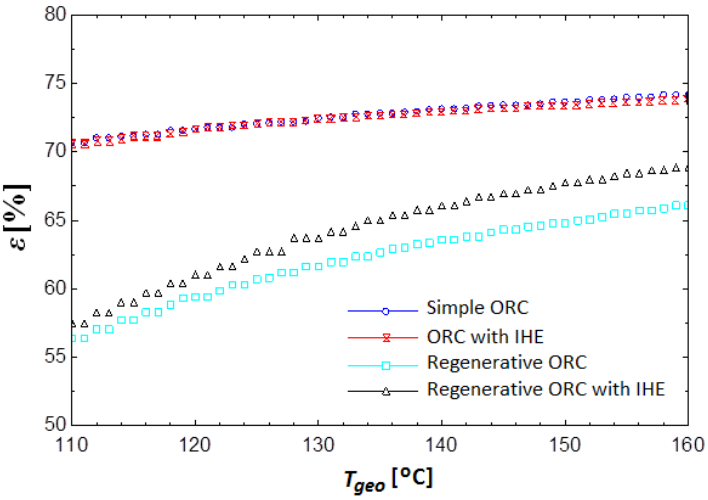

Figure 4. 21: Cycle effectiveness at the optimal operating conditions

In terms of the utilization of the available heat source, the regenerative ORCs were preferable for the conversion of low-to-moderate grade geothermal resource in the temperature range of 110°C to 160°C since they required less volume of organic binary fluid per unit mass flow rate of the geothermal fluid (Fig. 4.22). This could lower significantly the operating and maintenance (O&M) cost of the geothermal power plant.

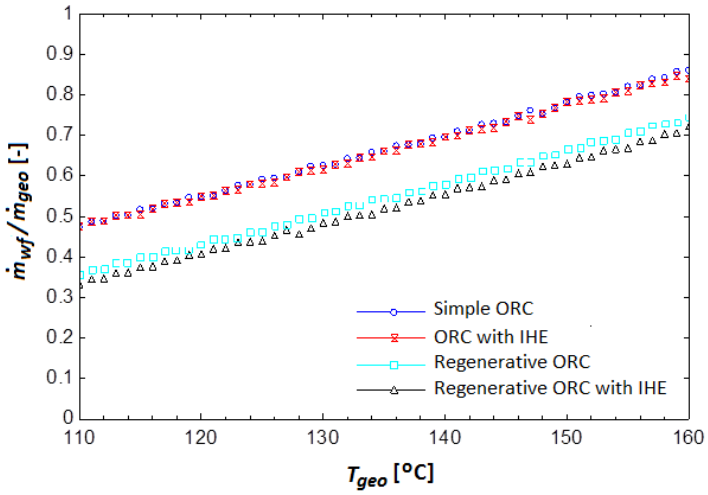

Figure 4. 22: Ratio of mass flow rates, working fluid to geofluid, at the optimal operating conditions

In Fig. 4.23, the recommended rejection temperature of the geofluid was plotted. For the regenerative ORCs, the geothermal fluid was discarded at relatively high temperature as compare to the basic ORCs. An attempt to operate at lower rejection temperature can produce silica oversaturation, scaling, fouling or deposition of the mineral in the piping system, valves and in the tubes of the primary heat exchanger, as discussed by Grassiani [117].

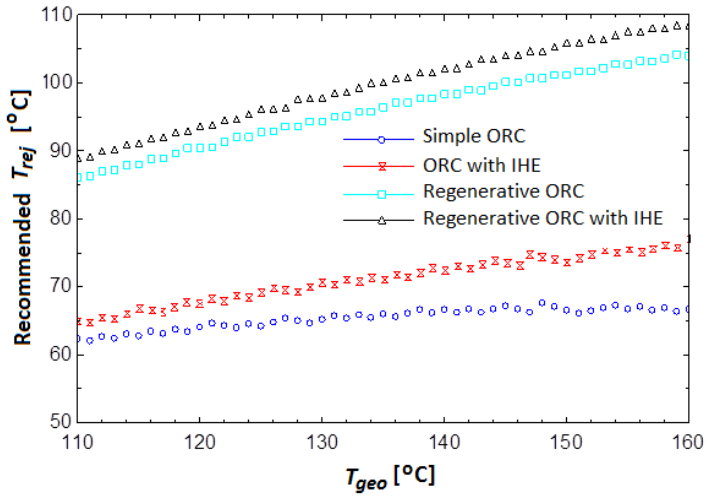

Figure 4. 23: Recommended rejection temperature at the optimal operating conditions

4.5. Design and Sizing of system components

4.5.1. Downhole coaxial heat exchanger

As pointed out by Lim JS et al. [118], there exists an optimal geothermal mass flow rate at which heat energy is extracted from a given hot-dry-rock (HDR) system to produce maximum net

power output. In the extreme cases of faster and slower circulation of the geothermal fluid, the resultant exergy is much lower due to no temperature raise of the rapidly flowing geothermal fluid or the lower mass flow rate, respectively. Hence, it was essential to determine an optimal geothermal mass flow rate for an enhanced geothermal system to generate both minimum pressure drop and entropy generation, while maximizing the extracted heat energy.

In Fig 4.24, the variation of the optimal mass flow rate of the geothermal fluid with the dimensionless Reynolds number was represented. The Reynolds number was varied from the laminar fully-developed flow regime to the large Reynolds number limit of the fully turbulent and fully rough regime. The increment in the optimal mass flow rate was observed to increase exponentially with the Reynolds number in the laminar regime and almost linearly with the large Reynolds number limit of the turbulent regime. A possible reason of such behaviour was the dependency of the fluid friction factor on the Reynolds number in the laminar region, whereas it was constant and independent on the Reynolds number in the fully turbulent and fully rough regime. In terms of the design variables, the optimal mass flow rate of the geothermal fluid was observed to decrease with the increase in either the underground temperature gradient (Fig. 4.24a) or the geothermal resource temperature (Fig. 4.24b). In other words, high underground temperature gradients and geothermal resource temperatures are susceptible to yield higher power output.

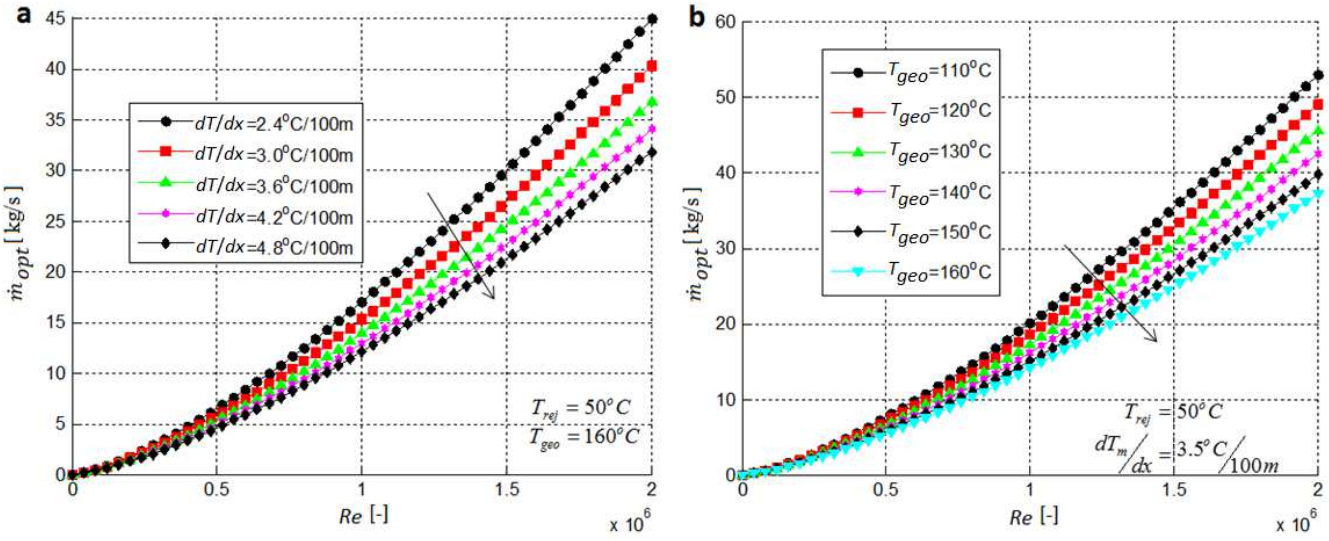

Figure 4. 24: Optimal mass flow rate of the geothermal fluid with variation in (a) temperature gradient and (b) geothermal resource temperature

In Fig. 4.25, the coaxial pipe outer diameter was plotted against the Reynolds number. A substantial variation of the geometry size was observed with the Earth's underground temperature gradient (Fig. 4.25a), rather with the geothermal resource temperature (Fig. 4.25b). Hence, geological and geographical sites with high Earth's underground temperature gradients were recommended to significantly minimize the size of the downhole coaxial heat exchanger for a given cycle power output, and therefore lowering the cost of the power plant.

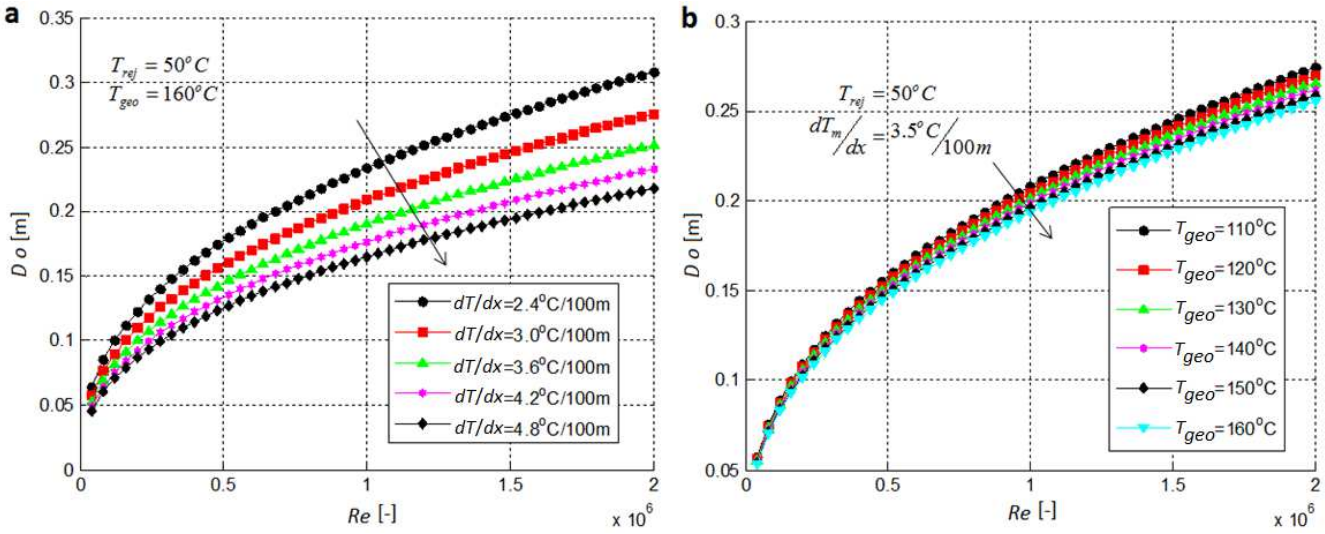

Figure 4. 25: Optimal downhole heat exchanger outer diameter with variation in (a) temperature gradient and (b) geothermal resource temperature

In Fig. 4.26, the minimum entropy generation rate per unit length of the downhole coaxial heat exchanger was observed to increase exponentially with the Reynolds number in both regions of the laminar and turbulent fully-developed flow regimes, to yield values approaching zero even at large Reynolds numbers limit of the fully turbulent and fully rough regime.

The maximum First- and Second-law efficiencies with respect to the reference temperature T_o, were plotted in Figs. 4.27a and 4.27b, respectively, as a function of the geothermal rejection temperature. The First-law efficiency, representing a quantitative measure of the effectiveness of the conversion of the available geothermal energy into useful work as discussed by Subbiah and Natarajan [75], was observed to be as little as 20% maximum (Fig. 4.27a). This was justified by the moderately low temperature of the liquid-dominated geothermal resource considered to be in the range of 110°C to 160°C. The Second-law efficiency, on the other hand, was quantified to more than 50% (Fig. 4.27b) since it accounted for the overall exergy input to the cycle with reference to the dead state environmental design conditions [75].

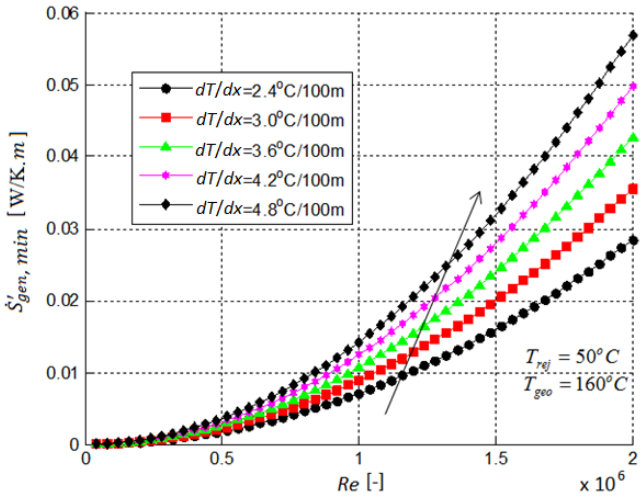

Figure 4. 26: Minimum entropy generation rate per unit length

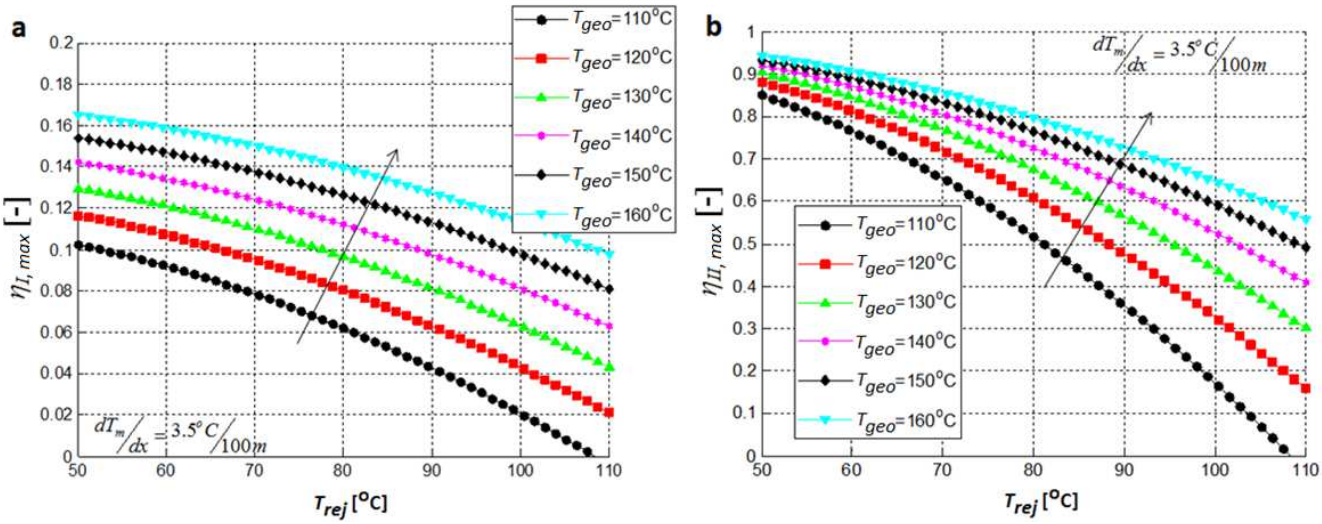

Figure 4. 27: Maximum (a) First- and (b) Second-law efficiency as a function of the geothermal rejection temperature

In addition, it was observed that both the First- and Second-law efficiencies decreased with the increase in the geothermal rejection temperature, which was varied from the lower limit temperature of the reference state to the upper limit temperature of the geothermal resource. The larger the temperature difference between the geothermal resource and the geofluid rejection, the higher the First- and Second-law efficiencies.

4.5.2. Preheater, Evaporator and Recuperator

Although a detail thermal design of shell-and-tube heat exchangers are nowadays performed by sophisticated computer softwares, the following analysis was conducted to emphasize the

principles used in their design. The thesis presented an effective design of the shell-and-tube heat exchangers subject to operating and geometric constraints. A dry cooling system was considered with the cooling air at ambient conditions of 25°C and 101.3 kPa, reference temperature and atmospheric pressure, respectively.

Subject to operating constraints, the shell-and-tube heat exchangers were sized for a given net turbine power output, chosen as one Megawatt. The heat exchangers effective tube lengths were determined while varying the total number of tubes. In Fig. 4.28, the effective tube length of the preheater, evaporator and recuperator were determined for a variation in the nominal tube diameter. For large values of the tube diameter, the effective length of the tubes required for the heat exchange process was high, and resulted in a rise in the flow velocity and pressure drop through the tubes of the heat exchangers. As the number of tubes was increased, the size of the heat exchangers was significantly reduced. In Fig. 4.29a, the effective length of the preheater tubes was observed to vary significantly with the geothermal resource temperature. In Fig. 4.29b and 4.29c, however, a marginal decrease in the effective tube length of the evaporator and recuperator was noticeable with the increment in the geothermal resource temperature. This was certainly dictated by the high optimal evaporating temperature.

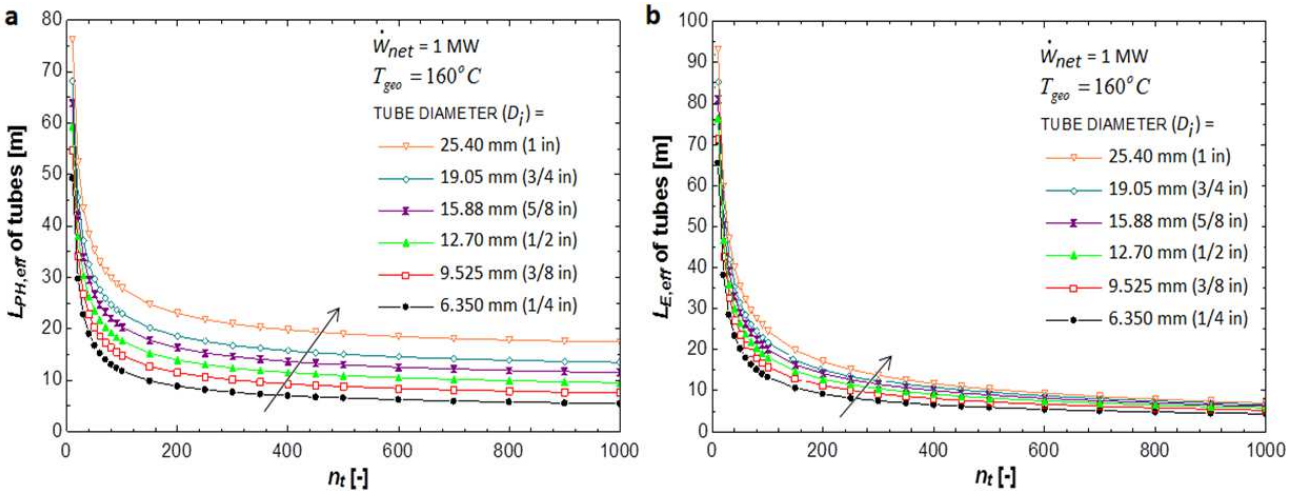

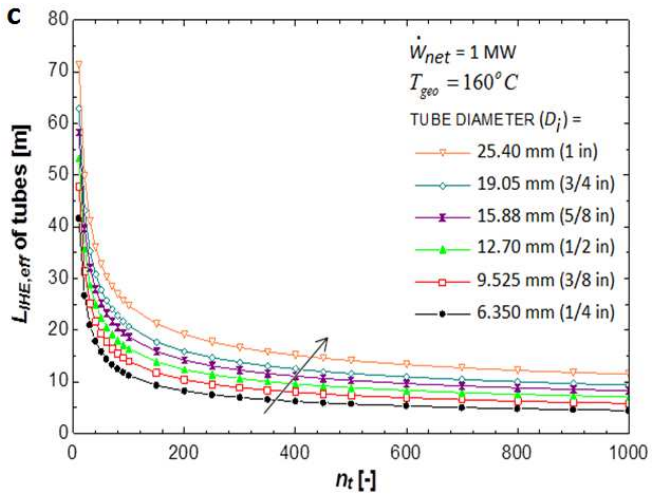

Figure 4. 28: Effective tube length of (a) preheater, (b) evaporator and (c) recuperator with variation in the tube nominal diameter

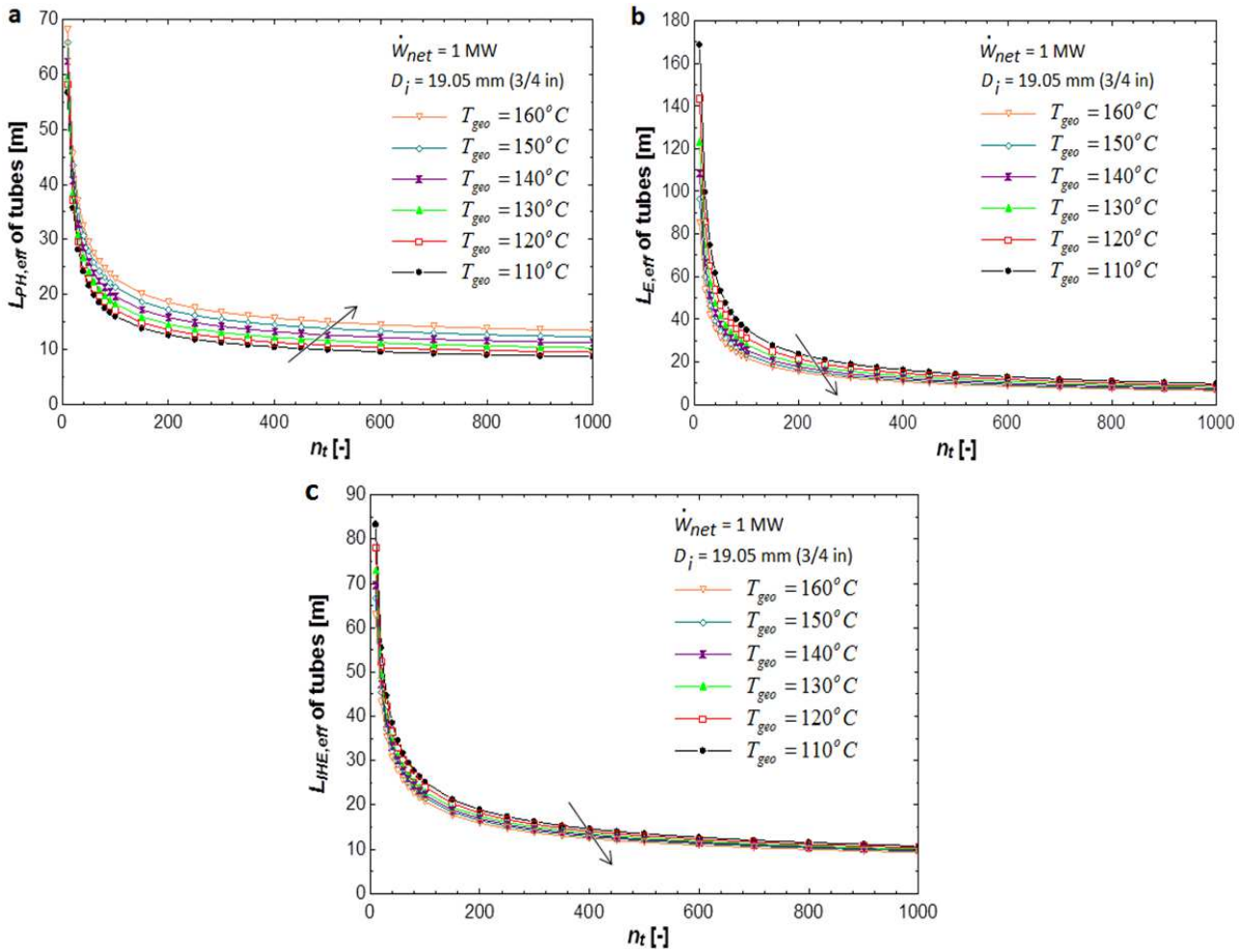

Figure 4. 29: Effective tube length of (a) preheater, (b) evaporator and (c) recuperator with variation in the geothermal resource temperature

Subject to geometric constraints, the shell-and-tube heat exchangers were sized for a given ratio of the overall volume of the exchanger to the total volume of the wall material. In Fig. 4.30, the effective length of the tubes of the heat exchangers were thus determined as a function of the mass flow rate of the geothermal fluid. As the geothermal fluid mass flow rate was varied, a minimum effective length of the preheater tubes was obtained (Fig. 4.30a).

Unlike the preheater model, the effective length of the evaporator tubes was observed to increase with the increment in the mass flow rate of the geothermal fluid, even at low mass flow rate values (Fig. 4.30b). While the effective tube length of the preheater was illustrated to vary significantly with the geothermal resource temperature, the change in the effective length of the evaporator tubes was seen to be nearly independent on the temperature of the geothermal resource. This robust behaviour was indeed justified by the unique optimal evaporating condition for every geothermal resource temperature.

In Fig. 4.30c, the effective length of the recuperator tubes was demonstrated to increase with the increment in both mass flow rate and temperature of the geothermal fluid.

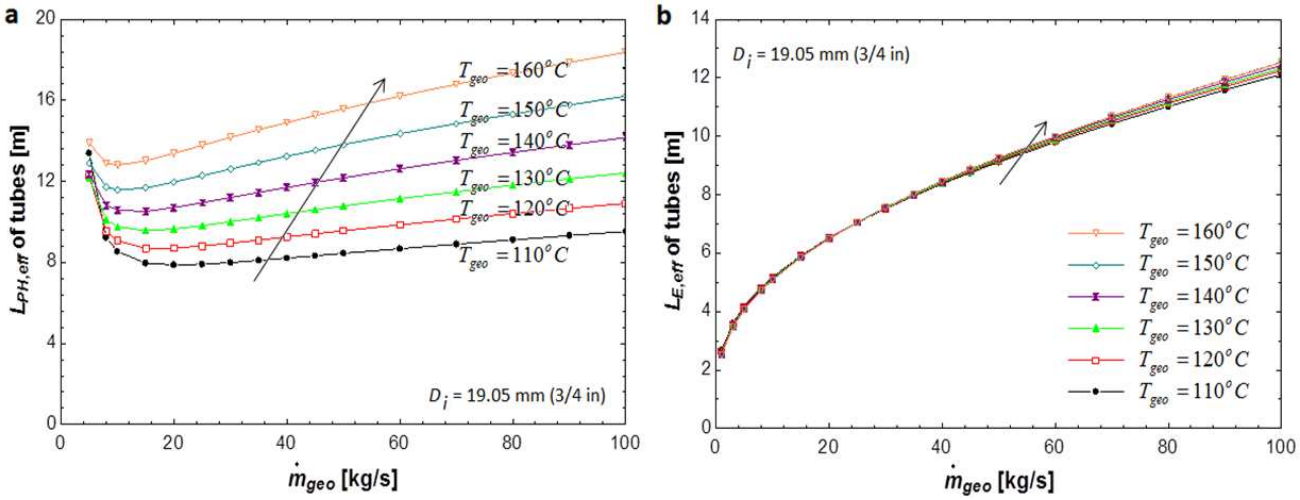

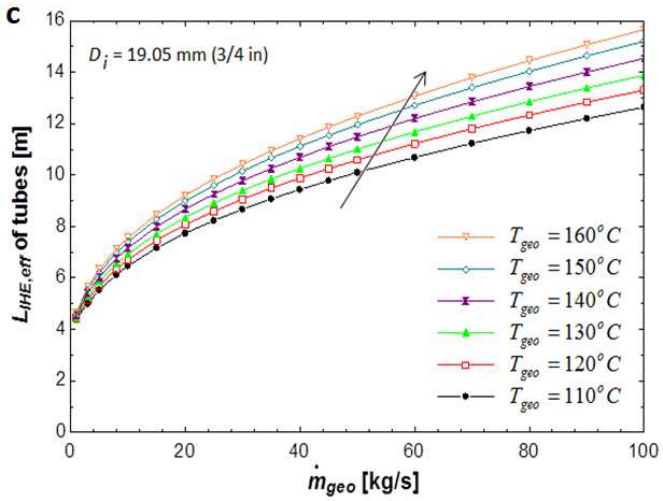

Figure 4. 30: Effective tube length of (a) preheater, (b) evaporator) and (c) recuperator) as a function of the geothermal mass flow rate

In Fig 4.31, the total pressure drop of the geothermal fluid and the pumping power requirement to move the desired amount of the geofluid through the preheater-evaporator unit were plotted as a function of the geothermal mass flow rate. The total pressure drop was determined from a summation of resulting pressure drop through each small increment section of the overall length of the preheater-evaporator unit and a nearly linear quality variation. As the geothermal fluid mass flow rate was increased, both the total pressure drop and the pumping power requirement were observed to increase exponentially. Moreover, it is worth mentioning the insignificant power requirement as compared to the total net power output from the turbine.

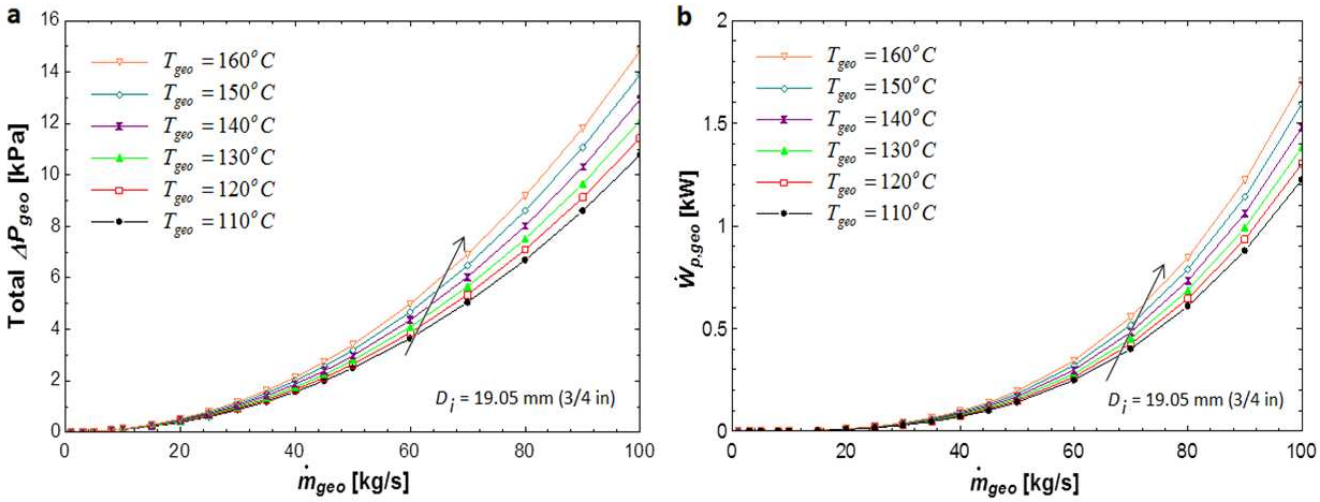

Figure 4. 31: (a) Total pressure drop and (b) pumping power requirement for the geofluid

4.5.3. Condenser

Likewise, the condenser was designed based on the operating and geometric constraints. Subject to operating constraints, the compact plate-fin-and-tube heat exchanger was sized for a given net turbine power output, chosen as one Megawatt. The heat exchanger effective tube length was determined while varying the number of tubes in the transversal direction. Three geometric design parameters were varied to optimize the effective length of the tubes required in the condensation process. These parameters include the number of rows or tubes in the longitudinal direction, the nominal tube diameter, and the fin spacing or pitch.

In Fig. 4.32a, the effective tube length of the condenser was determined for a variation in the number of rows or tubes in the longitudinal direction. For small values of the number of rows, the effective length of the tubes required for the condensation process was high. As the number of rows increased, the size of the condenser was significantly reduced. Similar conclusions can be drawn with the variation in the nominal tube diameter (Fig. 4.32b) and number of fins (Fig. 4.32c), where the size of the condenser was observed to decrease with the increase in both the diameter of the tubes and fin spacing, respectively. In Fig. 4.32d, only a marginal increase in the effective tube length of the condenser was observed with the increment in the geothermal resource temperature. This was certainly dictated by the nearly identical optimal condensing operating conditions at different geothermal resource temperatures.

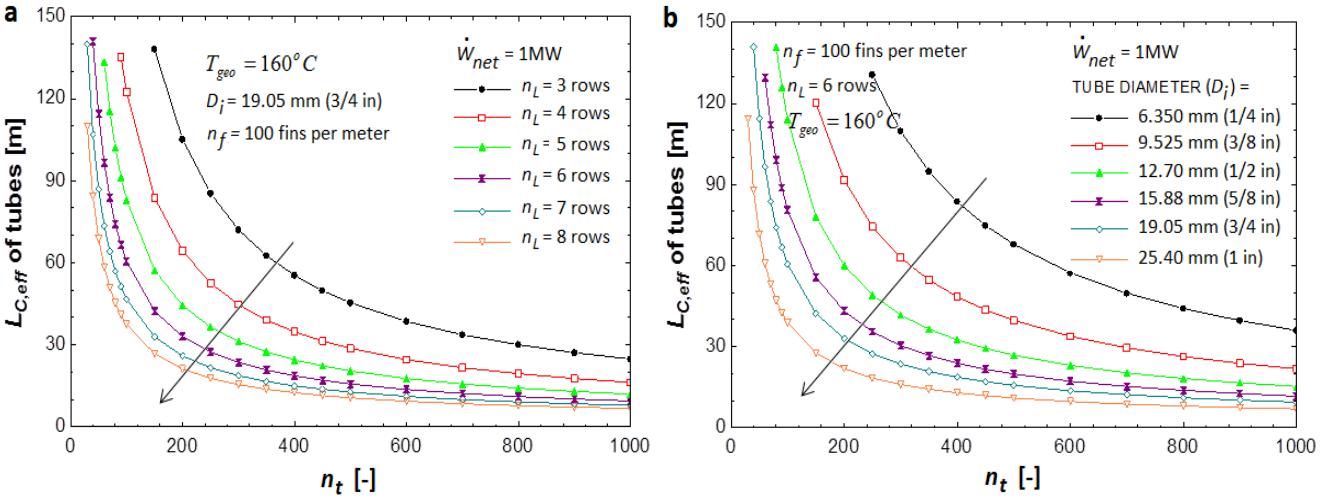

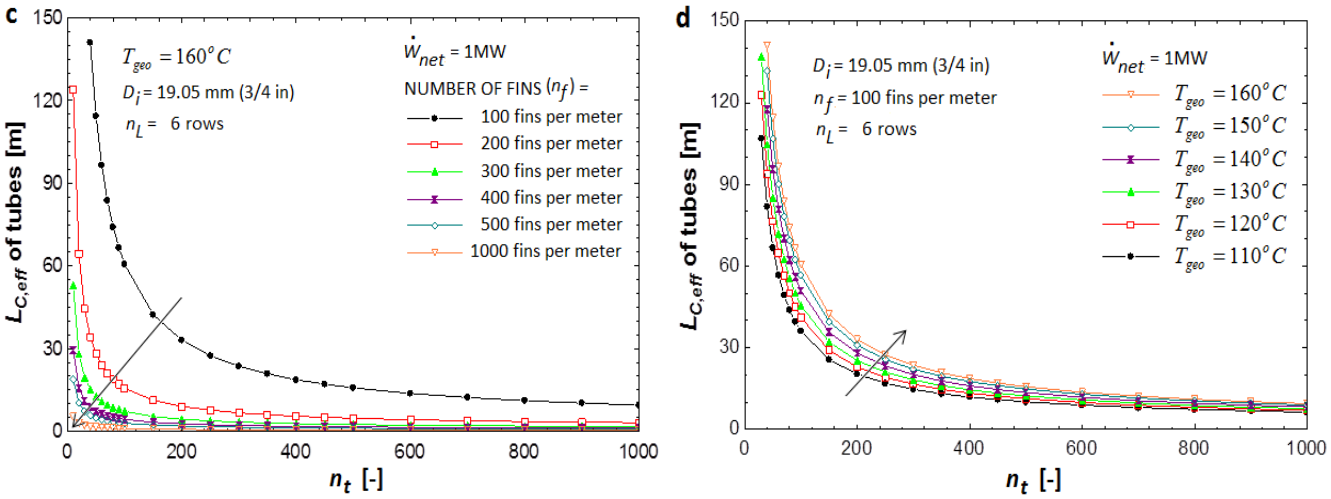

Figure 4. 32: Effective tube length of the condenser with variation in (a) number of rows, (b) tube diameter, (c) number of fins, and (d) geothermal resource temperature

Subject to the geometric constraints, the compact plate-fin-and-tube heat exchanger was sized for the fixed geometric design parameters and variation in the geothermal resource temperature. In Fig. 4.33, the effective tube length of the condenser was observed to increase exponentially with the increment in the frontal flow velocity of the cooling air. Alike the evaporator, the change in the effective length of the condenser tubes was seen to be nearly independent on the temperature of the geothermal resource. This robust behaviour can also be justified by the unique optimal condensing condition for every geothermal resource temperature.

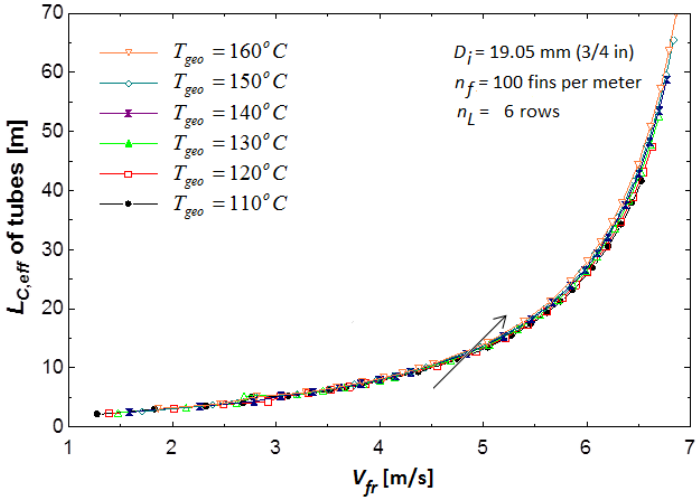

Figure 4. 33: Effective tube length of the condenser with variation in the frontal flow velocity of the cooling air

In Fig 4.34, both the total pressure drop and fan power requirement were observed to increase exponentially with the frontal flow velocity of the cooling air, and insignificantly with the temperature of the geothermal resource. It is worth mentioning the substantial fan power requirement.

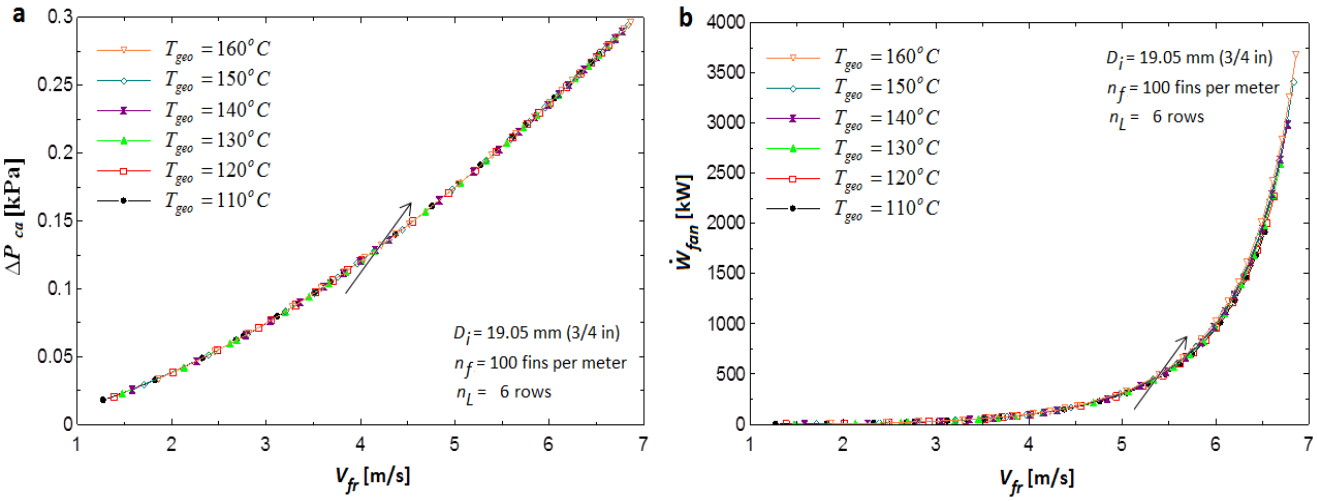

Figure 4. 34: (a) Total pressure drop and (b) fan power requirement for the cooling air

4.5.4. Turbine

A preliminary design and sizing of the turbine was considered. In Fig. 4.35, the turbine size parameter was plotted as a function of the geofluid mass flow rate. At low mass flow rate of the geothermal fluid, the turbine size parameter was observed to increase sharply as compared to a nearly linear increment at higher values of the geofluid mass flow rate. Moreover, the turbine size parameter was also observed to increase with the geothermal fluid temperature as a result of high optimal evaporating temperatures.

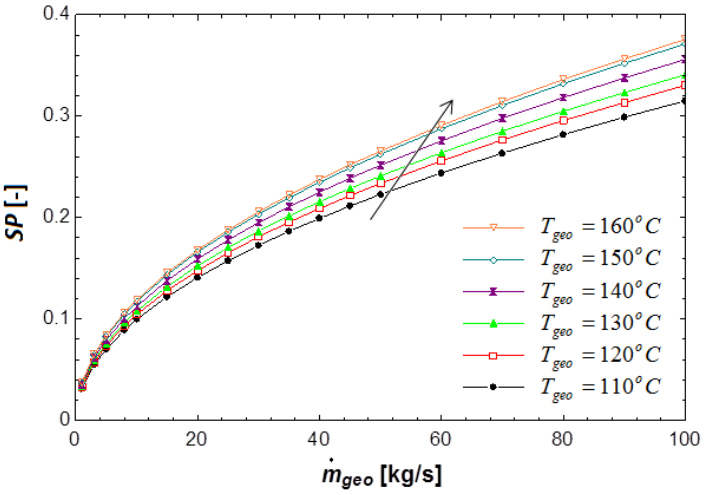

Figure 4. 35: Turbine size parameter as a function of the geothermal mass flow rate

4.6. Future work

One of the prospects for further study is an investigation on advanced geothermal energy conversion systems proposed by diverse researchers claiming to improve the plant thermal efficiency and raise the cycle power output of the geothermal power plants operating with moderately low-temperature geothermal resources. Among others, we may mention the dual-level binary geothermal power plant [18], the supercritical or trans-critical power cycles [25,120-123], a recovery heat exchanger (RHE) with a cascade of evaporators with both high- and low-pressure turbines operating in a Kalina cycle [26], a combined plant such as the hybrid fossil-geothermal system [26], a dual-fluid or multicycle with different thermodynamic properties [28], an advanced ORC using a secondary organic loop [91], power cycles with two or more back pressure steam turbines [91], etc.

A more detail design and optimization of the downhole heat exchanger can also be considered in further studies to account for the transient effect or time-dependent cooling of the Earth underground [118], while determining the optimum amount and size of perforations at the inner pipe entrance region to regulate the flow of the geothermal fluid.

Although the present study limited itself to the thermodynamic performance of pure organic fluids based on their thermodynamic properties, a more complete analysis has to consider also mixtures [41,79,119,124] and subject the selection to chemical stability and compatibility with materials, environmental impacts, safety concerns and economical operation of the organic binary fluids [77-80].

Finally, a thermoeconomic or exergoeconomic analysis is of most importance to discuss the viability and economic feasibility of electricity generation through advanced geothermal energy technologies [125-129].

CHAPTER 5

CONCLUSIONS AND RECOMMENDATIONS

Although the development of the geothermal energy for power generation has been exploited many decades ago, the technology related to viable and economical geothermal power generation is still immature. In this thesis, a thermodynamic optimization of small binary-cycle geothermal power plants operating with moderately low-temperature and liquid-dominated geothermal resources in the range of 110^{o}C to 160^{o}C, and cooling air at ambient conditions of 25^{o}C and 101.3 kPa, reference temperature and atmospheric pressure, respectively, was considered. The thermodynamic optimization process and entropy generation minimization (EGM) analysis were performed to minimize the overall exergy loss of the power plant, and the irreversibilities associated with heat transfer and fluid friction caused by the system components. The effect of the geothermal resource temperature to impact on the cycle power output of the ORC was studied, and it was found that the maximum cycle power output increases exponentially with the geothermal resource temperature. In addition, an optimal turbine inlet temperature was determined, and observed to increase almost linearly with the increase in the geothermal heat source.

Furthermore, a downhole coaxial geothermal heat exchanger was modeled and sized subject to a nearly linear increase in geothermal gradient with depth. The coaxial pipes dimensions and geofluid circulation flow rate were optimized to ensure minimum pumping power and maximum extracted heat energy from the Earth's deep underground (2 km and deeper below the surface). Transient effect or time-dependent cooling of the Earth underground, and the optimum amount and size of perforations at the inner pipe entrance region to regulate the flow of the geothermal fluid were disregarded to simplify the analysis. An optimal diameter ratio of the coaxial pipes for minimum pressure drop in both limits of the fully turbulent and laminar fully-developed flow were determined and observed to be nearly the same irrespective of the flow regime, whereas the optimal geofluid mass flow rate for maximum net power output increased exponentially with the flow Reynolds number. It is worth mentioning that the temperature of the geothermal resource was highly dependent on the site underground temperature gradient and the depth of the coaxial downhole heat exchanger to reach higher underground base temperatures, whereas the geofluid rejection temperature was limited by the dead state environmental design conditions.

Several organic Rankine Cycles were also considered as part of the study. The basic types of the ORCs were observed to yield maximum cycle power output. The addition of an IHE and/or an OFOH improved significantly the effectiveness of the conversion of the available geothermal energy into useful work, and increased the thermal efficiency of the geothermal power plant. Therefore, the regenerative ORCs were preferred for high-grade geothermal heat. However, to avoid a susceptible thermal pollution of the environment caused by the geofluid being discarded as waste heat at relatively high temperature, a combined power generation and direct use in process or district heating applications as a cogeneration system can be an additional option to improve the energy utilization [21,116].

In addition, a performance analysis of several organic binary fluids, namely refrigerants R123, R152a, isobutane and n-pentane, was conducted under saturation temperature and subcritical pressure operating conditions of the turbine. Organic fluids with higher boiling point temperature, such as n-pentane, were recommended for the basic type of ORCs, whereas those with lower vapour specific heat capacity, such as butane, were more suitable for the regenerative ORCs.

Finally, using basic thermal and heat transfer principles, all system components were designed, modeled and sized.

References

[1] EIA 2012, *Annual Energy Outlook 2012*, Report No.: DOE/EIA-0383(2012). U.S. Energy Information Administration, Washington, 258 pp.

[2] Yekoladio, PJ 2010, 'Solar Water Heating system for a household geyser', Graduate thesis, University of Pretoria, Pretoria.

[3] Bassfeld Technology Transfer 2009, *Geothermal Power Generation: Economically viable electricity generation through advanced geothermal energy technologies*, Switzerland.

[4] Threshold Energy Corporation, *Geothermal Basics*, viewed 10 December, 2010, <www.gothreshold.com/image/GT_solar_absorption.gif>.

[5] Turcotte, DL & Schubert, G 2002, *Geodynamics*, 2nd edn, Cambridge, England, UK: Cambridge University Press. pp. 136–137.

[6] Pollack, HN, Hurter, SJ & Johnson, JR 1993, 'Heat flow from the Earth's interior: Analysis of the Global Data Set', http://www.agu.org/pubs/crossref/1993/93RG01249.shtml, Rev, *Geophys*, vol. 30, no. 3, pp. 267-280, http://www.agu.org/pubs/crossref/1993/93RG01249.shtml.

[7] Fridleifsson, IB, Bertani, R, Huenges, E, Lund, JW, Ragnarsson, A, Rybach, L, Homhmeyer, O & Trittin, T 2009, *The possible role and contribution of geothermal energy to the mitigation of climate change*, (http://iga.igg.cnr.it/documenti/IGA/Fridleifsson_et_al_IPCC_Geothermal_paper_2008.pdf), Luebeck, Germany, pp.59-80. http://iga.igg.cnr.it/documenti/IGA/Fridleifsson_et_al_IPCC_Geothermal_paper_2008.pdf, retrieved 2009-04-06.

[8] Bertani, R 2012, 'Geothermal power generation in the world 2005-2010 update report', *Geothermics*, vol. 41, no.1, pp. 1-29.

[9] IEA ETSAP 2010, *Geothermal heat and power*, May 2010 edition, Energy Technology Systems Analysis Programme, USA.

[10] World Energy Council 2010, *2010 Survey of Energy Resources*, London.

[11] DiPippo, R 1998, 'Geothermal Power Systems', in Elliott, TC, Chen, K & Swanekamp, RC, *Standard handbook of power plant engineering*, 2nd edn, MacGraw-Hill, New York, pp. 8.27 - 8.60.

[12] Kutscher, FC 2000, *The Status and future of geothermal electric power*, American Solar Energy Society Conference, Madison, June 16-21, 2000, National Renewable Energy Laboratory, Colorado.

[13] EERE 2009, *Geothermal Technologies Program – Recovery Act Funding Opportunities*, Energy Efficiency & Renewable Energy, USA, 59 pp.

[14] Bejan, A 1999, 'Thermodynamic optimization Alternatives: Minimization of Physical Size Subject to Fixed Power', *International Journal of Energy Research*, vol. 23, no. 1, pp. 1111-1121.

[15] Yilmaz, M, Sara, ON & Karsli, S 2001, 'Performance evaluation criteria for heat exchangers based on the second law analysis', *Exergy, an International Journal*, vol. 4, no. 1, pp. 278-294.

[16] Koroneos, C, Spachos, T & Moussiopoulos, N 2003, 'Exergy analysis of renewable energy sources', *Renew Energy*, vol. 28, pp. 295–310.

[17] Hepbasli, A 2008, 'A key review on exergetic analysis and assessment of renewable energy resources for a sustainable future', *Renewable and Sustainable Energy Reviews*, vol. 12, pp. 593-661.

[18] Kanoglu, M 2002, 'Exergy analysis of a dual-level binary geothermal power plant', *Geothermics*, vol. 31, pp. 709–24.

[19] Yari, M 2010, 'Exergetic analysis of various types of geothermal power plants', *Renewable Energy*, vol. 35, no. 1, pp. 112-121.

[20] Bodvardson, G & Eggers, DE 1972, 'The exergy of thermal water', *Geothermics*, vol. 1, no. 3, pp. 93–5.

[21] Kanoglu, M & Bolatturk, A 2008, 'Performance and parametric investigation of a binary geothermal power plant by exergy', *Renewable Energy*, vol. 33, no. 1, pp. 2366–74.

[22] Franco, A 2011, 'Power production from a moderate temperature geothermal resource with regenerative Organic Rankine Cycles', *Energy for Sustainable Development*, vol. 15, pp. 411-419.

[23] DiPippo, R 2004, 'Second Law assessment of binary plants generating power from low-temperature geothermal fluids, *Geothermics*, vol. 33, no.1, pp. 565–86.

[24] Madhawa, HD, Mihajlo, G, Worek, WM & Yasuyuki, I 2007, 'Optimum design criteria for an organic Rankine cycle using low temperature geothermal heat sources', *Energy*, vol. 32, no. 1, pp. 1698–706.

[25] Gu, Z & Sato, H 2001, 'Optimization of cyclic parameters of a supercritical cycle for geothermal power generation', *Energy Conversion and Management,* vol. 42, pp. 1409-1416.

[26] DiPippo, R 2008, *Geothermal power plants principles, applications, case studies and environmental impact,* Butterworth-Heinemann, London.

[27] Desai, N & Bandyopadhyay, S 2009, 'Process integration of organic Rankine cycle', *Energy*, vol. 34, no. 1, pp. 1674-86.

[28] Gnutek, Z & Bryszewska-Mazurek, A 2001, 'The thermodynamic analysis of multicycle ORC engine', *Energy*, vol. 26, no. 1, pp. 1075-1082.

[29] Borsukiewicz-Gozdur, A & Nowak, W 2007, 'Maximising the working fluid flow as a way of increasing power output of geothermal power plant', *Applied Thermal Engineering*, vol. 27, pp. 2074–8.

[30] Calm, JM & Hourahan, GC, 2001, 'Refrigerant Data Summary', *Engineered Systems*, vol. 18, no. 11, pp. 74-88.

[31] Fridleifsson, Ingvar B., Bertani R., Huenges E., Lund, JW., Ragnarsson A., Rybach L., Hohmeyer O. & Trittin T. 2009, The possible role and contribution of geothermal energy to the mitigation of climate change, Luebeck, Germany, pp. 59–80.

[32] Alfe, D, Gillan, MJ & Price, GD 2003, 'Thermodynamics from first principles: temperature and composition of the Earth's core', *Mineralogical Magazine,* vol. 67, no. 1, pp. 113–123.

[33] The NEED project 2010, *Secondary Energy Infobook*, viewed on 10 December, 2010, <www.NEED.org>.

[34] EPRI 2010, *Geothermal Power: Issues, Technologies, and Opportunity for Research, Development, Demonstration, and Deployment.*

[35] Long, M et al 2003, *Geothermal Power Production: Steam for Free*, POWER Engineers, Idaho, viewed 10 December, 2010, <http://www.powereng.com/uploadedFiles/News/Articles/Power-Gen-Geothermal.pdf>.

[36] US department of Energy, *Low-Temperature and Co-produced Geothermal Resources*, viewed 10 December, 2010, <http://www1.eere.energy.gov/geothermal/low_temperature_resources.html>.

[37] EIA 2008, *Existing Electric Generating Units in the United States.*

[38] DiPippo, R, Khalifa, HE, Correia, RJ & Kestin, J 1979, 'Fossil Superheating in Geothermal Steam Power Plants', *Geothermal Energy Magazine*, vol. 7, no. 1, pp. 17-23.

[39] Khalifa, HE, DiPippo, R & Kestin, J 1978, 'Geothermal Preheating in Fossil-Fired Steam Power Plants', *in proceedings of the Thirteenth Intersociety Energy Conversion Engineering Conference*, vol. 2, pp. 1068-1073.

[40] DiPippo, R & Ellis, P 1990, *Geothermal Power Cycle Selection Guidelines*, EPRI Geothermal Information Series, Part 2, Palo Alto, CA.

[41] Lund, JW 2006, *Geothermal energy focus: tapping the earth's natural heat*, Refocus.

[42] Business Insights 2010, *Green Energy in Africa: Renewable sources, capacity growth, legislation, and the future outlook*, Business Insights Ltd, viewed on 10 December, 2010, <http://www.boplearninglab.dk/fileadmin/boplearninglab_uploads/dokumenter/external-docs/Green_Energy_in_Africa.pdf>.

[43] Tester, JW et al. 2006, *The Future of Geothermal Energy, Impact of enhanced geothermal systems (EGS) on the United States in the 21st Century: An Assessment*, Idaho National Laboratory, Idaho Falls, pp. 1–8 to 1–33.

[44] EERE 2009, *2008 Geothermal Technologies Market Report*, Energy Efficiency & Renewable Energy (EERE), US Department of Energy, viewed on 10 December, 2010, <http://www.nrel.gov/applying_technologies/pdfs/46022.pdf>.

[45] Entingh, DJ, Easwaran, E & McLarty, L 1994, 'Small Geothermal Electric Systems for Remote Powering', *Geothermal Ressources Council Transactions*, vol. 18, no. 1, pp. 39-46.

[46] Gawlik, K & Kutscher, C 2000, 'Investigation of the opportunity for small-scale geothermal power plants in the western United States', *Geothermal Resources Council Transactions*, vol. 24, pp. 109-112.

[47] Geothermal Energy Association 2010, *Geothermal Energy: International Market Update*, Geothermal Energy Association, Washington.

[48] US Energy Information Administration 2010, *Annual Energy Outlook*, Washington.

[49] Bertani, R 2010, 'Geothermal Power Generation in the World 2005-2010: Update Report', *in proceedings of the World Geothermal Congress 2010*, Bali, Indonesia, paper no. 0008.

[50] Barbier, E 2002, 'Geothermal energy technology and current status: an overview', *Renewable and Sustainable Energy Reviews*, vol. 6, pp. 3-65.

[51] ATSE Stelr Project, *Renewable energy: Geothermal Energy*, viewed on 10 December, 2010 <http:// stelr.org.au/geothermal-energy>.

[52] Smit, P 2010, *Despite geolocal limitations, SA begins to weigh its geothermal options*, Engineering news, Johannesburg.

[53] Tsibalo, AE, Olivier, J & Venter, J 2010, *South Africa Geothermal Country Update (2005-2009)*, Country Updates: Africa, Johannesburg.

[54] Lund, JW 2007, 'Characteristics, Development and utilization of geothermal resources', *Geo-Heat Centre Quarterly Bulletin* (Klamath Falls, Oregon: Oregon Institute of Technology), Oregon.

[55] Bargagli, R, Catenil, D, Nellil, L, Olmastronil, S & Zagarese, B 1997, *Environmental Impact of Trace Element Emissions from Geothermal Power Plants, Environmental Contamination Toxicology*, Springer, New York.

[56] Sonntag, RE, Borgnakke, C & Van Wylen, GJ 2003, *Fundamentals of thermodynamics*, John Wiley, New York.

[57] Bejan, A, Tsatsaronis, G & Moran, M 1996, *Thermal design and optimization*, Wiley, New York.

[58] Dincer, I, Hussain, MM & Al-Zaharnah, I 2004, 'Energy and exergy use in public and private sector of Saudi Arabia', *Energy Policy*, vol. 32, no. 141, pp. 1615–24.

[59] Bejan, A 1988, *Advanced Engineering Thermodynamics*, Wiley, New York.

[60] Hesselgreaves, JE 2000, 'Rationalisation of Second Law analysis of heat exchangers', *International Journal of Heat and Mass Transfer*, vol. 43, pp. 4189–4204.

[61] Witte, LC & Shamsundar, N 1983, 'A thermodynamic efficiency concept for heat exchange devices', *Journal Engineering Power*, vol. 105, pp. 199–203.

[62] London, AL & Shah, RK 1983, 'Costs of irreversibilities in heat exchanger design', *Heat Transfer Engineering*, vol. 4, pp. 59– 73.

[63] Bejan, A 1982, *Entropy Generation through Heat and Fluid Flow*, Wiley, New York.

[64] Lee, KC 1996, 'Classification of geothermal resources an engineering approach', *in proceedings of 21st workshop on geothermal reservoir engineering*, Stanford University, 5pp.

[65] Lee, KC 2001, 'Classification of geothermal resources by exergy', *Geothermics*, vol. 30, pp. 431–42.

[66] Das, SK & Roetzel, W 1998, 'Second Law analysis of a plate exchanger with an axial dispersive wave', *Cryogenics*, vol. 38, pp. 791–798.

[67] Prasad, RC & Shen, J 1993, 'Performance evaluation of convective heat transfer enhancement devices using exergy analysis', *International Journal of Heat and Mass Transfer*, vol. 36, pp. 4193–4197.

[68] Bruges, EA 1959, *Available Energy and the Second Law Analysis*, Butterworhts, London.

[69] Reistad, GM 1970, 'Availability: concepts and applications', Ph.D. thesis, University of Wisconsin, Madison.

[70] Mukherjee, P, Biswas, G, & Nag, PK 1987, 'Second Law analysis of heat transfer in swirling through a cylindrical duct', *Journal of Heat Transfer*, vol. 109, no. 2, pp. 308–313.

[71] DiPippo, R 1994, 'Second Law analysis of flash-binary and multilevel binary geothermal power plants', *Geotherm Resource Council Transactions*, vol. 18, pp. 505–10.

[72] Van Gool, W 1997, 'Energy policy: fairly tales and factualities', *in Soares ODD, Martins da Cruz A, Costa Pereira G, Soares IMRT, Reis AJPS, editors*, innovation and technology-strategies and policies, Dordrecht: Kluwer, pp. 93–105.

[73] Aljundi, IH 2011, 'Effect of dry hydrocarbons and critical point temperature on the efficiencies of organic Rankine cycle', *Renewable Energy*, vol. 36, no.1, pp. 1196-1202.

[74] Kanoglu, M 2002, 'Exergy analysis of a dual-level binary geothermal power plant', *Geothermics*, vol. 31, no. 1, pp. 709-724.

[75] Subbiah, S & Natarajan, R 1988, 'Thermodynamic analysis of binary-fluid rankine cycles for geothermal power plants', *Energy Conversion and Management*, vol. 28, no. 1, pp. 47-52.

[76] Franco, A & Villani, M 2009, 'Optimum design of binary cycle power plants for water-dominated, medium-temperature geothermal fields', *Geothermics*, vol. 38, no.1, pp. 379-391.

[77] Tchanche, BF, Lambrinos, Gr, Frangoudakis, A & Papadakis G 2011, 'Low-grade heat conversion into power using organic Rankine cycles- A review of various applications', *Renewable and Sustainable Energy Review*, vol. 15, no.1, pp. 3963-3979.

[78] Saleh, B, Koglbauer, G, Wendland M & Fischer, J 2007, 'Working fluids for low-temperature organic Rankine cycles', *Energy*, vol. 32, no. 7, pp. 1210-1221.

[79] DiPippo, R 1999, 'Small geothermal power plants: Design, performance and economics', *Geothermal Resources Council BULLETIN*, pp. 1-8.

[80] Maizza, V & Maizza, A 1996, 'Working fluids in non-steady flows for waste energy recovery systems', *Applied Thermal Engineering*, vol. 16, no. 1, pp. 579–90.

[81] Klein, SA 2012, 'Engineering Equation Solver EES Academic Commercial V7.933', McGraw Hill. See also https://www.fchart.com.

[82] Chen, H, Goswami, DY & Stefanakos, EK 2010, 'A review of thermodynamic cycles and working fluids for the conversion of low-grade heat', *Renewable and sustainable energy reviews*, vol. 14, no. 1, pp. 3059-3067.

[83] Bejan, A 1993, *Heat transfer*, Wiley, New York.

[84] Demuth, OJ & Kochan, RJ 1981, *Analyses of mixed hydrocarbon binary thermodynamic cycles for moderate temperature geothermal resources using regeneration techniques*, INEL Rep. EGG-GTH-05710, Idaho Falls, ID.

[85] Mago, PJ, Chamra, LM, Srinivasan, K & Somayaji, C, 2008, 'An examination of regenerative organic Rankine cycles using dry fluids', *Applied Thermal Engineering*, vol. 28, no. 1, pp. 998-1007.

[86] Gu, Z & Sato, H 2001, 'Optimization of cyclic parameters of a supercritical cycle for geothermal power generation', *Energy Conversion and Management*, vol. 42, no. 1, pp. 1409-1416.

[87] Bejan, A & Lorente, S 2008, *Design with constructal theory*, John Wiley & Sons, New Jersey.

[88] White, FM 2008, *Fluid mechanics*, 6th edn, McGraw-Hill, New York.

[89] Zimparov, V 2001, 'Extended performance evaluation criteria for enhanced heat transfer surfaces: heat transfer through ducts with constant heat flux', *International Journal of heat and Mass Transfer*, vol. 44, no. 1, pp. 169-180.

[90] Gnielinski, V 1983, 'Forced convection in ducts', in Spalding, DB & Taborek, J, *Heat Exchanger Design Handbook*, Hemisphere Publishing Corporation, Dusseldorf, pp. 2.5.1-1 to 2.5.1-10.

[91] Kaplan, U 2007, *Advanced organic Rankine cycles in binary geothermal power plants*, World Energy Council, Ormat Technologies, inc.

[92] Wark, KJ 1995, *Advanced thermodynamics for engineers*, McGraw-Hill, New York.

[93] Lopez, A, Dodson, C & Razani, A 2008, 'Second Law analysis and optimization of regenerators using regen 3.2', *AIP conference proceedings 985*, 720; doi:10.1063/1.2908663.

[94] Lakew, AA & Bolland, O 2010, 'Working fluids for low-temperature heat source', *Applied Thermal Engineering*, vol. 30, no. 1, pp. 1262-1268.

[95] Badr, O & Probert, D 1990, 'Thermal-Design Data for Evaporators of ORC Engines Utilising Low-Temperature Heat Sources', *Applied Energy*, vol. 37, no. 1, pp. 111-138.

[96] Wang, Y, Pan, M, Bulatov, I, Smith, R & Kim, JK 2012, 'Application of intensified heat transfer for the retrofit of heat exchanger network, *Applied Energy*, vol. 89, no. 1, pp. 45-59.

[97] Kern, DQ 1950, *Process Heat Transfer*, McGraw-Hill, New York.

[98] Kakac, S & Liu, H 2002, *Heat exchangers: Selection, Rating and Thermal design*, 2nd edn, CRC Press, Florida.

[99] Schmidt, TE 1945, 'La Production Calorifique des Surfaces Munies d'ailettes', *Annexe Du bulletin De L'Institut International Du Froid*, Annexe G-5.

[100] Wright, MF 2000, 'Plate-fin-and-tube condenser performance and design for refrigerant R-410a air conditioner', Masters Theses, Georgia Institute of Technology, Atlanta.

[101] Thome, JR 2004, *Engineering data book III*, Wolverine Tube, Lausanne.

[102] Bejan, A & Kraus, A 2003, *Heat Transfer Handbook*, John Wiley & Sons, New Jersey.

[103] Andersen, WC & Bruno, TJ 2005, 'Rapid screening of fluids for chemical stability in organic Rankine cycle applications', *Industrial and Engineering Chemistry Research*, vol. 44, pp. 5560–6.

[104] Invernizzi, C, Iora, P & Silva, P 2007, 'Bottoming micro-Rankine cycles for micro-gas turbines', *Applied Thermal Engineering*, vol. 27, pp. 100–110.

[105] Gnielinski, V 1976, 'New Equations for Heat and Mass Transfer in Turbulent Pipe and Channel Flow', *International Chemical Engineering*, vol. 16, pp. 359–366.

[106] Ganguli, A, Tung, SS & Taborek, J 1985, 'Parametric Study of Air Cooled Heat Exchanger Finned Tube Geometry', *AIChE Symp. Ser.*, vol. 81, no. 245, pp. 122-128.

[107] Kern, DQ & Kraus, AD 1972, *Extended Surface Heat Transfer*, McGraw-Hill, New York.

[108] Rich, DG 1973, 'The Effect of Fin Spacing on the Heat Transfer and Friction Performance of Multi-Row, Smooth Plate Fin-and-Tube Heat Exchangers', *ASHRAE Transactions*, vol. 79, no. 2, pp. 137-145.

[109] Robinson, KK & Briggs, DE 1966, 'Pressure Drop of Air Flowing Across Triangular Pitch Banks of Finned Tubes',*AIChE Chem. Eng. Prog. Symp. Ser.*, Vol. 62, no. 64, pp. 177-184.

[110] Gungor, KE & Winterton, RHS 1987, 'Simplified general correlation for saturated flow boiling and comparisons of correlations with data', *Chemical Engineering Research and Design*, vol. 65, no. 1, pp. 148–156.

[111] Steiner, D 1993, *VDI-Wärmeatlas (VDI Heat Atlas)*, Verein Deutscher Ingenieure, VDI-Gesellschaft Verfahrenstechnik und Chemieingenieurwesen (GCV), Düsseldorf, Capter Hbb.

[112] Friedel, L 1979, 'Improved Friction Pressure Drop Correlations for Horizontal and Vertical Two-Phase Pipe Flow', in *European Two-Phase Flow Group Meeting, Ispra, Italy, June*, Paper E2.

[113] Shah, MM 1979, 'A General correlation for heat transfer during film condensation inside pipes', *International Journal of Heat and Mass Transfer*, vol. 22, no. 1, pp. 547–556.

[114] Çengel, YA 2006, *Heat and Mass Transfer*, 3rd edition, McGraw-Hill, New York.

[115] Hammock, GL 2011, 'Cross-Flow, Staggered-Tube Heat Exchanger Analysis for High Enthalpy Flows', Masters Theses, University of Tennessee, Knoxville.

[116] Guo, T, Wang, HX & Zhang, SJ 2011, 'Fluids and parameters optimization for a novel cogeneration system driven by low-temperature geothermal sources', *Energy*, vol. 36, no. 1, pp. 2639-2649.

[117] Grassiani, M 2000, 'Siliceous scaling aspects of geothermal power generation using binary cycle heat recovery', *in proceedings of the 2000 World Geothermal Congress, 28 May- 10 June*, Kyushu-Tohoku, Japan, pp. 3167-3171.

[118] Lim, JS, Bejan, A & Kim, JH 1992, 'Thermodynamics of energy extraction from fractured hot dry rock', *International journal of heat and fluid flow*, vol. 13, no. 1, pp. 71-77.

[119] Wang, JL, Zhao, L & Wang, XD 2010, 'A comparative study of pure and zeotropic mixtures in low-temperature solar Rankine cycle', *Applied Energy*, vol. 87, pp. 3366–73.

[120] Gu, Z & Sato, H 2002, 'Performance of supercritical cycles for geothermal binary design', *Energy conversion and management*, vol. 43, no.7, pp. 961-971.

[121] Shengjun, Z, Huaixin, W & Tao, G 2011, 'Performance comparison and parametric optimization of subcritical Organic Rankine Cycle (ORC) and transcritical power cycle system for low-temperature geothermal power generation', *Applied Energy*, vol. 88, pp. 2740–54.

[122] Chen, H, Goswami, DY, Rahman, MM & Stefanakos, EK 2011, 'Energetic and exergetic analysis of CO2- and R32-based transcritical Rankine cycles for low-grade heat conversion', *Applied Energy*, vol. 88, pp. 2802–8.

[123] Chen, H, Goswami, DY, Rahman, MM & Stefanakos, EK 2011, 'A supercritical Rankine cycle using zeotropic mixture working fluids for the conversion of low-grade heat into power', *Energy*, vol. 36, pp. 549–55.

[124] Demuth, OJ 1981, *Analyses of mixed hydrocarbon binary thermodynamic cycles for moderate temperature geothermal resources*, INEL Rep. EGG-GTH-5753, Idaho Falls, ID.

[125] Karytsas, C & Mendiros, D 2007, 'Efficient low temperature geothermal binary power (Low-Bin)', *in the proceedings of DG-TREN Funded Strep Programme, European Geothermal Congress EGC 2007, May 30–June 1, 2007*, Unterhaching, Germany.

[126] Rentizelas, A, Karellas, S, Kakaras, E & Tatsiopoulos, I 2009, 'Comparative techno-economic analysis of ORC and gasification for bioenergy applications', *Energy Conversion and Management*, vol 50, no. 3, pp. 674–81.

[127] Schuster, A, Karellas, S, Kakaras, E & Spliethoff, H 2009, 'Energetic and economic investigation of organic Rankine cycle applications', *Applied Thermal Engineering*, vol. 29, no. 6, pp. 1809–17.

[128] Manolakos, D, Mohamed, ES, Karagiannis, I & Papadakis, G 2008, 'Technical and economic comparison between PV-RO system and RO-solar Rankine system, Case study: Thirasia Island', *Desalination*, vol. 221, no. 3, pp.37–46.

[129] Kosmadakis, G, Manolakos, D, Kyritsis, S & Papadakis, G 2009, 'Economic assessment of a two-stage solar organic Rankine cycle for reverse osmosis desalination', *Renewable Energy*, vol. 34, pp. 1579–86.

Appendix A: Typical characteristics of the geothermal power plants

Geothermal power plants	Dry-steam	Flash-Steam	Binary-cycle
Power cycle & Energy conversion			
Loops	1	1	2
Primary heat transfer medium	Dry steam	High-pressure superheated water	Hot geothermal water
Secondary heat transfer medium	-	-	Refrigerant R-114 or R-134a, Propane, Isobutane or Isopentane hydrocarbons
Geofluid flow rate, tons/h	400 – 1,000	500 – 2,800	700 – 3,600
Reservoir depth, km	≤ 1.5	≥ 1.5	1.5 - 3
Rating, MW	From small (10-15) to moderate size (55-60) and up to 135 per unit	15 - 60	1 - 65
Thermal hydraulics			
Resource temperature, ^{o}C	170 – 370 (Vapour-dominated)	170 - 250 (Liquid-dominated)	70 -170
Wellhead pressure, MPa	0.5 - 0.8	0.5 - 1.0	1.0 - 4.0
Ejectate temperature, ^{o}C	35 - 40	25 - 50	65 - 85
Exhaust pressure, MPa	0.007 - 0.010	0.004 - 0.013	0.2 - 0.5
Equipment			
Downwell pumps and motors	-	-	- Multistage centrifugal pumps, lineshaft-driven from surface-mounted electric motors or submersible electric pumps
Noise abatement system	- Rock mufflers for stacked steam - Acoustic insulation for noisy fluid-handling components	- Rock mufflers for stacked steam - Acoustic insulation for noisy fluid-handling components	-

Geothermal power plants	Dry-steam	Flash-Steam	Binary-cycle
Turbine-generator and controls	- Steam (Multistage, impulse/reaction turbine-generator with accessories - Control system - Air compressor	- Steam (Multistage, impulse/reaction turbine-generator with accessories - Control system - Air compressor Additional to Double-Flash plants: - Dual-pressure steam turbine-generator with accessories	- Working fluid turbine (axial or radial flow), generator and accessories - Control system
Brine and steam supply system	- Wellhead valves and controls - Sand/ particulate removal system - Steam purifier - Steam piping, insulation and supports - Steam header - Final moisture remover	- Wellhead valves and controls - Atmospheric discharge silencers - Steam cyclone separators - Ball-check valves - Steam purifier - Steam piping, insulation and supports - Brine piping, insulation and supports - Steam header - Final moisture remover for high-pressure steam line Additional to Double-Flash plants: - Flash vessels - Final moisture remover for low-pressure steam line	- Wellhead valves and controls - Sand/ particulate removal system and solid knock-out drum - Brine piping, insulation and supports - Preheater - Evaporator/superheater (Surface-Type)
Backup and Fire (if working fluid is flammable) protection systems	- Standby power supply	- Standby power supply	- Standby power supply - High-pressure sprinkler system - Flare stack

Geothermal power plants	Dry-steam	Flash-Steam	Binary-cycle
Condenser, gas ejection, and pollution control	- Condenser (Surface-Type or Direct-Contact) - Condensate pumps and motors - Gas removal system - NonCondensable Gases (NGS) treatment system	- Condenser (Direct-Contact) - Condensate pumps and motors - Gas removal system - NonCondensable Gases (NGS) treatment system	- Condenser (Surface-Type, Finned tube or Evaporative) - Condensate pumps and motors - Booster pumps - Dump tank and accumulator - Evacuation pumps to remove working fluid to storage during maintenance
Heat rejection system	- Water cooling tower - Cooling water pumps and motors - Cooling water treatment system	- Water cooling tower - Cooling water pumps and motors - Cooling water treatment system	Wet cooling system: - Water cooling tower with external source of makeup water - Cooling water pumps and motors - Cooling water treatment system Dry cooling system: - Air-cooled condensers with manifolds and accumulator - Induced-draft fans and motors
Brine and Condensate disposal system	- Injection wells for excess condensate and cooling tower blowdown	- Injection wells for excess condensate and cooling tower blowdown - Emergency holding pond Additional to Double-Flash plants: - Scale control system to mitigate deposition from waste brine before injection	- Brine return pumps and piping

Appendix B: Geothermal energy production, 2005, 2007 & 2010

Country	Installed Capacity [MW_e]			Annual energy Produced [GWh/year]			No. of units
	2005	2007	2010	2005	2007	2010	
Australia	0.2	0.2	1.1	0.5	n/a	0.5	2
Austria	1.1	1.1	1.4	3.2	n/a	3.8	3
China	27.8	27.8	24	96	178	150	8
Costa Rica	163.0	162.5	166	1145	1039	1131	6
El Salvador	151.0	204.2	204	967	1306	1422	7
Ethiopia	7.3	7.3	7.3	0	n/a	10	2
France (Guadeloupe)	14.7	14.7	16	102	94	95	3
Germany	0.2	8.4	7.1	1.5	54	50	4
Guatemala	33.0	53.0	52	212	339	289	8
Iceland	202.0	421.2	575	1483	2693	4597	25
Indonesia	797.0	992.0	1197	6085	6344	9600	22
Italy	791.0	810.5	843	5340	5183	5520	33
Japan	535.0	535.2	535	3467	3422	3064	20
Kenya	129.0	128.8	202	1088	824	1430	14
Mexico	953.0	953.0	958	6282	6094	7047	37
New Zealand	435.0	471.6	762	2774	3016	4055	43
Nicaragua	77.0	87.4	88	271	559	310	5
Papua New Guinea	6.0	56.0	56	17	358	450	6
Philippines	1930.0	1969.7	1904	9253	12,596	10,311	56
Portugal	16.0	23.0	29	90	147	175	5
Russia	79.0	79.0	82	85	505	441	11
Taiwan	n/a	n/a	3.3	n/a	n/a	n/a	n/a
Thailand	0.3	0.3	0.3	1.8	n/a	2.0	1
Turkey	20.0	38.0	91	105	243	490	5
United States	2564.0	2687.0	3098	17,917	15,883	16,603	210
TOTAL	8933	9732	10,898	56,786	60,877	67,246	536
No. of producing countries				24	24	46	

n/a: Data not available

Appendix C: Geothermal energy under development in Africa

Country	Installed capacity in 2010 [MW]	Estimated capacity by 2015 [MW]	Estimated geothermal potential [MW]	Project under development (location, time frame)	Utilities
Algeria	0	-	-	● Construction of a Binary cycle power plant (Guelma, -)	-
Comoros Island	0	-	3-10	● Feasibility studies, development and implementation of a geothermal program (Grand Comoro Island, April 2008-)	KenGen, GDA
Djibouti	0	-	230-460	● Construction of a 50MW geothermal power plant (Asal area, to be completed by 2012)	CERD, EDD, Reykjavik Energy
Ethiopia	7.3	45	640-1710	● Expansion to a full 30MW capacity of the Aluto-Langano Geothermal power plant (Southern Ethiopia) ● Rehabilitation of OEC (Aluto-Langano, 2006-July 2009) ● Rehabilitation of GCCU (Aluto-Langano, 2007) ● Development of a 5MW geothermal field with a 20MW reservoir potential (Tendaho, 2013) ● Geoscientific studies and the drilling of temeperature gradient wells (Corbetti and Tulu-Moye) ● Detailed scientific studies (Abaya, Fantale and Dofan areas) ● Reconnaissance investigation (Teo, Danab, Meteka, Kone, etc)	EEPCo, JMC, GDA, GSE

Country	Installed capacity in 2010 [MW]	Estimated capacity by 2015 [MW]	Estimated geothermal potential [MW]	Project under development (location, time frame)	Utilities
Kenya	167	530	850-1810	● Construction of 4x70 MW geothermal plants (Olkaria and Naivasha, early 2010-): * A contract between KenGen and Sinclair Knight Merz (from New Zealand) * Financed by Kenyan government, JICA, AFT, and the World Bank. * Project cost: US$1.4 billion ● Olkaria III Plant expansion (Olkaria, October 2010-2015) ● Development of Olkaria IV geothermal field, financed by the German Development Bank KfW ● Construction of a regional geothermal training centre, financed by Iceland, KenGen and UNU ● Construction of a small binary pilot plant (Eburru)	GDC, Ormat Technologies Inc, ARGeo, KenGen
Madagascar	0	-	-	● Development of a prototype (micro-geothermal) pre-feasibility study for a 50-100kW facility on 8 geothermal sites, to be financed by France	-
Rwanda	0	-	50-170	● Development of 300MW geothermal energy in 7 years To be financed by germany (BGR) and Chevron in conjunction with the Ministry of Environment and Natural Resources (MININFRA), the World Bank's Global Environment Facility (grant of US$4.5 million) and the Nordic Development Fund (grant of US$5.3 million).	-

Country	Installed capacity in 2010 [MW]	Estimated capacity by 2015 [MW]	Estimated geothermal potential [MW]	Project under development (location, time frame)	Utilities
Rwanda				● Further geological, geochemical and geophysical surface surveys and construction of 3 drilling exploration wells (Gishenyi, Western Rwanda, 2011-) for electricity production: * Geological surveys involve structural and geological mapping, dating of rocks, and alteration studies * Geochemical surveys involve the use of geothermometers to evaluate reservoir temperatures * Geophysical surveys involve electrical resistivity measurements, heat flow and microearthquake studies Project cost: US$20 million (R138 million),	-
South Africa	0	-	-	● Feasibility study on power generation from 87 thermal spring (with temperature ranging from 25^{o}C to 67.5^{o}C) binary systems identified and from hot granite.	-
Tunisia	0	-	-	● Expansion of the geothermal farming from 194,000 hectares to 310,000 hectares in 2010 ● Project to enhance energy capitalization of geothermal waters (2010-)	-
Yemen	0	-	50-100	● Feasibility studies (Al Lisi)	GEF, BGR
Zambia	0	-	20-90	● Development of the Kapisya Geothermal Project (Sumbu, on the shores of Lake Tanganyika) ● Development of a health resort and construction of a geothermal power plant (Chinyunyu Hot Springs) A number of additional sites were identified, but no funding is available	DAL SpA, JICA, ZGS

Appendix D: Initial development of the geothermal energy in Africa

Country	Geothermal potential	Location
Eritrea	● Fumaroles and thermal pools in at least 11 small (about 1-2 ha) sites over about 10 km^2	Alid Volcanic Centre (south of the Gulf of Zula in the Danakil, Afar Rift)
Morocco	● Hot water (<50^oC) to be used for soil heating in greenhouses and fish ponds	Northeastern of Morocco and the sedimentary basins of the Sahara
Mozambique	● At least 38 thermal springs identified	East of Africa Rift (North of Metangula)
	● Low temperature (<60^oC) springs	Espungabera-Manica Areas (near the border with Zimbabwe)
Tanzania	● At least 15 thermal areas with hot (T>40^oC) springs	Over and near active rift segments with Quaternary volcanism and over the Tanzanian (Archean) craton and its Precambrian surrounds
Uganda	● 3 geothermal field of hot-water of temperature 140^oC and above	East African Rift System (Katwe, Buranga and Kibiro)

Appendix E: Geothermal potential by world regions

GEOTHERMAL POTENTIAL BY WORLD REGIONS
(all countries)

EIA Region	Geothermal Potential (Billion kWh)	Current Electricity Use (Billion kWh)	% Geothermal
North America	200	4,333	4.6%
Central & S. America	224	623	36.0%
w/Caribbean	354	669	52.9%
Europe/Former USSR	97	4155	2.3%
Asia and Pacific	337	3304	10%
Africa	101	357	28%
WORLD TOTAL	1089	13,142	8.3%

Appendix F: Geothermal potential by African country, 1999

Country	Today's Technology		Enhanced Technology		Potential (Billion kwh)	Current Use (Billion kwh)	% Geothermal Possible	Pop., 1998 (Thousand)	People served by Geothermal
	TT High-MW	TT Low-MW	ET High-MW	ET Low-MW					
Burundi	80	20	170	50	1.34	0.12	10.99	6457	6457
Comoros Islands	30	10	70	20	0.65	0.02	36.79	658	658
Djibouti	460	230	860	380	6.78	0.18	38.74	623	623
Ethiopia	1710	640	2930	1230	23.1	1.32	17.50	59649	59649
Kenya	1810	850	3000	1450	23.65	3.81	6.21	29008	29008
Malagasy	240	70	470	140	3.71	0.60	6.23	15057	15057
Malawi	90	20	230	60	1.81	0.80	2.27	10346	10346
Mozambique	80	20	210	60	1.66	0.55	3.01	18880	18880
Rwanda	170	50	340	120	2.68	0.16	16.34	6604	6604
Somalia	100	30	210	60	1.66	0.26	6.42	9237	9237
Sudan	220	70	490	180	3.86	1.32	2.94	28292	28292
Tanzania	380	140	680	260	5.36	1.82	2.95	32102	32102
Uganda	330	120	610	250	4.81	0.79	6.11	20554	20554
Congo (Kinshasa)	320	130	640	250	5.05	6.4	0.79	49139	38741
Zambia	90	20	200	60	1.58	7.84	0.20	8781	1766
Zimbabwe	90	20	200	60	1.58	8.50	0.19	11377	2111
Eritrea	150	50	1250	600	9.86	N/A	N/A	3577	N/A
Yemen	100	50	300	100	2.37	1.86	1.27	16887	16887
Total Africa	**6450**	**2540**	**12860**	**5330**	**101.51**	**36.35**	**279.26**	**327228**	**296972**

Appendix G: Countries which could be 100% geothermal powered

39 COUNTRIES WHICH COULD BE 100% GEOTHERMAL POWERED

Country	Population
Bolivia	7,957,000
Burundi	6,457,000
Comoros Islands	658,000
Costa Rica	3,841,000
Djibouti	623,000
Dominica	71,000
Ecuador	12,175,000
El Salvador	6,032,000
Ethiopia	59,649,000
Fiji	796,000
Grenada	93,000
Guadeloupe	443,000
Guatemala	10.801,000
Honduras	6,147,000
Iceland	276,000
Indonesia	206,338,000
Kenya	29,008,000
Malagasy Republic	15,057,000
Malawi	10.346,000
Martinique	389,000
Montserrat	11,000
Mozambique	18,880,000
Nicaragua	4,807,000
Panama	2,767,000
Papua New Guinea	4,600,000
Peru	24,797,000
Philippines	72,944,000
Rwanda	6,604,000
Solomon Islands	417,000
Somalia	9,237,000
St Kitts & Nevis	39,000
St. Lucia	150,000
St. Vincent	112,000
Sudan	28,292,000
Tanzania	32,102,000
Tonga	98,000
Uganda	20,554,000
Vanuatu	182,000
Yemen	16,887,000
TOTAL	620,637,000

Appendix H: Countries which could be 50% geothermal powered

Burma
Chile
Congo
New Zealand

Appendix I: Countries which could be 20% geothermal powered

Argentina
Columbia
Macedonia
Mexico
Zambia

Appendix J: Countries which could be 10% geothermal powered

Australia
Dominican Republic
Greece
Hungary
Turkey
Venezuela
Vietnam
Zimbabwe

Appendix K: Mass, energy and exergy balance relations for the components of a simple ORC

Subsystem	Mass analysis	Energy balance	Exergy balance	Energetic efficiency	Exergetic efficiency
Condensate Pump	$\dot{m}_1 = \dot{m}_2 = \dot{m}_{wf}$	$\dot{W}_p = \dot{m}_{wf}(h_{2,s} - h_1)/\eta_p$	$\dot{I}_p = \dot{E}x_1 - \dot{E}x_2 + \dot{W}_p$ $= \dot{m}_{wf}(\psi_1 - \psi_2) + \dot{W}_p$	$\eta_{I,p} = \frac{h_{2s} - h_1}{h_2 - h_1}$	$\eta_{II,p} = \frac{\dot{W}_p - \dot{I}_p}{\dot{W}_p}$
Preheater	$\dot{m}_2 = \dot{m}_3 = \dot{m}_{wf}$ $\dot{m}_7 = \dot{m}_8 = \dot{m}_{geo}$	$\dot{m}_{wf}(h_3 - h_2) = \dot{m}_{geo}(h_7 - h_8)$	$\dot{I}_{PH} = \dot{E}x_2 + \dot{E}x_7 - \dot{E}x_3 - \dot{E}x_8$ $= \dot{m}_{wf}(\psi_2 - \psi_3) + \dot{m}_{geo}(\psi_7 - \psi_8)$	$\eta_{I,PH} = \frac{T_3 - T_2}{T_7 - T_2} = \frac{T_7 - T_8}{T_7 - T_2}$	$\eta_{II,PH} = \frac{\dot{m}_{wf}(\psi_3 - \psi_2)}{\dot{m}_{geo}(\psi_7 - \psi_8)}$
Evaporator	$\dot{m}_3 = \dot{m}_4 = \dot{m}_{wf}$ $\dot{m}_6 = \dot{m}_7 = \dot{m}_{geo}$	$\dot{Q}_E = \dot{m}_{wf}(h_4 - h_3)$ $= \dot{m}_{geo}(h_6 - h_7)$	$\dot{I}_E = \dot{E}x_3 + \dot{E}x_6 - \dot{E}x_4 - \dot{E}x_7$ $= \dot{m}_{wf}(\psi_3 - \psi_4) + \dot{m}_{geo}(\psi_6 - \psi_7)$	$\eta_{I,E} = \frac{T_4 - T_3}{T_6 - T_3} = \frac{T_6 - T_7}{T_6 - T_3}$	$\eta_{II,E} = \frac{\dot{m}_{wf}(\psi_4 - \psi_3)}{\dot{m}_{geo}(\psi_6 - \psi_7)}$
Turbine	$\dot{m}_4 = \dot{m}_5 = \dot{m}_{wf}$	$\dot{W}_t = \dot{m}_{wf}(h_4 - h_{5,s}).\eta_t$	$\dot{I}_t = \dot{E}x_4 - \dot{E}x_5 - \dot{W}_t$ $= \dot{m}_{wf}(\psi_4 - \psi_5) - \dot{W}_t$	$\eta_{I,t} = \frac{h_4 - h_5}{h_4 - h_{5s}}$	$\eta_{II,t} = \frac{\dot{W}_t}{\dot{W}_t + \dot{I}_t}$
Condenser	$\dot{m}_5 = \dot{m}_1 = \dot{m}_{wf}$ $\dot{m}_9 = \dot{m}_{10} = \dot{m}_{ca}$	$\dot{Q}_c = \dot{m}_{wf}(h_5 - h_1)$ $= \dot{m}_{ca}(h_{10} - h_9)$	$\dot{I}_c = \dot{E}x_5 + \dot{E}x_9 - \dot{E}x_1 - \dot{E}x_{10}$ $= \dot{m}_{wf}(\psi_5 - \psi_1) + \dot{m}_{ca}(\psi_9 - \psi_{10})$	$\eta_{I,c} = \frac{T_{10} - T_9}{T_5 - T_9} = \frac{T_5 - T_1}{T_5 - T_9}$	$\eta_{II,c} = \frac{\dot{m}_{ca}(\psi_{10} - \psi_9)}{\dot{m}_{wf}(\psi_5 - \psi_1)}$
Reinjection	$\dot{m}_6 = \dot{m}_8 = \dot{m}_{geo}$		$\dot{I}_{rej} = \dot{E}x_8 - \dot{E}x_o$ $= \dot{m}_{geo}(\psi_8 - \psi_o)$		

Appendix L: Mass, energy and exergy balance relations for the components of an ORC with an IHE

Subsystem	Mass analysis	Energy balance	Exergy balance	Energetic efficiency	Exergetic efficiency
Condensate Pump	$\dot{m}_1 = \dot{m}_2 = \dot{m}_{wf}$	$\dot{W}_p = \dot{m}_{wf}(h_{2,s} - h_1)/\eta_p$	$\dot{I}_p = \dot{E}x_1 - \dot{E}x_2 + \dot{W}_p$ $= \dot{m}_{wf}(\psi_1 - \psi_2) + \dot{W}_p$	$\eta_{I,p} = \frac{h_{2s} - h_1}{h_2 - h_1}$	$\eta_{II,p} = \frac{\dot{W}_p - \dot{I}_p}{\dot{W}_p}$
Recuperator	$\dot{m}_2 = \dot{m}_3 = \dot{m}_{wf}$ $\dot{m}_6 = \dot{m}_7 = \dot{m}_{wf}$	$h_3 - h_2 = h_6 - h_7$	$\dot{I}_{IHE} = \dot{E}x_2 + \dot{E}x_6 - \dot{E}x_3 - \dot{E}x_7$ $= \dot{m}_{wf}[(\psi_2 - \psi_3) + (\psi_6 - \psi_7)]$	$\eta_{I,IHE} = \frac{T_3 - T_2}{T_6 - T_2} = \frac{T_6 - T_7}{T_6 - T_2}$	$\eta_{II,IHE} = \frac{(\psi_3 - \psi_2)}{(\psi_6 - \psi_7)}$
Preheater	$\dot{m}_3 = \dot{m}_4 = \dot{m}_{wf}$ $\dot{m}_9 = \dot{m}_{10} = \dot{m}_{geo}$	$\dot{m}_{wf}(h_4 - h_3) = \dot{m}_{geo}(h_9 - h_{10})$	$\dot{I}_{PH} = \dot{E}x_3 + \dot{E}x_9 - \dot{E}x_4 - \dot{E}x_{10}$ $= \dot{m}_{wf}(\psi_3 - \psi_4) + \dot{m}_{geo}(\psi_9 - \psi_{10})$	$\eta_{I,PH} = \frac{T_4 - T_3}{T_9 - T_3} = \frac{T_9 - T_{10}}{T_9 - T_3}$	$\eta_{II,PH} = \frac{\dot{m}_{wf}(\psi_4 - \psi_3)}{\dot{m}_{geo}(\psi_9 - \psi_{10})}$
Evaporator	$\dot{m}_4 = \dot{m}_5 = \dot{m}_{wf}$ $\dot{m}_8 = \dot{m}_9 = \dot{m}_{geo}$	$\dot{Q}_E = \dot{m}_{wf}(h_5 - h_4)$ $= \dot{m}_{geo}(h_8 - h_9)$	$\dot{I}_E = \dot{E}x_4 + \dot{E}x_8 - \dot{E}x_5 - \dot{E}x_9$ $= \dot{m}_{wf}(\psi_4 - \psi_5) + \dot{m}_{geo}(\psi_8 - \psi_9)$	$\eta_{I,E} = \frac{T_5 - T_4}{T_8 - T_4} = \frac{T_8 - T_9}{T_8 - T_4}$	$\eta_{II,E} = \frac{\dot{m}_{wf}(\psi_5 - \psi_4)}{\dot{m}_{geo}(\psi_8 - \psi_9)}$
Turbine	$\dot{m}_5 = \dot{m}_6 = \dot{m}_{wf}$	$\dot{W}_t = \dot{m}_{wf}(h_5 - h_{6,s}).\eta_t$	$\dot{I}_t = \dot{E}x_5 - \dot{E}x_6 - \dot{W}_t$ $= \dot{m}_{wf}(\psi_5 - \psi_6) - \dot{W}_t$	$\eta_{I,t} = \frac{h_5 - h_6}{h_5 - h_{6s}}$	$\eta_{II,t} = \frac{\dot{W}_t}{\dot{W}_t + \dot{I}_t}$
Condenser	$\dot{m}_7 = \dot{m}_1 = \dot{m}_{wf}$ $\dot{m}_{11} = \dot{m}_{12} = \dot{m}_{ca}$	$\dot{Q}_c = \dot{m}_{wf}(h_7 - h_1)$ $= \dot{m}_{ca}(h_{12} - h_{11})$	$\dot{I}_c = \dot{E}x_7 + \dot{E}x_{11} - \dot{E}x_1 - \dot{E}x_{12}$ $= \dot{m}_{wf}(\psi_7 - \psi_1) + \dot{m}_{ca}(\psi_{11} - \psi_{12})$	$\eta_{I,c} = \frac{T_{12} - T_{11}}{T_7 - T_{11}} = \frac{T_7 - T_1}{T_7 - T_{11}}$	$\eta_{II,c} = \frac{\dot{m}_{ca}(\psi_{12} - \psi_{11})}{\dot{m}_{wf}(\psi_7 - \psi_1)}$
Reinjection	$\dot{m}_8 = \dot{m}_{10} = \dot{m}_{geo}$		$\dot{I}_{rej} = \dot{E}x_{10} - \dot{E}x_o$ $= \dot{m}_{geo}(\psi_{10} - \psi_o)$		

Appendix M: Mass, energy and exergy balance relations for the components of a regenerative ORC

Subsystem	Mass analysis	Energy balance	Exergy balance	Energetic efficiency	Exergetic efficiency
Condesate Pump	$\dot{m}_1 = \dot{m}_2 = \dot{m}_{wf}$	$\dot{W}_{p1} = \dot{m}_{wf}(h_{2,s} - h_1)/\eta_p$	$\dot{I}_p = \dot{E}x_1 - \dot{E}x_2 + \dot{W}_p$ $= \dot{m}_{wf}(\psi_1 - \psi_2) + \dot{W}_p$	$\eta_{I,p} = \frac{h_{2s} - h_1}{h_2 - h_1}$	$\eta_{II,p} = \frac{\dot{W}_p - \dot{I}_p}{\dot{W}_p}$
OFOH	$\dot{m}_2 + \dot{m}_7 = \dot{m}_3$ $\dot{m}_3 = \dot{m}_{wf}$	$(h_3 - h_2) = y(h_7 - h_2)$	$\dot{I}_{OFOH} = (1-y)\dot{E}x_2 + y\dot{E}x_7 - \dot{E}x_3$ $= \dot{m}_{wf}[(1-y)\psi_2 + y\psi_7 - \psi_3]$	$\eta_{I,OFOH} = \frac{T_3 - T_2}{T_7 - T_2}$	$\eta_{II,OFOH} = \frac{\psi_3}{[(1-y)\psi_2 + y\psi_7]}$
Feed Pump	$\dot{m}_3 = \dot{m}_4 = \dot{m}_{wf}$	$\dot{W}_{p2} = \dot{m}_{wf}(h_{4,s} - h_3)/\eta_p$	$\dot{I}_p = \dot{E}x_3 - \dot{E}x_4 + \dot{W}_p$ $= \dot{m}_{wf}(\psi_3 - \psi_4) + \dot{W}_p$	$\eta_{I,p} = \frac{h_{4s} - h_3}{h_4 - h_3}$	$\eta_{II,p} = \frac{\dot{W}_p - \dot{I}_p}{\dot{W}_p}$
Preheater	$\dot{m}_4 = \dot{m}_5 = \dot{m}_{wf}$ $\dot{m}_{10} = \dot{m}_{11} = \dot{m}_{geo}$	$\dot{m}_{wf}(h_5 - h_4) = \dot{m}_{geo}(h_{10} - h_{11})$	$\dot{I}_{PH} = \dot{E}x_4 + \dot{E}x_{10} - \dot{E}x_5 - \dot{E}x_{11}$ $= \dot{m}_{wf}(\psi_4 - \psi_5) + \dot{m}_{geo}(\psi_{10} - \psi_{11})$	$\eta_{I,PH} = \frac{T_{10} - T_{11}}{T_{10} - T_4}$	$\eta_{II,PH} = \frac{\dot{m}_{wf}(\psi_5 - \psi_4)}{\dot{m}_{geo}(\psi_{10} - \psi_{11})}$
Evaporator	$\dot{m}_5 = \dot{m}_6 = \dot{m}_{wf}$ $\dot{m}_9 = \dot{m}_{10} = \dot{m}_{geo}$	$\dot{Q}_E = \dot{m}_{wf}(h_6 - h_5)$ $= \dot{m}_{geo}(h_9 - h_{10})$	$\dot{I}_E = \dot{E}x_5 + \dot{E}x_9 - \dot{E}x_6 - \dot{E}x_{10}$ $= \dot{m}_{wf}(\psi_5 - \psi_6) + \dot{m}_{geo}(\psi_9 - \psi_{10})$	$\eta_{I,E} = \frac{T_9 - T_{10}}{T_9 - T_5}$	$\eta_{II,E} = \frac{\dot{m}_{wf}(\psi_6 - \psi_5)}{\dot{m}_{geo}(\psi_9 - \psi_{10})}$
Turbine	$\dot{m}_6 = y\dot{m}_7 + (1-y)\dot{m}_8$ $= \dot{m}_{wf}$	$\dot{W}_{t1} = \dot{m}_{wf}(h_6 - h_{7,s}).\eta_t$ $\dot{W}_{t2} = \dot{m}_{wf}(h_7 - h_{8,s}).\eta_t$	$\dot{I}_t = (\dot{E}x_6 - \dot{E}x_7) + (1-y)(\dot{E}x_7 - \dot{E}x_8) - \dot{W}_t$ $= \dot{m}_{wf}[(\psi_6 - \psi_7) + (1-y)(\psi_7 - \psi_8)] - \dot{W}_t$	$\eta_{I,t} = \frac{h_6 - h_7}{h_6 - h_{7s}}$	$\eta_{II,t} = \frac{\dot{W}_t}{\dot{W}_t + \dot{I}_t}$
Condenser	$\dot{m}_8 = \dot{m}_1 = \dot{m}_{wf}$ $\dot{m}_{12} = \dot{m}_{13} = \dot{m}_{ca}$	$\dot{Q}_c = \dot{m}_{wf}(h_8 - h_1)$ $= \dot{m}_{ca}(h_{13} - h_{12})$	$\dot{I}_c = \dot{E}x_8 + \dot{E}x_{12} - \dot{E}x_1 - \dot{E}x_{13}$ $= \dot{m}_{wf}(\psi_8 - \psi_1) + \dot{m}_{ca}(\psi_{12} - \psi_{13})$	$\eta_{I,c} = \frac{T_8 - T_1}{T_8 - T_{12}}$	$\eta_{II,c} = \frac{\dot{m}_{ca}(\psi_{13} - \psi_{12})}{\dot{m}_{wf}(\psi_8 - \psi_1)}$
Reinjection	$\dot{m}_9 = \dot{m}_{11} = \dot{m}_{geo}$		$\dot{I}_{rej} = \dot{E}x_{11} - \dot{E}x_o$ $= \dot{m}_{geo}(\psi_{11} - \psi_o)$		

Appendix N: Mass, energy and exergy balance relations for the components of a regenerative ORC with an IHE

Subsystem	Mass analysis	Energy balance	Exergy balance	Energetic efficiency	Exergetic efficiency
Condesate Pump	$\dot{m}_1 = \dot{m}_2 = \dot{m}_{wf}$	$\dot{W}_{p1} = \dot{m}_{wf}(h_{2,s} - h_1)/\eta_p$	$\dot{I}_p = \dot{E}x_1 - \dot{E}x_2 + \dot{W}_p$ $= \dot{m}_{wf}(\psi_1 - \psi_2) + \dot{W}_p$	$\eta_{I,p} = \frac{h_{2s} - h_1}{h_2 - h_1}$	$\eta_{II,p} = \frac{\dot{W}_p - \dot{I}_p}{\dot{W}_p}$
Recuperator	$\dot{m}_2 = \dot{m}_3 = \dot{m}_{wf}$ $\dot{m}_9 = \dot{m}_{10} = \dot{m}_{wf}$	$h_3 - h_2 = h_9 - h_{10}$	$\dot{I}_{IHE} = \dot{E}x_2 + \dot{E}x_9 - \dot{E}x_3 - \dot{E}x_{10}$ $= \dot{m}_{wf}[(\psi_2 - \psi_3) + (\psi_9 - \psi_{10})]$	$\eta_{I,IHE} = \frac{T_9 - T_{10}}{T_9 - T_2}$	$\eta_{II,IHE} = \frac{(\psi_3 - \psi_2)}{(\psi_9 - \psi_{10})}$
OFOH	$\dot{m}_3 + \dot{m}_8 = \dot{m}_4$ $\dot{m}_4 = \dot{m}_{wf}$	$(h_4 - h_3) = y(h_8 - h_3)$	$\dot{I}_{OFOH} = (1-y)\dot{E}x_3 + y\dot{E}x_8 - \dot{E}x_4$ $= \dot{m}_{wf}[(1-y)\psi_3 + y\psi_8 - \psi_4]$	$\eta_{I,OFOH} = \frac{T_4 - T_3}{T_8 - T_3}$	$\eta_{II,OFOH} = \frac{\psi_4}{[(1-y)\psi_3 + y\psi_8]}$
Feed Pump	$\dot{m}_4 = \dot{m}_5 = \dot{m}_{wf}$	$\dot{W}_{p2} = \dot{m}_{wf}(h_{5,s} - h_4)/\eta_p$	$\dot{I}_p = \dot{E}x_4 - \dot{E}x_5 + \dot{W}_p$ $= \dot{m}_{wf}(\psi_4 - \psi_5) + \dot{W}_p$	$\eta_{I,p} = \frac{h_{5s} - h_4}{h_5 - h_4}$	$\eta_{II,p} = \frac{\dot{W}_p - \dot{I}_p}{\dot{W}_p}$
Preheater	$\dot{m}_5 = \dot{m}_6 = \dot{m}_{wf}$ $\dot{m}_{12} = \dot{m}_{13} = \dot{m}_{geo}$	$\dot{m}_{wf}(h_6 - h_5) = \dot{m}_{geo}(h_{12} - h_{13})$	$\dot{I}_{PH} = \dot{E}x_5 + \dot{E}x_{12} - \dot{E}x_6 - \dot{E}x_{13}$ $= \dot{m}_{wf}(\psi_5 - \psi_6) + \dot{m}_{geo}(\psi_{12} - \psi_{13})$	$\eta_{I,PH} = \frac{T_{12} - T_{13}}{T_{12} - T_5}$	$\eta_{II,PH} = \frac{\dot{m}_{wf}(\psi_6 - \psi_5)}{\dot{m}_{geo}(\psi_{12} - \psi_{13})}$
Evaporator	$\dot{m}_6 = \dot{m}_7 = \dot{m}_{wf}$ $\dot{m}_{11} = \dot{m}_{12} = \dot{m}_{geo}$	$\dot{Q}_E = \dot{m}_{wf}(h_7 - h_6)$ $= \dot{m}_{geo}(h_{11} - h_{12})$	$\dot{I}_E = \dot{E}x_6 + \dot{E}x_{11} - \dot{E}x_7 - \dot{E}x_{12}$ $= \dot{m}_{wf}(\psi_6 - \psi_7) + \dot{m}_{geo}(\psi_{11} - \psi_{12})$	$\eta_{I,E} = \frac{T_{11} - T_{12}}{T_{11} - T_6}$	$\eta_{II,E} = \frac{\dot{m}_{wf}(\psi_7 - \psi_6)}{\dot{m}_{geo}(\psi_{11} - \psi_{12})}$
Turbine	$\dot{m}_7 = y\dot{m}_8 + (1-y)\dot{m}_9$ $= \dot{m}_{wf}$	$\dot{W}_{t1} = \dot{m}_{wf}(h_7 - h_{8,s}).\eta_t$ $\dot{W}_{t2} = \dot{m}_{wf}(h_8 - h_{9,s}).\eta_t$	$\dot{I}_t = (\dot{E}x_7 - \dot{E}x_8) + (1-y)(\dot{E}x_8 - \dot{E}x_9) - \dot{W}_t$ $= \dot{m}_{wf}[(\psi_7 - \psi_8) + (1-y)(\psi_8 - \psi_9)] - \dot{W}_t$	$\eta_{I,t} = \frac{h_7 - h_8}{h_7 - h_{8s}}$	$\eta_{II,t} = \frac{\dot{W}_t}{\dot{W}_t + \dot{I}_t}$
Condenser	$\dot{m}_{10} = \dot{m}_1 = \dot{m}_{wf}$ $\dot{m}_{14} = \dot{m}_{15} = \dot{m}_{ca}$	$\dot{Q}_c = \dot{m}_{wf}(h_{10} - h_1)$ $= \dot{m}_{ca}(h_{15} - h_{14})$	$\dot{I}_c = \dot{E}x_{10} + \dot{E}x_{14} - \dot{E}x_1 - \dot{E}x_{15}$ $= \dot{m}_{wf}(10 - \psi_1) + \dot{m}_{ca}(\psi_{14} - \psi_{15})$	$\eta_{I,c} = \frac{T_{10} - T_1}{T_{10} - T_{14}}$	$\eta_{II,c} = \frac{\dot{m}_{ca}(\psi_{15} - \psi_{14})}{\dot{m}_{wf}(\psi_{10} - \psi_1)}$
Reinjection	$\dot{m}_{11} = \dot{m}_{13} = \dot{m}_{geo}$		$\dot{I}_{rej} = \dot{E}x_{13} - \dot{E}x_o = \dot{m}_{geo}(\psi_{13} - \psi_o)$		

Appendix O: MaTlab code-EGM analysis of a downhole coaxial heat exchanger

```
clear all
close all
clc
%-----------Input values-----------------
n=1;
To=25+273.15; %oC
Trej=50+273.15; %oC
Tgeo=160+273.15; %oC
Tm=(Trej+Tgeo)/2; %K
L=100; %m
for Tb=300.55:0.6:302.95 %oC
%Tb=270+273.15;  %oC
%for Tm=80+273.15:5:105+273.15   %oC
if n==1; Spec1='-ok'; Spec2='MarkerFaceColor'; Spec3='k';end
if n==2; Spec1='-sr'; Spec2='MarkerFaceColor'; Spec3='r';end
if n==3; Spec1='-^g'; Spec2='MarkerFaceColor'; Spec3='g';end
if n==4; Spec1='-hm'; Spec2='MarkerFaceColor'; Spec3='m';end
if n==5; Spec1='-dk'; Spec2='MarkerFaceColor'; Spec3='k';end
if n==6; Spec1='-vc'; Spec2='MarkerFaceColor'; Spec3='c';end
grad=(Tb-To)/L
Re=linspace(0,2e6,51);
col=length(Re);
%-----------Water properties-------------
co_r=999.79684;     co_c=4.2174356000;   co_k=0.5650285;
co_m=557.82468;         co_p=0.074763403;
c1_r=0.068317355;   c1_c=-0.0056181625;  c1_k=0.00263638950;
c1_m=19.408782;         c1_p=0.002902098;
c2_r=-0.010740248;  c2_c=0.001299253;    c2_k=-0.00012516934;
c2_m=0.1360459;         c2_p=2.8606181e-5;
c3_r=0.000821409;   c3_c=-0.000115354;   c3_k=-1.5154915e-6;    c3_m=-
3.1160832e-4;     c3_p=-8.1395537e-8;
c4_r=-2.30310e-5;   c4_c=4.15e-6;        c4_k=-0.0009412945;
rho=co_r+c1_r*(Tm-273.15)+c2_r*(Tm-273.15)^2+c3_r*(Tm-273.15)^2.5+c4_r*(Tm-
273.15)^3;
Cp=1000*(co_c+c1_c*(Tm-273.15)+c2_c*(Tm-273.15)^1.5+c3_c*(Tm-
273.15)^2+c4_c*(Tm-273.15)^2.5);
k=co_k+c1_k*(Tm-273.15)+c2_k*(Tm-273.15)^1.5+c3_k*(Tm-273.15)^2+c4_k*(Tm-
273.15)^0.5;
```

```
mu=1/(co_m+c1_m*(Tm-273.15)+c2_m*(Tm-273.15)^2+c3_m*(Tm-273.15)^3);
Pr=1/(co_p+c1_p*(Tm-273.15)+c2_p*(Tm-273.15)^2+c3_p*(Tm-273.15)^3);
%------------Optimization-------------------------------------------------
Do_opt=zeros;Sgen_min=zeros;Bo=zeros;m_opt=zeros;
Ex_dest=zeros;Ex=zeros;Exo=zeros;ratio1=zeros;ratio2=zeros;Wnet=zeros;En_eff=
zeros;Ex_eff=zeros;
for i=1:col
if Re(i)>2300
r=0.653;
Bo(i)=(mu^6*Tm/(rho^2*Cp*Pr^0.6*grad^2))*(1-r)^4.6*(1/r^0.8-
0.14/r^0.2)*(1/((1-r)^2.8*(1+r)^2)+1/r^4.8);
m_opt(i)=0.238*Re(i)^1.4*Bo(i)^0.25;
Sgen_min(i)=(13.84*m_opt(i)^2*Cp*Pr^0.6*(1-r)^0.2*grad^2)/(mu*(1/r^0.8-
0.14/r^0.2)*Tm^2*Re(i)^0.8)+(0.0446*Re(i)^4.8*mu^5*(1-
r)^4.8)/(rho^2*Tm*m_opt(i)^2)*(1/((1-r)^2.8*(1+r)^2)+1/r^4.8);
Do_opt(i)=(4*m_opt(i))/(pi*mu*(1-r)*Re(i));
elseif Re(i)<2300
r=0.683;
Bo(i)=(mu^6*Tm/(rho^2*Cp*Pr*grad^2))*(1-r)^3*(3.66+1.2*r^0.5)*(((1-
r)/(1+r))/(1-r^4-(1+r^2)^2/log(1/r)+1/r^4));
m_opt(i)=2.642*Re(i)*Bo(i)^0.25;
Sgen_min(i)=(m_opt(i)^2*Cp*Pr*(1-
r)*grad^2)/(pi*mu*(3.66+1.2*r^0.5)*Tm^2)+(15.50*Re(i)^4*mu^5*(1-
r)^4)/(rho^2*Tm*m_opt(i)^2)*(((1-r)/(1+r))/(1-r^4-(1+r^2)^2/log(1/r)+1/r^4));
Do_opt(i)=(4*m_opt(i))/(pi*mu*(1-r)*Re(i));
end
Ex_dest(i)=To*Sgen_min(i)*L;
Ex(i)=Tgeo-Trej-To*log(Tgeo/Trej);
Exo(i)=Tgeo-To-To*log(Tgeo/To);
ratio1(i)=Ex(i)/(Tgeo-To);
ratio2(i)=Ex(i)/Exo(i);
Wnet(i)=Ex(i)-Ex_dest(i)/(m_opt(i)*Cp);
En_eff(i)=Wnet(i)/(Tgeo-To);
Ex_eff(i)=Wnet(i)/(Tgeo-To-To*log(Tgeo/To));
end
figure (1)
hold on
plot (Re,m_opt,Spec1,Spec2,Spec3)
xlabel('Re (-)')
```

```
ylabel('m_o_p_t (kg/s)')
legend('dT/dx=2.4^oC/100m','dT/dx=3.0^oC/100m','dT/dx=3.6^oC/100m','dT/dx=4.2
^oC/100m','dT/dx=4.8^oC/100m',5);
%legend('T_g_e_o=110^oC','T_g_e_o=120^oC','T_g_e_o=130^oC','T_g_e_o=140^oC','
T_g_e_o=150^oC','T_g_e_o=160^oC',6);
grid on
hold off
figure (2)
hold on
plot (m_opt,Do_opt,Spec1,Spec2,Spec3)
xlabel('m_d_o_t (kg/s)')
ylabel('Do_o_p_t (m)')
legend('dT/dx=2.4^oC/100m','dT/dx=3.0^oC/100m','dT/dx=3.6^oC/100m','dT/dx=4.2
^oC/100m','dT/dx=4.8^oC/100m',5);
%legend('T_g_e_o=110^oC','T_g_e_o=120^oC','T_g_e_o=130^oC','T_g_e_o=140^oC','
T_g_e_o=150^oC','T_g_e_o=160^oC',6);
grid on
hold off
figure (3)
hold on
plot (Re,Do_opt,Spec1,Spec2,Spec3)
xlabel('Re (-)')
ylabel('Do (m)')
legend('dT/dx=2.4^oC/100m','dT/dx=3.0^oC/100m','dT/dx=3.6^oC/100m','dT/dx=4.2
^oC/100m','dT/dx=4.8^oC/100m',5);
%legend('T_g_e_o=110^oC','T_g_e_o=120^oC','T_g_e_o=130^oC','T_g_e_o=140^oC','
T_g_e_o=150^oC','T_g_e_o=160^oC',6);
grid on
hold off
figure (4)
hold on
plot (Re,Sgen_min,Spec1,Spec2,Spec3)
xlabel('Re (-)')
ylabel('Sgen, min (J/K.s.m)')
legend('dT/dx=2.4^oC/100m','dT/dx=3.0^oC/100m','dT/dx=3.6^oC/100m','dT/dx=4.2
^oC/100m','dT/dx=4.8^oC/100m',5);
%legend('T_g_e_o=110^oC','T_g_e_o=120^oC','T_g_e_o=130^oC','T_g_e_o=140^oC','
T_g_e_o=150^oC','T_g_e_o=160^oC',6);
grid on
```

```
hold off
n=n+1;
end
```

Appendix P: MATlab code- Energy and Exergy analysis of a downhole coaxial heat exchanger

```
clear all
close all
clc
%-----------Input values-----------------
n=1;
To=25+273.15; %oC
Trej=50+273.15; %oC
Tgeo=160+273.15; %oC
L=7000; %m
%for Tb=300.55:0.6:302.95 %oC
Tb=270+273.15;  %oC
%grad=(Tb-To)/L;
Trej=linspace(50+273.15,110+273.15,51); %K
%for Tb=300.55:0.6:302.95 %oC
grad=(Tb-To)/L;
for Tgeo=110+273.15:10:160+273.15; %K
Do_opt=zeros;Sgen_min=zeros;Bo=zeros;m_opt=zeros;
Ex_dest=zeros;Ex=zeros;Exo=zeros;ratio1=zeros;ratio2=zeros;Wnet=zeros;En_eff=
zeros;Ex_eff=zeros;
Re=1e6;%linspace(0,2e6,51);
col=length(Trej);
for i=1:col
Tm=(Trej(i)+Tgeo)/2; %K
if n==1; Spec1='-ok'; Spec2='MarkerFaceColor'; Spec3='k';end
if n==2; Spec1='-sr'; Spec2='MarkerFaceColor'; Spec3='r';end
if n==3; Spec1='-^g'; Spec2='MarkerFaceColor'; Spec3='g';end
if n==4; Spec1='-hm'; Spec2='MarkerFaceColor'; Spec3='m';end
if n==5; Spec1='-dk'; Spec2='MarkerFaceColor'; Spec3='k';end
if n==6; Spec1='-vc'; Spec2='MarkerFaceColor'; Spec3='c';end
%-----------Water properties-------------
co_r=999.79684;     co_c=4.2174356000;   co_k=0.5650285;
co_m=557.82468;         co_p=0.074763403;
c1_r=0.068317355;   c1_c=-0.0056181625;  c1_k=0.00263638950;
c1_m=19.408782;         c1_p=0.002902098;
c2_r=-0.010740248;  c2_c=0.001299253;    c2_k=-0.00012516934;
c2_m=0.1360459;         c2_p=2.8606181e-5;
```

```
c3_r=0.000821409;   c3_c=-0.000115354;   c3_k=-1.5154915e-6;    c3_m=-
3.1160832e-4;     c3_p=-8.1395537e-8;
c4_r=-2.30310e-5;   c4_c=4.15e-6;        c4_k=-0.0009412945;
rho=co_r+c1_r*(Tm-273.15)+c2_r*(Tm-273.15)^2+c3_r*(Tm-273.15)^2.5+c4_r*(Tm-
273.15)^3;
Cp=1000*(co_c+c1_c*(Tm-273.15)+c2_c*(Tm-273.15)^1.5+c3_c*(Tm-
273.15)^2+c4_c*(Tm-273.15)^2.5);
k=co_k+c1_k*(Tm-273.15)+c2_k*(Tm-273.15)^1.5+c3_k*(Tm-273.15)^2+c4_k*(Tm-
273.15)^0.5;
mu=1/(co_m+c1_m*(Tm-273.15)+c2_m*(Tm-273.15)^2+c3_m*(Tm-273.15)^3);
Pr=1/(co_p+c1_p*(Tm-273.15)+c2_p*(Tm-273.15)^2+c3_p*(Tm-273.15)^3);
%------------Optimization-----------------------------------------------------
if Re>2300
r=0.653;
Bo(i)=(mu^6*Tm/(rho^2*Cp*Pr^0.6*grad^2))*(1-r)^4.6*(1/r^0.8-
0.14/r^0.2)*(1/((1-r)^2.8*(1+r)^2)+1/r^4.8);
m_opt(i)=0.238*Re^1.4*Bo(i)^0.25;
Sgen_min(i)=(13.84*m_opt(i)^2*Cp*Pr^0.6*(1-r)^0.2*grad^2)/(mu*(1/r^0.8-
0.14/r^0.2)*Tm^2*Re^0.8)+(0.0446*Re^4.8*mu^5*(1-
r)^4.8)/(rho^2*Tm*m_opt(i)^2)*(1/((1-r)^2.8*(1+r)^2)+1/r^4.8);
Do_opt(i)=(4*m_opt(i))/(pi*mu*(1-r)*Re);
elseif Re<2300
r=0.683;
Bo(i)=(mu^6*Tm/(rho^2*Cp*Pr*grad^2))*(1-r)^3*(3.66+1.2*r^0.5)*(((1-
r)/(1+r))/(1-r^4-(1+r^2)^2/log(1/r)+1/r^4));
m_opt(i)=2.642*Re*Bo(i)^0.25;
Sgen_min(i)=(m_opt(i)^2*Cp*Pr*(1-
r)*grad^2)/(pi*mu*(3.66+1.2*r^0.5)*Tm^2)+(15.50*Re^4*mu^5*(1-
r)^4)/(rho^2*Tm*m_opt(i)^2)*(((1-r)/(1+r))/(1-r^4-(1+r^2)^2/log(1/r)+1/r^4));
Do_opt(i)=(4*m_opt(i))/(pi*mu*(1-r)*Re);
end
%----------------Performance evaluation-----------------------------------
Ex_dest(i)=To*Sgen_min(i)*L;
Ex(i)=Tgeo-Trej(i)-To*log(Tgeo/Trej(i));
Exo(i)=Tgeo-To-To*log(Tgeo/To);
ratio1(i)=Ex(i)/(Tgeo-To);
ratio2(i)=Ex(i)/Exo(i);
Wnet(i)=Ex(i)-Ex_dest(i)/(m_opt(i)*Cp);
En_eff(i)=Wnet(i)/(Tgeo-To);
```

```
Ex_eff(i)=Wnet(i)/(Tgeo-To-To*log(Tgeo/To));
end
figure (1)
hold on
plot((Trej-273.15),En_eff,Spec1,Spec2,Spec3)
xlabel('T_r_e_j (^oC)')
ylabel('Energy efficiency (-)')
%title('Energy efficiency','fontsize',14,'fontweight','b')
legend('T_g_e_o=110^oC','T_g_e_o=120^oC','T_g_e_o=130^oC','T_g_e_o=140^oC','T
_g_e_o=150^oC','T_g_e_o=160^oC',6);
axis([50 110 0 0.20])
grid on
hold off
figure (2)
hold on
plot((Trej-273.15),Ex_eff,Spec1,Spec2,Spec3)
xlabel('T_r_e_j (^oC)')
ylabel('Exergy efficiency (-)')
%title('Exergy efficiency','fontsize',14,'fontweight','b')
legend('T_g_e_o=110^oC','T_g_e_o=120^oC','T_g_e_o=130^oC','T_g_e_o=140^oC','T
_g_e_o=150^oC','T_g_e_o=160^oC',6);
axis([50 110 0 1])
grid on
hold off
n=n+1;
end
```

Appendix Q: MATlab code- Thermodynamic analysis of a simple ORC

```
"-------------------------PREHEATED  CYCLE-----------------------------"
"-----------------------------------INPUT-----------------------------------------"
"Fluid"
wf$='R123'
cw$='air'
geo$='water'
"Data"
T_o=25 [C]
P_o=Po#
h_o=Enthalpy(geo$,T=T_o, x=0)
s_o=Entropy(geo$,T=T_o, x=0)
m_dot_geo=1 [kg/s]
T_geo=110[C]
DELTAT_pp=5 [C]
T_E=68 [C]
P_E=P_sat(wf$,T=T_E)
T_c=28.9 [C]
P_c=P_sat(wf$,T=T_c) "Condenser pressure"
T_9=T_o                  "Cooling water inlet temperature"
n_t = 0.80               "Isentropic efficiency"
n_p = 0.90             "Isentropic efficiency"
"-------------------------PUMP-----------------------------------"
"Losses due to friction, heat dissipation, ...."
P_loss = 0 [kPa]
T_loss = 0 [C]
"Inlet"
P_1=P_c- P_loss
T_1= T_c- T_loss
v_1 = Volume(wf$,T=T_1,x=0)
h_1 = Enthalpy(wf$, T=T_1,x=0)
s_1 = Entropy(wf$, T=T_1,x=0)
"Outlet"
T_2s=Temperature(wf$,s=s_2s,P=P_2s)
P_2s = P_4
h_2s=h_1+v_1*(P_2s-P_1)/n_p
s_2s=s_1
P_2 = P_2s
T_2= Temperature(wf$,h=h_2,P=P_2)
```

```
h_2=h_1+(h_2s-h_1)/n_p
s_2=Entropy(wf$, T=T_2,P=P_2)
"Output"
h_2 = h_1 + w_p "1st law:"
"-------------------------PREHEATER-----------------------------------"
T_3=T_4
P_3=P_4
h_3=Enthalpy(wf$, T=T_3,x=0)
s_3=Entropy(wf$, T=T_3,x=0)
h_2+q_IN=h_4
percent_Q_PH=(h_3-h_2)/(h_4-h_2)
m_dot_geo*Cp_geo*(T_7-T_8)=m_dot_wf*(h_3-h_2)
DELTAT_LMTD_PH=((T_8-T_2)- (T_7-T_3))/ln((T_8-T_2)/ (T_7-T_3))
Q_dot_PH=m_dot_wf*(h_3-h_2)
"----------------------------EVAPORATOR-----------------------------------"
"Pitch point"
DELTAT_pp= T_pp-T_3
T_7=T_pp
P_7=P_6
h_7=Enthalpy(geo$,T=T_7, x=0)
s_7=Entropy(geo$,T=T_7, x=0)
m_dot_geo*Cp_geo*(T_6-T_7)=m_dot_wf*(h_4-h_3)
percent_Q_E=(h_4-h_3)/(h_4-h_2)
DELTAT_LMTD_E=((T_6-T_4)- (T_7-T_3))/ln((T_6-T_4)/ (T_7-T_3))
Q_dot_E=m_dot_wf*(h_4-h_3)
"-----------------------------------TURBINE---------------------------------"
"Inlet"
T_4=T_E
P_4 =P_sat(wf$,T=T_4)
h_4 =Enthalpy(wf$,T=T_4,x=1)
s_4 =Entropy(wf$,T=T_4,x=1)
"Outlet"
P_5=P_sat(wf$,T=T_c)
T_5s=Temperature(wf$,P=P_5,s=s_5s)
h_5s=Enthalpy(wf$,P=P_5,s=s_5s)
s_5s=s_4 "2nd law: Isentropic process"
h_5=h_4-n_t*(h_4-h_5s)
T_5=Temperature(wf$,P=P_5,h=h_5)
"Output"
```

```
h_4 = h_5 + w_t "1st law:"
"----------CONDENSER----------"
"Inlet of Condenser = outlet of Turbine"
h_c=Enthalpy(wf$,T=T_c,x=1)
s_c=Entropy(wf$,T=T_c,x=1)
h_5=h_1+q_c
s_5 = Entropy(wf$, h=h_5,P=P_5)
m_dot_cw*Cp_cw*(T_10-T_cw)=m_dot_wf*(h_5-h_c)
DELTAT_LMTD_c=((T_5-T_10)- (T_1-T_9))/ln((T_5-T_10)/ (T_1-T_9))
m_dot_cw*Cp_cw*(T_10-T_9)=m_dot_wf*(h_5-h_1)
Q_dot_c=m_dot_wf*q_c
"Cooling water"
"T_10=30"
3= T_c-T_cw
Cp_cw=Cp(cw$, T=T_9)
P_9=P_o
h_9=Enthalpy(cw$,T=T_9)
s_9=Entropy(cw$,T=T_9,P=P_o)
P_10=P_o
h_10=Enthalpy(cw$,T=T_10)
s_10=Entropy(cw$,T=T_10,P=P_o)
"----------DOWNHOLE HEAT EXCHANGER----------"
"Inlet"
T_8=T_rej
P_8=P_6
h_8=Enthalpy(geo$,T=T_8, P=P_8)
s_8=Entropy(geo$,T=T_8, P=P_8)
"Outlet"
Cp_geo=Cp(geo$,T=T_geo,x=0)
T_6=T_geo
P_6=P_sat(geo$,T=T_6)
h_6=Enthalpy(geo$,T=T_6, x=0)
s_6=Entropy(geo$,T=T_6, x=0)
"---------OVERALL EFFICIENCY OF THE CYCLE----------"
w_net = w_t - w_p
W_dot_p=m_dot_wf*w_p
W_dot_t=m_dot_wf*w_t
W_dot_net=m_dot_wf*w_net
n_th = w_net /q_IN
```

```
n_th2 = 1-(q_c /q_IN)
n_I=(W_dot_net/(m_dot_geo*Cp_geo*(ConvertTEMP(C,K,T_geo)-ConvertTEMP(C,K,T_o))))*100
n_I2=(W_dot_net/(m_dot_geo*Cp_geo*(ConvertTEMP(C,K,T_geo)-ConvertTEMP(C,K,T_rej))))*100
n_I2a=(W_dot_net/(m_dot_wf*(h_4-h_2)))*100
n_II=(W_dot_net/(m_dot_geo*Cp_geo*(ConvertTEMP(C,K,T_geo)-ConvertTEMP(C,K,T_o)-
ConvertTEMP(C,K,T_o)*ln(ConvertTEMP(C,K,T_geo)/ConvertTEMP(C,K,T_o)))))*100
n_II2=(W_dot_net/(m_dot_geo*Cp_geo*(ConvertTEMP(C,K,T_geo)-ConvertTEMP(C,K,T_rej)-
ConvertTEMP(C,K,T_o)*ln(ConvertTEMP(C,K,T_geo)/ConvertTEMP(C,K,T_rej)))))*100
n_III=(W_dot_net/(m_dot_wf*((h_4-h_2)-ConvertTEMP(C,K,T_o)*(s_4-s_2))))*100
beta=m_dot_wf/m_dot_geo
gamma=m_dot_cw/m_dot_wf
 "--------------------IRREVERSIBILITY ANALYSIS----------------------"
I_dot_p=m_dot_wf*((h_1-h_2)-ConvertTEMP(C,K,T_o) *(s_1-s_2))+W_dot_p
I_dot_PH=m_dot_wf*((h_2-h_3)-ConvertTEMP(C,K,T_o) *(s_2-s_3))+m_dot_geo*((h_7-h_8)-
ConvertTEMP(C,K,T_o) *(s_7-s_8))
I_dot_E=m_dot_wf*((h_3-h_4)-ConvertTEMP(C,K,T_o) *(s_3-s_4))+m_dot_geo*((h_6-h_7)-
ConvertTEMP(C,K,T_o) *(s_6-s_7))
I_dot_t=m_dot_wf*((h_4-h_5)-ConvertTEMP(C,K,T_o) *(s_4-s_5))-W_dot_t
I_dot_c=m_dot_wf*((h_5-h_1)-ConvertTEMP(C,K,T_o) *(s_5-s_1))+m_dot_cw*((h_9-h_10)-
ConvertTEMP(C,K,T_o) *(s_9-s_10))
I_dot_rej=m_dot_geo*((h_8-h_o)-ConvertTEMP(C,K,T_o)*(s_8-s_o))
I_dot_HX=I_dot_PH+I_dot_E
I_dot_cycle=I_dot_p+I_dot_PH+I_dot_E+I_dot_t+I_dot_c
I_dot_plant=E_dot_in-W_dot_net
I_dot_planta=I_dot_cycle+I_dot_CA+I_dot_rej
I_dot_CA=m_dot_cw*((h_10-h_9)-ConvertTEMP(C,K,T_o)*(s_10-s_9))
"-------------------------------------------------------------------------------------"
E_dot_in=m_dot_geo*((h_6-h_o)-ConvertTEMP(C,K,T_o)*(s_6-s_o))
E_dot_p=m_dot_wf*((h_1-h_o)-ConvertTEMP(C,K,T_o)*(s_1-s_o))
E_dot_PH=m_dot_wf*((h_2-h_o)-ConvertTEMP(C,K,T_o)*(s_2-s_o))
E_dot_E=m_dot_wf*((h_3-h_o)-ConvertTEMP(C,K,T_o)*(s_3-s_o))
E_dot_t=m_dot_wf*((h_4-h_o)-ConvertTEMP(C,K,T_o)*(s_4-s_o))
E_dot_c=m_dot_wf*((h_5-h_o)-ConvertTEMP(C,K,T_o)*(s_5-s_o))
E_dot_rej=m_dot_wf*((h_8-h_o)-ConvertTEMP(C,K,T_o)*(s_8-s_o))
E_dot_total=E_dot_p+E_dot_PH+E_dot_E+E_dot_t+E_dot_c
"-------------------------------------------------------------------------------------"
Y_p=I_dot_p/E_dot_in*100
Y_PH=I_dot_PH/E_dot_in*100
Y_E=I_dot_E/E_dot_in*100
```

```
Y_t=I_dot_t/E_dot_in*100
Y_c=I_dot_c/E_dot_in*100
Y_rej=I_dot_rej/E_dot_in*100
Y_CA=I_dot_CA/E_dot_in*100
Y_HX=I_dot_HX/E_dot_in*100
Y_W=W_dot_net/E_dot_in*100
Y_cycle=I_dot_cycle/E_dot_in*100
Y_plant=I_dot_plant/E_dot_in*100
Y_total=Y_p+Y_PH+Y_E+Y_t+Y_c+Y_W+Y_rej+Y_CA
"-----------------------------------------------------------------------------------------"
X_p=I_dot_p/I_dot_plant*100
X_PH=I_dot_PH/I_dot_plant*100
X_E=I_dot_E/I_dot_plant*100
X_t=I_dot_t/I_dot_plant*100
X_c=I_dot_c/I_dot_plant*100
X_rej=I_dot_rej/I_dot_plant*100
X_CA=I_dot_CA/I_dot_plant*100
X_total=X_p+X_PH+X_E+X_t+X_c+X_rej+X_CA
"-----------------------------------------------------------------------------------------"
eff_p=(h_2s-h_1)/(h_2-h_1)*100
eff_PH=(T_7-T_8)/(T_7-T_2)*100
eff_E=(T_6-T_7)/(T_6-T_3)*100
eff_t=(h_4-h_5)/(h_4-h_5s)*100
eff_c=(T_5-T_1)/(T_5-T_9)*100
"-----------------------------------------------------------------------------------------"
efx_p=(W_dot_p-I_dot_p)/W_dot_p*100
efx_PH=(m_dot_wf*((h_3-h_2)-ConvertTEMP(C,K,T_o) *(s_3-s_2)))/(m_dot_geo*((h_7-h_8)-
ConvertTEMP(C,K,T_o) *(s_7-s_8)))*100
efx_E=(m_dot_wf*((h_4-h_3)-ConvertTEMP(C,K,T_o) *(s_4-s_3)))/(m_dot_geo*((h_6-h_7)-
ConvertTEMP(C,K,T_o) *(s_6-s_7)))*100
efx_t=W_dot_t/(W_dot_t+I_dot_t)*100
efx_c=(m_dot_cw*((h_10-h_9)-ConvertTEMP(C,K,T_o) *(s_10-s_9)))/(m_dot_wf*((h_5-h_1)-
ConvertTEMP(C,K,T_o) *(s_5-s_1)))*100
"-----------------------------------------------------------------------------------------"
```

Appendix R: MATlab code- Thermodynamic analysis of an ORC with an IHE

```
"-------------------------RECUPERATED  CYCLE-------------------------------"
"-----------------------------------INPUT-----------------------------------------"
"Fluid"
wf$='n-pentane'
cw$='air'
geo$='water'
"Data"
T_o=25 [C]
P_o=Po#
h_o=Enthalpy(geo$,T=T_o, x=0)
s_o=Entropy(geo$,T=T_o, x=0)
m_dot_geo=1[kg/s]
T_geo=110 [C]
DELTAT_pp= 5 [C]
T_E=68 [C]
P_E=P_sat(wf$,T=T_E)
T_c=29.4 [C]
P_c=P_sat(wf$,T=T_c) "Condenser pressure"
T_11=T_o                  "Cooling water inlet temperature"
n_t = 0.80                "Isentropic efficiency"
n_p = 0.90                "Isentropic efficiency"
"-------------------------PUMP-----------------------------------"
 "Losses due to friction, heat dissipation, ...."
P_loss = 0 [kPa]
T_loss = 0 [C]
"Inlet"
P_1=P_c- P_loss
T_1= T_c- T_loss
v_1 = Volume(wf$,T=T_1,x=0)
h_1 = Enthalpy(wf$, T=T_1,x=0)
s_1 = Entropy(wf$, T=T_1,x=0)
"Outlet"
T_2s=Temperature(wf$,s=s_2s,P=P_2s)
P_2s = P_E
h_2s=h_1+v_1*(P_2s-P_1)/n_p
s_2s=s_1
P_2 = P_2s
T_2= Temperature(wf$,h=h_2,P=P_2)
```

```
h_2=h_1+(h_2s-h_1)/n_p
s_2=Entropy(wf$, T=T_2,P=P_2)
"Output"
h_2 = h_1 + w_p "1st law:"
"-------------------------PREHEATER-----------------------------------"
"Inlet"
P_3=P_E
T_3=Temperature(wf$,h=h_3,P=P_3)
s_3=Entropy(wf$,T=T_3,P=P_3)
"Outlet"
T_4=T_5
P_4=P_E
h_4=Enthalpy(wf$, T=T_4,x=0)
s_4=Entropy(wf$, T=T_4,x=0)
h_3+q_IN=h_5
percent_Q_PH=(h_4-h_3)/(h_5-h_2)
m_dot_geo*Cp_geo*(T_9-T_10)=m_dot_wf*(h_4-h_3)
Q_dot_PH=m_dot_wf*(h_4-h_3)
"----------------------------EVAPORATOR-----------------------------------"
"Pitch point"
DELTAT_pp= T_pp-T_4
T_9=T_pp
P_9=P_8
h_9=Enthalpy(geo$,T=T_9, x=0)
s_9=Entropy(geo$,T=T_9, x=0)
m_dot_geo*Cp_geo*(T_8-T_9)=m_dot_wf*(h_5-h_4)
percent_Q_E=(h_5-h_4)/(h_5-h_2)
DELTAT_LMTD_E=((T_8-T_5)- (T_9-T_4))/ln((T_8-T_5)/ (T_9-T_4))
Q_dot_E=m_dot_wf*(h_5-h_4)
"-----------------------------------TURBINE---------------------------------"
"Inlet"
T_5 =T_E
P_5 =P_E
h_5 =Enthalpy(wf$,T=T_5,x=1)
s_5 =Entropy(wf$,T=T_5,x=1)
"Outlet"
P_6=P_c
T_6s=Temperature(wf$,P=P_6,s=s_6s)
h_6s=Enthalpy(wf$,P=P_6,s=s_6s)_
```

```
s_6s=s_5 "2nd law: Isentropic process"
h_6=h_5-n_t*(h_5-h_6s)
T_6=Temperature(wf$,P=P_6,h=h_6)
s_6 = Entropy(wf$,P=P_6,h=h_6)
"Output"
h_5 = h_6 + w_t "1st law:"
"----------RECUPERATOR----------"
"Heat exchange"
EPSILON=0.8
EPSILON=(T_6-T_7)/ (T_6-T_2)
(h_6-h_7)=(h_3-h_2)
percent_Q_IHE=(h_3-h_2)/(h_5-h_2)
DELTAT_LMTD_IHE=((T_7-T_2)- (T_6-T_3))/ln((T_7-T_2)/ (T_6-T_3))
Q_dot_IHE=m_dot_wf*(h_6-h_7)
"Q_dot_IHE=U_IHE*A_SH*DELTAT_LMTD_IHE"
"----------CONDENSER----------"
"Inlet of Condenser = outlet of Turbine"
h_c=Enthalpy(wf$,T=T_c,x=1)
s_c=Entropy(wf$,T=T_c,x=1)
h_7=h_1+q_c
P_7=P_c
h_7=Enthalpy(wf$, T=T_7,P=P_7)
s_7 = Entropy(wf$, T=T_7,P=P_7)
m_dot_cw*Cp_cw*(T_12-T_cw)=m_dot_wf*(h_7-h_c)
m_dot_cw*Cp_cw*(T_cw-T_11)=m_dot_wf*(h_c-h_1)
DELTAT_LMTD_c=((T_7-T_12)- (T_1-T_11))/ln((T_7-T_12)/ (T_1-T_11))
Q_dot_c=m_dot_wf*q_c
2=T_c-T_cw
{T_12=35}
"Cooling water"
Cp_cw=Cp(cw$, T=T_11)
P_11=P_o
h_11=Enthalpy(cw$,T=T_11)
s_11=Entropy(cw$,T=T_11,P=P_o)
P_12=P_o
h_12=Enthalpy(cw$,T=T_12)
s_12=Entropy(cw$,T=T_12,P=P_o)
"----------DOWNHOLE HEAT EXCHANGER----------"
"Inlet"
```

```
T_10=T_rej
P_10=P_8
h_10=Enthalpy(geo$,T=T_10, P=P_10)
s_10=Entropy(geo$,T=T_10, P=P_10)
"Outlet"
Cp_geo=Cp(geo$,T=T_geo,x=0)
T_8=T_geo
P_8=P_sat(geo$,T=T_8)
h_8=Enthalpy(geo$,T=T_8, x=0)
s_8=Entropy(geo$,T=T_8, x=0)
"---------OVERALL EFFICIENCY OF THE CYCLE-----------"
w_net = w_t - w_p
W_dot_p=m_dot_wf*w_p
W_dot_t=m_dot_wf*w_t
W_dot_net=m_dot_wf*w_net
n_th = w_net /q_IN
n_th2 = 1-(q_c /q_IN)
n_I=(W_dot_net/(m_dot_geo*Cp_geo*(ConvertTEMP(C,K,T_geo)-ConvertTEMP(C,K,T_o))))*100
n_I2=(W_dot_net/(m_dot_geo*Cp_geo*(ConvertTEMP(C,K,T_geo)-ConvertTEMP(C,K,T_rej))))*100
n_I2a=(W_dot_net/(m_dot_wf*(h_5-h_2)))*100
n_II=(W_dot_net/(m_dot_geo*Cp_geo*(ConvertTEMP(C,K,T_geo)-ConvertTEMP(C,K,T_o)-
ConvertTEMP(C,K,T_o)*ln(ConvertTEMP(C,K,T_geo)/ConvertTEMP(C,K,T_o)))))*100
n_II2=(W_dot_net/(m_dot_geo*Cp_geo*(ConvertTEMP(C,K,T_geo)-ConvertTEMP(C,K,T_rej)-
ConvertTEMP(C,K,T_o)*ln(ConvertTEMP(C,K,T_geo)/ConvertTEMP(C,K,T_rej)))))*100
n_III=(W_dot_net/(m_dot_wf*((h_5-h_3)-ConvertTEMP(C,K,T_o)*(s_5-s_3))))*100
beta=m_dot_wf/m_dot_geo
gamma=m_dot_cw/m_dot_wf
"--------------------IRREVERSIBILITY ANALYSIS----------------------"
E_dot_in=m_dot_geo*((h_8-h_o)-ConvertTEMP(C,K,T_o)*(s_8-s_o))
I_dot_p=m_dot_wf*((h_1-h_2)-ConvertTEMP(C,K,T_o) *(s_1-s_2))+W_dot_p
I_dot_IHE=m_dot_wf*((h_2-h_3)-ConvertTEMP(C,K,T_o) *(s_2-s_3))+m_dot_wf*((h_6-h_7)-
ConvertTEMP(C,K,T_o) *(s_6-s_7))
I_dot_PH=m_dot_wf*((h_3-h_4)-ConvertTEMP(C,K,T_o) *(s_3-s_4))+m_dot_geo*((h_9-h_10)-
ConvertTEMP(C,K,T_o) *(s_9-s_10))
I_dot_E=m_dot_wf*((h_4-h_5)-ConvertTEMP(C,K,T_o) *(s_4-s_5))+m_dot_geo*((h_8-h_9)-
ConvertTEMP(C,K,T_o) *(s_8-s_9))
I_dot_t=m_dot_wf*((h_5-h_6)-ConvertTEMP(C,K,T_o) *(s_5-s_6))-W_dot_t
I_dot_c=m_dot_wf*((h_7-h_1)-ConvertTEMP(C,K,T_o) *(s_7-s_1))+m_dot_cw*((h_11-h_12)-
ConvertTEMP(C,K,T_o) *(s_11-s_12))
```

```
I_dot_rej=m_dot_geo*((h_10-h_o)-ConvertTEMP(C,K,T_o)*(s_10-s_o))
I_dot_HX=m_dot_wf*((h_3-h_5)-ConvertTEMP(C,K,T_o) *(s_3-s_5))+m_dot_geo*((h_8-h_10)-
ConvertTEMP(C,K,T_o) *(s_8-s_10))
I_dot_cycle=I_dot_p+I_dot_IHE+I_dot_PH+I_dot_E+I_dot_t+I_dot_c
I_dot_plant=E_dot_in-W_dot_net
I_dot_planta=I_dot_cycle+I_dot_CA+I_dot_rej
I_dot_CA=m_dot_cw*((h_12-h_11)-ConvertTEMP(C,K,T_o)*(s_12-s_11))
"-----------------------------------------------------------------------------------------"
Y_p=I_dot_p/E_dot_in*100
Y_IHE=I_dot_IHE/E_dot_in*100
Y_PH=I_dot_PH/E_dot_in*100
Y_E=I_dot_E/E_dot_in*100
Y_t=I_dot_t/E_dot_in*100
Y_c=I_dot_c/E_dot_in*100
Y_rej=I_dot_rej/E_dot_in*100
Y_CA=I_dot_CA/E_dot_in*100
Y_HX=I_dot_HX/E_dot_in*100
Y_W=W_dot_net/E_dot_in*100
Y_cycle=I_dot_cycle/E_dot_in*100
Y_plant=I_dot_plant/E_dot_in*100
Y_total=Y_p+Y_PH+Y_E+Y_t+Y_c+Y_W+Y_rej+Y_IHE+Y_CA
"-----------------------------------------------------------------------------------------"
X_p=I_dot_p/I_dot_plant*100
X_IHE=I_dot_IHE/I_dot_plant*100
X_PH=I_dot_PH/I_dot_plant*100
X_E=I_dot_E/I_dot_plant*100
X_t=I_dot_t/I_dot_plant*100
X_c=I_dot_c/I_dot_plant*100
X_rej=I_dot_rej/I_dot_plant*100
X_CA=I_dot_CA/I_dot_plant*100
X_total=X_p+X_PH+X_E+X_t+X_c+X_rej+X_CA+X_IHE
"-----------------------------------------------------------------------------------------"
efx_p=(W_dot_p-I_dot_p)/W_dot_p*100
efx_IHE=((h_3-h_2)-ConvertTEMP(C,K,T_o) *(s_3-s_2))/((h_6-h_7)-ConvertTEMP(C,K,T_o) *(s_6-
s_7))*100
efx_PH=(m_dot_wf*((h_4-h_3)-ConvertTEMP(C,K,T_o) *(s_4-s_3)))/(m_dot_geo*((h_9-h_10)-
ConvertTEMP(C,K,T_o) *(s_9-s_10)))*100
efx_E=(m_dot_wf*((h_5-h_4)-ConvertTEMP(C,K,T_o) *(s_5-s_4)))/(m_dot_geo*((h_8-h_9)-
ConvertTEMP(C,K,T_o) *(s_8-s_9)))*100
```

```
efx_t=W_dot_t/(W_dot_t+I_dot_t)*100
efx_c=(m_dot_cw*((h_12-h_11)-ConvertTEMP(C,K,T_o) *(s_12-s_11)))/(m_dot_wf*((h_7-h_1)-
ConvertTEMP(C,K,T_o) *(s_7-s_1)))*100
"-------------------------------------------------------------------------------------"
eff_p=(h_2s-h_1)/(h_2-h_1)*100
eff_PH=(T_9-T_10)/(T_9-T_3)*100
eff_E=(T_8-T_9)/(T_8-T_4)*100
eff_t=(h_5-h_6)/(h_5-h_6s)*100
eff_IHE=(T_6-T_7)/(T_6-T_2)*100
eff_c=(T_7-T_1)/(T_7-T_11)*100
```

Appendix S: MATlab code- Thermodynamic analysis of a regenerative ORC

```
"-------------------REGENERATIVE-RECUPERATED  CYCLE-----------------------"
"-----------------------------------INPUT-----------------------------------------"
"Fluid"
wf$='n-pentane'
cw$='air'
geo$='water'
"Data"
T_o=25 [C]
P_o=Po#
h_o=Enthalpy(geo$,T=T_o, x=0)
s_o=Entropy(geo$,T=T_o, x=0)
m_dot_geo=1 [kg/s]
T_geo=110 [C]
DELTAT_pp=5 [C]
T_E=105 [C]
P_E=P_sat(wf$,T=T_E)
T_c=40 [C]
P_c=P_sat(wf$,T=T_c)
T_12=T_o                    "Cooling water inlet temperature"
T_13=T_o+10 [C]                    "Cooling water outlet temperature"
n_t = 0.80                  "Isentropic efficiency"
n_p = 0.90                "Isentropic efficiency"
"--------------CONDENSATE PUMP-------------------------------------"
"Losses due to friction, heat dissipation, ...."
P_loss = 0 [kPa]
T_loss = 0 [C]
"Inlet"
P_1=P_c- P_loss
T_1= T_c- T_loss
v_1 = Volume(wf$,T=T_1,x=0)
h_1 = Enthalpy(wf$, T=T_1,x=0)
s_1 = Entropy(wf$, T=T_1,x=0)
"Outlet"
T_2s=Temperature(wf$,s=s_2s,P=P_2s)
P_2s =494 [kPa]
h_2s=h_1+v_1*(P_2s-P_1)/n_p
s_2s=s_1
P_2 = P_2s
```

```
T_2= Temperature(wf$,h=h_2,P=P_2)
h_2=h_1+(h_2s-h_1)/n_p
s_2=Entropy(wf$, h=h_2,P=P_2)
"Output"
h_2 = h_1 + w_p1 "1st law:"
"-------------------OPEN FEED ORGANIC HEATER-------------------"
y=(h_3-h_2)/(h_7-h_2)
percent_Q_OFOH=(h_3-h_2)/(h_6-h_2)
"----------------------------FEED PUMP-----------------------------------"
"Inlet"
P_3=P_2
T_3= Temperature(wf$,P=P_3,x=0)
v_3 = Volume(wf$,T=T_3,x=0)
h_3 = Enthalpy(wf$, T=T_3,x=0)
s_3 = Entropy(wf$, T=T_3,x=0)
"Outlet"
T_4s=Temperature(wf$,s=s_4s,P=P_4s)
P_4s = P_E
h_4s=h_3+v_3*(P_4s-P_3)/n_p
s_4s=s_3
P_4 = P_4s
T_4= Temperature(wf$,h=h_4,P=P_4)
h_4=h_3+(h_4s-h_3)/n_p
s_4=Entropy(wf$, h=h_4,P=P_4)
"Output"
h_4 = h_3 + w_p2 "1st law:"
"-------------------------PREHEATER-------------------------------------"
T_5=T_6
P_5=P_6
h_5=Enthalpy(wf$, T=T_5,x=0)
s_5=Entropy(wf$, T=T_5,x=0)
h_4+q_IN=h_6
percent_Q_PH=(h_5-h_4)/(h_6-h_2)
m_dot_geo*Cp_geo*(T_10-T_11)=m_dot_wf*(h_5-h_4)
DELTAT_LMTD_PH=((T_11-T_4)- (T_10-T_5))/ln((T_11-T_4)/ (T_10-T_5))
Q_dot_PH=m_dot_wf*(h_5-h_4)
"----------------------------EVAPORATOR-----------------------------------"
"Pitch point"
DELTAT_pp= T_pp-T_5
```

```
T_10=T_pp
h_10=Enthalpy(geo$,T=T_10, x=0)
s_10=Entropy(geo$,T=T_10, x=0)
m_dot_geo*Cp_geo*(T_9-T_10)=m_dot_wf*(h_6-h_5)
percent_Q_E=(h_6-h_5)/(h_6-h_2)
DELTAT_LMTD_E=((T_9-T_6)- (T_10-T_5))/ln((T_9-T_6)/ (T_10-T_5))
Q_dot_E=m_dot_wf*(h_6-h_5)
"-----------------------------------TURBINE----------------------------------------"
"Inlet"
T_6=T_E
P_6 =P_sat(wf$,T=T_6)
h_6 =Enthalpy(wf$,T=T_6,x=1)
s_6 =Entropy(wf$,T=T_6,x=1)
"Extracted"
P_7=P_3
h_7=h_6-n_t*(h_6-h_7s)
T_7=Temperature(wf$,P=P_7,h=h_7)
s_7=Entropy(wf$,P=P_7,h=h_7)
T_7s=Temperature(wf$,P=P_7,s=s_7s)
h_7s=Enthalpy(wf$,P=P_7,s=s_7s)
s_7s=s_6 "2nd law: Isentropic process"
"Output"
h_6 = h_7 + w_t1 "1st law:"
"Outlet"
P_8=P_c
T_8s=Temperature(wf$,P=P_8,s=s_8s)
h_8s=Enthalpy(wf$,P=P_8,s=s_8s)
s_8s=s_7 "2nd law: Isentropic process"
h_8=h_7-n_t*(h_7-h_8s)
T_8=Temperature(wf$,P=P_8,h=h_8)
s_8=Entropy(wf$,P=P_8,h=h_8)
"Output"
h_7 = h_8 + w_t2 "1st law:"
"----------------------CONDENSER-------------------------------"
"Inlet of Condenser = outlet of Turbine"
h_c=Enthalpy(wf$,T=T_c,x=1)
s_c=Entropy(wf$,T=T_c,x=1)
h_8=h_1+q_c
m_dot_cw*Cp_cw*(T_13-T_12)=(1-y)*m_dot_wf*(h_8-h_1)
```

```
DELTAT_LMTD_c=((T_8-T_13)- (T_1-T_12))/ln((T_8-T_13)/ (T_1-T_12))
Q_dot_c=(1-y)*m_dot_wf*q_c
"Cooling water"
Cp_cw=Cp(cw$, T=T_12)
h_12=Enthalpy(cw$,T=T_12)
s_12=Entropy(cw$,T=T_12,P=P_o)
h_13=Enthalpy(cw$,T=T_13)
s_13=Entropy(cw$,T=T_13,P=P_o)
"----------DOWNHOLE HEAT EXCHANGER----------"
"Inlet"
T_11=T_rej
P_11=P_9
h_11=Enthalpy(geo$,T=T_11, P=P_11)
s_11=Entropy(geo$,T=T_11, P=P_11)
"Outlet"_
Cp_geo=Cp(geo$,T=T_geo,x=0)
T_9=T_geo
P_9=P_sat(geo$,T=T_9)
h_9=Enthalpy(geo$,T=T_9, x=0)
s_9=Entropy(geo$,T=T_9, x=0)__
"---------OVERALL EFFICIENCY OF THE CYCLE----------"
w_net = w_t1+(1-y)*w_t2 - (1-y)*w_p1-w_p2
W_dot_p=m_dot_wf*(  (1-y)*w_p1+w_p2)
W_dot_t=m_dot_wf*(w_t1+(1-y)*w_t2)
W_dot_net=m_dot_wf*w_net
n_th = w_net /q_IN
n_th2 = 1-((1-y)*q_c /q_IN)
n_I=(W_dot_net/(m_dot_geo*Cp_geo*(ConvertTEMP(C,K,T_geo)-ConvertTEMP(C,K,T_o))))*100
n_I2=(W_dot_net/(m_dot_geo*Cp_geo*(ConvertTEMP(C,K,T_geo)-ConvertTEMP(C,K,T_rej))))*100
n_I2a=(W_dot_net/(m_dot_wf*(h_6-h_2)))*100
n_II=(W_dot_net/(m_dot_geo*Cp_geo*(ConvertTEMP(C,K,T_geo)-ConvertTEMP(C,K,T_o)-
ConvertTEMP(C,K,T_o)*ln(ConvertTEMP(C,K,T_geo)/ConvertTEMP(C,K,T_o)))))*100
n_II2=(W_dot_net/(m_dot_geo*Cp_geo*(ConvertTEMP(C,K,T_geo)-ConvertTEMP(C,K,T_rej)-
ConvertTEMP(C,K,T_o)*ln(ConvertTEMP(C,K,T_geo)/ConvertTEMP(C,K,T_rej)))))*100
n_III=(W_dot_net/(m_dot_wf*((h_6-h_4)-ConvertTEMP(C,K,T_o)*(s_6-s_4))))*100
beta=m_dot_wf/m_dot_geo
gamma=m_dot_cw/m_dot_wf
"--------------------IRREVERSIBILITY ANALYSIS----------------------"
E_dot_in=m_dot_geo*((h_9-h_o)-ConvertTEMP(C,K,T_o)*(s_9-s_o))
```

```
I_dot_p=(1-y)*m_dot_wf*((h_1-h_2)-ConvertTEMP(C,K,T_o)*(s_1-s_2))+m_dot_wf*((h_3-h_4)-
ConvertTEMP(C,K,T_o)*(s_3-s_4))+W_dot_p
I_dot_PH=m_dot_wf*((h_4-h_5)-ConvertTEMP(C,K,T_o) *(s_4-s_5))+m_dot_geo*((h_10-h_11)-
ConvertTEMP(C,K,T_o) *(s_10-s_11))
I_dot_E=m_dot_wf*((h_5-h_6)-ConvertTEMP(C,K,T_o) *(s_5-s_6))+m_dot_geo*((h_9-h_10)-
ConvertTEMP(C,K,T_o) *(s_9-s_10))
I_dot_t=m_dot_wf*((h_6-h_7)-ConvertTEMP(C,K,T_o) *(s_6-s_7))+(1-y)*m_dot_wf*((h_7-h_8)-
ConvertTEMP(C,K,T_o) *(s_7-s_8))-W_dot_t
I_dot_OFOH=m_dot_wf*(((1-y)*h_2+y*h_7-h_3)-ConvertTEMP(C,K,T_o)*((1-y)*s_2+y*s_7-s_3))
I_dot_c=(1-y)*m_dot_wf*((h_8-h_1)-ConvertTEMP(C,K,T_o) *(s_8-s_1))+m_dot_cw*((h_12-h_13)-
ConvertTEMP(C,K,T_o) *(s_12-s_13))
I_dot_rej=m_dot_geo*((h_11-h_o)-ConvertTEMP(C,K,T_o)*(s_11-s_o))
I_dot_HX=m_dot_wf*((h_4-h_6)-ConvertTEMP(C,K,T_o) *(s_4-s_6))+m_dot_geo*((h_9-h_11)-
ConvertTEMP(C,K,T_o) *(s_9-s_11))
I_dot_cycle=I_dot_p+I_dot_PH+I_dot_E+I_dot_t+I_dot_c+I_dot_OFOH
I_dot_plant=E_dot_in-W_dot_net
I_dot_planta=I_dot_cycle+I_dot_CA+I_dot_rej
I_dot_CA=m_dot_cw*((h_13-h_12)-ConvertTEMP(C,K,T_o)*(s_13-s_12))
"-------------------------------------------------------------------------------------"
Y_p=I_dot_p/E_dot_in*100
Y_PH=I_dot_PH/E_dot_in*100
Y_E=I_dot_E/E_dot_in*100
Y_t=I_dot_t/E_dot_in*100
Y_c=I_dot_c/E_dot_in*100
Y_rej=I_dot_rej/E_dot_in*100
Y_HX=I_dot_HX/E_dot_in*100
Y_cycle=I_dot_cycle/E_dot_in*100
Y_plant=I_dot_plant/E_dot_in*100
Y_OFOH=I_dot_OFOH/E_dot_in*100
Y_CA=I_dot_CA/E_dot_in*100
Y_W=W_dot_net/E_dot_in*100
Y_total=Y_p+Y_PH+Y_E+Y_t+Y_c+Y_W+Y_rej+Y_OFOH+Y_CA
"-------------------------------------------------------------------------------------"
X_p=I_dot_p/I_dot_plant*100
X_OFOH=I_dot_OFOH/I_dot_plant*100
X_PH=I_dot_PH/I_dot_plant*100
X_E=I_dot_E/I_dot_plant*100
X_t=I_dot_t/I_dot_plant*100
X_c=I_dot_c/I_dot_plant*100
```

```
X_rej=I_dot_rej/I_dot_plant*100
X_CA=I_dot_CA/I_dot_plant*100
X_total=X_p+X_PH+X_E+X_t+X_c+X_rej+X_CA+X_OFOH
"----------------------------------------------------------------------------------------"
efx_p=(W_dot_p-I_dot_p)/W_dot_p*100
efx_PH=(m_dot_wf*((h_5-h_4)-ConvertTEMP(C,K,T_o) *(s_5-s_4)))/(m_dot_geo*((h_10-h_11)-
ConvertTEMP(C,K,T_o) *(s_10-s_11)))*100
efx_E=(m_dot_wf*((h_6-h_5)-ConvertTEMP(C,K,T_o) *(s_6-s_5)))/(m_dot_geo*((h_9-h_10)-
ConvertTEMP(C,K,T_o) *(s_9-s_10)))*100
efx_t=W_dot_t/(W_dot_t+I_dot_p)*100
efx_OFOH=((h_3-h_o)-ConvertTEMP(C,K,T_o) *(s_3-s_o))/((y*h_7+(1-y)*h_2-h_o)-
ConvertTEMP(C,K,T_o) *(y*s_7+(1-y)*s_2-s_o))*100
efx_c=(m_dot_cw*((h_13-h_12)-ConvertTEMP(C,K,T_o) *(s_13-s_12)))/((1-y)*m_dot_wf*((h_8-h_1)-
ConvertTEMP(C,K,T_o) *(s_8-s_1)))*100
"----------------------------------------------------------------------------------------"
eff_p=(h_2s-h_1)/(h_2-h_1)*100
eff_PH=(T_10-T_11)/(T_10-T_4)*100
eff_E=(T_9-T_10)/(T_9-T_5)*100
eff_t=(h_6-h_7)/(h_6-h_7s)*100
eff_OFOH=(T_3-T_2)/(T_7-T_2)*100
eff_c=(T_8-T_1)/(T_8-T_12)*100
"----------------------------------------------------------------------------------------"
```

Appendix T: MATlab code- Thermodynamic analysis of a regenerative ORC with an IHE

```
"------------------REGENERATIVE-RECUPERATED  CYCLE-----------------------"
"-----------------------------------INPUT-----------------------------------------"
"Fluid"
wf$='n-pentane'
cw$='air'
geo$='water'
"Data"
T_o=25 [C]
P_o=Po#
h_o=Enthalpy(geo$,T=T_o, x=0)
s_o=Entropy(geo$,T=T_o, x=0)
m_dot_geo=1 [kg/s]
T_geo=110 [C]
DELTAT_pp=5 [C]
T_E=107 [C]      "Turbine inlet temperature"
P_E=P_sat(wf$,T=T_E)    "Turbine inlet pressure"
T_c=29.3 [C]                "Condenser temperature"
P_c=P_sat(wf$,T=T_c) "Condenser pressure"
T_14=T_o                   "Cooling water inlet temperature"
T_15=35 [C]                    "Cooling water outlet temperature"
n_t = 0.80                  "Isentropic efficiency"
n_p = 0.90                "Isentropic efficiency"
"--------------CONDENSATE PUMP-------------------------------------"
"Losses due to friction, heat dissipation, ...."
P_loss = 0 [kPa]
T_loss = 0 [C]
"Inlet"
P_1=P_c- P_loss
T_1= T_c- T_loss
v_1 = Volume(wf$,T=T_1,x=0)
h_1 = Enthalpy(wf$, T=T_1,x=0)
s_1 = Entropy(wf$, T=T_1,x=0)
"Outlet"
T_2s=Temperature(wf$,s=s_2s,P=P_2s)
P_2s = 581 [kPa]
h_2s=h_1+v_1*(P_2s-P_1)/n_p
s_2s=s_1
P_2 = P_2s
```

```
T_2= Temperature(wf$,h=h_2,P=P_2)
h_2=h_1+(h_2s-h_1)/n_p
s_2=Entropy(wf$, h=h_2,P=P_2)
"Output"
h_2 = h_1 + w_p1 "1st law:"
"-------------------OPEN FEED ORGANIC HEATER-------------------"
P_3=P_2
T_3=Temperature(wf$,h=h_3,P=P_3)
s_3=Entropy(wf$,h=h_3,P=P_3)
y=(h_4-h_3)/(h_8-h_3)
percent_Q_OFOH=(h_5-h_3)/(h_7-h_2)
"-----------------------------FEED PUMP-----------------------------------"
"Inlet"
P_4=P_2s
T_4= Temperature(wf$,P=P_4,x=0)
v_4 = Volume(wf$,T=T_4,x=0)
h_4 = Enthalpy(wf$, T=T_4,x=0)
s_4 = Entropy(wf$, T=T_4,x=0)
"Outlet"
T_5s=Temperature(wf$,s=s_5s,P=P_5s)
P_5s = P_E
h_5s=h_4+v_4*(P_5s-P_4)/n_p
s_5s=s_4
P_5 = P_5s
T_5= Temperature(wf$,h=h_5,P=P_5)
h_5=h_4+(h_5s-h_4)/n_p
s_5=Entropy(wf$, h=h_5,P=P_5)
"Output"
h_5 = h_4 + w_p2 "1st law:"
"-------------------------PREHEATER-----------------------------------"
T_6=T_7
P_6=P_7
h_6=Enthalpy(wf$, T=T_6,x=0)
s_6=Entropy(wf$, T=T_6,x=0)
h_5+q_IN=h_7
percent_Q_PH=(h_6-h_5)/(h_7-h_2)
m_dot_geo*Cp_geo*(T_12-T_13)=m_dot_wf*(h_6-h_5)
DELTAT_LMTD_PH=((T_13-T_5)- (T_12-T_6))/ln((T_13-T_5)/ (T_12-T_6))
Q_dot_PH=m_dot_wf*(h_6-h_5)
```

```
"----------------------------EVAPORATOR-----------------------------------"
"Pitch point"
DELTAT_pp= T_pp-T_6
T_12=T_pp
P_12=P_11
h_12=Enthalpy(geo$,T=T_12, x=0)
s_12=Entropy(geo$,T=T_12, x=0)
m_dot_geo*Cp_geo*(T_11-T_12)=m_dot_wf*(h_7-h_6)
percent_Q_E=(h_7-h_6)/(h_7-h_2)
DELTAT_LMTD_E=((T_11-T_7)- (T_12-T_6))/ln((T_11-T_7)/ (T_12-T_6))
Q_dot_E=m_dot_wf*(h_7-h_6)
"-----------------------------------TURBINE---------------------------------------"
"Inlet"
T_7=T_E
P_7 =P_sat(wf$,T=T_7)
h_7 =Enthalpy(wf$,T=T_7,x=1)
s_7 =Entropy(wf$,T=T_7,x=1)
"Extracted"
T_8s=Temperature(wf$,P=P_8,s=s_8s)
P_8s=P_8
h_8s=Enthalpy(wf$,P=P_8,s=s_8s)
s_8s=s_7 "2nd law: Isentropic process"
T_8=Temperature(wf$,P=P_8,h=h_8)
P_8=P_4
h_8=h_7-n_t*(h_7-h_8s)
s_8=Entropy(wf$,P=P_8,h=h_8)
"Output"
h_7 = h_8 + w_t1 "1st law:"
"Outlet"
P_9=P_c
P_9s=P_c
T_9s=Temperature(wf$,P=P_9,s=s_9s)
h_9s=Enthalpy(wf$,P=P_9,s=s_9s)
s_9s=s_8 "2nd law: Isentropic process"
h_9=h_8-n_t*(h_8-h_9s)
T_9=Temperature(wf$,P=P_9,h=h_9)
s_9=Entropy(wf$,P=P_9,h=h_9)
"Output"
h_8 = h_9 + w_t2 "1st law:"
```

```
"----------------------RECUPERATOR---------------------------"
"Heat exchange"
EPSILON=0.8
EPSILON=(T_9-T_10)/ (T_9-T_2)
(h_9-h_10)=(h_3-h_2)
percent_Q_IHE=(h_3-h_2)/(h_7-h_2)
DELTAT_LMTD_IHE=((T_10-T_2)- (T_9-T_3))/ln((T_10-T_2)/ (T_9-T_3))
Q_dot_IHE=(1-y)*m_dot_wf*(h_9-h_10)
"----------------------CONDENSER-------------------------------"
"Inlet of Condenser = outlet of Turbine"
h_c=Enthalpy(wf$,T=T_c,x=1)
s_c=Entropy(wf$,T=T_c,x=1)
h_10=Enthalpy(wf$, T=T_10,P=P_10)
P_10=P_c
h_10=h_1+q_c
s_10 = Entropy(wf$, h=h_10,P=P_10)
m_dot_cw*Cp_cw*(T_15-T_14)=(1-y)*m_dot_wf*(h_10-h_1)
DELTAT_LMTD_c=((T_10-T_15)- (T_1-T_14))/ln((T_10-T_15)/ (T_1-T_14))
Q_dot_c=(1-y)*m_dot_wf*q_c
"Cooling water"
Cp_cw=Cp(cw$, T=T_14)
P_14=P_o
h_14=Enthalpy(cw$,T=T_14)
s_14=Entropy(cw$,T=T_14,P=P_o)
P_15=P_o
h_15=Enthalpy(cw$,T=T_15)
s_15=Entropy(cw$,T=T_15,P=P_o)
"----------------DOWNHOLE HEAT EXCHANGER-----------------------"
"Inlet"
T_13=T_rej
P_13=P_11
h_13=Enthalpy(geo$,T=T_13, P=P_13)
s_13=Entropy(geo$,T=T_13, P=P_13)
"Outlet"
Cp_geo=Cp(geo$,T=T_geo,x=0)
T_11=T_geo
P_11=P_sat(geo$,T=T_11)
h_11=Enthalpy(geo$,T=T_11, x=0)
s_11=Entropy(geo$,T=T_11, x=0)
```

```
"---------OVERALL EFFICIENCY OF THE CYCLE-----------"
w_net = w_t1+(1-y)*w_t2 - (1-y)*w_p1-w_p2
W_dot_p=m_dot_wf*(  (1-y)*w_p1+w_p2)
W_dot_t=m_dot_wf*(w_t1+(1-y)*w_t2)
W_dot_net=m_dot_wf*w_net
n_th = w_net /q_IN
n_th2 = 1-((1-y)*q_c /q_IN)
n_I=(W_dot_net/(m_dot_geo*Cp_geo*(ConvertTEMP(C,K,T_geo)-ConvertTEMP(C,K,T_o))))*100
n_I2=(W_dot_net/(m_dot_geo*Cp_geo*(ConvertTEMP(C,K,T_geo)-ConvertTEMP(C,K,T_rej))))*100
n_I2a=(W_dot_net/(m_dot_wf*(h_7-h_2)))*100
n_II=(W_dot_net/(m_dot_geo*Cp_geo*(ConvertTEMP(C,K,T_geo)-ConvertTEMP(C,K,T_o)-
ConvertTEMP(C,K,T_o)*ln(ConvertTEMP(C,K,T_geo)/ConvertTEMP(C,K,T_o)))))*100
n_II2=(W_dot_net/(m_dot_geo*Cp_geo*(ConvertTEMP(C,K,T_geo)-ConvertTEMP(C,K,T_rej)-
ConvertTEMP(C,K,T_o)*ln(ConvertTEMP(C,K,T_geo)/ConvertTEMP(C,K,T_rej)))))*100
n_III=(W_dot_net/(m_dot_wf*((h_7-h_5)-ConvertTEMP(C,K,T_o)*(s_7-s_5))))*100
beta=m_dot_wf/m_dot_geo
gamma=m_dot_cw/m_dot_wf
"--------------------IRREVERSIBILITY ANALYSIS----------------------"
E_dot_in=m_dot_geo*((h_11-h_o)-ConvertTEMP(C,K,T_o)*(s_11-s_o))
I_dot_p=(1-y)*m_dot_wf*((h_1-h_2)-ConvertTEMP(C,K,T_o)*(s_1-s_2))+m_dot_wf*((h_4-h_5)-
ConvertTEMP(C,K,T_o)*(s_4-s_5))+W_dot_p
I_dot_PH=m_dot_wf*((h_5-h_6)-ConvertTEMP(C,K,T_o) *(s_5-s_6))+m_dot_geo*((h_12-h_13)-
ConvertTEMP(C,K,T_o) *(s_12-s_13))
I_dot_E=m_dot_wf*((h_6-h_7)-ConvertTEMP(C,K,T_o) *(s_6-s_7))+m_dot_geo*((h_11-h_12)-
ConvertTEMP(C,K,T_o) *(s_11-s_12))
I_dot_t=m_dot_wf*((h_7-h_8)-ConvertTEMP(C,K,T_o) *(s_7-s_8))+(1-y)*m_dot_wf*((h_8-h_9)-
ConvertTEMP(C,K,T_o) *(s_8-s_9))-W_dot_t
I_dot_IHE=(1-y)*m_dot_wf*((h_2-h_3)-ConvertTEMP(C,K,T_o) *(s_2-s_3))+(1-y)*m_dot_wf*((h_9-h_10)-
ConvertTEMP(C,K,T_o) *(s_9-s_10))
I_dot_OFOH=m_dot_wf*(((1-y)*h_3+y*h_8-h_4)-ConvertTEMP(C,K,T_o)*((1-y)*s_3+y*s_8-s_4))
I_dot_c=(1-y)*m_dot_wf*((h_10-h_1)-ConvertTEMP(C,K,T_o) *(s_10-s_1))+m_dot_cw*((h_14-h_15)-
ConvertTEMP(C,K,T_o) *(s_14-s_15))
I_dot_rej=m_dot_geo*((h_13-h_o)-ConvertTEMP(C,K,T_o)*(s_13-s_o))
I_dot_HX=m_dot_wf*((h_5-h_7)-ConvertTEMP(C,K,T_o) *(s_5-s_7))+m_dot_geo*((h_11-h_13)-
ConvertTEMP(C,K,T_o) *(s_11-s_13))
I_dot_cycle=I_dot_p+I_dot_PH+I_dot_E+I_dot_t+I_dot_c+I_dot_OFOH+I_dot_IHE
I_dot_plant=E_dot_in-W_dot_net
I_dot_planta=I_dot_cycle+I_dot_CA+I_dot_rej
I_dot_CA=m_dot_cw*((h_15-h_14)-ConvertTEMP(C,K,T_o)*(s_15-s_14))
```

```
"-------------------------------------------------------------------------------"
Y_p=I_dot_p/E_dot_in*100
Y_PH=I_dot_PH/E_dot_in*100
Y_E=I_dot_E/E_dot_in*100
Y_t=I_dot_t/E_dot_in*100
Y_IHE=I_dot_IHE/E_dot_in*100
Y_OFOH=I_dot_OFOH/E_dot_in*100
Y_c=I_dot_c/E_dot_in*100
Y_rej=I_dot_rej/E_dot_in*100
Y_CA=I_dot_CA/E_dot_in*100
Y_HX=I_dot_HX/E_dot_in*100
Y_W=W_dot_net/E_dot_in*100
Y_total=Y_p+Y_PH+Y_E+Y_t+Y_c+Y_W+Y_rej+Y_OFOH+Y_CA+Y_IHE
Y_cycle=I_dot_cycle/E_dot_in*100
Y_plant=I_dot_plant/E_dot_in*100
"-------------------------------------------------------------------------------"
X_p=I_dot_p/I_dot_plant*100
X_IHE=I_dot_IHE/I_dot_plant*100
X_OFOH=I_dot_OFOH/I_dot_plant*100
X_PH=I_dot_PH/I_dot_plant*100
X_E=I_dot_E/I_dot_plant*100
X_t=I_dot_t/I_dot_plant*100
X_c=I_dot_c/I_dot_plant*100
X_rej=I_dot_rej/I_dot_plant*100
X_CA=I_dot_CA/I_dot_plant*100
X_total=X_p+X_PH+X_E+X_t+X_c+X_rej+X_CA+X_IHE+X_OFOH
"-------------------------------------------------------------------------------"
efx_p=(W_dot_p-I_dot_p)/W_dot_p*100
efx_PH=(m_dot_wf*((h_6-h_5)-ConvertTEMP(C,K,T_o) *(s_6-s_5)))/(m_dot_geo*((h_12-h_13)-
ConvertTEMP(C,K,T_o) *(s_12-s_13)))*100
efx_E=(m_dot_wf*((h_7-h_6)-ConvertTEMP(C,K,T_o) *(s_7-s_6)))/(m_dot_geo*((h_11-h_12)-
ConvertTEMP(C,K,T_o) *(s_11-s_12)))*100
efx_t=W_dot_t/(W_dot_t+I_dot_p)*100
efx_IHE=((1-y)*m_dot_wf*((h_3-h_2)-ConvertTEMP(C,K,T_o) *(s_3-s_2)))/((1-y)*m_dot_wf*((h_9-h_10)-
ConvertTEMP(C,K,T_o) *(s_9-s_10)))*100
efx_OFOH=((h_4-h_o)-ConvertTEMP(C,K,T_o) *(s_4-s_o))/((y*h_8+(1-y)*h_3-h_o)-
ConvertTEMP(C,K,T_o) *(y*s_8+(1-y)*s_3-s_o))*100
efx_c=(m_dot_cw*((h_15-h_14)-ConvertTEMP(C,K,T_o) *(s_15-s_14)))/((1-y)*m_dot_wf*((h_10-h_1)-
ConvertTEMP(C,K,T_o) *(s_10-s_1)))*100
```

```
"--------------------------------------------------------------------------------"
eff_p=(h_2s-h_1)/(h_2-h_1)*100
eff_PH=(T_12-T_13)/(T_12-T_5)*100
eff_E=(T_11-T_12)/(T_11-T_6)*100
eff_t=(h_7-h_8)/(h_7-h_8s)*100
eff_OFOH=(T_4-T_3)/(T_8-T_3)*100
eff_IHE=(T_9-T_10)/(T_9-T_2)*100
eff_c=(T_10-T_1)/(T_10-T_14)*100
"--------------------------------------------------------------------------------"
```

Appendix U: MATlab code- Design and sizing of the system components of an ORC with an IHE

```
"----------------------------ORC  WITH IHE CYCLE-----------------------------"
"----------------------------PREHEATER SIZING-----------------------------"
procedure Preheater(D_s,N_PH, wf$,
geo$,cw$,T_3,P_3,h_3,T_4,P_4,h_4,T_9,P_9,h_9,T_10,P_10,h_10,m_dot_geo,m_dot_wf,m_dot_cw,n_t
PH,d_iPH,pass:Area_PH,Length_PH,DELTAp_tPH,DELTAp_sPH,W_dot_ghPH,
Volume_tPH,Volume_wPH,Volume_zPH)
value_PH:=0
surface_PH:=0
dp_tPH:=0
dp_sPH:=0
n_p=0.90

N_pPH=pass;F=1 "One tube pass"
d_oPH=1.2*d_iPH
t_wallPH=d_oPH-d_iPH
P_tPH=1.5*d_oPH
A_iPH=(pi/4)*d_iPH^2

CL_PH=1
CTP_PH=0.93   "one tube pass"

D_ePH=4*(P_tPH^2-(pi/4*d_oPH^2))/(pi*d_oPH)
C_PH=P_tPH-d_oPH
D_sPH=D_s
n_tPH=0.785*(CTP_PH/CL_PH)*D_sPH^2/((P_tPH/d_oPH)^2*d_oPH^2)
G_tPH=m_dot_wf/(A_iPH*n_tPH)

B_PH=0.60*D_sPH
A_sPH=D_sPH*C_PH*B_PH/P_tPH
G_sPH=m_dot_geo/A_sPH
T_PHwf=(T_4-T_3)/N_PH
T_PHgeo=(T_9-T_10)/N_PH
h_PHwf=(h_4-h_3)/N_PH
rho_oPH=Density(geo$,T=(T_9+T_10)/2,P=(P_9+P_10)/2)
rho_iPH=Density(wf$,T=(T_3+T_4)/2,P=(P_3+P_4)/2)
V_tPH=G_tPH/rho_iPH
```

V_sPH=G_sPH/rho_oPH

Repeat
T_PHwfin=T_3+(N_PH-1)*T_PHwf
T_PHwfout=T_3+N_PH*T_PHwf
mu_iPH=Viscosity(wf$,T=(T_PHwfin+T_PHwfout)/2,P=(P_3+P_4)/2)
k_iPH=Conductivity(wf$,T=(T_PHwfin+T_PHwfout)/2,P=(P_3+P_4)/2)
Pr_iPH=Prandtl(wf$,T=(T_PHwfin+T_PHwfout)/2,P=(P_3+P_4)/2)
rho_iPH=Density(wf$,T=(T_PHwfin+T_PHwfout)/2,P=(P_3+P_4)/2)

h_PHwfin=h_3+(N_PH-1)*h_PHwf
h_PHwfout=h_3+N_PH*h_PHwf

T_PHgeoin=T_10+N_PH*T_PHgeo
T_PHgeoout=T_10+(N_PH-1)*T_PHgeo
mu_oPH=Viscosity(geo$,T=(T_PHgeoin+T_PHgeoout)/2,P=(P_9+P_10)/2)
k_oPH=Conductivity(geo$,T=(T_PHgeoin+T_PHgeoout)/2,P=(P_9+P_10)/2)
Pr_oPH=Prandtl(geo$,T=(T_PHgeoin+T_PHgeoout)/2,P=(P_9+P_10)/2)
rho_oPH=Density(geo$,T=(T_PHgeoin+T_PHgeoout)/2,P=(P_9+P_10)/2)

Cp_geo=Cp(geo$,T=T_PHgeoin,x=0)
Q_dot_PH=m_dot_geo*Cp_geo*(T_PHgeoin-T_PHgeoout)
Q_dot_PH=m_dot_wf*(h_PHwfout-h_PHwfin)

T_wPH=(T_PHwfin+T_PHwfout+T_PHgeoin+T_PHgeoout)/4
P_wPH=(P_3+P_4+P_9+P_10)/4
mu_wPH=Viscosity(geo$,T=T_wPH,P=P_wPH)
k_tube=k_('Stainless_AISI316', T=T_wPH)

DELTAT_LMTD_PH=((T_PHgeoout-T_PHwfin)- (T_PHgeoin-T_PHwfout))/ln((T_PHgeoout-T_PHwfin)/(T_PHgeoin-T_PHwfout))

Re_iPH=(4*m_dot_wf)/(pi*mu_iPH*d_iPH*n_tPH)
Nu_iPH=0.012*(Re_iPH^0.87-280)*Pr_iPH^0.40
h_iPH=Nu_iPH*k_iPH/d_iPH
Re_oPH=G_sPH*D_ePH/mu_oPH
Nu_oPH=0.36*Re_oPH^0.55*Pr_oPH^(1/3)*(mu_oPH/mu_wPH)^0.14
h_oPH=Nu_oPH*k_oPH/D_ePH
U_PH=1/((d_oPH/(d_iPH*h_iPH))+((d_oPH*ln(d_oPH/d_iPH))/(2*k_tube))+(1/h_oPH))

```
A_PH=Q_dot_PH/(F*U_PH*DELTAT_LMTD_PH)*1000
L_PH=A_PH/(N_pPH*n_tPH*pi*d_oPH)
surface_PH:=surface_PH+A_PH
value_PH:=value_PH+L_PH
f_iPH=(1.58*ln(Re_iPH)-3.28)^(-2)
dp_iPH=G_tPH^2/(2*rho_iPH)*(4*f_iPH*N_pPH*L_PH/d_iPH+4*(N_pPH-1))
dp_tPH=dp_iPH+dp_tPH
f_oPH=exp(0.576-0.19*ln(Re_oPH))
N_bPH=(L_PH/B_PH)-1
dp_oPH=f_oPH*G_sPH^2*D_sPH*(N_bPH+1)/(2*rho_oPH*D_ePH*(mu_oPH/mu_wPH)^0.14)
dp_sPH=dp_oPH+dp_sPH
N_PH:=N_PH-1;
Until (N_PH=0)
Area_PH:=surface_PH
Length_PH:=value_PH
Volume_tPH=(pi/4)*Length_PH*(D_sPH+2*t_wallPH)^2
Volume_wPH=(pi/4)*Length_PH*(n_tPH*(d_oPH^2-d_iPH^2)+((D_sPH+2*t_wallPH)^2-D_sPH^2))
Volume_zPH=Volume_wPH/Volume_tPH
DELTAp_tPH:=dp_tPH/1000 "kPa"
DELTAp_sPH:=dp_sPH/1000 "kPa"
W_dot_ghPH=(m_dot_geo*DELTAp_sPH)/(rho_oPH*n_p)
End
"------------------------------RECUPERATOR SIZING--------------------------------"
procedure Recuperator(D_s,N_IHE, wf$,
geo$,cw$,T_3,P_3,h_3,T_2,P_2,h_2,T_6,P_6,h_6,T_7,P_7,h_7,m_dot_geo,m_dot_wf,m_dot_cw,n_tIHE,
d_iIHE,pass:Area_IHE,Length_IHE,DELTAp_tIHE, DELTAp_sIHE,W_dot_ghIHE,
Volume_tIHE,Volume_wIHE,Volume_zIHE)
m_dot_hot=m_dot_wf
value_IHE:=0
surface_IHE:=0
dp_tIHE:=0
dp_sIHE:=0
n_p=0.90
hot$=wf$
N_pIHE=pass;F=1 "One tube pass"
d_oIHE=1.2*d_iIHE
t_wallIHE=d_oIHE-d_iIHE
P_tIHE=1.5*d_oIHE
A_iIHE=(pi/4)*d_iIHE^2
```

```
CL_IHE=1
CTP_IHE=0.93   "one tube pass"

D_eIHE=4*(P_tIHE^2-(pi/4*d_oIHE^2))/(pi*d_oIHE)
C_IHE=P_tIHE-d_oIHE
D_sIHE=D_s
n_tIHE=0.785*(CTP_IHE/CL_IHE)*D_sIHE^2/((P_tIHE/d_oIHE)^2*d_oIHE^2)
G_tIHE=m_dot_hot/(A_iIHE*n_tIHE)
B_IHE=0.60*D_sIHE
A_sIHE=D_sIHE*C_IHE*B_IHE/P_tIHE
G_sIHE=m_dot_wf/A_sIHE
T_IHEwf=(T_3-T_2)/N_IHE
T_IHEhot=(T_6-T_7)/N_IHE
h_IHEwf=(h_3-h_2)/N_IHE
h_IHEhot=(h_6-h_7)/N_IHE
rho_oIHE=Density(wf$,T=(T_6+T_7)/2,P=(P_6+P_7)/2)
rho_iIHE=Density(wf$,T=(T_3+T_2)/2,P=(P_3+P_2)/2)
V_tIHE=G_tIHE/rho_iIHE
V_sIHE=G_sIHE/rho_oIHE

Repeat
T_IHEhotin=T_7+N_IHE*T_IHEhot
T_IHEhotout=T_7+(N_IHE-1)*T_IHEhot
mu_iIHE=Viscosity(hot$,T=(T_IHEhotin+T_IHEhotout)/2,P=(P_6+P_7)/2)
k_iIHE=Conductivity(hot$,T=(T_IHEhotin+T_IHEhotout)/2,P=(P_6+P_7)/2)
Pr_iIHE=Prandtl(hot$,T=(T_IHEhotin+T_IHEhotout)/2,P=(P_6+P_7)/2)
rho_iIHE=Density(hot$,T=(T_IHEhotin+T_IHEhotout)/2,P=(P_6+P_7)/2)
h_IHEhotin=h_7+(N_IHE-1)*h_IHEhot
h_IHEhotout=h_7+N_IHE*h_IHEhot
h_IHEwfin=h_2+(N_IHE-1)*h_IHEwf
h_IHEwfout=h_2+N_IHE*h_IHEwf
T_IHEwfin=T_2+(N_IHE-1)*T_IHEwf
T_IHEwfout=T_2+N_IHE*T_IHEwf
mu_oIHE=Viscosity(wf$,T=(T_IHEwfin+T_IHEwfout)/2,P=(P_2+P_3)/2)
k_oIHE=Conductivity(wf$,T=(T_IHEwfin+T_IHEwfout)/2,P=(P_2+P_3)/2)
Pr_oIHE=Prandtl(wf$,T=(T_IHEwfin+T_IHEwfout)/2,P=(P_2+P_3)/2)
rho_oIHE=Density(wf$,T=(T_IHEwfin+T_IHEwfout)/2,P=(P_2+P_3)/2)
Q_dot_IHE=m_dot_hot*(h_IHEhotin-h_IHEhotout)
Q_dot_IHE=m_dot_wf*(h_IHEwfout-h_IHEwfin)
```

```
T_wIHE=(T_IHEwfin+T_IHEwfout+T_IHEhotin+T_IHEhotout)/4
P_wIHE=(P_2+P_3+P_6+P_7)/4
mu_wIHE=Viscosity(hot$,T=T_wIHE,P=P_wIHE)
k_tube=k_('Stainless_AISI316', T=T_wIHE)

DELTAT_LMTD_IHE=((T_IHEhotout-T_IHEwfin)- (T_IHEhotin-T_IHEwfout))/ln((T_IHEhotout-
T_IHEwfin)/(T_IHEhotin-T_IHEwfout))
Re_iIHE=(4*m_dot_hot)/(pi*mu_iIHE*d_iIHE*n_tIHE)
Nu_iIHE=0.012*(Re_iIHE^0.87-280)*Pr_iIHE^0.40
h_iIHE=Nu_iIHE*k_iIHE/d_iIHE
Re_oIHE=G_sIHE*D_eIHE/mu_oIHE
Nu_oIHE=0.36*Re_oIHE^0.55*Pr_oIHE^(1/3)*(mu_oIHE/mu_wIHE)^0.14
h_oIHE=Nu_oIHE*k_oIHE/D_eIHE
U_IHE=1/((d_oIHE/(d_iIHE*h_iIHE))+((d_oIHE*ln(d_oIHE/d_iIHE))/(2*k_tube))+(1/h_oIHE))
A_IHE=Q_dot_IHE/(F*U_IHE*DELTAT_LMTD_IHE)*1000
L_IHE=A_IHE/(N_pIHE*n_tIHE*pi*d_oIHE)
surface_IHE:=surface_IHE+A_IHE
value_IHE:=value_IHE+L_IHE
f_iIHE=(1.58*ln(Re_iIHE)-3.28)^(-2)
dp_iIHE=G_tIHE^2/(2*rho_iIHE)*(4*f_iIHE*N_pIHE*L_IHE/d_iIHE+4*(N_pIHE-1))
dp_tIHE=dp_iIHE+dp_tIHE
f_oIHE=exp(0.576-0.19*ln(Re_oIHE))
N_bIHE=(L_IHE/B_IHE)-1
dp_oIHE=f_oIHE*G_sIHE^2*D_sIHE*(N_bIHE+1)/(2*rho_oIHE*D_eIHE*(mu_oIHE/mu_wIHE)^0.14)
dp_sIHE=dp_oIHE+dp_sIHE
N_IHE:=N_IHE-1;
Until (N_IHE=0)
Area_IHE:=surface_IHE
Length_IHE:=value_IHE
Volume_tIHE=(pi/4)*Length_IHE*(D_sIHE+2*t_wallIHE)^2
Volume_wIHE=(pi/4)*Length_IHE*(n_tIHE*(d_oIHE^2-d_iIHE^2)+((D_sIHE+2*t_wallIHE)^2-D_sIHE^2))
Volume_zIHE=Volume_wIHE/Volume_tIHE
DELTAp_tIHE:=dp_tIHE/1000 "kPa"
DELTAp_sIHE:=dp_sIHE/1000 "kPa"
W_dot_ghIHE=(m_dot_hot*DELTAp_sIHE)/(rho_oIHE*n_p)
End

"----------------------------EVAPORATOR SIZING-------------------------------"
```

```
procedure Evaporator(D_s,N_E, wf$,
geo$,cw$,T_4,P_4,h_4,T_5,P_5,h_5,T_8,P_8,h_8,T_9,P_9,h_9,m_dot_geo,m_dot_wf,m_dot_cw,n_tE,d
_iE,pass:Area_E,Length_E,DELTAp_tE,DELTAp_sE,W_dot_ghE, Volume_tE,Volume_wE,Volume_zE)
value_E:=0
surface_E:=0
dp_tE:=0
dp_sE:=0
n_p = 0.90
F=1 "CONDENSATION"
N_pE=pass
d_oE=1.2*d_iE
t_wallE=d_oE-d_iE
P_tE=1.5*d_oE
A_iE=(pi/4)*d_iE^2
CL_E=1
CTP_E=0.93   "one tube pass"

D_eE=4*(P_tE^2-(pi/4*d_oE^2))/(pi*d_oE)
C_E=P_tE-d_oE
D_sE=D_s
n_tE=0.785*(CTP_E/CL_E)*D_sE^2/((P_tE/d_oE)^2*d_oE^2)
G_tE=m_dot_wf/(A_iE*n_tE)
B_E=0.60*D_sE
A_sE=D_sE*C_E*B_E/P_tE
G_sE=m_dot_geo/A_sE
rho_oE=Density(geo$,T=(T_8+T_9)/2,P=(P_8+P_9)/2)
rho_iE=Density(wf$,T=(T_4+T_5)/2,x=0)
V_tE=G_tE/rho_iE
V_sE=G_sE/rho_oE
x_Einc=1/N_E
T_Ewf=(T_5-T_4)/N_E
T_Egeo=(T_8-T_9)/N_E
h_Ewf=(h_5-h_4)/N_E

Repeat
x_Eout=N_E*x_Einc
x_Ein=x_Eout-x_Einc
T_Ewfin=T_4+(N_E-1)*T_Ewf
T_Ewfout=T_4+N_E*T_Ewf
```

```
mu_lE=Viscosity(wf$,T=(T_Ewfin+T_Ewfout)/2,x=0)
k_lE=Conductivity(wf$,T=(T_Ewfin+T_Ewfout)/2,x=0)
Pr_lE=Prandtl(wf$,T=(T_Ewfin+T_Ewfout)/2,x=0)
rho_lE=Density(wf$,T=(T_Ewfin+T_Ewfout)/2,x=0)
mu_vE=Viscosity(wf$,T=(T_Ewfin+T_Ewfout)/2,x=1)
k_vE=Conductivity(wf$,T=(T_Ewfin+T_Ewfout)/2,x=1)
Pr_vE=Prandtl(wf$,T=(T_Ewfin+T_Ewfout)/2,x=1)
rho_vE=Density(wf$,T=(T_Ewfin+T_Ewfout)/2,x=1)
rho_H=1/(x_Ein/rho_vE+(1-x_Ein)/rho_lE)
g=9.81
sigma_in=SurfaceTension(wf$,T=T_Ewfin)
sigma_out=SurfaceTension(wf$,T=T_Ewfout)

h_Ewfin=h_4+(N_E-1)*h_Ewf
h_Ewfout=h_4+N_E*h_Ewf

T_Egeoin=T_9+N_E*T_Egeo
T_Egeoout=T_9+(N_E-1)*T_Egeo
mu_oE=Viscosity(geo$,T=(T_Egeoin+T_Egeoout)/2,P=(P_8+P_9)/2)
k_oE=Conductivity(geo$,T=(T_Egeoin+T_Egeoout)/2,P=(P_8+P_9)/2)
Pr_oE=Prandtl(geo$,T=(T_Egeoin+T_Egeoout)/2,P=(P_8+P_9)/2)
rho_oE=Density(geo$,T=(T_Egeoin+T_Egeoout)/2,P=(P_8+P_9)/2)

Cp_geo=Cp(geo$,T=T_Egeoin,x=0)
Q_dot_E=m_dot_geo*Cp_geo*(T_Egeoin-T_Egeoout)
Q_dot_E=m_dot_wf*(h_Ewfout-h_Ewfin)

T_wE=(T_Ewfin+T_Ewfout+T_Egeoin+T_Egeoout)/4
P_wE=(P_4+P_5+P_8+P_9)/4
mu_wE=Viscosity(geo$,T=T_wE,P=P_wE)
k_tube=k_('Stainless_AISI316', T=T_wE)

DELTAT_LMTD_E=((T_Egeoout-T_Ewfin)- (T_Egeoin-T_Ewfout))/ln((T_Egeoout-T_Ewfin)/(T_Egeoin-
T_Ewfout))
Bo=(Q_dot_E)/(G_tE*(h_5-h_4))

if x_Ein=0 then
Re_lE=(4*m_dot_wf)/(pi*mu_lE*d_iE*n_tE)
Re_vE=(4*m_dot_wf)/(pi*mu_vE*d_iE*n_tE)
```

```
Nu_iEin=0.012*(Re_lE^0.87-280)*Pr_lE^0.40
h_iEin=Nu_iEin*k_lE/d_iE
Nu_iEout=0.023*(G_tE*(1-x_Eout)*(d_iE/mu_lE))^0.8*Pr_lE^0.4*(1+3000*Bo^0.86+1.12*(x_Eout/(1-
x_Eout))^0.75*(rho_lE/rho_vE)^0.41)
h_iEout=Nu_iEout*k_lE/d_oE

Re_oE=G_sE*D_eE/mu_oE
Nu_oE=0.36*Re_oE^0.55*Pr_oE^(1/3)*(mu_oE/mu_wE)^0.14
h_oE=Nu_oE*k_oE/D_eE
U_Ein=1/((d_oE/(d_iE*h_iEin))+((d_oE*ln(d_oE/d_iE))/(2*k_tube))+(1/h_oE))
U_Eout=1/((d_oE/(d_iE*h_iEout))+((d_oE*ln(d_oE/d_iE))/(2*k_tube))+(1/h_oE))
U_E=(U_Ein+U_Eout)/2
A_E=Q_dot_E/(F*U_E*DELTAT_LMTD_E)*1000
L_E=A_E/(N_pE*n_tE*pi*d_oE)
eps_E=(x_Eout/rho_vE)/((1+0.12*(1-x_Eout))*(x_Eout/rho_vE+((1-x_Eout)/rho_lE)+1.18*(1-
x_Eout)*(g*sigma_in*(rho_lE-rho_vE))^0.25/(G_tE^2*rho_lE^0.5)))
dp_iEmom=G_tE^2*((((1-x_Eout)^2/(rho_lE*(1-eps_E))+(x_Eout^2/(rho_vE*eps_E))))-((1-
x_Ein)^2/(rho_lE*(1-eps_E))+(x_Ein^2/(rho_vE*eps_E))))
f_L=0.079/Re_lE^0.25
f_G=0.079/Re_vE^0.25
Fr_H=G_tE^2/(g*d_iE*rho_H^2)
E=(1-x_Ein)^2+x_Ein^2*(rho_lE*f_G)/(rho_vE*f_L)
F_E=x_Ein^0.78*(1-x_Ein)^0.224
H=(rho_lE/rho_vE)^0.91*(mu_vE/mu_lE)^0.19*(1-mu_vE/mu_lE)^0.7
We_L=(G_tE^2*d_iE)/(sigma_in*rho_H)
dp_iEfrict=4*f_L*(L_E/d_iE)*G_tE^2/(2*rho_lE)*(E+(3.24*F_E*H)/(Fr_H^0.045*We_L^0.035))
dp_iE=dp_iEmom+dp_iEfrict
dp_tE=dp_iE+dp_tE
 f_oE=exp(0.576-0.19*ln(Re_oE))
N_bE=(L_E/B_E)-1
dp_oE=f_oE*G_sE^2*D_sE*(N_bE+1)/(2*rho_oE*D_eE*(mu_oE/mu_wE)^0.14)
dp_sE=dp_oE+dp_sE
surface_E:=surface_E+A_E
value_E:=value_E+L_E
endIF

if x_Eout=1 then
Re_lE=(4*m_dot_wf)/(pi*mu_lE*d_iE*n_tE)
Re_vE=(4*m_dot_wf)/(pi*mu_vE*d_iE*n_tE)
```

```
Nu_iEin=0.023*(G_tE*(1-x_Ein)*(d_iE/mu_lE))^0.8*Pr_lE^0.4*(1+3000*Bo^0.86+1.12*(x_Ein/(1-
x_Ein))^0.75*(rho_lE/rho_vE)^0.41)
h_iEin=Nu_iEin*k_lE/d_iE
Nu_iEout=0.012*(Re_vE^0.87-280)*Pr_vE^0.40
h_iEout=Nu_iEout*k_vE/d_iE

Re_oE=G_sE*D_eE/mu_oE
Nu_oE=0.36*Re_oE^0.55*Pr_oE^(1/3)*(mu_oE/mu_wE)^0.14
h_oE=Nu_oE*k_oE/D_eE
U_Ein=1/((d_oE/(d_iE*h_iEin))+((d_oE*ln(d_oE/d_iE))/(2*k_tube))+(1/h_oE))
U_Eout=1/((d_oE/(d_iE*h_iEout))+((d_oE*ln(d_oE/d_iE))/(2*k_tube))+(1/h_oE))
U_E=(U_Ein+U_Eout)/2
A_E=Q_dot_E/(F*U_E*DELTAT_LMTD_E)*1000
L_E=A_E/(n_tE*pi*d_oE)
eps_E=(x_Ein/rho_vE)/((1+0.12*(1-x_Ein))*(x_Ein/rho_vE+((1-x_Ein)/rho_lE)+1.18*(1-
x_Ein)*(g*sigma_in*(rho_lE-rho_vE))^0.25/(G_tE^2*rho_lE^0.5)))
dp_iEmom=G_tE^2*((((1-x_Eout)^2/(rho_lE*(1-eps_E))+(x_Eout^2/(rho_vE*eps_E))))-((1-
x_Ein)^2/(rho_lE*(1-eps_E))+(x_Ein^2/(rho_vE*eps_E))))
f_L=0.079/Re_lE^0.25
f_G=0.079/Re_vE^0.25
Fr_H=G_tE^2/(g*d_iE*rho_H^2)
E=(1-x_Ein)^2+x_Ein^2*(rho_lE*f_G)/(rho_vE*f_L)
F_E=x_Ein^0.78*(1-x_Ein)^0.224
H=(rho_lE/rho_vE)^0.91*(mu_vE/mu_lE)^0.19*(1-mu_vE/mu_lE)^0.7
We_L=(G_tE^2*d_iE)/(sigma_in*rho_H)
dp_iEfrict=4*f_L*(L_E/d_iE)*G_tE^2/(2*rho_lE)*(E+(3.24*F_E*H)/(Fr_H^0.045*We_L^0.035))
dp_iE=dp_iEmom+dp_iEfrict
dp_tE=dp_iE+dp_tE
f_oE=exp(0.576-0.19*ln(Re_oE))
N_bE=(L_E/B_E)-1
dp_oE=f_oE*G_sE^2*D_sE*(N_bE+1)/(2*rho_oE*D_eE*(mu_oE/mu_wE)^0.14)
dp_sE=dp_oE+dp_sE
surface_E:=surface_E+A_E
value_E:=value_E+L_E

else
Re_lE=(4*m_dot_wf)/(pi*mu_lE*d_iE*n_tE)
Re_vE=(4*m_dot_wf)/(pi*mu_vE*d_iE*n_tE)
```

```
Nu_iEin=0.023*(G_tE*(1-x_Ein)*(d_iE/mu_lE))^0.8*Pr_lE^0.4*(1+3000*Bo^0.86+1.12*(x_Ein/(1-
x_Ein))^0.75*(rho_lE/rho_vE)^0.41)
h_iEin=Nu_iEin*k_lE/d_iE
Nu_iEout=0.023*(G_tE*(1-x_Eout)*(d_iE/mu_lE))^0.8*Pr_lE^0.4*(1+3000*Bo^0.86+1.12*(x_Eout/(1-
x_Eout))^0.75*(rho_lE/rho_vE)^0.41)
h_iEout=Nu_iEout*k_lE/d_iE

Re_oE=G_sE*D_eE/mu_oE
Nu_oE=0.36*Re_oE^0.55*Pr_oE^(1/3)*(mu_oE/mu_wE)^0.14
h_oE=Nu_oE*k_oE/D_eE
U_Ein=1/((d_oE/(d_iE*h_iEin))+((d_oE*ln(d_oE/d_iE))/(2*k_tube))+(1/h_oE))
U_Eout=1/((d_oE/(d_iE*h_iEout))+((d_oE*ln(d_oE/d_iE))/(2*k_tube))+(1/h_oE))
U_E=(U_Ein+U_Eout)/2
A_E=Q_dot_E/(F*U_E*DELTAT_LMTD_E)*1000
L_E=A_E/(n_tE*pi*d_oE)
eps_E=(x_Eout/rho_vE)/((1+0.12*(1-x_Eout))*(x_Eout/rho_vE+((1-x_Eout)/rho_lE)+1.18*(1-
x_Eout)*(g*sigma_in*(rho_lE-rho_vE))^0.25/(G_tE^2*rho_lE^0.5)))
dp_iEmom=G_tE^2*((((1-x_Eout)^2/(rho_lE*(1-eps_E))+(x_Eout^2/(rho_vE*eps_E))))-((1-
x_Ein)^2/(rho_lE*(1-eps_E))+(x_Ein^2/(rho_vE*eps_E))))
f_L=0.079/Re_lE^0.25
f_G=0.079/Re_vE^0.25
Fr_H=G_tE^2/(g*d_iE*rho_H^2)
E=(1-x_Ein)^2+x_Ein^2*(rho_lE*f_G)/(rho_vE*f_L)
F_E=x_Ein^0.78*(1-x_Ein)^0.224
H=(rho_lE/rho_vE)^0.91*(mu_vE/mu_lE)^0.19*(1-mu_vE/mu_lE)^0.7
We_L=(G_tE^2*d_iE)/(sigma_in*rho_H)
dp_iEfrict=4*f_L*(L_E/d_iE)*G_tE^2/(2*rho_lE)*(E+(3.24*F_E*H)/(Fr_H^0.045*We_L^0.035))
dp_iE=dp_iEmom+dp_iEfrict
dp_tE=dp_iE+dp_tE
f_oE=exp(0.576-0.19*ln(Re_oE))
N_bE=(L_E/B_E)-1
dp_oE=f_oE*G_sE^2*D_sE*(N_bE+1)/(2*rho_oE*D_eE*(mu_oE/mu_wE)^0.14)
dp_sE=dp_oE+dp_sE
surface_E:=surface_E+A_E
value_E:=value_E+L_E
endIF
N_E:=N_E-1;
Until (N_E=0)
Area_E:=surface_E
```

```
Length_E:=value_E
Volume_tE=(pi/4)*Length_E*(D_sE+2*t_wallE)^2
Volume_wE=(pi/4)*Length_E*(n_tE*(d_oE^2-d_iE^2)+((D_sE+2*t_wallE)^2-D_sE^2))
Volume_zE=Volume_wE/Volume_tE
DELTAp_tE:=dp_tE/1000 "kPa"
DELTAp_sE:=dp_sE/1000 "kPa"
W_dot_ghE=(m_dot_geo*DELTAp_sE)/(rho_oE*n_p)
End

"----------------------------CONDENSER SIZING-------------------------------"
procedure Condenser(N_C, wf$,
geo$,cw$,T_1,P_1,h_1,T_7,P_7,h_7,T_11,P_11,h_11,T_12,P_12,h_12,T_c,P_c,h_c,m_dot_geo,m_dot_
wf,m_dot_cw,n_trans,n_long,
d_iC:Area_C1,Area_C2,Area_C,Length_C1,Length_C2,Length_C,DELTAp_tC,DELTAp_sC,W_dot_fan,V
_frC,n_fin_m,P_tC,P_lC)
Length_C=1
repeat
L_Cprev=Length_C
N_Co=N_C
n_fan = 0.90
value_C:=0
surface_C:=0
dp_tC:=0
dp_sC:=0
P_cw=Po#
F=1
Cp_cw=Cp(cw$,T=T_12)
Q_dot_C=m_dot_wf*(h_c-h_1)
T_cw=T_11+Q_dot_C/(m_dot_cw*Cp_cw)

d_oC=1.2*d_iC
t_w=(d_iC+d_oC)/2
P_tC=2.5*d_oC
P_lC=2*d_oC
P_dC=((P_tC/2)^2+P_lC^2)^(1/2)
t_fin=0.0003
C1=P_tC/d_oC
C2=(1/P_tC)*(P_lC^2+P_tC^2/4)^(1/2)
R_e=1.27*(d_oC/2)*C1*(C2-0.3)^(1/2)
```

```
D_sC=2*R_e
phi=(D_sC/d_oC-1)*(1+0.35*ln(D_sC/d_oC))
z=P_tC-d_oC
A_iC=(pi/4)*d_iC^2
n_tC=n_trans*n_long
G_tC=m_dot_wf/(A_iC*n_tC)
A_fr=n_trans*D_sC*L_Cprev
n_fin_m=100   "fins per meter"
n_fin=n_fin_m*L_Cprev*n_tC
P_fin=(1/n_fin)-t_fin
A_fin=n_fin*((pi/2)*(D_sC^2-d_oC^2)+pi*D_sC*t_fin)
A_unfin=n_tC*pi*d_oC*L_Cprev-n_fin*pi*d_oC*t_fin
A_T=A_unfin+A_fin
P_test=2*P_dC-d_oC-(2*z*t_fin)/(z+t_fin)
if P_tC>P_test then
A_min=n_trans*L_Cprev*(P_tC-d_oC-(2*z*t_fin)/(z+t_fin))
else
A_min=2*n_trans*L_Cprev*(P_dC-d_oC-(2*z*t_fin)/(z+t_fin))
endIF
D_eq=d_oC*(1-n_fin_m*t_fin)+n_fin_m*((1/2)*(D_sc^2-d_oC^2)+D_sC*t_fin)
D_h=4*D_sC*(A_min/A_T)
L_fin=(D_sC-d_oC)/2+(t_fin/2)
A_isC=n_tC*pi*d_iC*L_Cprev
A_osC=n_tC*pi*(d_iC+t_w)*L_Cprev
rho_cwC=Density(cw$,T=(T_11+T_12)/2,P=(P_11+P_12)/2)
rho_wfC=Density(wf$,T=(T_1+T_7)/2,P=(P_1+P_7)/2)
V_fr1=m_dot_cw/(rho_cwC*A_fr)
V_tC=G_tC/rho_wfC
G_oC=m_dot_cw/A_min
"------------------------------DESUPERHEATING------------------------------"
x_Cinc=1/N_C
T_Cwf=(T_7-T_c)/N_C
T_Ccw=(T_12-T_cw)/N_C
h_Cwf=(h_7-h_c)/N_C
"----------------------------------------x>1----------------------------------------"
Repeat
T_Cwfin=T_c+N_C*T_Cwf
T_Cwfout=T_c+(N_C-1)*T_Cwf
mu_iC=Viscosity(wf$,T=(T_Cwfin+T_Cwfout)/2,P=(P_7+P_c)/2)
```

```
k_iC=Conductivity(wf$,T=(T_Cwfin+T_Cwfout)/2,P=(P_7+P_c)/2)
Pr_iC=Prandtl(wf$,T=(T_Cwfin+T_Cwfout)/2,P=(P_7+P_c)/2)
rho_iC=Density(wf$,T=(T_Cwfin+T_Cwfout)/2,P=(P_7+P_c)/2)

h_Cwfin=h_c+N_C*h_Cwf
h_Cwfout=h_c+(N_C-1)*h_Cwf

T_Ccwin=T_cw+(N_C-1)*T_Ccw
T_Ccwout=T_cw+N_C*T_Ccw
mu_oC=Viscosity(cw$,T=(T_Ccwin+T_Ccwout)/2)
k_oC=Conductivity(cw$,T=(T_Ccwin+T_Ccwout)/2)
Pr_oC=Prandtl(cw$,T=(T_Ccwin+T_Ccwout)/2)
rho_oC=Density(cw$,T=(T_Ccwin+T_Ccwout)/2,P=(P_12+P_cw)/2)
Cp_oC=Cp(cw$, T=(T_Ccwin+T_Ccwout)/2)

Cp_cw=Cp(cw$,T=T_Ccwin)
Q_dot_C=m_dot_cw*Cp_cw*(T_Ccwout-T_Ccwin)
Q_dot_C=m_dot_wf*(h_Cwfin-h_Cwfout)

T_wC=(T_Cwfin+T_Cwfout+T_Ccwin+T_Ccwout)/4
k_tube=k_('Stainless_AISI316', T=T_wC)
Pr_wC=Prandtl(cw$,T=T_wC)
mu_wC=Viscosity(cw$,T=T_wC)
DELTAT_LMTD_C=((T_Cwfin-T_Ccwout)-(T_Cwfout-T_Ccwin))/ln((T_Cwfin-T_Ccwout)/(T_Cwfout-
T_Ccwin))

Re_iC=(4*m_dot_wf)/(pi*mu_iC*d_iC*n_tC)
Nu_iC=0.012*(Re_iC^0.87-280)*Pr_iC^0.40
h_iC=Nu_iC*k_iC/d_iC
Re_oC=(d_oC*G_oC)/mu_oC
Nu_oC=0.38*Re_oC^0.6*Pr_oC^(1/3)*(A_unfin/A_T)^0.15
h_oC=Nu_oC*k_oC/d_oC
m_es=((2*h_oC)/(k_tube*t_fin))^(1/2)
eta_f=tanh(m_es*R_e*phi)/(m_es*R_e*phi)
eta_o=1-A_fin*(1-eta_f)/A_T
U_C=1/((1/(h_iC))+((d_iC*ln(d_oC/d_iC))/(2*k_tube))+(A_isC/(h_oC*eta_o*A_T)))
A_C=Q_dot_C/(F*U_C*DELTAT_LMTD_C)*1000
L_C=A_C/(n_tC*pi*D_eq)
f_iC=(1.58*ln(Re_iC)-3.28)^(-2)
```

```
dp_iC=G_tC^2/(2*rho_iC)*(4*f_iC*L_C/d_iC)
dp_tC=dp_iC+dp_tC
dp_oCtube=18.03*(G_oC^2/rho_oC)*n_long*Re_oC^(-0.316)*(P_tC/d_oC)^(-0.927)*(P_tC/P_dC)^0.515
Re_long=G_oC*P_lC/mu_oC
f_fin=1.7*Re_long^(-0.5)
dp_oCfin=(f_fin*G_oC^2*A_fin)/(2*rho_oC*A_min)
dp_oC=dp_oCfin+dp_oCtube
dp_sC=dp_oC+dp_sC
dp_sC1=dp_sC
value_C:=value_C+L_C
surface_C:=surface_C+A_C
N_C:=N_C-1;
Until (N_C=0)
N_C=N_Co
Area_C1:=surface_C
Length_C1=value_C
"-----------------------------------------CONDENSING-----------------------------------------"
N_C=N_Co
value_C:=0
surface_C:=0
x_Cinc=1/N_Co
T_Cwf=(T_c-T_1)/N_Co
T_Ccw=(T_cw-T_11)/N_Co
h_Cwf=(h_c-h_1)/N_Co
PC=P_crit(wf$)
P_sat=P_sat(wf$,T=T_c)
p_r=P_sat/PC
Repeat
x_Cin=N_Co*x_Cinc
x_Cout=x_Cin-x_Cinc
T_Cwfin=T_1+N_Co*T_Cwf
T_Cwfout=T_1+(N_Co-1)*T_Cwf
mu_lC=Viscosity(wf$,T=(T_Cwfin+T_Cwfout)/2,x=0)
k_lC=Conductivity(wf$,T=(T_Cwfin+T_Cwfout)/2,x=0)
Pr_lC=Prandtl(wf$,T=(T_Cwfin+T_Cwfout)/2,x=0)
rho_lC=Density(wf$,T=(T_Cwfin+T_Cwfout)/2,x=0)
rho_vC=Density(wf$,T=(T_Cwfin+T_Cwfout)/2,x=1)

mu_vC=Viscosity(wf$,T=(T_Cwfin+T_Cwfout)/2,x=1)
```

```
k_vC=Conductivity(wf$,T=(T_Cwfin+T_Cwfout)/2,x=1)
Pr_vC=Prandtl(wf$,T=(T_Cwfin+T_Cwfout)/2,x=1)
rho_vC=Density(wf$,T=(T_Cwfin+T_Cwfout)/2,x=1)
rho_H=1/(x_Cin/rho_vC+(1-x_Cin)/rho_lC)

g=9.81
sigma_in=SurfaceTension(wf$,T=T_Cwfin)
sigma_out=SurfaceTension(wf$,T=T_Cwfout)

mu_iC=mu_lC
k_iC=k_lC
Pr_iC=Pr_lC
rho_iC=rho_lC

h_Cwfin=h_1+N_Co*h_Cwf
h_Cwfout=h_1+(N_Co-1)*h_Cwf

T_Ccwin=T_11+(N_Co-1)*T_Ccw
T_Ccwout=T_11+N_Co*T_Ccw
mu_oC=Viscosity(cw$,T=(T_Ccwin+T_Ccwout)/2)
k_oC=Conductivity(cw$,T=(T_Ccwin+T_Ccwout)/2)
Pr_oC=Prandtl(cw$,T=(T_Ccwin+T_Ccwout)/2)
rho_oC=Density(cw$,T=(T_Ccwin+T_Ccwout)/2,P=(P_11+P_cw)/2)
Cp_oC=Cp(cw$, T=(T_Ccwin+T_Ccwout)/2)

Cp_cw=Cp(cw$,T=T_Ccwin)
Q_dot_C=m_dot_cw*Cp_cw*(T_Ccwout-T_Ccwin)
Q_dot_C=m_dot_wf*(h_Cwfin-h_Cwfout)

T_wC=(T_Cwfin+T_Cwfout+T_Ccwin+T_Ccwout)/4
Pr_wC=Prandtl(cw$,T=T_wC)
k_tube=k_('Stainless_AISI316', T=T_wC)
DELTAT_LMTD_C=((T_Cwfin-T_Ccwout)- (T_Cwfout-T_Ccwin))/ln((T_Cwfin-T_Ccwout)/(T_Cwfout-
T_Ccwin))

if x_Cout=0 then
Re_lC=(4*m_dot_wf)/(pi*mu_lC*d_iC*n_tC)
Re_vC=(4*m_dot_wf)/(pi*mu_vC*d_iC*n_tC)
```

```
Nu_iCin=0.023*(G_tC*(d_iC/mu_lC))^0.8*Pr_lC^0.4*((1-x_Cin)^0.8+(3.8*x_Cin^0.76*(1-
x_Cin)^0.04)/p_r^0.38)
h_iCin=Nu_iCin*k_lC/d_iC
Re_iC=(4*m_dot_wf)/(pi*mu_iC*d_oC*n_tC)
Nu_iCout=0.012*(Re_iC^0.87-280)*Pr_iC^0.40
h_iCout=Nu_iCout*k_lC/d_iC
Re_oC=(d_oC*G_oC)/mu_oC
Nu_oC=0.38*Re_oC^0.6*Pr_oC^(1/3)*(A_unfin/A_T)^0.15
h_oC=Nu_oC*k_oC/d_oC
m_es=((2*h_oC)/(k_tube*t_fin))^(1/2)
eta_f=tanh(m_es*R_e*phi)/(m_es*R_e*phi)
eta_o=1-A_fin*(1-eta_f)/A_T
U_Cin=1/((1/(h_iCin))+((d_iC*ln(d_oC/d_iC))/(2*k_tube))+(A_isC/(h_oC*eta_o*A_T)))
U_Cout=1/((1/(h_iCout))+((d_iC*ln(d_oC/d_iC))/(2*k_tube))+(A_isC/(h_oC*eta_o*A_T)))
U_C=(U_Cin+U_Cout)/2
A_C=Q_dot_C/(F*U_C*DELTAT_LMTD_C)*1000
L_C=A_C/(n_tC*pi*D_eq)
surface_C:=surface_C+A_C
value_C:=value_C+L_C
eps_C=(x_Cin/rho_vC)/((1+0.12*(1-x_Cin))*(x_Cin/rho_vC+((1-x_Cin)/rho_lC)+1.18*(1-
x_Cin)*(g*sigma_in*(rho_lC-rho_vC))^0.25/(G_tC^2*rho_lC^0.5)))
dp_iCmom=G_tC^2*((((1-x_Cin)^2/(rho_lC*(1-eps_C))+(x_Cin^2/(rho_vC*eps_C))))-((1-
x_Cin)^2/(rho_lC*(1-eps_C))+(x_Cin^2/(rho_vC*eps_C))))
f_L=0.079/Re_lC^0.25
f_G=0.079/Re_vC^0.25
Fr_H=G_tC^2/(g*d_iC*rho_H^2)
E=(1-x_Cin)^2+x_Cin^2*(rho_lC*f_G)/(rho_vC*f_L)
F_C=x_Cin^0.78*(1-x_Cin)^0.224
H=(rho_lC/rho_vC)^0.91*(mu_vC/mu_lC)^0.19*(1-mu_vC/mu_lC)^0.7
We_L=(G_tC^2*d_iC)/(sigma_in*rho_H)
dp_iCfrict=4*f_L*(L_C/d_iC)*G_tC^2/(2*rho_lC)*(E+(3.24*F_C*H)/(Fr_H^0.045*We_L^0.035))
dp_iC=dp_iCmom+dp_iCfrict
dp_tC=dp_iC+dp_tC
dp_oCtube=18.03*(G_oC^2/rho_oC)*n_long*Re_oC^(-0.316)*(P_tC/d_oC)^(-0.927)*(P_tC/P_dC)^0.515
Re_long=G_oC*P_lC/mu_oC
f_fin=1.7*Re_long^(-0.5)
dp_oCfin=(f_fin*G_oC^2*A_fin)/(2*rho_oC*A_min)
dp_oC=dp_oCfin+dp_oCtube
dp_sC=dp_oC+dp_sC
```

```
endIF

if x_Cin=1 then
Re_lC=(4*m_dot_wf)/(pi*mu_lC*d_iC*n_tC)
Re_vC=(4*m_dot_wf)/(pi*mu_vC*d_iC*n_tC)
Re_iC=(4*m_dot_wf)/(pi*mu_iC*d_oC*n_tC)
Nu_iCin=0.012*(Re_iC^0.87-280)*Pr_iC^0.40
h_iCin=Nu_iCin*k_lC/d_iC
Nu_iCout=0.023*(G_tC*(d_iC/mu_lC))^0.8*Pr_lC^0.4*((1-x_Cout)^0.8+(3.8*x_Cout^0.76*(1-
x_Cout)^0.04)/p_r^0.38)
h_iCout=Nu_iCout*k_lC/d_iC
Re_oC=(d_oC*G_oC)/mu_oC
Nu_oC=0.38*Re_oC^0.6*Pr_oC^(1/3)*(A_unfin/A_T)^0.15
h_oC=Nu_oC*k_oC/d_oC
m_es=((2*h_oC)/(k_tube*t_fin))^(1/2)
eta_f=tanh(m_es*R_e*phi)/(m_es*R_e*phi)
eta_o=1-A_fin*(1-eta_f)/A_T
U_Cin=1/((1/(h_iCin))+((d_iC*ln(d_oC/d_iC))/(2*k_tube))+(A_isC/(h_oC*eta_o*A_T)))
U_Cout=1/((1/(h_iCout))+((d_iC*ln(d_oC/d_iC))/(2*k_tube))+(A_isC/(h_oC*eta_o*A_T)))
U_C=(U_Cin+U_Cout)/2
A_C=Q_dot_C/(F*U_C*DELTAT_LMTD_C)*1000
L_C=A_C/(n_tC*pi*D_eq)
surface_C:=surface_C+A_C
value_C:=value_C+L_C
eps_C=(x_Cout/rho_vC)/((1+0.12*(1-x_Cout))*(x_Cout/rho_vC+((1-x_Cout)/rho_lC)+1.18*(1-
x_Cout)*(g*sigma_in*(rho_lC-rho_vC))^0.25/(G_tC^2*rho_lC^0.5)))
dp_iCmom=G_tC^2*((((1-x_Cout)^2/(rho_lC*(1-eps_C))+(x_Cout^2/(rho_vC*eps_C))))-((1-
x_Cin)^2/(rho_lC*(1-eps_C))+(x_Cin^2/(rho_vC*eps_C))))
f_L=0.079/Re_lC^0.25
f_G=0.079/Re_vC^0.25
Fr_H=G_tC^2/(g*d_iC*rho_H^2)
E=(1-x_Cin)^2+x_Cin^2*(rho_lC*f_G)/(rho_vC*f_L)
F_C=x_Cin^0.78*(1-x_Cin)^0.224
H=(rho_lC/rho_vC)^0.91*(mu_vC/mu_lC)^0.19*(1-mu_vC/mu_lC)^0.7
We_L=(G_tC^2*d_iC)/(sigma_in*rho_H)
dp_iCfrict=4*f_L*(L_C/d_iC)*G_tC^2/(2*rho_lC)*(E+(3.24*F_C*H)/(Fr_H^0.045*We_L^0.035))
dp_iC=dp_iCmom+dp_iCfrict
dp_tC=dp_iC+dp_tC
dp_oCtube=18.03*(G_oC^2/rho_oC)*n_long*Re_oC^(-0.316)*(P_tC/d_oC)^(-0.927)*(P_tC/P_dC)^0.515
```

```
Re_long=G_oC*P_lC/mu_oC
f_fin=1.7*Re_long^(-0.5)
dp_oCfin=(f_fin*G_oC^2*A_fin)/(2*rho_oC*A_min)
dp_oC=dp_oCfin+dp_oCtube
dp_sC=dp_oC+dp_sC

else
Re_lC=(4*m_dot_wf)/(pi*mu_lC*d_iC*n_tC)
Re_vC=(4*m_dot_wf)/(pi*mu_vC*d_iC*n_tC)
Nu_iCin=0.023*(G_tC*(d_iC/mu_lC))^0.8*Pr_lC^0.4*((1-x_Cin)^0.8+(3.8*x_Cin^0.76*(1-
x_Cin)^0.04)/p_r^0.38)
h_iCin=Nu_iCin*k_lC/d_iC
Nu_iCout=0.023*(G_tC*(1-x_Cout)*(d_iC/mu_lC))^0.8*Pr_lC^0.4*((1-x_Cout)^0.8+(3.8*x_Cout^0.76*(1-
x_Cout)^0.04)/p_r^0.38)
h_iCout=Nu_iCout*k_lC/d_iC
Re_oC=(d_oC*G_oC)/mu_oC
Nu_oC=0.38*Re_oC^0.6*Pr_oC^(1/3)*(A_unfin/A_T)^0.15

h_oC=Nu_oC*k_oC/d_oC
m_es=((2*h_oC)/(k_tube*t_fin))^(1/2)
eta_f=tanh(m_es*R_e*phi)/(m_es*R_e*phi)
eta_o=1-A_fin*(1-eta_f)/A_T
U_Cin=1/((1/(h_iCin))+((d_iC*ln(d_oC/d_iC))/(2*k_tube))+(A_isC/(h_oC*eta_o*A_T)))
U_Cout=1/((1/(h_iCout))+((d_iC*ln(d_oC/d_iC))/(2*k_tube))+(A_isC/(h_oC*eta_o*A_T)))
U_C=(U_Cin+U_Cout)/2
A_C=Q_dot_C/(F*U_C*DELTAT_LMTD_C)*1000
L_C=A_C/(n_tC*pi*D_eq)
surface_C:=surface_C+A_C
value_C:=value_C+L_C
eps_C=(x_Cin/rho_vC)/((1+0.12*(1-x_Cin))*(x_Cin/rho_vC+((1-x_Cin)/rho_lC)+1.18*(1-
x_Cin)*(g*sigma_in*(rho_lC-rho_vC))^0.25/(G_tC^2*rho_lC^0.5)))
dp_iCmom=G_tC^2*((((1-x_Cout)^2/(rho_lC*(1-eps_C))+(x_Cout^2/(rho_vC*eps_C))))-((1-
x_Cin)^2/(rho_lC*(1-eps_C))+(x_Cin^2/(rho_vC*eps_C))))
f_L=0.079/Re_lC^0.25
f_G=0.079/Re_vC^0.25
Fr_H=G_tC^2/(g*d_iC*rho_H^2)
E=(1-x_Cin)^2+x_Cin^2*(rho_lC*f_G)/(rho_vC*f_L)
F_C=x_Cin^0.78*(1-x_Cin)^0.224
H=(rho_lC/rho_vC)^0.91*(mu_vC/mu_lC)^0.19*(1-mu_vC/mu_lC)^0.7
```

```
We_L=(G_tC^2*d_iC)/(sigma_in*rho_H)
dp_iCfrict=4*f_L*(L_C/d_iC)*G_tC^2/(2*rho_lC)*(E+(3.24*F_C*H)/(Fr_H^0.045*We_L^0.035))
dp_iC=dp_iCmom+dp_iCfrict
dp_tC=dp_iC+dp_tC
dp_oCtube=18.03*(G_oC^2/rho_oC)*n_long*Re_oC^(-0.316)*(P_tC/d_oC)^(-0.927)*(P_tC/P_dC)^0.515
Re_long=G_oC*P_lC/mu_oC
f_fin=1.7*Re_long^(-0.5)
dp_oCfin=(f_fin*G_oC^2*A_fin)/(2*rho_oC*A_min)
dp_oC=dp_oCfin+dp_oCtube
dp_sC=dp_oC+dp_sC
dp_sC2=dp_sC-dp_sC1
endIF

N_Co:=N_Co-1;
Until (N_Co=0)
Length_C2:=value_C
Area_C2:=surface_C
Area_C=Area_C1+Area_C2
Length_C=Area_C/(pi*n_tC*D_eq)
until (Length_C=L_Cprev)
A_fr=n_trans*D_sC*Length_C
V_frC=m_dot_cw/(rho_cwC*A_fr)
DELTAp_tC:=dp_tC/1000 "kPa"
DELTAp_sC:=(dp_sC/N_C)/1000 "kPa"
W_dot_fan=(G_oC*A_min*DELTAp_sC)/(rho_cwC*n_fan)
End
"------------------------------TURBINE SIZING-------------------------------"
procedure Turbine(wf$,
geo$,cw$,T_5,h_5,P_5,T_6s,h_6s,T_6,P_6,m_dot_geo,m_dot_wf,m_dot_cw:VFR,SP)
rho_in=Density(wf$,T=T_5,x=1)
rho_out=Density(wf$,T=T_6s,P=P_6)
V_dot_in=m_dot_wf/rho_in
V_dot_out=m_dot_wf/rho_out
VFR=V_dot_out/V_dot_in
DELTAH_is=h_5-h_6s
SP=(V_dot_out)^(1/2)/(DELTAH_is*1000)^(1/4)
End
"-------------------------RECUPERATED  CYCLE-------------------------------"
"-----------------------------------INPUT-----------------------------------"
```

```
"Fluid"
wf$='n-pentane'
cw$='air'
geo$='water'
"Data"
T_o=25 [C]
P_o=Po#
h_o=Enthalpy(geo$,T=T_o, x=0)
s_o=Entropy(geo$,T=T_o, x=0)
m_dot_geo=21.31287298[kg/s]
T_geo=160 [C]
DELTAT_pp= 5 [C]
T_E=97[C]
P_E=P_sat(wf$,T=T_E)
T_c=29.3 [C]
P_c=P_sat(wf$,T=T_c) "Condenser pressure"
T_11=T_o                "Cooling water inlet temperature"
n_t = 0.80              "Isentropic efficiency"
n_p = 0.90              "Isentropic efficiency"
"-------------------------PUMP-------------------------------------"
 "Losses due to friction, heat dissipation, ...."
P_loss = 0 [kPa]
T_loss = 0 [C]
"Inlet"
P_1=P_c- P_loss
T_1= T_c- T_loss
v_1 = Volume(wf$,T=T_1,x=0)
h_1 = Enthalpy(wf$, T=T_1,x=0)
s_1 = Entropy(wf$, T=T_1,x=0)
"Outlet"
T_2s=Temperature(wf$,s=s_2s,P=P_2s)
P_2s = P_E
h_2s=h_1+v_1*(P_2s-P_1)/n_p
s_2s=s_1
P_2 = P_2s
T_2= Temperature(wf$,h=h_2,P=P_2)
h_2=h_1+(h_2s-h_1)/n_p
s_2=Entropy(wf$, T=T_2,P=P_2)
"Output"
```

```
h_2 = h_1 + w_p "1st law:"
"-------------------------PREHEATER-------------------------------------"
"Inlet"
P_3=P_E
T_3=Temperature(wf$,h=h_3,P=P_3)
s_3=Entropy(wf$,T=T_3,P=P_3)
"Outlet"
T_4=T_5
P_4=P_E
h_4=Enthalpy(wf$, T=T_4,x=0)
s_4=Entropy(wf$, T=T_4,x=0)
h_3+q_IN=h_5
percent_Q_PH=(h_4-h_3)/(h_5-h_2)
m_dot_geo*Cp_geo*(T_9-T_10)=m_dot_wf*(h_4-h_3)
Q_dot_PH=m_dot_wf*(h_4-h_3)
"----------------------------EVAPORATOR-------------------------------------"
"Pitch point"
DELTAT_pp= T_pp-T_4
T_9=T_pp
P_9=P_8
h_9=Enthalpy(geo$,T=T_9, x=0)
s_9=Entropy(geo$,T=T_9, x=0)
m_dot_geo*Cp_geo*(T_8-T_9)=m_dot_wf*(h_5-h_4)
percent_Q_E=(h_5-h_4)/(h_5-h_2)
DELTAT_LMTD_E=((T_8-T_5)- (T_9-T_4))/ln((T_8-T_5)/ (T_9-T_4))
Q_dot_E=m_dot_wf*(h_5-h_4)
"-----------------------------------TURBINE---------------------------------------"
"Inlet"
T_5 =T_E
P_5 =P_E
h_5 =Enthalpy(wf$,T=T_5,x=1)
s_5 =Entropy(wf$,T=T_5,x=1)
"Outlet"
P_6=P_c
T_6s=Temperature(wf$,P=P_6,s=s_6s)
h_6s=Enthalpy(wf$,P=P_6,s=s_6s)
s_6s=s_5 "2nd law: Isentropic process"
h_6=h_5-n_t*(h_5-h_6s)
T_6=Temperature(wf$,P=P_6,h=h_6)
```

```
s_6 = Entropy(wf$,P=P_6,h=h_6)
"Output"
h_5 = h_6 + w_t "1st law:"
"-----------------------------RECUPERATOR-------------------------------------"
"Heat exchange"
EPSILON=0.8
EPSILON=(T_6-T_7)/ (T_6-T_2)
(h_6-h_7)=(h_3-h_2)
percent_Q_IHE=(h_3-h_2)/(h_5-h_2)
DELTAT_LMTD_IHE=((T_7-T_2)- (T_6-T_3))/ln((T_7-T_2)/ (T_6-T_3))
Q_dot_IHE=m_dot_wf*(h_6-h_7)
"----------------------CONDENSER-------------------------------"
"Inlet of Condenser = outlet of Turbine"
h_c=Enthalpy(wf$,T=T_c,x=1)
s_c=Entropy(wf$,T=T_c,x=1)
h_7=h_1+q_c
P_7=P_c
h_7=Enthalpy(wf$, T=T_7,P=P_7)
s_7 = Entropy(wf$, T=T_7,P=P_7)
m_dot_cw*Cp_cw*(T_12-T_cw)=m_dot_wf*(h_7-h_c)
m_dot_cw*Cp_cw*(T_cw-T_11)=m_dot_wf*(h_c-h_1)
DELTAT_LMTD_c=((T_7-T_12)- (T_1-T_11))/ln((T_7-T_12)/ (T_1-T_11))
Q_dot_c=m_dot_wf*q_c
2=T_c-T_cw
"Cooling water"
Cp_cw=Cp(cw$, T=T_11)
P_11=P_o
h_11=Enthalpy(cw$,T=T_11)
s_11=Entropy(cw$,T=T_11,P=P_o)
P_12=P_o
h_12=Enthalpy(cw$,T=T_12)
s_12=Entropy(cw$,T=T_12,P=P_o)
"---------------DOWNHOLE HEAT EXCHANGER----------------------"
"Inlet"
T_10=T_rej
P_10=P_8
h_10=Enthalpy(geo$,T=T_10, P=P_10)
s_10=Entropy(geo$,T=T_10, P=P_10)
"Outlet"
```

```
Cp_geo=Cp(geo$,T=T_geo,x=0)
T_8=T_geo
P_8=P_sat(geo$,T=T_8)
 h_8=Enthalpy(geo$,T=T_8, x=0)
s_8=Entropy(geo$,T=T_8, x=0)
"---------OVERALL EFFICIENCY OF THE CYCLE-----------"
w_net = w_t - w_p
W_dot_p=m_dot_wf*w_p
W_dot_t=m_dot_wf*w_t
W_dot_net=m_dot_wf*w_net
n_th = w_net /q_IN
n_th2 = 1-(q_c /q_IN)
n_I=(W_dot_net/(m_dot_geo*Cp_geo*(ConvertTEMP(C,K,T_geo)-ConvertTEMP(C,K,T_o))))*100
n_I2=(W_dot_net/(m_dot_geo*Cp_geo*(ConvertTEMP(C,K,T_geo)-ConvertTEMP(C,K,T_rej))))*100
n_I2a=(W_dot_net/(m_dot_wf*(h_5-h_2)))*100
n_II=(W_dot_net/(m_dot_geo*Cp_geo*(ConvertTEMP(C,K,T_geo)-ConvertTEMP(C,K,T_o)-
ConvertTEMP(C,K,T_o)*ln(ConvertTEMP(C,K,T_geo)/ConvertTEMP(C,K,T_o)))))*100
n_II2=(W_dot_net/(m_dot_geo*Cp_geo*(ConvertTEMP(C,K,T_geo)-ConvertTEMP(C,K,T_rej)-
ConvertTEMP(C,K,T_o)*ln(ConvertTEMP(C,K,T_geo)/ConvertTEMP(C,K,T_rej)))))*100
n_III=(W_dot_net/(m_dot_wf*((h_5-h_3)-ConvertTEMP(C,K,T_o)*(s_5-s_3))))*100
beta=m_dot_wf/m_dot_geo
gamma=m_dot_cw/m_dot_wf
"--------------------IRREVERSIBILITY ANALYSIS----------------------"
E_dot_in=m_dot_geo*((h_8-h_o)-ConvertTEMP(C,K,T_o)*(s_8-s_o))
I_dot_p=m_dot_wf*((h_1-h_2)-ConvertTEMP(C,K,T_o) *(s_1-s_2))+W_dot_p
I_dot_IHE=m_dot_wf*((h_2-h_3)-ConvertTEMP(C,K,T_o) *(s_2-s_3))+m_dot_wf*((h_6-h_7)-
ConvertTEMP(C,K,T_o) *(s_6-s_7))
I_dot_PH=m_dot_wf*((h_3-h_4)-ConvertTEMP(C,K,T_o) *(s_3-s_4))+m_dot_geo*((h_9-h_10)-
ConvertTEMP(C,K,T_o) *(s_9-s_10))
I_dot_E=m_dot_wf*((h_4-h_5)-ConvertTEMP(C,K,T_o) *(s_4-s_5))+m_dot_geo*((h_8-h_9)-
ConvertTEMP(C,K,T_o) *(s_8-s_9))
I_dot_t=m_dot_wf*((h_5-h_6)-ConvertTEMP(C,K,T_o) *(s_5-s_6))-W_dot_t
I_dot_c=m_dot_wf*((h_7-h_1)-ConvertTEMP(C,K,T_o) *(s_7-s_1))+m_dot_cw*((h_11-h_12)-
ConvertTEMP(C,K,T_o) *(s_11-s_12))
I_dot_rej=m_dot_geo*((h_10-h_o)-ConvertTEMP(C,K,T_o)*(s_10-s_o))
I_dot_HX=m_dot_wf*((h_3-h_5)-ConvertTEMP(C,K,T_o) *(s_3-s_5))+m_dot_geo*((h_8-h_10)-
ConvertTEMP(C,K,T_o) *(s_8-s_10))
I_dot_cycle=I_dot_p+I_dot_IHE+I_dot_PH+I_dot_E+I_dot_t+I_dot_c
I_dot_plant=E_dot_in-W_dot_net
```

```
I_dot_planta=I_dot_cycle+I_dot_CA+I_dot_rej
I_dot_CA=m_dot_cw*((h_12-h_11)-ConvertTEMP(C,K,T_o)*(s_12-s_11))
"-------------------------------------------------------------------------------------"
Y_p=I_dot_p/E_dot_in*100
Y_IHE=I_dot_IHE/E_dot_in*100
Y_PH=I_dot_PH/E_dot_in*100
Y_E=I_dot_E/E_dot_in*100
Y_t=I_dot_t/E_dot_in*100
Y_c=I_dot_c/E_dot_in*100
Y_rej=I_dot_rej/E_dot_in*100
Y_CA=I_dot_CA/E_dot_in*100
Y_HX=I_dot_HX/E_dot_in*100
Y_W=W_dot_net/E_dot_in*100
Y_cycle=I_dot_cycle/E_dot_in*100
Y_plant=I_dot_plant/E_dot_in*100
Y_total=Y_p+Y_PH+Y_E+Y_t+Y_c+Y_W+Y_rej+Y_IHE+Y_CA
"-------------------------------------------------------------------------------------"
X_p=I_dot_p/I_dot_plant*100
X_IHE=I_dot_IHE/I_dot_plant*100
X_PH=I_dot_PH/I_dot_plant*100
X_E=I_dot_E/I_dot_plant*100
X_t=I_dot_t/I_dot_plant*100
X_c=I_dot_c/I_dot_plant*100
X_rej=I_dot_rej/I_dot_plant*100
X_CA=I_dot_CA/I_dot_plant*100
X_total=X_p+X_PH+X_E+X_t+X_c+X_rej+X_CA+X_IHE
"-------------------------------------------------------------------------------------"
efx_p=(W_dot_p-I_dot_p)/W_dot_p*100
efx_IHE=((h_3-h_2)-ConvertTEMP(C,K,T_o) *(s_3-s_2))/((h_6-h_7)-ConvertTEMP(C,K,T_o) *(s_6-
s_7))*100
efx_PH=(m_dot_wf*((h_4-h_3)-ConvertTEMP(C,K,T_o) *(s_4-s_3)))/(m_dot_geo*((h_9-h_10)-
ConvertTEMP(C,K,T_o) *(s_9-s_10)))*100
efx_E=(m_dot_wf*((h_5-h_4)-ConvertTEMP(C,K,T_o) *(s_5-s_4)))/(m_dot_geo*((h_8-h_9)-
ConvertTEMP(C,K,T_o) *(s_8-s_9)))*100
efx_t=W_dot_t/(W_dot_t+I_dot_t)*100
efx_c=(m_dot_cw*((h_12-h_11)-ConvertTEMP(C,K,T_o) *(s_12-s_11)))/(m_dot_wf*((h_7-h_1)-
ConvertTEMP(C,K,T_o) *(s_7-s_1)))*100
"-------------------------------------------------------------------------------------"
e_1=((h_1)-ConvertTEMP(C,K,T_o) *(s_1))
```

```
e_2=((h_2)-ConvertTEMP(C,K,T_o) *(s_2))
e_3=((h_3)-ConvertTEMP(C,K,T_o) *(s_3))
e_4=((h_4)-ConvertTEMP(C,K,T_o) *(s_4))
e_5=((h_5)-ConvertTEMP(C,K,T_o) *(s_5))
e_6=((h_6)-ConvertTEMP(C,K,T_o) *(s_6))
e_7=((h_7)-ConvertTEMP(C,K,T_o) *(s_7))
e_8=((h_8)-ConvertTEMP(C,K,T_o) *(s_8))
e_9=((h_9)-ConvertTEMP(C,K,T_o) *(s_9))
e_10=((h_10)-ConvertTEMP(C,K,T_o) *(s_10))
e_11=((h_11)-ConvertTEMP(C,K,T_o) *(s_11))
e_12=((h_12)-ConvertTEMP(C,K,T_o) *(s_12))
"-------------------------------------------------------------------------------"
efxb_p=e_2/(e_1+w_p)*100
efxf_p=(e_2-e_1)/w_p*100
efxb_IHE=(m_dot_wf*e_3+m_dot_wf*e_7)/(m_dot_wf*e_2+m_dot_wf*e_6)*100
efxf_IHE=(m_dot_wf*(e_3-e_2))/(m_dot_wf*(e_6-e_7))*100
efxb_PH=(m_dot_wf*e_4+m_dot_geo*e_10)/(m_dot_wf*e_3+m_dot_geo*e_9)*100
efxf_PH=(m_dot_wf*(e_4-e_3))/(m_dot_geo*(e_9-e_10))*100
efxb_E=(m_dot_wf*e_5+m_dot_geo*e_9)/(m_dot_wf*e_4+m_dot_geo*e_8)*100
efxf_E=(m_dot_wf*(e_5-e_4))/(m_dot_geo*(e_8-e_9))*100

efxb_t=(w_t+e_6)/e_5*100
efxf_t=w_t/(e_5-e_6)*100
efxb_C=(m_dot_cw*e_12+m_dot_wf*e_1)/(m_dot_cw*e_11+m_dot_wf*e_7)*100
efxf_C=(m_dot_cw*(e_12-e_11))/(m_dot_wf*(e_7-e_1))*100

"-------------------------------------------------------------------------------"
eff_p=(h_2s-h_1)/(h_2-h_1)*100
eff_PH=(T_9-T_10)/(T_9-T_3)*100
eff_E=(T_8-T_9)/(T_8-T_4)*100
eff_t=(h_5-h_6)/(h_5-h_6s)*100
eff_IHE=(T_6-T_7)/(T_6-T_2)*100
eff_c=(T_7-T_1)/(T_7-T_11)*100
"-------------------------------------------------NTU_PH_____________________________________________"
NTU=1
Cp_geo_PH=Cp(geo$,T=T_9,P=P_9)
Cp_wf_PH=Cp(wf$,T=T_3,P=P_3)
C_max_PH=m_dot_geo*Cp_geo_PH
C_min_PH=m_dot_wf*Cp_wf_PH
```

```
c_PH=C_min_PH/C_max_PH
e_PH=(1-exp(-NTU*(1-c_PH)))/(1-c_PH*exp(-NTU*(1-c_PH)))
Ns1_PH=T_3/(e_PH*(T_9-T_3))*(ln(1+e_PH*c_PH*(ConvertTEMP(C,K,T_9)/ConvertTEMP(C,K,T_3)-
1))/c_PH+(ln(1-e_PH*(1-ConvertTEMP(C,K,T_3)/ConvertTEMP(C,K,T_9)))))
Sgen_PH=m_dot_geo*Cp_geo*ln(ConvertTEMP(C,K,T_10)/ConvertTEMP(C,K,T_9))+m_dot_wf*Cp_geo
*ln(ConvertTEMP(C,K,T_4)/ConvertTEMP(C,K,T_3))
"----------------------------------------------------NTU_IHE_____________________________________________"
m_dot_hot=m_dot_wf
Cp_hot_IHE=Cp(wf$,T=T_6,P=P_6)
Cp_wf_IHE=Cp(wf$,T=T_2,P=P_2)
C_max_IHE=m_dot_hot*Cp_hot_IHE
C_min_IHE=m_dot_wf*Cp_wf_IHE
c_IHE=C_min_IHE/C_max_IHE
e_IHE=(1-exp(-NTU*(1-c_IHE)))/(1-c_IHE*exp(-NTU*(1-c_IHE)))
Ns1_IHE=T_2/(e_IHE*(T_6-T_2))*(ln(1+e_IHE*c_IHE*(ConvertTEMP(C,K,T_6)/ConvertTEMP(C,K,T_2)-
1))/c_IHE+(ln(1-e_IHE*(1-ConvertTEMP(C,K,T_2)/ConvertTEMP(C,K,T_6)))))
"-------------------------------------------------
NTU_Evap_____________________________________________"
Cp_geo_E=Cp(geo$,T=T_8,x=0)
Cp_wf_E=Cp(wf$,T=T_4,x=0)
C_max_E=m_dot_geo*Cp_geo_E
C_min_E=m_dot_wf*Cp_wf_E
c_E=C_min_E/C_max_E
e_E=1-exp(-NTU)
Ns1_E=ln(1-e_E*(1-
ConvertTEMP(C,K,T_4)/ConvertTEMP(C,K,T_8)))/(e_E*(ConvertTEMP(C,K,T_8)/ConvertTEMP(C,K,T_4
)-1))+1
"-------------------------------------------------
NTU_Cond_____________________________________________"
Cp_cw_C=Cp(wf$,T=T_11,P=P_11)
Cp_wf_C=Cp(wf$,T=T_7,P=P_7)
C_max_C=m_dot_cw*Cp_cw_C
C_min_C=m_dot_wf*Cp_wf_C
c_C=C_min_C/C_max_C
e_C=1-exp(-NTU)
Ns1_C=ln(1+e_C*(ConvertTEMP(C,K,T_7)/ConvertTEMP(C,K,T_11)-
1))/(e_C*(ConvertTEMP(C,K,T_7)/ConvertTEMP(C,K,T_11)-1))-
(ConvertTEMP(C,K,T_11)/ConvertTEMP(C,K,T_7))
```

```
"-----------------------------------------------------------------COMPONENTS SIZING-----------------------------------
-----------------------------------------------"
pass=1
d_iPH=0.01905
d_iIHE=0.01905
d_iE=0.01905
d_iC=0.00635

ratio_Volume=0.785*(CTP/CL)*((d_oPH^2-d_iPH^2)/(P_t^2*(1+2*t_wall/D_s)^2))-1/(1+2*t_wall/D_s)^2+1
ratio_Volume=0.11
CL=1
CTP=0.93   "one tube pass"
d_oPH=1.2*d_iPH
P_t=1.5*d_oPH
t_wall=d_oPH-d_iPH

n_tPH=400
n_tIHE=400
n_tE=400
n_trans=400
n_long=6
n_tC=n_trans*n_long

N_PH=10
N_IHE=10
N_E=10
N_C=1000
"----------------------------PREHEATER SIZING-------------------------------"
call Preheater(D_s,N_PH, wf$,
geo$,cw$,T_3,P_3,h_3,T_4,P_4,h_4,T_9,P_9,h_9,T_10,P_10,h_10,m_dot_geo,m_dot_wf,m_dot_cw,n_t
PH,d_iPH,pass:Area_PH,Length_PH,DELTAp_tPH,DELTAp_sPH,W_dot_ghPH,
Volume_tPH,Volume_wPH,Volume_zPH)
"----------------------------RECUPERATOR SIZING-----------------------------"
call Recuperator(D_s,N_IHE, wf$,
geo$,cw$,T_3,P_3,h_3,T_2,P_2,h_2,T_6,P_6,h_6,T_7,P_7,h_7,m_dot_geo,m_dot_wf,m_dot_cw,n_tIHE,
d_iIHE,pass:Area_IHE,Length_IHE,DELTAp_tIHE, DELTAp_sIHE,W_dot_ghIHE,
Volume_tIHE,Volume_wIHE,Volume_zIHE)
"----------------------------EVAPORATOR SIZING-----------------------------"
```

```
call Evaporator(D_s,N_E, wf$,
geo$,cw$,T_4,P_4,h_4,T_5,P_5,h_5,T_8,P_8,h_8,T_9,P_9,h_9,m_dot_geo,m_dot_wf,m_dot_cw,n_tE,d
_iE,pass:Area_E,Length_E,DELTAp_tE,DELTAp_sE,W_dot_ghE, Volume_tE,Volume_wE,Volume_zE)
"-----------------------------CONDENSER SIZING-------------------------------"
call Condenser(N_C, wf$,
geo$,cw$,T_1,P_1,h_1,T_7,P_7,h_7,T_11,P_11,h_11,T_12,P_12,h_12,T_c,P_c,h_c,m_dot_geo,m_dot_
wf,m_dot_cw,n_trans,n_long,d_iC:Area_C1,Area_C2,Area_C,Length_C1,Length_C2,Length_C,DELTAp
_tC,DELTAp_sC,W_dot_fan,V_frC,n_fin_m,P_tC,P_lC)
"-----------------------------TURBINE SIZING-------------------------------"
call Turbine(wf$, geo$,cw$,T_5,h_5,P_5,T_6s,h_6s,T_6,P_6,m_dot_geo,m_dot_wf,m_dot_cw:VFR,SP)
"---------------------------------------OVERALL-----------------------------------------"
Area_total=Area_PH+Area_E+Area_IHE+Area_C
W_dot_gh=W_dot_ghPH+W_dot_ghE
DELTAp_geo=DELTAp_sPH+DELTAp_sE
DELTAp_wf=DELTAp_tPH+DELTAp_tE
```